



**Investigation of the role of
poly(ADP-ribose)polymerase inhibition
in topoisomerase I
poison-induced cytotoxicity.**

PhD Thesis

PAWEL JACEK ZNOJEK

October 2011

ABSTRACT

The topoisomerase I (TopoI) poisons (*e.g.* camptothecin, CPT) cause stabilisation of the TopoI-DNA cleavable complex resulting in DNA single strand breaks (SSBs). DNA breakage and cytotoxicity are related to TopoI activity and TopoI poisons are thought to be primarily cytotoxic in S phase due to conversion of SSB to double strand breaks (DSB) through replication fork collision. DNA SSB are repaired by the base excision repair/SSB repair (BER/SSBR) pathway and DSB are predominantly repaired by homologous recombination repair (HRR) or non-homologous end joining (NHEJ). Poly (ADP-ribose) polymerase-1 (PARP-1) recognises SSB and DSB and promotes their repair. Previous studies in this laboratory demonstrate that PARP inhibitors enhance TopoI poison-induced cytotoxicity by a mechanism that involves elevation of DNA breaks level or retarding the repair of TopoI poison-induced DNA strand breaks. The role of BER/SSBR in this process was verified previously however, there is no data linking sensitisation of TopoI poison-induced cytotoxicity by PARP inhibitors to a specific cell cycle phase. The aim of this project was to test the hypothesis that a) PARP inhibition inhibits the repair of CPT-induced SSB, resulting in more replication-associated DSB in S phase cells, b) PARP inhibition further retards DSB repair and c) consequently the greatest sensitisation is seen in S phase cells. To elucidate the mechanisms DNA breakage, and cytotoxicity were determined in asynchronous cells and those separated into G1, S and G2/M phases by centrifugal elutriation, in cells exposed to the clinically active PARP-1 inhibitor, AG014699, and CPT. Cell cycle-specific variations in TopoI and PARP expression and activity were also investigated as possible contributors to ultimate cytotoxicity.

Survival of asynchronous Lovo colorectal cancer cells exposed to CPT was substantially reduced by co-incubation with AG014699. CPT cytotoxicity was greater in a 60% pure S phase population than in 90% pure G1 population. AG014699 increased the cytotoxicity of CPT in the S phase cells but not cells in G1. K562 leukaemia cells were used to confirm findings obtained with Lovo cells. Highly purified (>90% pure) cell cycle specific fraction of K562 cells were used to demonstrate that CPT was most cytotoxic to S phase cells and that potentiation of CPT-induced cytotoxicity by AG014699 is predominantly related to S phase cells whose survival was reduced by 2-fold. TopoI activity was greatest in S phase cells, corresponding to the greater cytotoxicity of CPT in this phase. However, the magnitude of the effect of AG014699 on survival did not correspond with the level of PARP-1 activity, which was highest in

G2 cells. The potentiation of CPT-induced cytotoxicity by AG014699 in S phase was shown to correlate with the level of SSB and DSB, which was highest in S phase. Repair of CPT-induced SSB and DSB was most rapid during S phase and AG014699 hindered the repair of both SSB and DSB to the greatest extent in S phase compared with other phases of the cell cycle. This suggests that collision with the replication fork is a major mechanism for the induction of DSB and resultant cytotoxicity. and that PARP is involved in the repair of CPT-induced DSB as well as SSB.

BER/SSBR requires XRCC1 as well as PARP, furthermore, PARP-1 is proposed to act in a backup NHEJ pathway that also involves XRCC1. To test these hypotheses the effect of AG014699 on the DNA repair and cytotoxicity of CPT, temozolomide (a DNA methylating agent that induces SSB) and neocarzinostatin (an inducer of DSB) was investigated in XRCC1 wild type (AA8) and mutant (EM9) cells. AG014699 enhanced the cytotoxicity of these agents in parallel with increasing the number of DSB and inhibition of their repair in EM9 as well as AA8 cells. Therefore PARP has an additional role in the protection of cells from DNA SSB and DSB independent of XRCC1.

Currently there are 9 PARP inhibitors undergoing clinical evaluation, including combinations with TopoI poisons. The data presented here demonstrate that PARP inhibitors reduce the repair of TopoI poison-induced DNA DSB as well as SSB and consequent cell survival primarily in S phase. Furthermore, we demonstrate that the activity of PARP inhibition is independent of XRCC1 indicating that tumours associated with XRCC1 polymorphisms will be similarly sensitive. These findings may have implications for the rational design of clinical trials involving PARP inhibitor – TopoI poison combinations.



This thesis is dedicated to my lovely wife Agnieszka, who was with me in most difficult moments and helps me realize what is the most important...

Acknowledgements

I would like to thank, in particular, my supervisors, Professor Nicola Curtin and Dr Elaine Willmore, without whose knowledge, compassion and assistance in difficult moments, this thesis have not been completed.

Participating in charity project financed by CR-UK I feel obligatory to thank this organization for supporting my research.

I would like also to thank everybody in NICR especially people in Drug Development Lab for their help, kind and friendly atmosphere conducive to scientific work.

ABREVIATION LIST

°C - Degrees Celsius
3-AB - 3-Aminobenzamide
AP - Abasic site
APC – anaphase promoting complex
APE1 - AP endonuclease
ATM - Ataxia telangiectasia mutated gene product
ATP - Adenosine 5'-triphosphate
ATR - Human Ataxia telangiectasia-related
BCA - Bicinchoninic acid
BER - Base excision repair
B-NHEJ - Back-up non-homologous end joining
Bp - Base pair
BRCA - Breast cancer susceptibility protein
BRCT - C-terminal region of breast cancer susceptibility protein-1
BSA - Bovine serum albumin
Cdk - Cyclin dependent kinase
Chk - Checkpoint kinase
CHO - Chinese hamster ovary
CPT - camptothecin
DAPI - 4',6'-diamidino-2-phenylindole dihydrochloride
DBD - DNA binding domain
DMS - dimethyl sulphate
DMSO - Dimethyl sulphoxide
DNA - Deoxyribonucleic acid
D-NHEJ - DNA-PK dependent non-homologous end joining
dRP - Deoxyribose-5-phosphate
DSB - Double strand break
e.g. - “*Exempli gratia*”/for example
EDTA - Ethylenediaminetetraacetic acid
FEN1 - Flap structure-specific endonuclease1
H2AX – Monophosphorylated histone variant
i.e. - “*id est*”/that is
IC₅₀ - Concentration at which 50% enzyme inhibition is observed
IR - Ionising radiation
MMR - Mismatch repair
MMS - Methylmethanesulfonate
MNNG - *N*-methyl-*N'*-nitro-*N*-nitrosoguanidine
MRN - Mre11-Rad50-Nbs1 complex
NAD⁺ - Nicotinamide adenine dinucleotide
NBS - Nijmegen breakage syndrome
NCS - Neocarzinostatin
NER - Nucleotide excision repair
NHEJ Non-homologous end joining
NLS - Nuclear localisation signal
OH - Hydroxyl radical
OTM - Olive tail moment
PAR - Poly(ADP-ribose) polymer
PARG - Poly(ADP-ribose) glycosylase

PARP - Poly(ADP-ribose) polymerase
PARP-1 - Poly(ADP-ribose) polymerase-1
PARPi - PARP inhibitors
PBS - Phosphate buffered saline
PCNA - Proliferating cell nuclear antigen
PI – propidium iodide
PMSF - Phenylmethanesulphonyl fluoride
PNK – Polynucleotide kinase
PNK Polynucleotide kinase
RFC - Recombinant Human Replication Factor C
RNA - Ribonucleic acid
ROS - Reactive oxygen species
RPA - Replication protein
RT - Room temperature
SSB - Single strand break
TCA - Trichloroacetic acid
TopoI - Topoisomerase I
TopoI-cc – Topoisomerase I cleavage complex
TopoII - Topoisomerase II
U - Uracil
UV - Ultra violet
V - Volt
v/v By volume
v-PARP - Vault Poly(ADP-ribose) polymerase
w/v By weight
XRCC1 – X-ray repair complementing defective repair in Chinese hamster cells 1.
ZnF1/ZnF2/ZnF3 - Zinc finger motifs found in PARP-1
 γ H2AX - Phosphorylated H2AX

TABLE OF CONTENTS

ABSTRACT	i
Acknowledgements	iv
ABREVIATION LIST	v
TABLE OF CONTENTS	vii
TABLE OF FIGURES	xii
TABLE OF TABLES	xvi
Chapter 1. Introduction	1
1.1. Cancer overview	1
1.2. Cell cycle control in cancer.	3
1.3. DNA damage and repair in cancer.	6
1.3.1. Source of DNA damage	6
1.3.2. DNA repair defect in cancer	8
1.4. DNA repair.	9
1.4.1. Base Excision Repair (BER).	9
1.4.2. Nucleotide Excision Repair (NER).	11
1.4.3. Non homologous end joining (NHEJ).	12
1.4.4. Homologous Recombination Repair (HRR).	13
1.5. Human DNA Topoisomerases.	16
1.5.1. TopoI structure and catalytic activity.	18
1.5.2. Regulation of TopoI activity.	20
1.5.3. Topoisomerases poisons.	21
1.5.4. Repair of TopoI-mediated DNA damage.	26
1.6. Poly (ADP-ribose) polymerases– PARP.	28
1.6.1. PARP-1 molecular structure.	30
1.6.2. PARP-1 catalytic mechanism – poly(ADP-ribosylation).	31
1.6.3. PAR acceptors	33
1.6.4. Role of PARP-1 in DNA repair	34

1.6.5. PARP inhibitors	36
1.7. PARP-1 and TopoI interaction.....	38
1.8. Aims.....	42
Chapter 2. Materials and methods	43
2.1. Materials	43
2.2. Equipment	43
2.3. Tissue culture	44
2.4. Growth inhibition and cytotoxicity assay.....	45
2.4.1. XTT cell proliferation assay.....	45
2.4.2. Clonogenic survival assay.....	45
2.4.3. Clonogenic survival assay by sloppy agar.	46
2.5. Staining cells for the cell cycle analysis by flow cytometry.	46
2.6. Centrifugal elutriation in JE – 5.0 rotor.....	49
2.6.1. Elutriation of K562 cells.....	51
2.7. Comet assay.....	52
2.8. Topoisomerase activity assay	54
2.8.1. Lysate preparation.....	55
2.8.2. TopoI relaxation activity.....	55
2.9. Parp-1 activity assay.....	55
2.10. γ H2AX detection by immunofluorescence.....	56
2.10.1. PZFociEZ - ImageJ custom macro.....	57
2.10.2. Comparing image analysis between ImageJ and Image ProPlus software. 60	
2.11. Western blotting.....	63
2.12. Statistical analysis.....	64
Chapter 3. Cell cycle dependent effect of PARP-1 inhibition on topoisomerase I poison-induced cytotoxicity in cells.	65
3.1. Introduction	65

3.2.	Aims	69
3.3.	Effect of PARP1 inhibition on TopoI poison-induced cell cytotoxicity in elutriated and asynchronously growing Lovo cells.....	70
3.3.1.	Effect of AG014699 on CPT induced cytotoxicity in Lovo cells after long and short exposure	70
3.3.2.	Separation of Lovo cell into different cell cycle fractions by centrifugal elutriation.....	73
3.3.3.	Effect of AG014699 on CPT-induced cytotoxicity in elutriated Lovo cells. 75	
3.4.	Effect of PARP1 inhibitor on TopoI poison-induced cell cytotoxicity in elutriated and asynchronously growing K562 cells.	76
3.4.1.	Growth of asynchronous K562 cells.....	77
3.4.2.	Separation of K562 cells into different cell cycle fractions by centrifugal elutriation.....	78
3.4.3.	Effect of elutriation process on K562 cell growth.	80
3.4.4.	Effect of AG014699 on TopoI poison-mediated growth inhibition in asynchronous and elutriated K562 cells.	81
3.4.5.	Effect of PARP1 inhibitor on TopoI poison-induced cell cytotoxicity in elutriated K562 cells.....	83
3.5.	Variation in TopoI activity in different cell cycle phases	85
3.6.	Variation in PARP1 activity in different cell cycle phases.....	88
3.7.	Variation in PARP-1 and TopoI proteins level in different cell cycle phases..	89
3.8.	Discussion	91
Chapter 4.	The effect of AG014699 on the formation and repair of CPT-induced DNA damage.....	96
4.1.	Introduction	96
4.2.	Aims	99
4.3.	The level of DNA damage in K562 cells measured directly after elutriation	100
4.4.	The effect of AG14699 on the level of DNA breaks induced by CPT in asynchronous cells and K562 cells separated into cell cycle subpopulations.....	103

4.5.	Determination of DSB level in K562 cells exposed to CPT± AG014699.	107
4.5.1.	The effect of AG14699 on the DSB level in asynchronous and elutriated K562 cells determined by neutral comet assay.....	107
4.5.2.	The effect of AG14699 on CPT-induced DSB in asynchronous K562 cells evaluated by γ -H2AX	110
4.6.	The effect of AG014699 on the repair of DNA breaks induced by CPT in asynchronous K562 cells.....	117
4.6.1.	Repair of CPT-induced total DNA breaks in asynchronous K562 cells.	117
4.6.2.	Effect of AG014699 on the repair of CPT-induced DSB in asynchronous population of K562 cells.....	121
4.6.2.1.	Neutral comet assay.....	121
4.6.2.2.	γ H2AX immunostaining.....	124
4.7.	The effect of AG014699 on the repair of CPT-induced DNA breaks in K562 cells in different phases of the cell cycle.....	127
4.7.1.	The effect of AG014699 on the repair of total CPT-induced DNA breaks.	127
4.7.2.	The role of PARP inhibition in the repair of CPT-induced DSB.....	131
4.8.	Discussion	135
Chapter 5.	The role of the interaction between PARP and XRCC1 in DSB induction and repair	139
5.1.	Introduction	139
5.2.	Aims	142
5.3.	Verification of XRCC1 expression in AA8 and EM9 cells by Western blot.	143
5.4.	Effect of AG014699 on the formation and repair of DNA breaks in EM9 and AA8 cells.....	144
5.4.1.	CPT induced total DNA breaks measured by alkaline comet assay.	144
5.4.2.	Effect of AG014699 on the formation and repair of CPT-induced DSB in EM9 and AA8 cells.....	148
5.4.3.	Effect of AG014699 on the formation and repair of CPT-induced DSB in EM9 and AA8 cells determined by H2AX immunofluorescence	151

5.4.4. Effect of AG014699 on the formation and repair of TMZ-induced DSB in EM9 and AA8 cells.....	153
5.4.5. Effect of AG014699 on the formation and repair of neocarzinostatin-induced DSB in EM9 and AA8 cells.....	155
5.5. The effect of PARP-1 inhibition on CPT, TMZ and neocarzinostatin induced cell cytotoxicity.....	156
5.6. Discussion.....	160
Chapter 6. Summary and final discussion.....	164
A. APPENDIX - PZFociEZ, ImageJ macro for γ H2AX foci analysis - documentation.....	172

TABLE OF FIGURES

Figure 1. 1. “Acquired Capabilities” - functional capabilities acquired by cells during their transformation into cancer cells (Hanahan and Weinberg, 2000).	2
Figure 1. 2. Cell cycle control.	4
Figure 1. 3. Factors causing DNA damage.	6
Figure 1. 4. Base Excision Repair process	10
Figure 1. 5. Nucleotide excision Repair mechanism (Wood, 2010).	11
Figure 1. 6. Non Homologous End Joining.	12
Figure 1. 7. Homologous Recombination (HR).	15
Figure 1. 8. Classification of human DNA topoisomerases.	17
Figure 1. 9. TopoI molecular structure.	18
Figure 1. 10. DNA relaxation catalysed by Topoisomerase I (Pommier et al., 2010).	19
Figure 1. 11. Natural source and molecular structure of camptothecin.	21
Figure 1. 12. Human TopoI in covalent complex with DNA and CPT (image adopted from PubMed webpage using Cn3D software).	22
Figure 1. 13. TopoI-mediated DNA damage (Pomier 2006).	24
Figure 1. 14. Pathways involved in repair of TopoI-cc.	27
Figure 1. 15. Molecular structure of PARP-1.	30
Figure 1. 16. Maintenance of ADP-ribose polymer by PARPs and PARG (Patel et al., 2005).	32
Figure 1. 17 Chemical features of potent PARP inhibitors. (Griffin et al., 1995)	36
Figure 1. 18. Molecular structure of AG014699.	38
Figure 2. 1. An example of FACS report produced with the aid of ModFit LT software	48
Figure 2. 2. The JE-5.0 elutriation system and process of cells separation inside elutriation chamber (picture from Beckman elutriation manual).	50
Figure 2. 3. Gel image showing the results of TopoI relaxation activity assay (from www.TopoGen.com).	54
Figure 2. 4. A sequence of operation during generation of the selections for DAPI stained nucleus implemented in MasKEZ panel of the PZFociEZ macro.	58
Figure 2. 5. A sequence of operation applied during analysis of images with γ H2AX foci by FociEZ panel.	59
Figure 2. 6. Images of γ H2AX foci obtained using two different microscopes.	61

Figure 2. 7. Comparison of the results analysis with the aid of PZFociEZ macro and Image ProPlus softwares of images obtained from Olympus and Leica microscopes ...	62
Figure 3. 1. Effect of 0.4 μ M AG014699 on CPT induced cytotoxicity in Lovo cell line.	72
Figure 3. 2. DNA histograms of asynchronous and elutriated Lovo cells.....	74
Figure 3. 3. Growth curve for K562 cells	77
Figure 3. 4. DNA histograms of asynchronous and elutriated K562 cells.....	78
Figure 3. 5. DNA histograms of progression through cell cycle of K562 cells elutriated on G1-phase K652.....	79
Figure 3. 6. Growth curve for asynchronous and elutriated on G1, S and G2 cell cycle phases K562 cells.	80
Figure 3. 7. Effect of AG4699 on camptothecin induced growth inhibition in asynchronous and elutriated K652 cells,.....	82
Figure 3. 8. Effect of AG14699 on CPT induced cytotoxicity in asynchronous and elutriated K562 cells.	84
Figure 3. 9. TopoI relaxation activity in asynchronous and elutriated on G1, S and G2 K562 cells.	87
Figure 3. 10. PARP activity.	88
Figure 3. 11. TopoI and PARP-1 protein level in elutriated fractions of K562 cells.....	90
Figure 4. 1. OTM measured measured in K562 cells directly after elutriation.	101
Figure 4. 2. Histograms of the Olive Tail Moment measured in populations of asynchronous and cell cycle separated K562 cells	102
Figure 4. 3. Comets observed after 30 min exposure to CPT \pm 0.4 μ M AG014699 and determined using alkaline comet assay	104
Figure 4. 4. The effect of PARP-1 inhibition on the level of DNA breaks in asynchronous and cell cycle phase separated K562 cells.	105
Figure 4. 5. Comets showing the level of DNA double strand breaks in K562 cells ...	108
Figure 4. 6 The effect of AG014699 on CPT-induced DSB in asynchronous and elutriated K562 cells.	109
Figure 4. 7. Sample image illustrating background subtractions (BG) using rolling ball algorithm.	111
Figure 4. 8. The measurements of H2AX analysis obtained with ImageJ macro.....	112

Figure 4. 9. γ H2AX immunostaining pattern found in K562 cells exposed to CPT \pm AG014699	115
Figure 4. 10. Plot of Foci Raw Integrated Density and Foci number categorised by cell cycle phase, PARP Inhibitor and CPT concentration	116
Figure 4. 11. The comets observed after 30 min exposure to 10 and 100 nM CPT followed by incubation in fresh medium \pm 0.4 μ M AG014699 as determined by alkaline comet assay.	118
Figure 4. 12. Effect of AG014699 on the repair of total DNA breaks formed during 30 min exposure to 100 nM CPT	119
Figure 4. 13. The comets observed after 30 min exposure to 100 nM CPT followed by incubation in fresh medium \pm 04 μ M AG014699 as determined by neutral comet assay	121
Figure 4. 14. The comets observed after 30 min exposure to 100 nM CPT \pm 04 μ M AG014699 as determined by neutral comet assay.	122
Figure 4. 15. Representative staining of γ H2AX foci in K562 cells.	124
Figure 4. 16. The fluorescence and foci numbers observed after 30 min exposure to 10 and 100 nM CPT \pm 04 μ M AG014699 as determined by γ H2AX fluorescence.....	126
Figure 4. 17. Comets observed in asynchronous and cell cycle separated K562 cells evaluated by alkaline comet assay	128
Figure 4. 18. The effect of PARP-1 inhibition on DNA SSB break repair in asynchronous and cell-cycle-phase-separated K562 cells	129
Figure 4. 19. The comets observed after 30 min exposure to 100 nM CPT followed by incubation in fresh medium \pm 04 μ M AG014699 as determined by neutral comet assay	132
Figure 4. 20. The effect of PARP-1 inhibition on DSB repair in asynchronous and cell cycle phase separated K562 cells.....	133
Figure 5. 1. Western blot of XRCC1 in AA8 and EM9 cells.....	143
Figure 5. 2. Images of comets showing induction and repair of CPT induced total DNA breaks.	146
Figure 5. 3. Effect of AG014699 on induction and repair of SSB induced by CPT.....	147
Figure 5. 4. Images of comets showing induction and repair of CPT induced DSB DNA breaks.	149
Figure 5. 5. Effect of AG014699 in induction and repair of DSB induced by CPT	150

Figure 5. 6 AG014699 effect on induction and repair of CPT-induced DSB.....	152
Figure 5. 7. AG014699 effect on induction and repair of TMZ-induced DSB.....	154
Figure 5. 8. The effect of AG014699 on neocarzinostatin-induced DSB.....	155
Figure 5. 9. Survival of AA8 and EM9 cells following increasing concentration of CPT±AG014699	158
Figure 5. 10. Survival of AA8 and EM9 cells exposed to TMZ±AG014699.....	158
Figure 5. 11. Effect of AG014699 on neocarzinostatin-induced cell cytotoxicity.	159

TABLE OF TABLES

Table 3. 1. Comparison of survival of adherent and suspension Lovo cells.....	73
Table 3. 2. Effect of AG14699 on TopoI poison (CPT) induced cytotoxicity in Lovo cells elutriated on G1, S, and G2 cell cycle phases.....	76
Table 4. 1 Effect of AG014699 on CPT-induced DNA breaks	105
Table 4. 2. Effect of AG014699 on CPT-induced DSB.....	109
Table 4. 3. The effect of AG014699 on the repair of DNA breaks induced by exposure to CPT for 30 min.	120
Table 4. 4. The effect of AG014699 on the repair of DSB induced by exposure to CPT for 30 min.....	123
Table 4. 5. The effect of 0.4 μ M AG014699 on the repair of CPT-induced DNA breaks in the K562 cells evaluated by alkaline comet assay	129
Table 4. 6. The effect of 0.4 μ M AG014699 on the repair of CPT-induced DSB in the K562 cells evaluated by neutral comet assay.....	133
Table 5. 1. Formation and repair of total DNA breaks in AA8 and EM9 cells	147
Table 5. 2 Effect of AG014699 in induction and repair of DSB induced by CPT.	150
Table 5. 3. Effect of AG014699 in induction and repair of DSB induced by CPT	152
Table 5. 4. Effect of AG014699 in induction and repair of DSB induced by TMZ	154

Chapter 1. Introduction

1.1. Cancer overview

Cancer is caused by genetic, epigenetic or translational changes that force the progressive transformation of normal cells into malignant derivatives (Baylin and Jones, 2011). Cancer cells are generally characterized by defects in the regulation of cell proliferation and homeostasis, destruction of adjacent tissues and eventually capability to spread (metastasis) to other locations in the body. The most life-threatening and difficult-to-cure stage of cancer occurs when the original tumour undergoes metastasis. The presence of cancer can be suspected based on symptoms (*e.g.* a lump you can find anywhere in the body), or findings from radiology. However, definitive diagnosis of cancer occurrence requires the microscopic examination of a biopsy specimen. It is difficult to estimate the reliable number of people susceptible to cancer, however according to statistics available from Cancer Research UK in United Kingdom in 2002 there were 41,720 women diagnosed with breast cancer and in the same year 22,504 men were diagnosed with lung cancer (www.cancerresearchuk.org).

Different types of cancer are classified based on the type of cell/tissue from which tumours originate. The major cancers types listed include Carcinoma (derived from epithelial cells. including breast, prostate, lung and colon.); Sarcoma: (derived from connective tissue, or mesenchymal cells); Lymphoma and leukaemia: (derived from hematopoietic blood-forming cells); Germ cell tumour (derived from pluripotent cells) and Blastoma (derived from immature or embryonic tissue).

A process that leads to cancer is complex therefore, difficult and far from being completely understood. However, the results of decades of research allow us to identify six features/capabilities that can be acquired by the cells during the transformation into cancer cells. These features were reviewed in detail by Hanahan and Weinberg, who refer to them as “Hallmarks of cancer” (Figure 1. 1) and involve, self-sufficiency in growth signals, insensitivity to antigrowth signals, evading apoptosis, limitless replicative potential, sustained angiogenesis, tissue invasion and metastasis (Hanahan and Weinberg, 2000). Genomic instability is an “enabling characteristic” and may be caused by defects or imbalances in DNA damage signalling or repair (Hanahan and Weinberg, 2011).

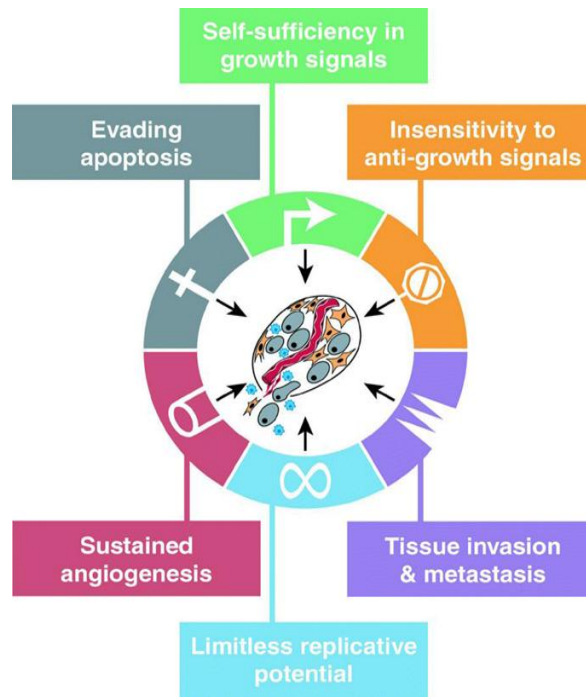


Figure 1. 1. “Acquired Capabilities” - functional capabilities acquired by cells during their transformation into cancer cells (Hanahan and Weinberg, 2000).

The main goal in the treatment of cancer is the complete removal of tumour tissue without damaging the rest of the body. The early diagnosis, location of the tumour, stage of the illness, and general condition of patient have a major impact on the choice of therapy, therapy limitation and survival prognosis.

Probably the most effective method used to treat cancer is surgery. Radiation therapy is another common method employed in cancer treatment. Ionizing radiation focused on tumour tissue kills cancer cells via induction of plethora of single and double strand breaks (Purdy, 2008). If tumour cannot be surgically removed it is necessary to apply radiation therapy and/or some form of chemotherapy that improve radiation effectiveness (Verheij et al.).

Examples of major classes of chemotherapeutics drugs include: DNA reactive drugs (Monofunctional or Bifunctional alkylating agents, Platinum compounds e.g. Temozolomide or Chlorambucil, Cisplatin); Topoisomerase I/II inhibitors (Topotecan Etoposide); alkylating agents (e.g. Temozolomide), Antimetabolites (Pyrimidine or Purine analogues e.g. 5-fluorouraci or 6-thioguanine); Tubulin binders (e.g. Paclitaxel, Vincristine). The general mechanism of action of these conventional chemotherapeutics is to stop the proliferation of cancer cells, mainly by DNA damage induction (Chabner and Roberts, 2005, DeVita and Chu, 2008).

Development of new anticancer drugs is currently focused to targeting specific proteins or metabolic pathways involving DNA damage repair proteins, cell cycle control regulators, growth factors and their receptors, apoptosis (Goldblatt and Lee, 2010).

1.2. Cell cycle control in cancer.

The cell cycle is a sequence of events occurring in living cells, covering the period between cell divisions (interphase) and the period in which cell divides into two daughter cells (mitosis). Based on the sequence of molecular events occurring in the interphase, this period is divided into four phases/Gaps referred to as G₀, G₁, S and G₂.

A family of serine/threonine kinases referred to as cyclin dependent kinases (Cdk) regulates the progression of cell through subsequent phase of the cell cycle. These kinases are formed by a catalytic kinase subunit (Cdk) and a regulatory subunit – a cyclin.

Several different cyclins control cell cycle phase progression. Cyclins also determine Cdk subcellular localization and the level of cyclins depends on the position of cell cycle. Cells begin cell cycle by entering the interphase. At the beginning of the cell cycle the level of G₁ cyclins rises and they bind to their Cdk partner. This gives the cell a signal to prepare chromosomes for replication. In the G₁ phase, Cyclin D combines with Cdk 4 or 6 and initiates progression to S phase of cell cycle. This complex phosphorylates pRb protein (retinoblastoma protein). pRb is a powerful growth inhibitory molecule which act as a break in cell cycle by binding and blocking the E2F transcription factor. E2F participates in turning on many genes involved in cell cycle progression. The Cyclin D/Cdk complex phosphorylates and inactivates pRb, which leads to the release of E2F that is free to drives cells through the cell cycle. When moving to S phase, the level of cyclin A increases and cyclin A binds to Cdk2 and E2F forming the S phase promoting factor (SPF). The SPF enters the nucleus and prepares cells to duplicate their DNA. Mitotic cyclins such as cyclin B complex with Cdk1 forming mitotic promoting factor (MPF) which initiates the assembly of the mitotic spindle, disaggregation of the nucleus envelope and condensation of chromosomes. At this point MPF activates anaphase-promoting complex (APC). This complex initiates anaphase by allowing sister chromatins to separate. At the end of mitosis, MPF is degraded by cyclin B, which completes mitosis and turns on the synthesis of G₁ cyclins (Lukas et al., 1999, Lukas and Bartek, 2004).

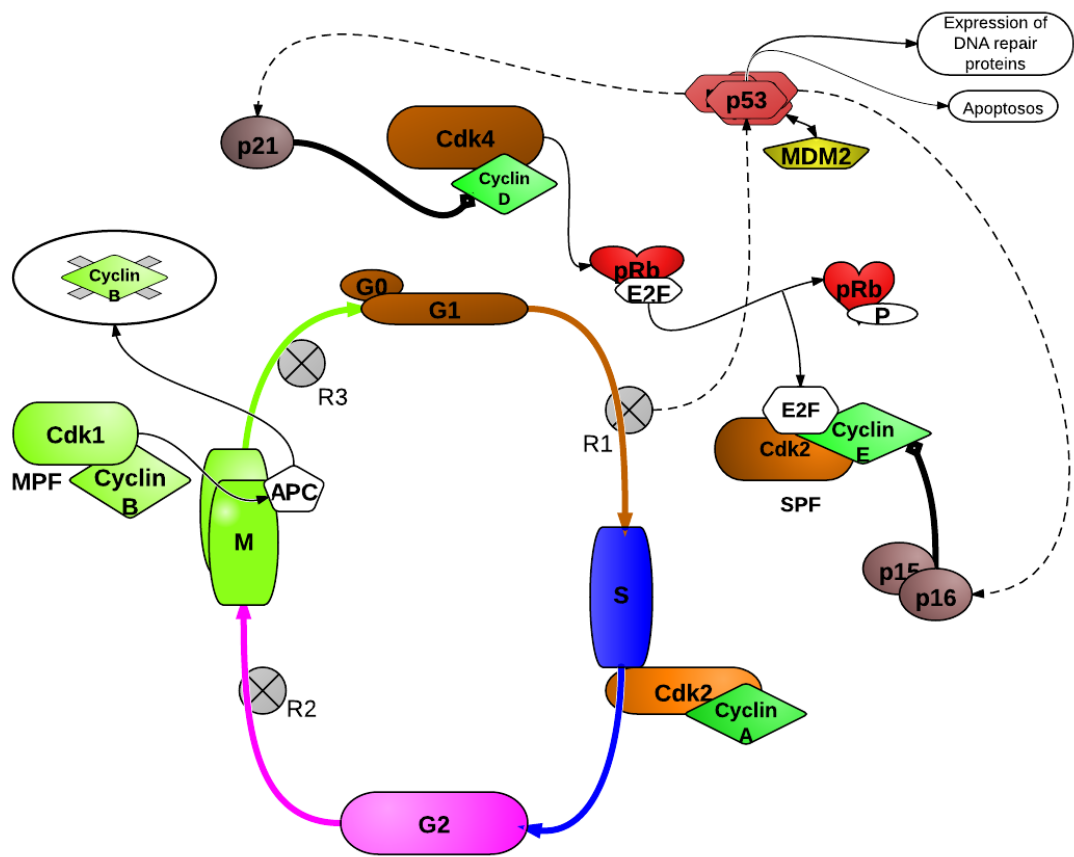


Figure 1. 2. Cell cycle control.

Schematic representation interaction of cell cycle control proteins.

Stressful conditions that cause DNA damage drive the cell response by the restriction points following activation of a complex network of checkpoint pathways to delay their cell cycle progression and repair the defects. As cells progress through cell cycle, they rely on major cell cycle checkpoints (R). At the transition between G1 and S phase, the first restriction point exists (R1) where cells check on their normal growth pattern which includes growth factor withdrawal, contact inhibition and DNA damage. Following S phase, the second major checkpoint exists (R2) in which cells determine whether the DNA has any damage or mismatched DNA bases introduced to DNA during replication. The last major checkpoint exists in M phase (R3) at which cells check if chromosomes are connected to mitotic spindle and kinetochore.

The cell cycle also contains inhibitory proteins that restrict movement through the cell cycle. Proteins p15 and p16 block the activity of Cdk partners of cyclin D and prevent progression from G1 to S phase. The proteins p21 inhibits both cyclin D and cyclin E (Busk et al., 2005).

p53 is a transcription factor that consists of four subunits (C-terminal regulatory domain, tetramerisation domain, DNA-binding domain, and N-terminal transactivation domain). Monomers of p53 following tetramerisation bind to its consensus DNA sequences of p53 target genes. Transcription factors bind to the transactivation domain and mediate gene transcription by DNA polymerase. Deletion of both alleles of p53 often occurs in cancer. When DNA is no longer synthesised, there is no expression of p53 dependent genes. When only one allele is mutated (some tumours have a point mutation in one allele), and the other is wild type, p53 monomers still form tetramer, however there is no binding with DNA. When cells sense DNA damage, p53 is activated leading to inhibition of progression through cell cycle. p53 blocks cell cycle progression by activating expression of proteins that bind and inactivate Cdk proteins. p53 may also activate expression of DNA damage response proteins involved in the repair of or it is capable to activate proteins that drive cells to apoptosis (Riley et al., 2008).

The *MDM2* gene product binds to p53 transactivation domain, preventing p53 from binding with DNA, thus blocking transcription of target genes. The *MDM2* gene is amplified in about 1/3 human soft tissue sarcomas and its product is a ubiquitin ligase. By binding with the N-terminal transactivation domain of p53 monomers, MDM2 ubiquitinates p53, which then is degraded in proteasomes. When the cell senses a DNA-damage, p53 is activated. This inhibits further steps in the cell cycle. p53 acts through stimulation of proteins, amongst others p21 (which binds to cyclin D or E). Cells exposed to DNA damaging agents accumulate changes in DNA that eventually can cause inactivation of tumour suppressor genes (p53, Rb) or activation of proto-oncogenes (e.g. c-myc, fos). Loss of the p53 protein is observed in almost 50% of tumour types (Hollstein et al., 1999). ATR (Ataxia telangiectasia and Rad3 related protein) with ATM (Ataxia telangiectasia mutated) are crucial players in a signalling response to DNA double strand breaks damage. These phosphoinositol 3-kinase like kinase (PIKK) enzymes are activated by the presence of DSBs leading to the phosphorylation of a range of downstream substrates (e.g. γ H2AX, CHK1, CHK2) and eventually to cell cycle checkpoint arrest and/or apoptosis (Shiloh, 2001).

1.3. DNA damage and repair in cancer.

1.3.1. Source of DNA damage

The human genome consists of three billion base pairs, which code for between 30,000-40,000 genes (Venter et al., 2001) which is about 5% of the whole human genome.

DNA is under constant attack of various destructive agents from endogenous as well as exogenous sources as summarised in Figure 1. 3.

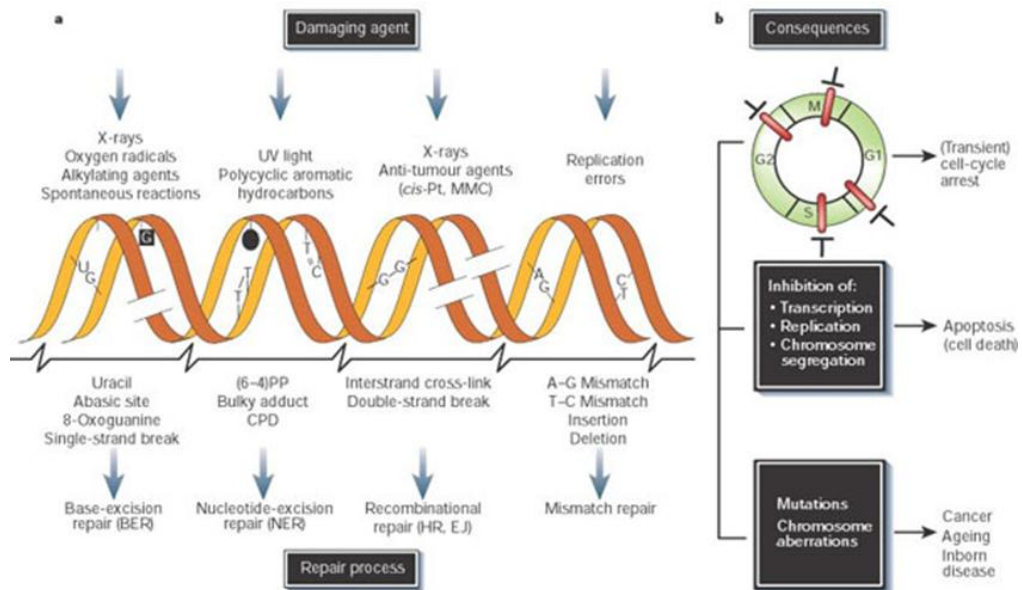


Figure 1. 3. Factors causing DNA damage.

Illustration summarising sources of DNA damaging agents, lesions they cause and DNA repair pathways employed to correct them. Also eventual consequences of repair failure are given (Hoeijmakers, 2001).

Inside the cell, DNA is prone to damaging by by-products of normal cellular metabolism. Metabolites capable of damage to DNA include reactive oxygen species (ROS), derived from oxidative respiration and products of lipid peroxidation (Cadet et al., 2011). Other endogenous genotoxic events include spontaneous loss of bases, various types of base modifications (*e.g.* cytosine deamination, converting it to uracil) or errors occurring during DNA replication (Lindahl, 1993, Hoeijmakers, 2001). Exogenous or environmental sources of factors that are harmful to DNA include UV light or ionizing radiation and mutagens present in the diet. These sources cause alterations in DNA structure, which, if left unrepaired, may lead to mutations that enhance cancer risk. Maintenance of genomic integrity is essential for cellular homeostasis, therefore during evolution an efficient defence system against genomic

instability was developed which involves an arsenal of DNA repair pathways each specialized in removing a specific subset of DNA lesions. When these pathways work properly, they protect cells from causes of genotoxic stress and suppress tumorigenesis. Malfunctions associated with the DNA repair pathway are closely linked to genomic instability, which is the factor that enables tumorigenesis. There are six main, partially overlapping repair pathways operating in mammalian cells: Direct Repair, BER/SSBR, NER, MMR, NHEJ and HRR. The choice of DNA repair pathway depends on the lesion type, availability of repair proteins and the cell cycle phase in which damage occurs.

Direct DNA repair relies on an enzyme that catalyses the reverse reaction to the reaction that caused damage DNA at the first place. An example of a direct DNA repair is repair of O6-alkyl guanine mediated by DNA alkyltransferase which transfers the alkyl group from the DNA to one of own cysteine (Eker et al., 2009)

The base excision repair (BER) mechanism efficiently repairs modified bases, AP-sites (apurinic/apyrimidinic sites) and SSB. Mis-paired bases, incorrectly inserted during replication are processed by mismatch repair (MMR). More bulky, DNA helix-distorting lesions, which obstruct normal transcription and replication, are caused mostly by environmental factors (UV light) are corrected by nucleotide excision repair (NER) (Zheng et al., 2005)

DNA double strand breaks (DSB) are more problematic lesions for repair and failure in repair of these lesions has the most dramatic consequence for cell survival. Two major (and some additional back-up systems) have developed in order to remove any DSB. These are nonhomologous end joining (NHEJ), and homologous recombination repair (HRR). The vast majority of DNA double strand breaks are repaired by the NHEJ pathway that operates throughout whole cell cycle. The HRR pathway is active only during late S and G2 phases, because it requires the sister chromatid as a template for accurate repair. This pathway is considered as highly efficient and virtually error free repair process, unlike NHEJ mechanism, which is error prone (Cline and Hanawalt, 2003)

1.3.2. DNA repair defect in cancer

Sustained genomic instability in cancer cells is often related to deficiency in one of the DNA repair pathways, which can account for the development of a more malignant phenotype. This is possibly due to redundancy in the function of the DNA repair pathways, and in many types of cancers, defects in one pathway, is compensated by upregulation of a complementary pathway. Upregulation of DNA repair pathways in cancer cells is one of the reasons that tumours become resistant to therapy, however, it can be also used as a target for improvement of the treatment efficiency. The absence of one DNA repair pathway results in a hyper-dependence on one or more other DNA repair pathways and targeting these pathways can be employed in cancer therapy. The system in which inactivation of complementary pathways when the other one is already defective is referred to as “synthetic lethality” and recently has been employed in cancer therapy.

The defects in BER/SSBR relevant in cancer therapy include XRCC1 gene polymorphisms which was linked with increase a predisposition to breast cancer (Ali, Meza et al. 2008). The defects in NER are linked to diseases such as Xeroderma pigmentosum (XP), Cockayne syndrome and trichothiodystrophy (TTD), and are all characterized by increased sensitivity to sun (de Waard, Sonneveld et al. 2008). Misfunctional components of HRR metabolic pathways are often acquired in cancer. For example, carriers of mutations in BRCA1 and/or BRCA2 genes are predisposed to develop ovarian and breast cancer. However, lack of some repair pathways in cancer cells is often compensated by a different complementary repair mechanism, allowing cancer cells to sustain efficient proliferation. This, phenomenon, provides the possibility to kill cancer cells during treatment (see section 1.1). PARP inhibitors can be synthetically lethal if used when various components of the HRR pathway exhibits mutations.

1.4. DNA repair.

1.4.1. Base Excision Repair (BER).

Spontaneous, alkylated, and oxidised DNA lesions, when occurring in DNA are repaired by base excision repair (BER). This DNA repair mechanism aims to remove and replace a damaged nucleotide with the aid of DNA glycosylases (Figure 1. 4.). DNA glycosylases belong to a family of several substrate-selective enzymes able to recognize and excise a range of various base modifications such as uracil, 8-oxoguanine (8-oxo-dG), and 3-methyladenine. (Hegde et al., 2008). Removal of a damaged base by DNA glycosylases create an empty space in DNA, which is referred as apurinic/apyrimidinic (AP-site). The AP-sites, which are also quite often formed by spontaneous, non-enzymatic hydrolysis of the N-glycosidic bond, become a substrate for AP-endonuclease (APE1) (Tell et al., 2009). In the next step of BER mechanism, the APE1 cleaves the AP site generating a single strand break. Further processing of damaged DNA depends on the structure of free DNA end follows by two pathways. If resulted terminus of single strand breaks is 3'-OH and 5'-phosphate it is processed by short patch BER (SP-BER). The other option, when 5'-terminus is occupied by reduced deoxyribose phosphate (dRP) follows by long path BER (LP-BER). This is because modified DNA ends must be restored to the conventional 3'-OH and 5-phosphate moieties in order for gap filling and subsequent ligation. The repair of DNA carried out by proteins involved in the LP-BER subpathway, involves removal of 5'-dRP moiety along with short 4–6 additional oligonucleotides by flap endonuclease (FEN-1). One of the DNA Polymerases ϵ , δ , or β then fill the missing strand and DNA Ligase reconnects broken ends. In SP-BER following removal of single nucleobases remaining 3'-OH and 5'-phosphate, DNA strand termini are recognized by DNA polymerase β (Pol β), which replaces the missing nucleotide then sealed by a DNA ligase III in complex with X-ray cross-complementing protein 1 (XRCC1). SSB repaired by BER are potent activators of PARP-1, which plays important role in DNA repair as a sensor of broken DNA (see section 1.6.4).

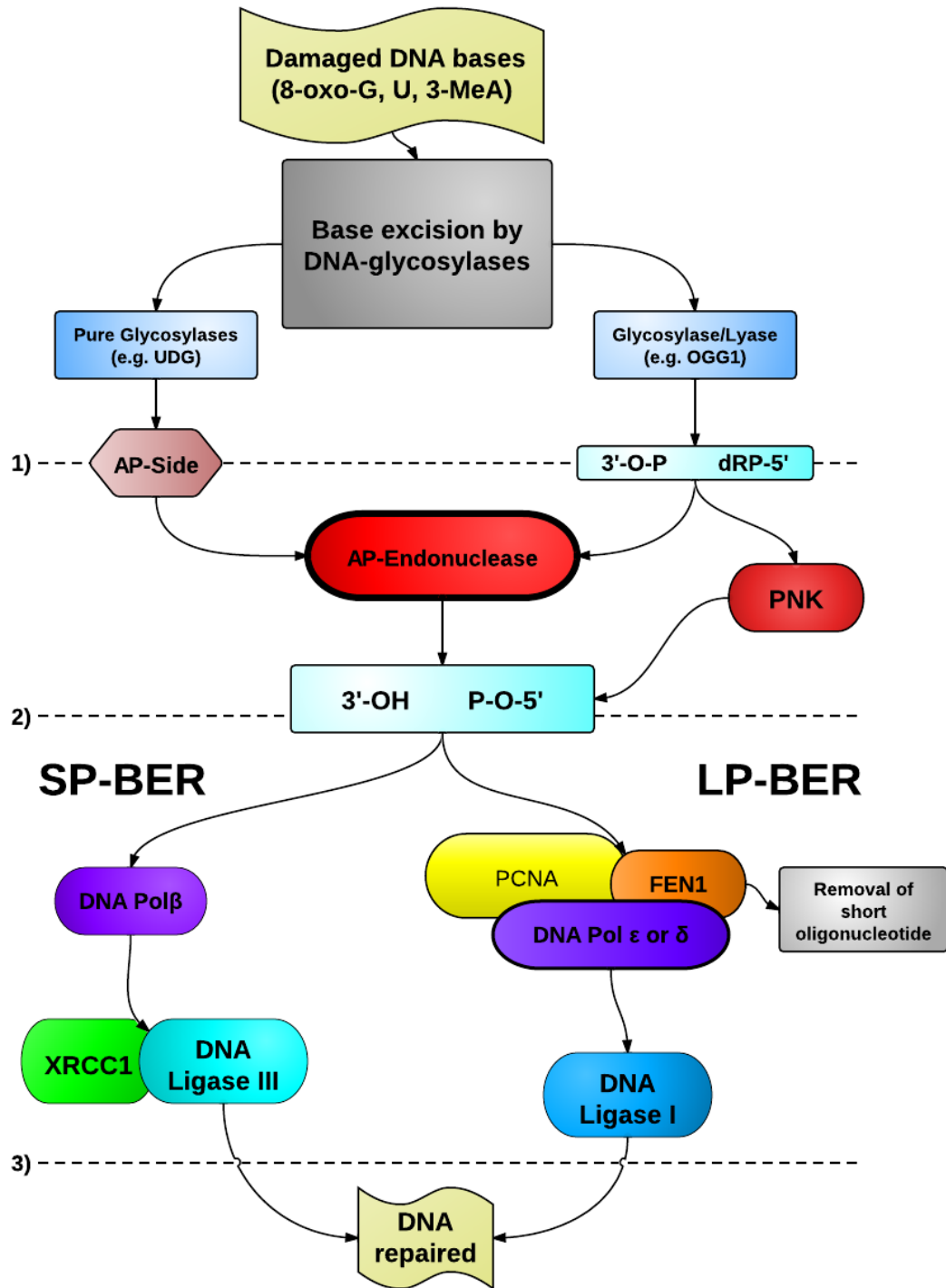


Figure 1. 4. Base Excision Repair process

Base excision repair regardless of the nature of damage, nature of DNA-glycosylases and DNA polymerases follows with three common steps. 1) Removal of the incorrect base by DNA-glycosylase. 2) AP-endonuclease nicks DNA on the 5' site of the AP-site to generate 3'-OH terminus. 3) Extension of the 3'-OH termini by a DNA polymerases and replacement of AP-site with the correct nucleotide

1.4.2. Nucleotide Excision Repair (NER).

Nucleotide excision repair (NER) is the primary DNA repair pathway that removes bulky, helix-distorting DNA damage. Most NER substrates arise from exogenous sources, with UV light as major source (Liu et al., 2010). DNA damage processed by NER includes therefore various intrastrand crosslink photoproducts, *e.g.* thymine dimers or cyclo-butane pyrimidine dimers. Mitomycin C or platinum-based chemotherapeutics agents also form intra and interstrand crosslinks. These lesions are potent blockers of DNA replication and transcription and if unrepaired can be toxic with mutagenic effects. Therefore, often NER is thought to be coupled with transcription, termed “transcription-coupled repair” (TCR) (Lagerwerf et al., 2011). Illustrated in Figure 1. 5. process of DNA repair by NER is carried on in sequential manner, usually divided into four stages. First XPC-RAD23B binds to DNA with base pairing disruption. Following that TFIIH is recruited to DNA with XPA, RPA and XPG to form the pre-incision complex. XPG processes 3’ incision and the XPF-ERCC1 nuclease complex produces a 5’ incision. After DNA incision in last step, DNA Polymerases along with PCNA fill in the gap created, releasing a single-stranded DNA fragment containing the lesion. The patch is sealed by a DNA ligase, either LIG3 or LIG1.

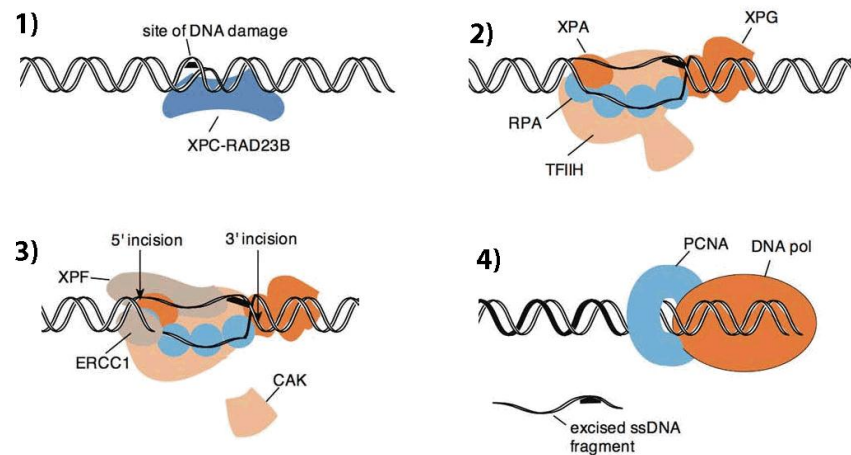


Figure 1. 5. Nucleotide excision Repair mechanism (Wood, 2010).

The illustration shows NER mechanism that is divided into 4 steps 1) recognition of distorted DNA 2) formation of pre-incision complex 3) incision and replacement of broken DNA fragment 4) ligation of fixed DNA.

1.4.3. Non homologous end joining (NHEJ).

The more general and commonly used pathway for DNA double strand break repair is non-homologous DNA end joining (NHEJ). NHEJ can repair a DSB at any time during the cell cycle and does not require a homologous sequence, however a few homologous nucleotides flanking broken DNA ends are often utilized by the NHEJ enzymes. Repair of DSBs by NHEJ is initiated by binding of Ku70 and Ku80 proteins with free DNA ends (Figure 1. 6.).

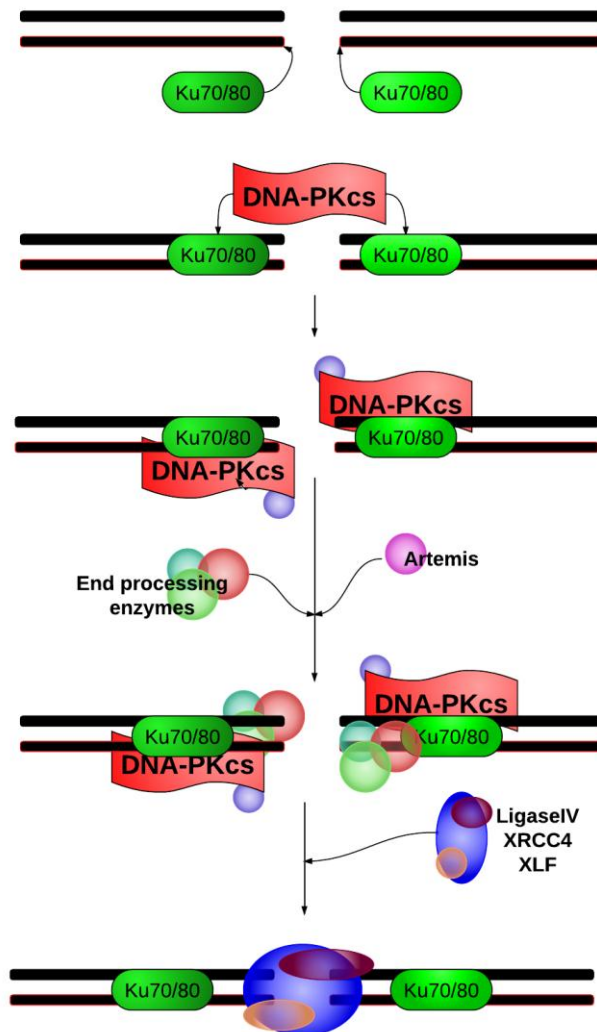


Figure 1. 6. Non Homologous End Joining.

The drawings show subsequent steps of Non homologues end joining. The process starts from recognition of broken DNA ends by complex Ku70/80 that recruits other proteins to DSB that process and join broken DNA ends (DNA-PK, Artemis), and ligate broken DNA strand (Ligase IV, XRCC4, XLF)

The heterodimer Ku70/80 has an asymmetrical ring shape with a positively charged amino acid interior in which the negatively charged DNA backbone is accommodated. Ku70/80 acts as primary damage sensor in NHEJ. By formation of a ring-shaped structure around DNA, Ku70/80 provides a mechanism for bringing DNA ends together and protecting free DNA ends from nucleolytic degradation and loss of genetic information. This function distinguishes NHEJ from HRR, in which of the one DNA strand is degraded to expose the second strand for searching homologous DNA sequences. Ku70/80 bound with DNA ends, recruit the DNA-dependent protein kinase (DNA-PK) and activate its protein kinase activity.

The Ku70/80 complex can bind to hairpin, overhang and blunt DNA ends and following recruitment of DNA-PK, end processing enzymes (Mre11/Rad54/Nbs1 and Artemis) join the complex. Artemis in addition to its endonuclease activity can be phosphorylated by ATM regulating cell cycle checkpoints (Kurosawa and Adachi, 2010). The assembled DNA dependent protein kinase (DNA-PK) complex phosphorylates downstream targets leading to activation of the DNA damage response and initiation of NHEJ. DNA-PK undergoes also autophosphorylation, which regulates its binding to DNA (Merkle et al., 2002). DNA-bound Ku also recruits DNA ligase IV/XRCC4 complex, which causes inward translocation of Ku, allowing the ligase complex to transiently attach to the DNA termini and promotion of ligation (Kysela et al., 2003).

1.4.4. Homologous Recombination Repair (HRR).

HRR allows recombination of genetic information but also provides a precise, error free way to repair of DSB. Unlike NHEJ, HRR takes place during late S and G2/M phase when homologous chromatids appear in close proximity. The HRR process involves recognition of DSB and generation of a single-stranded region of DNA by the MNR complex, which is believed to be one of the earliest sensors of the DSB (Figure 1. 7. I). The MRN complex consists of three proteins (RAD50/MRE11/NBS) and by its 5'-3' endonuclease activity allows resection of DNA strands exposing both 3' DNA ends of the DSB. In the following steps, (Figure 1. 7 II) resected single stranded DNA ends are coated with RPA proteins which subsequently recruits checkpoint protein complexes (*e.g.* Rad17/Rfc2-5, Rad9/Hus1/Rad1 and ATR/ATRIP) which form repair protein foci at the DSB site. These foci are dynamic structures actively recruiting multiple DNA repair proteins at DSB site, which can be detected immunocytochemically. The RPA protein is subsequently replaced by Rad51 proteins with the aid of BRCA2 (Figure 1. 7

III). The Rad51 and its family proteins (Rad52, Rad54) play a central role in HRR, participating in the displacement/invasion of the single-stranded DNA which pairs with the recipient (blue) homologous partner forming a heteroduplex while unpaired recipient DNA forms a “D-loop” (Figure 1. 7 IV). Strand exchange forms a Holliday junction structure (X-over). While one DNA strand is displaced, DNA Polymerases synthesize a new DNA strand. In the last step DNA helicases (BLM, WRN) cut and resolve Holliday junction structure (Figure 1. 7 V). Depending on the strand incision, the most common HHR scenario occurs when a part of both DNA strands from one of the sister chromatids is inserted to its homologous partner (“crossover”). Less common is the scenario when only one of the homologous strands is left in the sister chromatid and this is referred to as “non-crossover” homologous recombination.

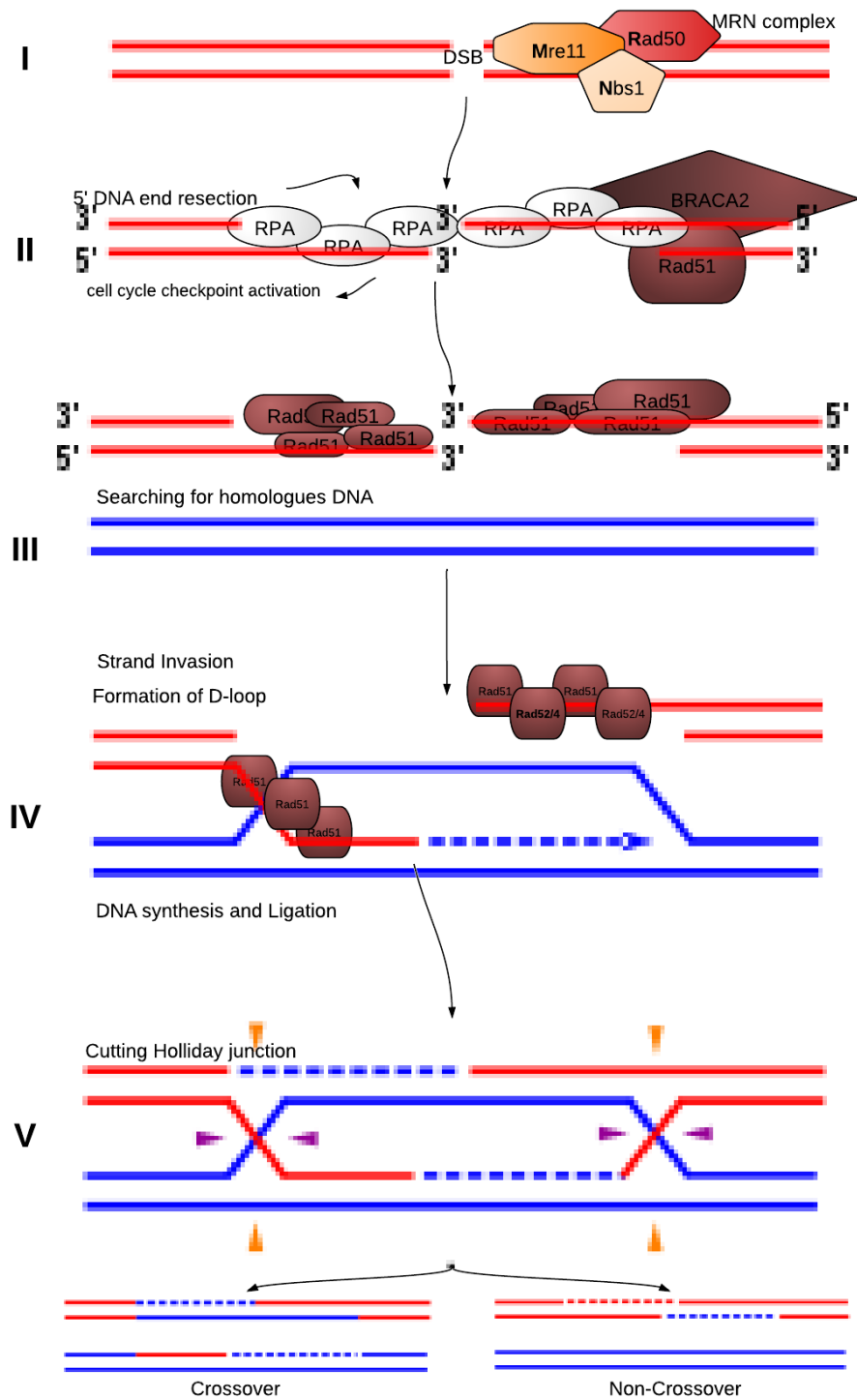


Figure 1. 7. Homologous Recombination (HR).

Schematic illustration that represent subsequent steps in HHR. Following of recognition of DSB by MRN complex in following steps (II-V), DSB is repaired using its homologous counterpart.

1.5. Human DNA Topoisomerases.

The processes of DNA replication and transcription lead to DNA supercoils, which can be positive or negative. The positive supercoils results from over-winding DNA, negative supercoils result from under-wound DNA. When DNA is unwound, two DNA strands pull apart, creating tension that builds up upstream in DNA. For each twist that is un-wound one twist is added in front of the place that undergoes un-winding. At some point, when strands cannot be separated anymore, the remaining DNA is too tightly twisted because there are no free ends to release the tension. This causes DNA to twist around itself and creates supercoils. To be able to separate DNA strands this tension has to be periodically removed. The way to remove DNA supercoils created by DNA metabolic processes is to cut and re-join DNA. The process of altering DNA topology *i.e.* relaxation of DNA supercoils is catalysed by ubiquitous nuclear enzymes called DNA topoisomerases.

Human genome structure is maintained by six topoisomerases subdivided into two distinct types, however the overall catalytic mechanism is similar for both types of enzymes. All topoisomerases cut the DNA strand by nucleophilic attack from a catalytic tyrosine residue, transiently linking it with the phosphate end of the DNA break. Then the DNA helix is rotated and the introduced break is re-joined, leaving the DNA sequence unchanged but topologically different (Wang, 2002).

Classification of human topoisomerases divides them into two types: Type I and Type II, depending on the catalytic functions (Vos et al., 2011). The Type I enzymes cleave one DNA strand whereas Type II cleave both strands at the time of reaction. Type I is further subdivided onto 2 subclasses: Type IA, Type IB. Members of the Type IA (Topo3 α , Topo3 β) during catalytic reaction are linked to the 5' end of DNA. Type IA enzymes relax only negative but not positive supercoiling. Unlike Type IB, Type IA topoisomerases requires divalent metal ions and energy cofactor for their function.

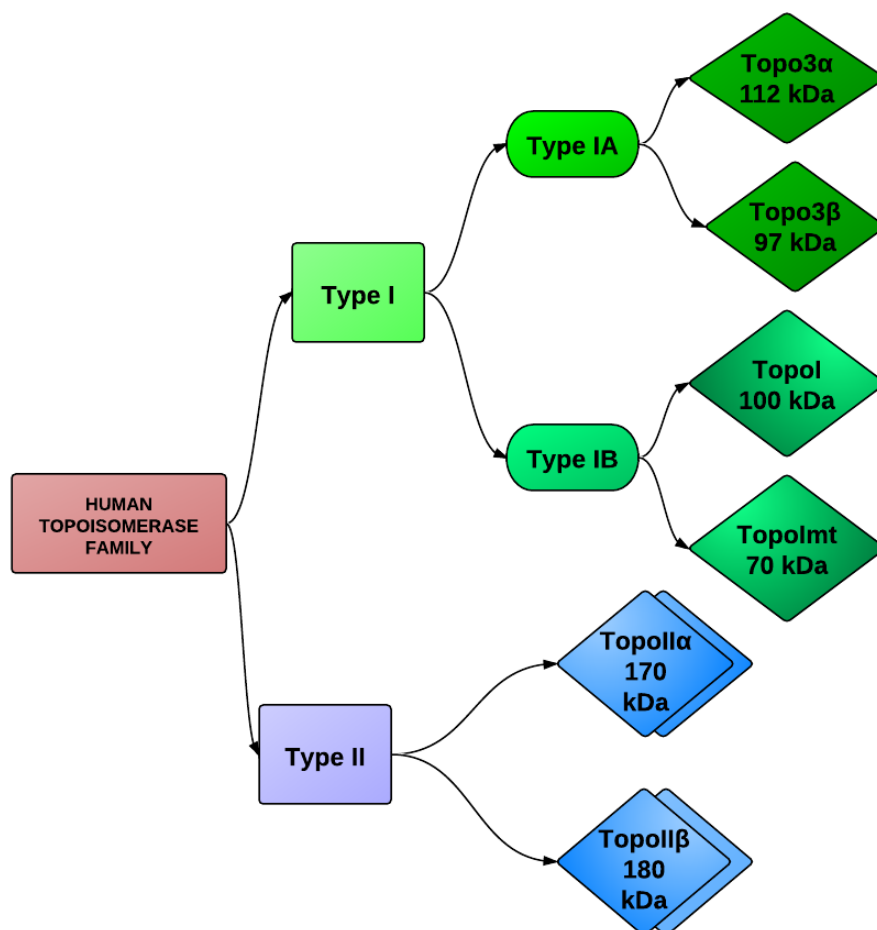


Figure 1. 8. Classification of human DNA topoisomerases.

Classification adopted from (Pommier et al., 2010)

Two members of Type IB subfamily include TopoI which operates in nucleus and TopoImt operating on mitochondrial DNA. Type IB topoisomerases form tyrosyl-DNA covalent complexes at the 3' end of cleaved DNA during catalysis and do not require ATP energy source to relax both negative and positive supercoils.

Type II topoisomerases (TopoII α , TopoII β), relax DNA supercoils and various other structures decantation by breaking both DNA strands. These topoisomerases act as dimers when processing DNA. TopoII α is closely linked to cell proliferation, because its expression and activity can increase by 3-fold in G2 / M, and it is much expressed in rapidly dividing cells compared to quiescent cells. In contrast to Topo2 β which effectively relaxes both positive and negative supercoils, TopoII α is more efficient at relaxing positive supercoils (McClendon et al., 2005). The reaction catalysed by Type II topoisomerases is similar to Type IA, is energy consuming and require divalent metal ions as cofactors.

1.5.1. TopoI structure and catalytic activity

Most topoisomerase related studies have focused on TopoI and TopoII α and β , because only these topoisomerases can be used as a target in cancer therapy (see section 1.5.3.)

Relevant to this thesis, TopoI is an essential enzyme in vertebrates, as mice embryos lacking TopoI die early during development stage (Goto and Wang, 1985, Morham et al., 1996). However, one human cell line (p388/CPT45) with low levels of TopoI was selected based on resistance to camptothecin (Eng et al., 1990). Without TopoI, these cells spontaneously accumulate genomic alterations and replication defects (Tuduri et al., 2009). The role of TopoI in the nucleus is relaxation of both positive and negative DNA supercoils, which arise prior to or after chromatin remodelling during transcription, replication or DNA repair. Expression of TopoI is relatively constant during the cell cycle, although its activity is variable. The number TopoI copies and its activity is kept at high level throughout the cell cycle (Kunze et al., 1990).

TopoI has a molecular mass of ~100 kDa, and is composed of 765 aa, divided into four functional domains as in Figure 1. 9. The N-terminal domain (aa 1 to 214) with a nuclear localisation signal (NLS), the core domain (aa 215-635), the linker domain (aa 636-712) and the C-terminal domain (aa 713 - 765) (Champoux, 2001b) .

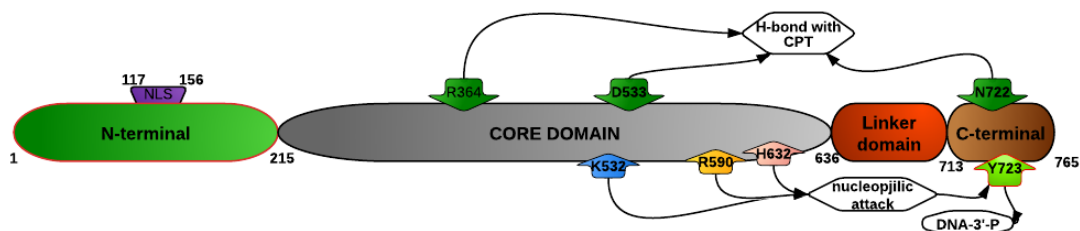


Figure 1. 9. TopoI molecular structure.

This illustration shows the molecular domain exemplified in TopoI molecular structure. Active site amino-acids of TopoI are exemplified by arrows. Amino acids involved in CPT interaction sites are marked in dark green.

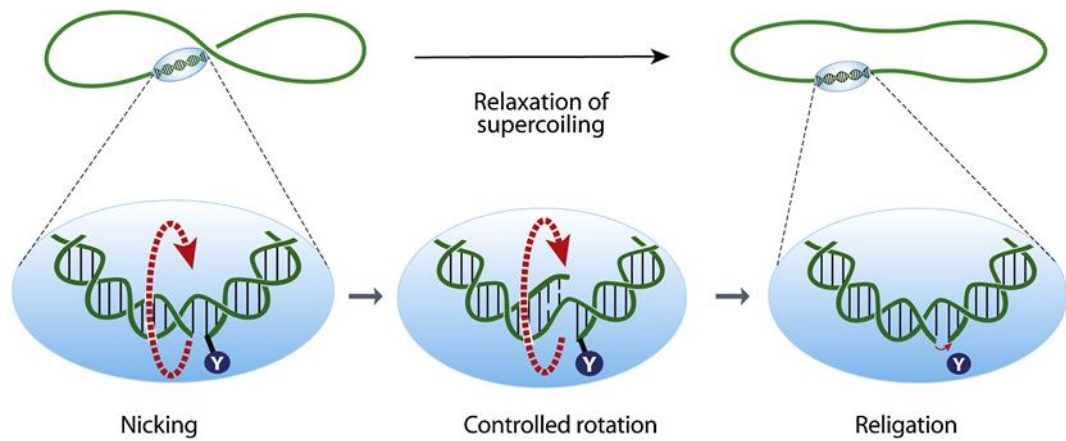


Figure 1. 10. DNA relaxation catalysed by Topoisomerase I (Pommier et al., 2010).

Nicking, DNA rotation around nicked strand and religation of broken strand are three steps of reaction catalysed by TopoI.

As it is schematically shown in Figure 1. 10, TopoI introduces single strand breaks in the DNA backbone by using an active site tyrosine as a nucleophile to attack and cut the phosphodiester bond generating a 3'-phosphotyrosyl linkage and a free 5'-OH group. The nicking results from the transesterification of an active-site tyrosine (Tyr-723) at a DNA phosphodiester bond forming a 3'-phosphotyrosine covalent enzyme–DNA complex. Introducing a gap in one DNA strand, TopoI then catalyses relaxation of DNA allowing rotation by one turn the free 5'-OH DNA end generated during cleavage, around the intact strand. After DNA relaxation, the covalent intermediate is reversed when the released 5'-OH of the broken strand restacks the phosphotyrosine intermediate in a second transesterification reaction. The generated 5'-OH group is used as a nucleophile in the subsequent ligation step, which restores intact DNA and releases the covalently bound enzyme. The intermediate step where TopoI is covalently bound to nicked DNA is referred to as “cleavage complex”. Under normal physiological conditions the rate of the religation step is much faster than the rate of cleavage, which ensures that the steady-state concentration of the covalent 3'-phosphotyrosyl TopoI–DNA complex remains low. In other words the cleavage complex is very transient and reaction equilibrium is moved toward religation step (Champoux, 2001a).

1.5.2. Regulation of TopoI activity.

TopoI activity and expression in tumour cells is usually greater than in normal cells. There are data indicating that the activity of TopoI varies between patients suffering from the same tumour type, as well as data indicating that TopoI activity varies depending on the type of cancer (Holden, 2001). TopoI level was found to be elevated in malignant cells of colorectal cancer compared to benign tumours or healthy tissue. Elevated levels of TopoI in human malignant colorectal tumours correlates with the progression of the disease (Giovanella et al., 1989). TopoI catalytic activity and protein levels were significantly elevated in colon cancer and prostate cancer compared with their normal counterparts (Husain et al., 1994). Increased TopoI level was also observed in malignant ovarian cancer in comparison with its less aggressive counterpart form of this type of cancer (van der Zee et al., 1991).

Low activity of TopoI was observed in lung cancer and breast cancer, while increased TopoI activity was found in colorectal cancer, cervical cancer and metastatic melanoma (Larsen and Gobert, 1999). TopoI expression level is usually higher in malignant tumor cells in comparison to primary tumors (Tsavaris et al., 2009).

TopoI poison-induced cell cytotoxicity correlates with the level of TopoI generated DNA breaks which in turn is dependent on TopoI activities. Therefore, cell cycle phase specific cytotoxicity will be dependent on the number of created SSB and their ability to convert to DSB in these phases. The activity and distribution of TopoI tends to change when cells traverse from G1 to G2 phase. Meyer et al. (using A431 lung cancer cells) showed that the level of TopoI increases towards mitosis but its activity in this phase decreases. Immunostaining of interphase cells shows that TopoI distribution exhibits a homogenous granular pattern with tendency to concentrate in nucleoli. During mitosis TopoI is attached to chromosomes (Meyer et al., 1997).

1.5.3. Topoisomerases poisons.

As described in the previous section, TopoI catalyses DNA relaxation by cleaving and religating DNA, forming an intermediate covalent enzyme-DNA complex. TopoI cleavage complexes are a selective target for camptothecins, which is isolated from the Chinese tree *Camptotheca acuminata* (Figure 1. 11.)

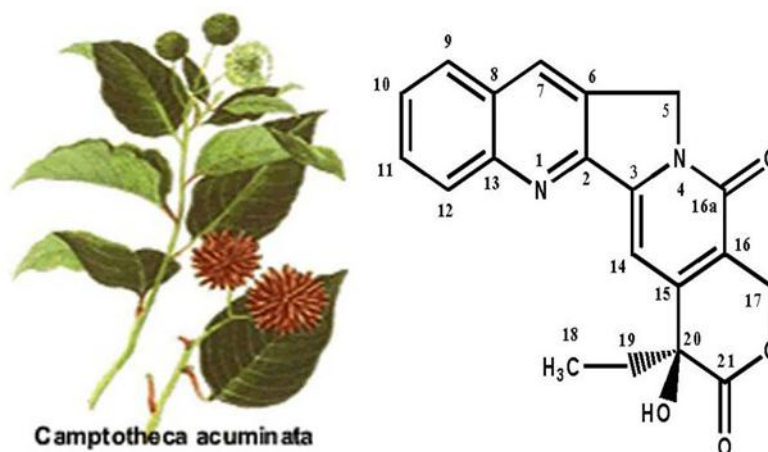


Figure 1. 11. Natural source and molecular structure of camptothecin.

Figure shows the plant that produces camptothecin and camptothecin molecular structure.

The trapping of TopoI cleavage complexes by CPT represent a model of interfacial inhibition, which is a common molecular mechanism for many compounds, that act blocking enzymes being in specific conformational states of macromolecular complexes (Figure 1. 12). CPT stabilize TopoI cleavage complex, forming H bonds with three amino acid residues at the TopoI active site (Figure 1. 12 C). The bonds are formed between camptothecin N-1 position in arginine 364, between the camptothecin 20-hydroxyl and aspartate 533, and between the camptothecin 17-carbonyl and asparagine 722 (Marchand et al., 2006).

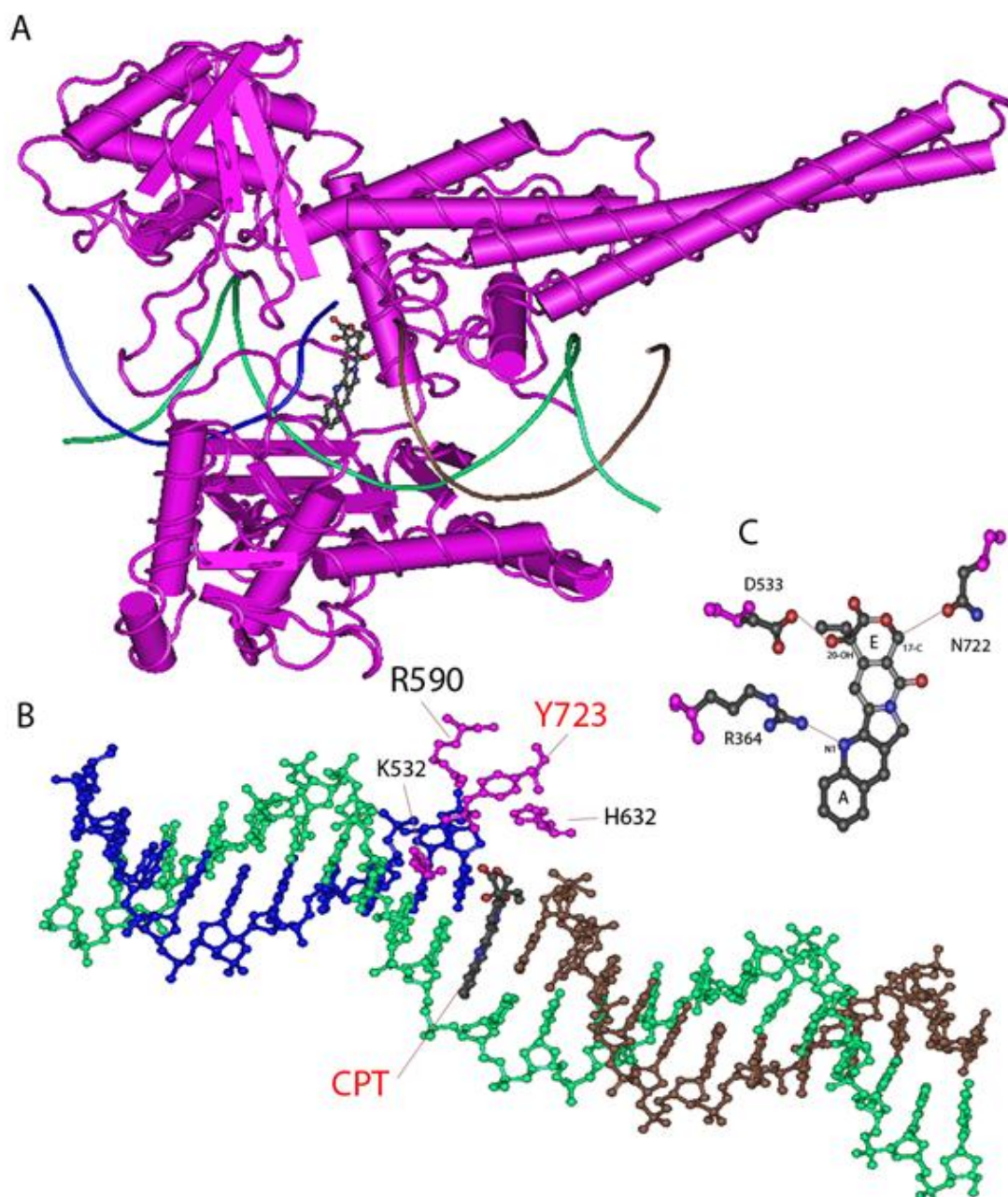


Figure 1. 12. Human TopoI in covalent complex with DNA and CPT (image adopted from PubMed webpage using Cn3D software).

A) Representation of crystal structure of TopoI-DNA cleavage complex with intercalated CPT molecule. B) DNA with basic amino acid residues (shown in purple) that catalyse the nucleophilic attack of DNA by the catalytic tyrosine Y723. C) CPT surrounded with hydrogen bond forming TopoI active side amino acid residues.

Under physiological conditions, CPT binds reversibly to the TopoI cleavage complexes, quickly establishing an equilibrium between the drug-enzyme-DNA and the dissociated complex. Once CPT is removed, the cleavage complexes reverse rapidly. Camptothecin inhibits only a fraction of the existing TopoI cleavage complexes with a guanine at the 5'-end of the break. The sequence selectivity of CPT makes it a relatively poor TopoI catalytic inhibitor because a substantial subset of the TopoI cleavage complexes not bearing a guanine are protected from the CPT action (Jaxel et al., 1991, Tanizawa et al., 1995).

Cleavage complexes can be readily reversed but under certain conditions can be irreversible. The irreversible cleavage complexes, referred to as “suicide complexes” can be formed if in close proximity to TopoI-cc complex DNA modification occurs (e.g. abasic site, mismatch, oxidized base). Such irreversible cleavage complexes have been (Figure 1. 13). DNA alterations which can be converted into suicide complexes include abasic sites, mismatched loops, single-strand breaks, IR-induced DNA breaks or apoptotic DNA fragments (Sordet et al., 2008). In stressful, CPT-mediated conditions, suicide complexes can be also generated from reversible cleavage complexes by collision with progressing DNA or RNA polymerases (Hsiang et al., 1989). Such collisions convert cleavage complexes into DNA double-strand breaks with TopoI covalently attached to the 3' DNA end. At the 5'-end DNA there can be DNA-RNA hybrids in the case of transcription-mediated damage or DNA duplexes formed by the newly synthesized leading strand in case of replication-mediated lesion (Figure 1. 13 B, C). CPT-induced cytotoxicity is thought to result from collision of the DNA replication fork with stabilized cleavage complex (Pommier, 2004).

The relative contribution of replication or transcription to CPT-induced cytotoxicity depends on the CPT concentration, and for non-dividing cells, a much higher concentration is required to obtain a similar effect than in frequently dividing cells. In support of this, it was shown that cells in S phase were at least 100-fold more sensitive to CPT-induced killing effect, although the amount of CPT-induced breaks and TopoI were equal in all phases of the cell cycle (Beidler and Cheng, 1995). Lesions induced by CPT were shown to be rapidly reversed after CPT removal, and therefore the important determinants of CPT cytotoxicity are the TopoI level, duration of the exposure to CPT and cell cycle phase (D'Arpa et al., 1990).

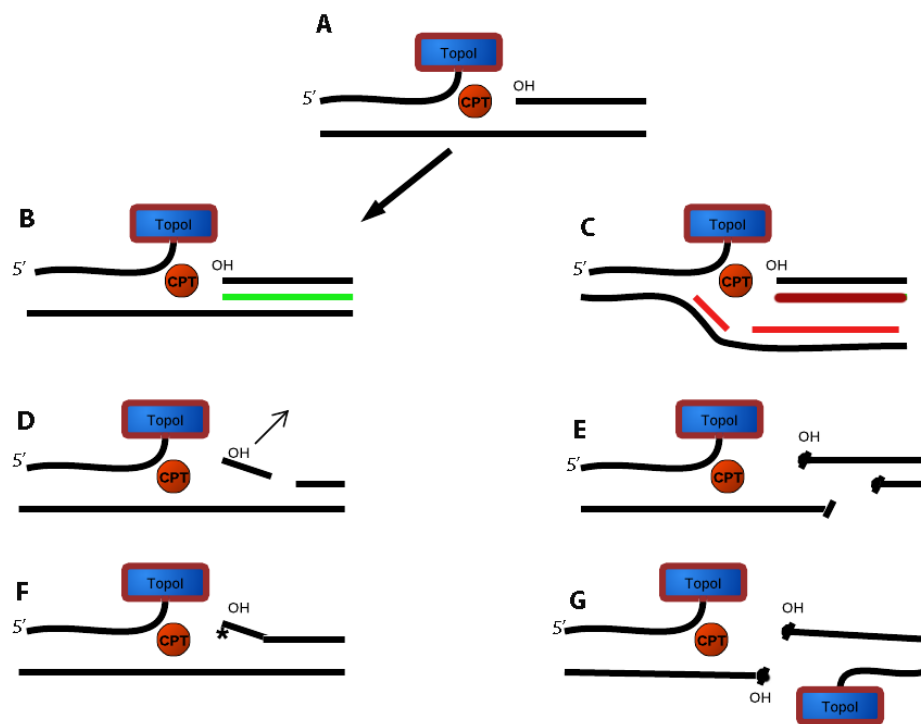


Figure 1. 13. TopoI-mediated DNA damage (Pomier 2006).

(A) TopoI cleavage complex trapped by camptothecin (CPT). TopoI is covalently bound to the 3'-end of the broken DNA. (B) Transcription related conversion of the cleavage complex into a covalent TopoI–DNA complex (the RNA is shown in green). (C) Replication related conversion of the cleavage into a covalent TopoI–DNA complex by a colliding replication fork (the leading replication is shown in red; the lagging replication in blue). (D and E) Formation of the suicide complex by a single-strand break on the same (D) or the opposite (E) strand from the TopoI scissile strand. (F) Formation of an irreversible TopoI cleavage complex by pre-existing base lesion ((*) abasic site, mismatch, oxidized base) at the 5'-end of the cleavage site. (G) The double-strand break formation at two TopoI cleavage sites close to each other. (Pommier et al., 2006).

CPT was first used in clinical trials in the 70s but because of the strong side effect, these trials were abandoned (O'Leary and Muggia, 1998). Development of the CPT analog characterized by greater solubility (Wall et al., 1993), resulted in the resumption of clinical trials and two of its derivatives (hycamtin - Topotecan and CPT-11/Irinotecan - Camptosar) have been approved for the treatment of platinum-refractory ovarian cancer topotecan (Creemers et al., 1996, Creemers, 1997) and irinotecan (CPT-11) (Armand et al., 1995, Armand et al., 1999) in colorectal cancer.

Clinically approved camptothecin derivatives, despite their established efficacy in anticancer therapy, have also some limitations including chemical instability, drug resistance, long infusions and side effects. These compounds are quickly inactivated at physiological pH due to opening the lactone E ring of CPT. Irinotecan (CPT-11) is an inactive prodrug that is converted to its active metabolite SN-38. Irinotecan is the basic drug used to treat patients with primary and relapsed colorectal cancer. However, only about 20% to 30% of patients exhibit positive response to treatment (Ikeguchi et al., 2011). Irinotecan treatment is often accompanied with frequent and severe side effects such as diarrhoea, neutropenia, nausea and vomiting. Assessment of the expression of TopoI can be an important tool utilized for increasing the effectiveness of therapy.

One of the reasons for resistance to TopoI poisons is as described in section 1.5.2. TopoI activity and expression level which varies between cancer type and malignancy stage. For resistance to camptothecin the TopoI N-terminal domain and linker domain play major role. Total or partial deletion of the linker domain reduces TopoI sensitivity to camptothecin (Ireton et al., 2000, Fiorani et al., 2003). The N-terminal domain is dispensable for the formation of the TopoI-DNA complex but seems to have influence on the sensitivity to camptothecin – induced inhibition of religation process. Truncation of the N-terminus of TopoI results in a 4-fold reduction in sensitivity to camptothecin. To overcome the resistance to CPT several strategies have been explored to develop more potent TopoI inhibitors.

For example, metabolically labile camptothecin in homocamptothecins lactone was replaced with a more stable beta-hydroxylactone which are potent anticancer agents. Gimatecan, a seven-position modified lipophilic camptothecin was developed to provide fast uptake and accumulation in the cells as well as stability of TopoI/DNA/drug ternary complex. Diflomotecan, homocamptothecin and gimatecan are in Phase II clinical trial. The non-camptothecins TopoI poisons edotecarin and indolocarbazole that results in cleavage of DNA by TopoI at C / TG in comparison with the TG /A specific for camptothecins, is currently in phase II clinical trial. Among non-camptothecins, edotecarin, an indolocarbazole that results in DNA C/T-G cleavage compared with T-G/A for camptothecins, is currently in Phase II clinical trial (Teicher, 2008).

1.5.4. Repair of TopoI-mediated DNA damage.

As described in the previous section, CPT-induced DNA damage can be repaired by several partially overlapping mechanisms (Figure 1. 14). Repair of TopoI-related DNA damage is less known in human cells, and most of the data on this process comes from budding yeast, in which the two redundant pathways that remove TopoI cleavage complexes from DNA exists. Removal of TopoI from DNA is mediated *via* hydrolysis of the bond between the TopoI tyrosine Y723 and 3' end of DNA by tyrosyl- DNA phosphodiesterase1 (TDP1). In this pathway, TopoI covalently attached to DNA undergoes ubiquitination and proteasome-dependent proteolysis. Partially degraded TopoI polypeptide is then removed by TDP1. Following the removal of TopoI, TDP1 generates a 3'-phosphate and a 5'-hydroxyl DNA terminus. BER-related enzymes further process the resulting gap in DNA. It was proposed that DNA breaks generated by TDP1 can be sensed by PARP-1 which mediates recruitment of XRCC1 protein, which in turn recruits polynucleotide kinase (PNK) which transfers the phosphate group from the 3' to the 5' terminus. In the next step, XRCC1 acts as a scaffold protein for DNA polymerase β and DNA ligase III to fill and ligate the gap, completing the repair process (Plo et al., 2003).

The removal of TopoI-cc can be carried out by several superimposed molecular pathways which involves endonuclease activity of Rad1–Rad10, Mre11–Rad50–Xrs2, Mus81–Mms4. As a result of endonuclease action TopoI is excised from the DNA along with a containing a few nucleotides segment of DNA. Rad1–Rad10 is an ortholog of human endonuclease XPF–ERCC1. Yeast Mre11–Rad50–Xrs2 is equivalent to human Mre11–Rad50–Nbs1 complex (MRN complex) which participates in homologous recombination. Those endonucleases cleave fragment DNA 5' from the damaged region where DNA strands are separated. XPF–ERCC1 is also a critical 5'-endonuclease in nucleotide excision repair (NER) both for global and transcription-coupled repair (TCR) (Pommier, 2006, Pommier, 2009).

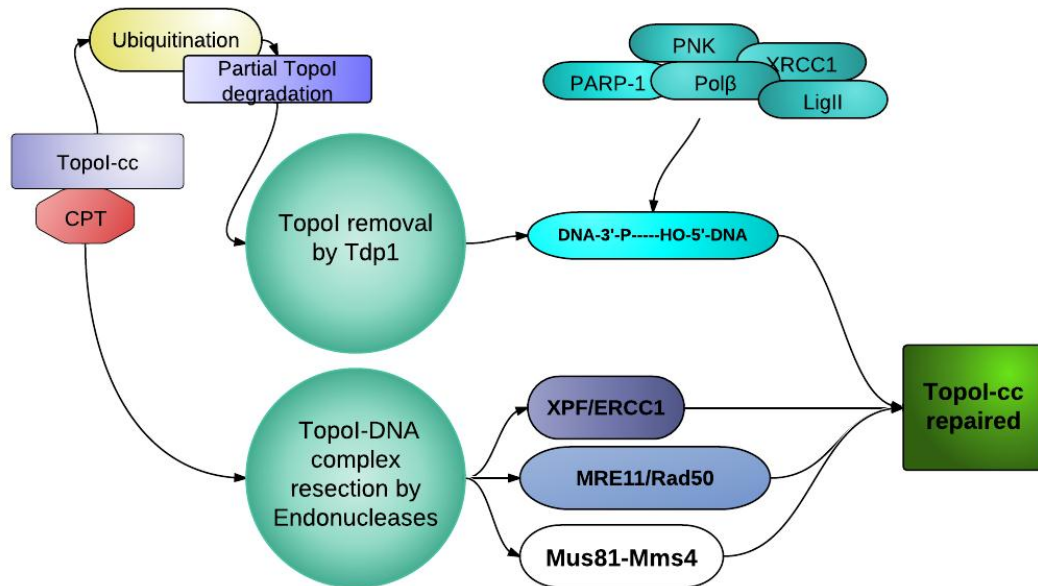


Figure 1. 14. Pathways involved in repair of TopoI-cc.

Diagram showing enzymatic pathways used by human cells to repair TopoI cleavage complexes.

Replication-related CPT cytotoxicity produces several well-characterized molecular responses. One of them is H2AX histone phosphorylation. The H2AX histone variant is phosphorylated within minutes after the formation of camptothecin-induced double-strand breaks (DSB). The phosphorylated form of H2AX, (termed γ H2AX) accumulates around each DSB and can be detected by immunofluorescence (Furuta et al., 2003). γ H2AX is considered as a very sensitive marker of double-strand breaks produced by DNA damaging agents. γ H2AX is also functionally important, because its genetic inactivation sensitizes cells to camptothecin. Other biomarkers of CPT-induced DNA breaks are ATM (Ataxia Telangiectasia Mutated) activation by autophosphorylation at serine 1981 and phosphorylation of Chk2 (Checkpoint kinase 2) at threonine 68 by ATM and DNA-PK (Flatten, 2005).

1.6. Poly (ADP-ribose) polymerases– PARP.

Poly(ADP-ribose) (PAR) is a complex, nucleic acid-like biopolymer synthesised in cells by poly(ADP-ribose) polymerases using NAD⁺ as a substrate. Poly(ADP-ribosyl)ation influences a number of factors, including DNA repair and cell cycle checkpoints and plays a role in the recruitment of DNA repair enzymes to strand breaks. The biological processes affected include maintenance of genome integrity, cell cycle progression, initiation of the DNA damage response, apoptosis, and regulation of transcription.

The enzymes which catalyses this reaction belong to the family of poly(ADP-ribosyl)ases of which the founding and best investigated member is PARP-1 (see section 1.11). Since its discovery almost 50 years ago (Chambon et al., 1963), 17 poly(ADP-ribose) polymerases have been identified. Although, they vary in molecular size and enzymatic capabilities, all have in common a ~50 aa long catalytic domain called the “PARP signature”. The PARP signature is highly conserved among vertebrates and between other species. This module is responsible for all PARP-1 catalytic activities, including NAD hydrolysis, initiation, elongation, branching, and termination of ADP-ribose polymers.

Some of the PARP family members can interact with each other and share common partners and common subcellular localizations (Ame et al., 2004). At present the nomenclature, and classification and number of 17 PARP-family members varies between published reports (Hottiger et al., 2010), however the most commonly-used classification of PARP proteins is based on their molecular domains or established function and includes DNA-dependent PARPs (PARP-1, PARP-2 and PARP-3), tankyrases, CCCH-type zinc-finger PARPs, and macroPARPs (Schreiber et al., 2006a).

The DNA-dependent PARPs are PARP-1 and PARP-2 and PARP-3, which have been shown to be stimulated by DNA damage. The second most studied PARP family member is PARP-2, discovered many years later after PARP-1 in PARP-1 deficient cells which exhibited residual PARP activity (Masutani et al., 2000). There is a growing amount of evidence regarding to the role of PARP-1 and PARP-2 in DNA repair. Three independent groups have created PARP-1 or PARP-2 knockout mice, which develop normally but show serious DNA damage defects caused by alkylating agents and ionizing radiation (Shall and de Murcia, 2000, Boehler et al., 2011a). It is believed that both PARP-1 and PARP-2 have overlapping cellular function as indicated by embryonic lethality of the PARP-1 and PARP-2 double knockout (Ame et al., 1999).

Both PARPs are activated by DNA breaks, and can form homo or heterodimers and poly (ADP-ribosyl)ate each other. Moreover these proteins have common partners in BER (Schreiber et al., 2002)

PARP-3 (67 kDa) is not activated upon binding to DNA and is a poly-ADP-ribosylase. Originally, PARP-3 was identified as a core component of the centrosome, preferentially localized to the daughter centriole throughout the cell cycle. It was shown that amplification of PARP-3 interferes with the G1/S cell cycle progression (Augustin et al., 2003). PARP-3 interacts with PARP-1 and activates PARP-1 in the absence of DNA, resulting in synthesis of polymers of ADP-ribose. Recently it has been demonstrated that PARP-3 can interact with Ku70/Ku80 and DNA-PK, contributing to the DNA damage response (Rouleau et al., 2009). Another study has implicated the role of PARP-3 in the accumulation of APLF (*aprataxin polynucleotide kinase PNK-like factor*) at DSBs. APLF promotes ligase IV XRCC4/DNA complex conservation in chromatin at DSBs, therefore PARP-3 interacting with APLF may accelerate DNA ligation during nonhomologous end-joining (NHEJ) (Rulten et al., 2011).

PARP-4/vPARP (193-kD) lacks the N-terminal DNA binding domain. PARP-4 is one of three proteins that compose large ribonucleoprotein complexes, known as vaults, which are involved in drug resistance and nucleo-cytoplasmic transport (Berger et al., 2009). This PARP isoform was also shown to localize with the mitotic spindle (Kickhoefer et al., 1999).

Tankyrase-1 and Tankyrase-2 plays a role in maintaining telomere length, and although the molecular structure of these two enzymes differ, their functions overlap. Phosphorylation of tankyrase during mitosis ensures correct mitotic spindle formation . The target partner for Tankyrase-1 is a protein TRF1 which is a negative regulator of telomere length. Knockout of both tankyrases genes in mice is lethal to embryos in the early development stage, however mice with only single-gene knockout are viable but grow smaller.

1.6.1. PARP-1 molecular structure.

Poly(ADP-ribose) polymerase-1 (EC. 2.4.2.30) is a 113 kDa protein, and beside histones is the most abundant nuclear protein with the number of copies estimated at between 10^5 and 10^6 per cell (Benjamin and Gill, 1980, de Murcia et al., 1994). The PARP-1 gene is located on chromosome 1q41-42, and encodes a 1014 amino acid long PARP-1 polypeptide which has a modular architecture with six molecular domains placed within 3 major functional units (Figure 1. 15): 46 kDa N-terminal DNA-binding domain (DBD), a 22 kDa central automodification region and a 54 kDa C-terminal catalytic domain (Dantzer et al., 2006b, Hakme et al., 2008).

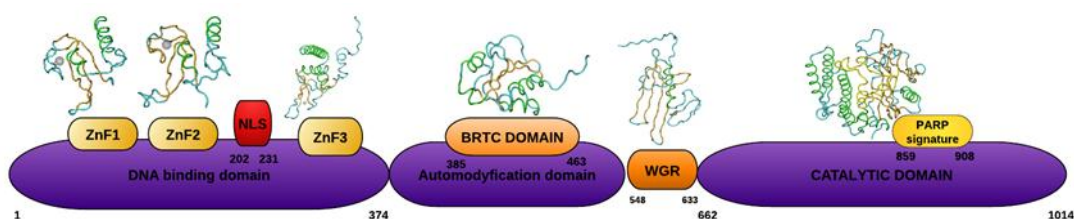


Figure 1. 15. Molecular structure of PARP-1.

The DNA-binding domain (aa 1 to 374) contains two Cys-X₂-Cys-X₂₈₋₃₀-His-X₂-Cys (X-any other aminoacid) zinc fingers (ZnF1 and ZnF2) that mediate binding of PARP-1 to DNA. PARP-1 zinc-fingers are structurally and functionally unique showing similarities only to zinc-fingers present in DNA polymerase ϵ and DNA ligase III (Petrucco, 2003). Among the first two Zinc Fingers, ZnF2 has the highest affinity to DNA damage. The ZnF1 also recognises DNA damage and additionally plays role in PARP-1 activation. Although both Zinc Fingers are required for binding with DNA breaks, only the first one is required for DSB binding (Ikejima et al., 1990). This zinc finger recognises single strand breaks and interacts in this place with the DNA helix covering seven amino acids in either side around the break (Menissier-de Murcia et al., 1989). A newly discovered third zinc binding domain (ZnF3), is placed between the NLS and BRCT domain and its major role in PARP-1 activation following binding with DNA damage (Langelier et al., 2008). The N-terminal domain contains also a bipartite nuclear localization signal (NLS), and a caspase-3 cleavage site (Schreiber et al., 2006b, Hakme et al., 2008).

The auto-modification domain (aa 375 to 525) has a BRCT domain which mediates protein-protein interactions. A molecular motif within the automodification domain

allows PARP-1 to form homodimers and ADP-ribosylate the adjacent PARP-1 molecule. This reaction takes place on 15 conserved glutamic acid residues and has impact on DNA-binding due to charge repulsion between DNA and ADP-ribose polymers. The BRCT motif is common among many DNA repair or cell cycle checkpoint proteins and plays a role in physical interactions between DNA repair enzymes. Using the auto modification domain PARP-1 is able to bind with transcription factors like YY1 (Yin-Yang-1). The catalytic domain of PARP-1 bears the PARP-signature – a 50 aa long highly conserved sequence with almost 100% sequence homology in vertebrates. C terminal domain is responsible for all catalytic activities of PARP-1 including initiation and elongation of PAR branches even up to 200 residues long (Masson et al., 1995).

1.6.2. PARP-1 catalytic mechanism – poly(ADP-ribosylation).

The majority of ADP-ribose polymers found in cells are produced by PARP-1. When activated upon binding to DNA, PARP-1 mediates rapid and reversible covalent attachment of ADP-ribose subunits onto target proteins. As a post-translational modification, PAR markedly changes biochemical properties of a protein, altering the DNA-binding affinity, the protein-interaction properties, and cellular location of target proteins (D'Amours et al., 1999). Using NAD⁺ as a precursor, PARP-1 catalyse the formation of long ADP-ribose polymers by cleaving of the glycosidic bond between the ribose and the nicotinamide in NAD⁺, freeing nicotinamide as a by-product which is also a weak PARP-1 inhibitor (Figure 1. 16). PAR synthesis is initiated by transfer an ADP-ribose unit from NAD⁺ onto of glutamate, lysine, arginine, cysteine, phosphoserine or asparagine amino acid residues of target proteins. Elongation and formation of branched polymers of the ADP-ribose involves addition of the ribose moiety to the 2'-hydroxyl of the nicotinamide ribose or adenine ribose respectively (Alvarez-Gonzalez et al., 1994, Alvarez-Gonzalez and Mendoza-Alvarez, 1995). Autoribosylation of PARP-1 decreases its affinity to DNA and results in reduction of PARP-1 catalytic activity. This in turn allows DNA repair proteins to gain access to the damaged DNA. A widespread DNA damage leads to hyper-activation of PARP-1, drastic consumption of NAD⁺, and depletion of cellular energy stores. Under extensive stressful conditions PAR acts also as caspase independent activator of cell death (Yu et al., 2002, Koh et al., 2005).

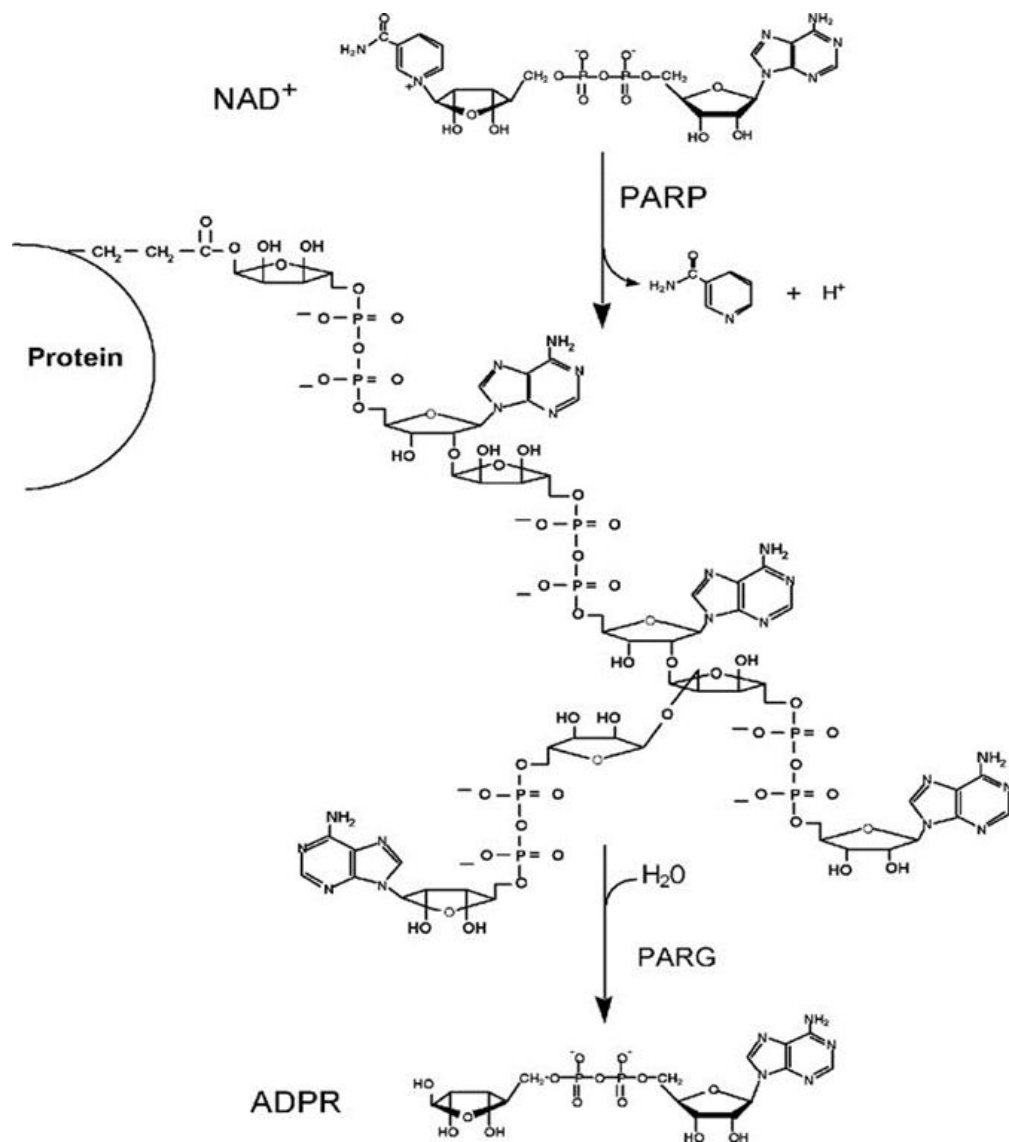


Figure 1. 16. Maintenance of ADP-ribose polymer by PARPs and PARG (Patel et al., 2005).

PARP-1, using NAD⁺ as a substrate, catalyses addition of ADP-ribose to target proteins and formation of growing polymer chain releasing nicotinamide as a by-product. ADP-ribose polymers can be rapidly degraded by PARG.

ADP-ribose polymers are degraded by poly(ADP-ribose) glycohydrolase (PARG), due to hydrolysis of alpha (1''- 2') or alpha (1'''- 2'') O-glycosidic bonds of ADP-ribose polymers to produce free ADP-ribose (Isabelle et al., 2010, Blenn et al., 2011, Davidovic et al., 2001). The cycle of formation and degradation of ADP-ribose polymers is measured in a few minutes following polymer formation. Degradation of the (ADP-ribose) polymers restores the catalytic activity of PARP-1 enzyme enabling it to bind with DNA again and start the next round of poly (ADP-ribosyl)ation. This rapid NAD^+ consumption, synthesis and turnover of the polymer imposes a high energy cost to the cells therefore in cells, undergoing apoptosis PARG and PARP-1 are one of the first proteins cleaved, by caspases-3 (Boulares et al., 1999, Affar et al., 2001). Degradation of the (ADP-ribose) polymers allows re-association of the histones with DNA. The degradation of PAR to ADP-ribose units by PARG might be coordinated with action of at the site of DNA break by incorporation of free DNA pol β -released phosphates into ATP providing local energy source for completion of the repair process by DNA ligase III (Oei and Ziegler, 2000).

1.6.3. PAR acceptors

In response to DNA damage, nearly 90% of ADP-ribose polymers are synthesized on PARP-1 (automodification), whereas the remaining is found on other acceptor proteins. Activated PARP-1 catalyses dynamic poly(ADP-ribosyl)ation of a 20 amino acid poly(ADP-ribose) binding motif which contains two conserved regions. One is rich in basic amino acids, and the second has a pattern of basic amino acids scattered with basic residues. The main PAR acceptors are histones, especially histone H1 and H2B. Covalent binding of PAR to histones is strong and resistant to treatment with detergents or solutions with high salt concentration. The accumulation of negatively charged poly (ADP-ribose) on histone H1 and H2B tails causes local relaxation of chromatin structure facilitating the access of DNA repair proteins (Dantzer et al., 2006a). PAR can be attached to many nuclear proteins. Proteins identified based on PAR binding motive include p53, p21(CIP1/WAF1), xeroderma pigmentosum group A complementing protein(XPA), MSH6, DNA ligase III, XRCC1, DNA polymerase epsilon, DNA-PK(CS), Ku70, NF- κ B, inducible nitric-oxide synthase, caspase-activated DNase, and telomerase (Pleschke et al., 2000).

PARP-1 also plays an important role during apoptosis, where it is cleaved by caspase 3 with the formation of a N-terminal 24 kDa fragment containing the DNA binding motif

(Kaufmann et al., 1993). The 24 kDa fragment competes with full length PARP-1 and is able to inhibit poly(ADP-ribosyl)ation that promotes DNA repair and inhibit necrosis caused by over-activation of PARP-1 (Sukhanova et al., 2007).

1.6.4. Role of PARP-1 in DNA repair

One of the first reports providing evidence for the role of PARP in DNA damage repair was published by Durkacz *et al.*, 1980. These authors discovered that inhibition of PARP activity by specific inhibitors (*e.g.* 3-aminobenzamide (3-AB)) or depletion of cellular NAD pool decreased the re-joining of DNA breaks induced by the methylating agent, dimethyl sulphate (DMS) in L1210 cells (Durkacz et al., 1980).

The role of PARP in DNA damage was also confirmed in molecular studies. The cytotoxic effect of MNNG (N-methyl-N'-nitro-N-nitrosoguanidine) and IR was intensified when PARP was inhibited by overexpression of the PARP DNA binding domain (DBD) in CV-1 monkey cells (Molinete et al., 1993, Schreiber et al., 1995). Similarly, potentiation of MMS-induced cytotoxicity in HeLa cells was observed following depletion of PARP activity by antisense RNA construct (Ding and Smulson, 1994).

A comprehensive source of knowledge about the role of PARP in DNA repair becomes available with generation of viable mice deficient in PARP-1 (Shall and de Murcia, 2000). The viability of cells taken from these animals is considerably reduced following the exposure to IR or alkylating agents (*e.g.* MMS). Moreover, these cells treated with alkylating agents exhibit increased levels of genomic instability indicated by a higher rate of sister chromatid exchange. There is also evidence that the repair of DNA damage induced by MNU was slower in MEF cells derived from PARP-1 null mice (Trucco et al., 1998).

The number of studies that provide direct evidence for PARP-1 interaction with proteins involved in BER/SSBR is overwhelming. PARP-1 has a high affinity for SSB detection and is believed to be one of the first proteins that sense and responds to SSB. The interaction of PARP-1 with BER/SSB repair proteins is mediated *via* the BRCT or zinc finger domains. For example, the BCRT motive allows interaction between automodified PARP-1 and XRCC1. Histones and chromatin modifying proteins are major PAR acceptors implicating PARP-1 in maintenance of chromatin structure. Addition of negatively charged PAR to histone causes chromatin relaxation and allows

other proteins to access a damaged site. Recruitment of XRCC1 negatively regulates PARP-1 activity removing it from damaged DNA site (Masson et al., 1998). This was demonstrated in PARP-1 null cells exposed to the DNA damaging agent, MMS, which were incapable of forming XRCC1 foci at the site of DNA breaks (El-Khamisy et al., 2003). A direct interaction of XRCC1 with BER proteins, allows recruitment of DNA polymerase β and DNA ligase III to the damaged site, which are also able to bind directly to PARP-1 and facilitate short patch BER (see section 1.4.1). PARP-1 has been shown to be involved in long patch BER where it participates in FEN1-dependent strand displacement during DNA synthesis by DNA pol β . Inhibition of poly (ADP-ribose) synthesis by 3-aminobenzamide greatly reduces the interaction between XRCC1 and PARP-1.

The main mechanism used by cells to repair DSB repair is NHEJ, which is dependent on a complex of DNA-PK, and XRCC4-DNA Ligase IV. A study by Audebert et al. 2004 provided evidence for an alternative method for repair of DSB, independent of DNA-PK, in which the main role is played by PARP-1 with XRCC1-DNA Ligase III complex. This PARP-1 dependent mechanism involved in joining DSB was proposed by the authors to be an alternative or backup end joining (B-NHEJ) in contrast to the DNA-PK-dependent NHEJ often referred to as D-NHEJ (Audebert et al., 2004). Further studies by these authors have shown the B-NHEJ depends on the presence of C: G base pairs at the ends of the broken microhomology DNA sequences (Audebert et al., 2008). These observations points to PARP-1 as a bridge connecting BER/SSBR with NHEJ.

The role of PARP-1 in HRR was demonstrated, when following PARP inhibition in Chinese hamster ovary cells with 3-Aminobenzamide, an increase in sister chromatid exchanges was observed (Morgan and Cleaver, 1982). These observations were further confirmed using cells derived from PARP-1 knockout mice (de Murcia et al., 1997). PARP-1 activity is essential to survival of cells in which progression of replication forks was blocked (*e.g.* by hydroxyurea). Stalled replication forks create DNA breaks, which can be recognized by PARP-1. The authors of this paper suggest that the activation of PARP-1 promotes replication fork restart by the employment of Mre11 endonuclease, which is required for DNA strand resection in HRR. Therefore, PARP-1 recruiting Mre11 promotes the restart of blocked replication forks (Bryant et al., 2009b).

Using DT40 PARP-1^{-/-} cells, it was shown that the replication forks were not slowed down when these cells were incubated in the presence of camptothecin. These results

were confirmed in PARP^{+/+} cells in which PARP-1 activity was reduced by PARP inhibitor or PARP-1-specific siRNA (Sugimura et al., 2008). These studies show PARP-1 participates in the regulation of HR at the time of HR start and inhibits the replication fork progression when DNA damage occurs in DNA.

1.6.5. PARP inhibitors

Identification of enhancement of cytotoxicity induced by radiation and monofunctional DNA alkylating agents by 3-aminobenzamide (3-AB) (a nicotinamide analogue) provided the rationale for development of PARP inhibitors as chemo- and radiosensitisers for cancer therapy (Durkacz et al., 1981). Nicotinamide is a by-product of the PARP reaction and a weak PARP inhibitor however its pharmacophore properties led to the design of further PARP inhibitors with optimal molecular interactions. The benzamide analogues including 3-AB were the first generation of PARP inhibitors. 3-AB was a 10-fold more potent inhibitor than nicotinamide but acts non-specifically and its effective concentration is too high for clinical application. At concentrations between 3-10 mM that are required for chemo- and radiopotentialiation 3-AB was also affecting *de novo* purine biosynthesis (Milam et al., 1986). Structure-activity studies indicated desirable features for a potent PARP-1 inhibitor (Figure 1. 17). Such inhibitors should have an aromatic or poly aromatic heterocyclic ring system and a carboxamide group constrained the *anti*-conformation to 1,2 -bond, which is essential for inhibitor activity. An amide proton is required for putative hydrogen bonding. Finally a non-cleaved bond is required at the position corresponding to the 3-position of the benzamide (Griffin *et al.*, 1995).

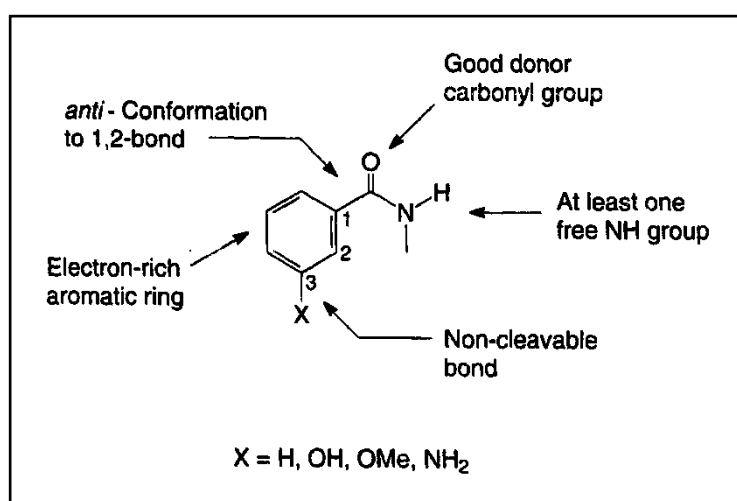


Figure 1. 17 Chemical features of potent PARP inhibitors. (Griffin et al., 1995)

A second-generation of benzamide analogues were developed in the 1990s. The inhibitors identified in these studies were PD128763 (Suto et al., 1991, Arundel-Suto et al., 1991) and NU1025 (Griffin et al., 1995) which were 50-fold more potent than 3AB in enzyme inhibition studies.

Significant progress in development of second-generation PARP inhibitors was achieved after screening nicotinamide-resembling compounds (Banasik et al., 1992). These studies identified several very potent PARP inhibitors (*e.g.* phenanthridinones, phthalazinones) that further were used as a lead molecule for development of new PARP inhibitors. The PJ34 (phenanthridinone) inhibitor was used for development of INO-1001, which entered clinical trial in 2005 (Jagtap et al., 2005, Morrow et al., 2009). The phthalazinones resulted in development of KU58684 with an IC₅₀ of 5 nM and AZ2281 - olaparib (Menear et al., 2008) and the tetracyclic phthalazinone, GPI 15427, with an IC₅₀ of 31 nM (Tentori et al., 2003). The development of third generation of PARP inhibitors started with crystallization of PP128763 and NU1025 inhibitors in the NAD⁺ binding site of chicken PARP (Ruf et al., 1998). These tricyclic lactam indoles and benzamidazoles include AG14361 and AG014699, which was the first PARP-1 inhibitor used in clinical trial for the treatment of cancer (Plummer et al., 2008).

Many studies were dedicated to the use of the PARP inhibitors as chemo sensitizers in cancer therapy. For example, PD128763 was shown to be able to increase the cytotoxicity of temozolomide by 5-fold (Arundel-Suto et al., 1991)

One of the most advanced PARP inhibitors to date is AG014699 showed in Figure 1. 18. The PARP inhibitor AG14447 was identified as the most potent inhibitor (Tomas, Calabrese et al 2007) and its phosphate soluble salt (AG014699) entered clinical trial in combination with temozolomide in 2003. After promising phase I of clinical trials of this compound in patients with melanoma (Plummer et al., 2005), AG014699 is currently undergoing a phase II trial.

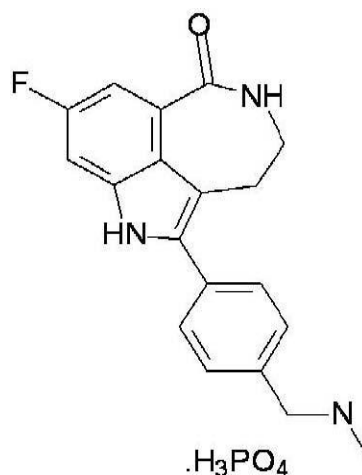


Figure 1. 18. Molecular structure of AG014699

PARP inhibitors were shown to potentiate the cytotoxic effects of ionising radiation which is particularly valuable for cancer patients as most them receive radiotherapy as part of the treatment. PARP inhibitors increases the cytotoxicity and antitumor activity not only of ionizing radiation or DNA alkylating agents (*e.g.* temozolomide) but also are extensively tested in combination with topoisomerase I poisons (Plummer 2006).

1.7. PARP-1 and TopoI interaction.

TopoI poison-based cancer therapy gives promising results however, the resistance to treatment is commonly observed (Liu, Desai et al. 2000). PARP inhibitors are undergoing clinical trials with TopoI poisons. To date the emerging data suggest increased toxicity. The combination of the PARP inhibitor, ABT-888 (veliparib), with topotecan was investigated in Phase I trials in patients with lymphomas and refractory solid tumours. The combination of veliparib with the standard dose of topotecan caused myelosuppression and dose reductions were needed. In this study, the maximum tolerated dose of topotecan was 0.6 mg/m²/day and ABT-888 10 mg BID on days 1–5 of 21- day cycles. Co-administration of veliparib with topotecan resulted in increased γ H2AX response in circulating tumor cells (CTC) and peripheral blood mononuclear cells (PBMCs), and more than 50% reduction of PAR level was observed in PBMCs. (Kummar et al., 2011). In another Phase I study, the PARP inhibitor Olaparib (AZD2281) in combination with topotecan dose-limiting toxicities of neutropenia and thrombocytopenia were observed and these were dose-related. A common adverse events (AEs) including fatigue and gastrointestinal consequences was observed

resulting in termination of this trials (Samol et al., 2011). Therefore, a proper understanding of the interaction between PARP and TopoI poisons is essential to maximise efficacy and reduce toxicity.

There are several studies where PARP inhibitors have been used to enhance topoisomerase I poisons. Early studies revealed that PARP activity was stimulated by camptothecin in L1210 cells and inhibition of PARP with NU1025 was able to enhance CPT -induced DNA breaks and cytotoxicity to a similar ~2.6-fold extent, connecting these two events (Bowman et al., 2001b). NU1025 and NU1085 also enhanced the cytotoxicity of topotecan up to 5-fold in a panel of 12 different cell lines including colon breast, lung and ovarian cancer cell lines. The effect of PARP inhibition on topotecan induced cytotoxicity in these studies was not related to p53 status in these cell lines and tissue specificity (Delaney et al., 2000). Support for the role of PARP-1 in TopoI poison-mediated cytotoxicity comes from genetic manipulation studies. Genetic inactivation of PARP-1 sensitizes cells to TopoI poisons (Chatterjee et al., 1989, Hochegger et al., 2006) and PARP-1 null mice are hypersensitive to TopoI poison toxicity; 64% of PARP null mice died within 2 weeks of exposure to CPT-11 (140 mg/kg) but all of the PARP wt mice were still alive 8 weeks later (Burkle, 2000).

In cell-based studies, AG14361 (the pre-clinical lead that led to AG014699 that went into clinical trial) was shown to be effective in potentiation of topotecan-induced growth inhibition in human colon (Lovo, SW620) and lung (A549) cancer cell lines. These *in vitro* data were supported by *in vivo* study in which irinotecan (2.5 mg/kg daily) antitumor activity in human colon cancer xenograft models was enhanced by AG14361 with a 2 to 3-fold enhancement of the irinotecan-induced tumour growth delay. In this study there was only mild body weight loss caused by irinotecan, which was not substantially increased by AG14361 (Calabrese et al., 2004). The *in vivo* activity of other PARP inhibitors has been investigated in combination with TopoI poisons: CEP-6800 caused a 60% enhancement of irinotecan-induced delay in the growth of human colon cancer (Miknyoczki et al., 2007).; xenografts, and GPI 15427 also enhanced irinotecan antitumour activity (Tentori et al., 2006), confirming the *in vitro* data.

As a direct prelude to the study described in this thesis the effect of AG14361 in combination with TopoI poisons on TopoI activity, DNA repair and cytotoxicity was investigated in K562 cells and various repair defective cell types. In this study (Smith et

al. 2005) PARP-1^{-/-} mouse embryonic fibroblasts were shown to be 3-fold more sensitive to topotecan than PARP-1^{+/+} cells. AG14361 potentiated topotecan-induced cytotoxicity in PARP-1^{+/+} cells approximately 3-fold. In comparison, these authors found only a 1.4-fold potentiation of topotecan in PARP-1^{-/-} cells, which was thought to be due to a contribution of PARP-2. PARP-1^{-/-} cells sensitivity to topotecan was not due to TopoI level, because the Western blot analysis of cell extracts showed that TopoI level was the same in both cell types. AG14361 also had no effect on TopoI activity, because relaxation of supercoiled plasmid by nuclear lysates obtained from K562 cells treated with or without AG14361 was the same. In contrast, alkaline elution data showed that AG14361 significantly retarded the re-joining of CPT-induced DNA breaks caused its accumulation after CPT removal (Smith et al., 2005). The extended persistence of these breaks was proposed to be *via* inhibition of PARP-1 dependent BER (Smith et al., 2005). The mechanisms explaining the role of PARP in repair of TopoI-induced DNA damage have not been elucidated. Cytotoxicity of TopoI poisons is related to formation of DSB mostly during DNA replication but, also to some extent during transcription. TopoI has several binding sites to PARP-1. With a native form of PARP-1, TopoI binds by its core and C-terminal domain, and to poly(ADP-ribosyl)ated PARP-1 via the TopoI N-terminal and core domain (Bauer et al., 2001). PARP-1 as one of the key BER enzymes is also involved in the repair of TopoI-mediated DNA damage. BER is significantly reduced in PARP-1 deficient cells, and BER deficient cells are hypersensitive to camptothecin (Caldecott and Jeggo, 1991). Autoribosylated PARP-1 may recruit XRCC1 protein which in turn recruits tyrosyl DNA phosphodiesterase1 as described in section 1.5.4. It was shown that BER protects non-replicating cells from TopoI poisons. AA8 cells were only sensitive to CPT during S-phase, and BER deficient EM9 cells were CPT hypersensitive in the presence of replication inhibitor aphidicolin (Barrows, Holden et al. 1998).

PARP inhibitors in response to TopoI-cc increase DNA breaks without increasing the number of TopoI–DNA complexes (Bowman et al., 2001b, Smith, 2005). PARP inactivation is also associated with deficiency of Tdp1 and, Ku / DNA-PK toxic interference in homologous recombination (HR) pathway, which are most important for repair of TopoI-cc (Hohegger et al., 2006, Zhang et al., 2011) .

There are two basic theories regarding the mechanism of sensitization of TopoI poisons-induced cytotoxicity by PARP inhibitors: firstly, that PARP-1 modulates TopoI activity and secondly that PARP-1 repairs TopoI poison-induced DNA damage. In support of

the first hypothesis several authors show that PARP-1 can interact with TopoI and modulate its activity. These two proteins interact noncovalently and co-localise throughout the cell cycle (Elias et al., 2003). TopoI activity may be regulated by PARP-1 depending on its autophosphorylation status. An interaction of these two proteins is weaker when PARP-1 is autophosphorylated (Yung et al., 2004). It was shown, that PARP-1 in the presence of NAD inhibited TopoI DNA relaxation activity (Ferro et al., 1983). The mechanism responsible for PARP-1 inhibitory activity on TopoI was suggested to be due to the accumulation on TopoI of a large negative charge from ADP-ribose that eventually causes repulsion between TopoI and DNA.

For the project described here, the most important aim is to determine the role of PARP-1 in repair of TopoI/camptotecin induced damage. If TopoI is trapped by camptotecin, the religation step is blocked and in consequence toxic SSB or DSB can be created. There is still an open question what kind of DNA breaks are accumulated due to PARP-1 inhibition (Veuger et al., 2004). Repair of those SSB and probably DSB lesions may involve binding and activation of PARP-1.

1.8. Aims.

The overall aim of this project is to determine the nature and physiological relevance of the potentiation of TopoI poison-induced cytotoxicity by inhibition of PARP-1 activity. TopoI poisons have been used in cancer therapy with promising results, however the resistance to these anti-cancer drugs is commonly observed (Liu et al., 2000). PARP-1 inhibitors are currently clinically tested and were proved not only as promising single-agent therapeutic, but also as efficient agents that can be used to increase the therapeutic efficiency of the other common anticancer agents (Plummer et al., 2005). Based on the promising pre-clinical evidence PARP inhibitors are undergoing clinical trial with TopoI poisons, but the mechanism of the chemosensitisation has not yet been fully determined .

Since the TopoI poison-induced cytotoxicity is predominantly restricted to S phase of the cell cycle the drug-resistant non-replicating pool of tumour cells can repopulate the tumour after chemotherapy withdrawal, therefore the enhancement of non- replication-associated drug cytotoxicity is clinically relevant.

The very potent and clinically active PARP inhibitor AG014699 and very specific TopoI poison Camptothecin will be used to answer on following main questions addressed in this thesis.

These questions are:

1. Is the sensitisation of TopoI poison-induced cytotoxicity by PARP inhibitors cell cycle specific?
2. Does PARP inhibition cause the accumulation of single strand breaks and does this elevated level of SSB can increase the amount of DSB in specific phase of cell cycle?
3. Does PARP inhibition have an effect on TopoI poison-induced DNA damage repair?
4. What kind of DNA breaks (SSB or DSB) are more important for mediation of cellular cytotoxicity?
5. What is the possible mechanism by which PARP-1 plays in its role in the repair of SSB and DSB?

Chapter 2. Materials and methods

2.1. Materials

All chemicals and reagents, including tissue culture media were provided by Sigma (Poole, Dorset, UK) unless otherwise stated. The PARP-1 inhibitor AG0140699 (1-(4-dimethylaminomethylphenyl)-8-9-dihydro-7H-2,7,9a-benzo[cd]azulen-6-one)) was provided by Aguron/Pfizer Pharmaceuticals GRD, La Jolla, CA, USA. The powder form of AG014699 was dissolved in water, and 5 mM stock solution was stored in small aliquots at -20 °C. In all experiments AG0140699 was used at a final concentration of 0.4 µM. Camptothecin was dissolved in anhydrous DMSO, and small 10 mM stock aliquots were stored at -20 °C. Temozolomide, a gift from Cancer Research UK (London, UK), was made up at a concentration of 150 mM in DMSO and stored at -20 °C.

2.2. Equipment

All tissue culture plastic-ware was purchased from NUNC (Fisher Scientific, Loughborough, UK). An MRX_{TC} Spectrophotometer (Dynex Technologies, UK) plate reader was used to measure the absorbance of XTT. Cell cycle analysis was performed on FACScan (Becton Dickinson, USA) flow cytometer. Centrifugal elutriation was carried out using Beckman Avanti J-20 centrifuge equipped with JE-5.0 elutriation rotor and Sanderson elutriation chamber. Peristaltic pump (Model no. 7550-50) and tubing size 8 or 16 was supplied by Master Flex, Vernon Hills, USA. Digital pictures were taken using an Epi-fluorescence microscope (DMR, Leica, Wetzlar, Germany) in 8-bit CCD camera (RTcolor SPOT, Diagnostic Instrument Inc., Sterling Heights, USA). The MIEF-SYS Isoelectric Focusing horizontal electrophoresis unit used for comet assay was supplied by VWR, Radnor, USA or by ScotLabs, Chagrin Falls, USA. Z1 Coulter counter (Beckman Coulter, Bucks) Cell colonies were automatically counted with the aid of ColCount™ Oxford Optronix.

2.3. Tissue culture

All cell lines were maintained in exponential growth phase in RPMI 1640 HEPES modified medium supplemented with 10% (v/v) foetal calf serum, glutamine, penicillin (100 units/ml) and streptomycin (100 µg/ml) at 37 °C in a humidified atmosphere of 5% CO².

Cell lines

K562

The K562 cell line was isolated from 53-year-old woman with chronic myelogenous leukaemia in blast crisis, positive for the Philadelphia chromosome (Lozzio and Lozzio, 1975). K562 cells exhibit various erythroid characteristics with possible multipotentiality (Horton et al., 1981). These suspension cells with rounded regular shape are known to be convenient for elutriation (Kauffman et al., 1990). Cells were obtained from the ATCC (Manassas VA, USA).

Lovo

The Lovo cell line was isolated from a 56-year-old male patient with adenocarcinoma of the colon. The karyotype of this cell has been characterised as near diploid, with some stocks found to become tetraploid. (Trainer et al., 1988). Cells were obtained from the ATCC (Manassas VA, USA.)

AA8

AA8, Chinese hamster ovary cell line, was isolated as a spontaneous clone, which was heterozygous in adenine phosphoribosyltransferase. Cells were obtained from Penny Jeggo, Sussex University.

EM9

EM9 cell line is a clone derived from AA8 cells. This line was obtained by isolation of resistant AA8 clones resistant to EMS (Thompson et al., 1982). The survival of EM9 cells subjected to the action of DNA-alkylating agents, IR or CPT is significantly lower as compared to the survival of AA8 (VanAnkeren et al., 1988). These cells are characterized by high frequency of SCE. Overall sensitivity to DNA-damaging agents is related to the lack of functional XRCC1 protein. (Thompson et al., 1990). Cells were obtained from Penny Jeggo, Sussex University.

2.4. Growth inhibition and cytotoxicity assay.

2.4.1. XTT cell proliferation assay.

The XTT reagent (2,3-bis(2-methoxy-4-nitro-5-sulfophenyl)-S[(phenylamino)carbonyl]-2H-tetrazolium hydroxide) is a yellow tetrazolium salt, that can be metabolised by mitochondrial dehydrogenases of the live cells to a spectrally different (orange), water soluble formazan product (Scudiero et al.,1988). The XTT assay has been commonly used to determine the effect of drugs on cell growth. For the purpose of the experiments done for this thesis, the growth of Lovo and K562 cells exposed to CPT±AG014699 was evaluated using commercially available XTT Cell Proliferation Kit II (Roche Diagnostics, GmbH) according to manufacturer's manual, and optimized by lab co-workers (Elaine Willmore, Clark Crawford – personal communication). After exposing cells to drug for the required duration, drug was removed by centrifugation and cells were plated in fresh medium in 96 well plates in density 1000 cells/well and left to grow for 4-5 days. The working XTT reagent mixture was prepared by mixing the XTT reagent (1 mg/mL) with the electron-coupling reagent (phenazine methosulfate) at a ratio of 50/1 (v/v). After adding 50 µl of the XTT reagent mixture to each well, plates were incubated for 4 hours in a humidified atmosphere at 37 °C and 5% CO₂, to allow cells to metabolize the tetrazolium salt. The absorbance of the formazan product was then measured on a MRX_{TC}spectrophotometer at 450 nm.

2.4.2. Clonogenic survival assay.

The clonogenic assay was used to investigate the cytotoxicity induced by CPT and AG014699 in Lovo and K562 cells. This method enables evaluation of the capability of individual cells to survive after exposure to drug treatment. Cells exposed to anticancer agents when returned to drug-free medium may still be able to reproduce and form colonies. Cell survival is then estimated by counting the number of colonies.

Exponentially growing Lovo cells, following drug exposure, were detached from plates using trypsin and counted using a haemocytometer or Coulter counter (Beckman). In the next step, several serial cell dilutions were prepared in fresh culture medium, from which cells were seeded at low densities into 90 mm plates (starting from 100, 250 and 500 cells for the lowest and up to 10,000 cells for the highest drug concentration).The plates were then incubated up to 12 days allowing cells to form colonies. After the incubation period colonies were fixed using Carnoy's fixative (methanol: acetic acid,

3:1), and stained with crystal violet (0.4% v/v in water) to aid counting. Colonies containing more than 30 cells were counted using an automatic colony counter (Oxford Optronix, UK). Only colonies which number contain more than 30 cells were counted on plates containing at least 5 colonies. Assuming that each colony comes from a single cell, the number of counted colonies estimates the number of cells that survived drug treatment. The plating efficiency of the cells was calculated as the percentage of colonies formed on the plates compared to the number of cells originally seeded. The clonogenic survival of drug treated-cells was calculated as the plating efficiency of treated cells expressed as a percentage of the plating efficiency of the DMSO alone or DMSO+AG014699 treated controls.

2.4.3. Clonogenic survival assay by sloppy agar.

The sloppy agar clonogenic assay enables measurement of cytotoxicity of cells growing in suspension. Cells are mixed with agarose that holds them suspended in one place where they can divide and form colonies. The K562 cells in exponential growth phase were separated into different cell cycle phases by elutriation performed in sterile conditions. The purity of each collected fraction was analysed by flow cytometry, and cell fractions containing the highest number of cells in G1, S and G2 cell cycle phase cells were used for the cytotoxicity assay. Asynchronous and elutriated cells at a density of 2.5×10^5 cell/ml were exposed to drug for the desired time and used for clonogenic assay by sloppy agar. Following treatment, drug was removed by centrifugation and cells were diluted to a density of 1×10^3 or 1×10^4 cells/ml in fresh medium. Three different cell dilutions, containing from 100 to 10000 cells were used depending on cell cycle phase and drug concentration, mixed with 0.15% SeaKem ME agarose and plated in 6-well plates. Cells were left for 12 days for colonies formation. To visualise colonies in the gel, MTT dye at a concentration of 0.4 mg/ml was used.

2.5. Staining cells for the cell cycle analysis by flow cytometry.

The flow cytometer is a machine that enables counting, examining and sorting of individual cells suspended in fluid. A hydro-dynamically focused stream of fluid in which the cells are dispersed is passed through a beam of laser light of single wavelength. At this point a number of detectors are aimed at it: one in the line of the light beam (Forward scatter - FSC) and several perpendicular to it (Side scatter - SSC) and one or more fluorescent detectors. Each cell passing through the light beam scatters the light and excites fluorescent chemicals present in the cells that emit fluorescent light

at a different frequency than light source. The detectors pick up a combination of scattered and fluorescent lights. Analysing the light fluctuation with each detector, it is possible to extrapolate various types of information about the physical and chemical properties of each cell.

The forward scatter correlates with cell volume and side scatter reflects the inner complexity of the cell (i.e. shape of nucleus, amount of cytoplasmic granules). The flow cytometric analysis of cell cycle described in this thesis was always performed directly after elutriation and just before any next planned experiments. This was an important time scheduling restriction, which must be carefully considered while planning and arranging further experiments. As described in section 3.4.2, progression of elutriated K562 cells to the next phase of cell cycle is rapid, therefore an efficient protocol for staining DNA, allowing analysis of 16 fractions collected during elutriation by flow cytometry within less than 1h, was adapted from a method described earlier (Krishan, 1975). 0.5×10^6 cells were suspended in 0.5 ml PBS and 0.5 ml of staining buffer (0.5g sodium citrate, 1.5 ml Triton-X100, 0.05g propidium iodide (PI), 0.01 g ribonuclease A, 250 ml of distilled water, stored in 4 °C protected from light) was added drop wise to the cell suspension. Staining was carried out at 4 °C for 20 min, and cells were subjected to cell cycle analysis by flow cytometry on a FASCcan (Becton Dickson) with the aid of CellQuest software. A minimum of fifteen thousand events per sample were collected and the data were stored as list mode files. PI signals derived from cells being analysed for their DNA content was gated out to exclude aggregates and distinct population of events with very low width and area, which were probably a debris resulted from staining procedures. Acquired data were then processed on ModFit LT software (Verity Software, Topsham, ME) using a manual analysis type that allows adjusting the place of G1 and G2 peaks of DNA on histograms plotted from events gated on FSC versus SSC scatter-grams. The AutoFit option on ModFit LT can analyse input data, generating report file showing analysis settings, DNA histogram and corresponding dot-plot with gated region (Figure 2. 1). The output report, provides also a summary statistics describing how model fits to experimental.

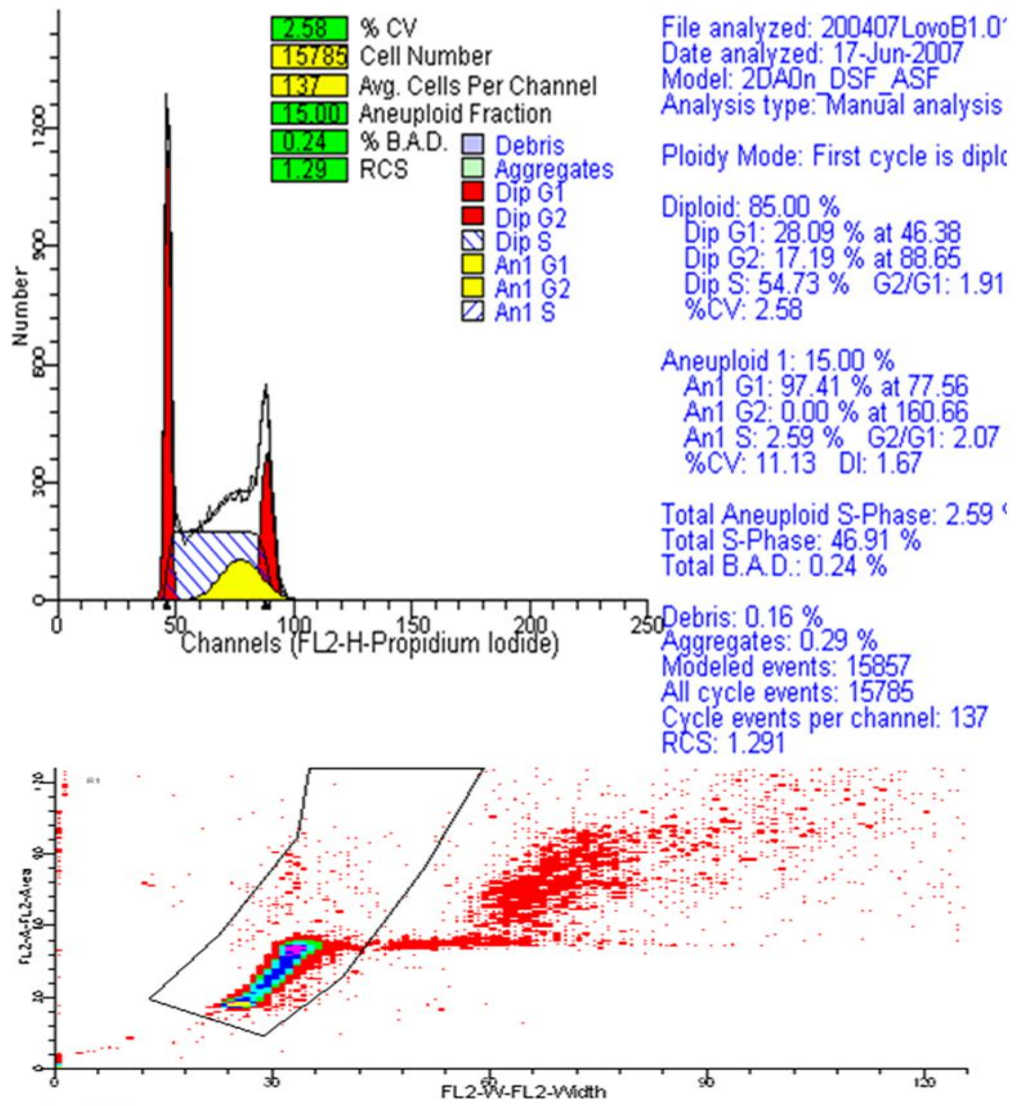


Figure 2. 1. An example of FACS report produced with the aid of ModFit LT software

A design of FACS report template generated with ModFit that include DNA histogram with indicated cell cycle phases, two types of histogram legend, scatterplot and results of analysis. One histogram legend shows various statistics (% CV, cell number) that illustrates goodness of fit, second indicates the meaning of each peak on histogram. Blue text indicates the results of sample analysis. Along with a histogram, corresponding scatterplot with gating can be generated.

2.6. Centrifugal elutriation in JE – 5.0 rotor.

Elutriation is a method which allows the separation of cells according to their size and shape. Each cell can be characterized by its size (shape, volume) and density. Cells in culture do not differ from each other according to their density so differences in their size can be used to separate them. The smallest cells are in the G1 phase and the biggest in G2, therefore it is possible to separate cells in each cell cycle phase.

Centrifugal elutriation in the JE – 5.0 rotor (Beckman Coulter, High-Wycombe, Bucks) showed in Figure 2. 1 combines two separation technologies: centrifugation (sedimentation under the influence of centrifugal force), and counterflow elutriation (separation by washing). Separation takes place in a funnel shaped elutriation chamber. Each cell in the elutriation chamber is acted upon by two opposing forces: a centrifugal force that is driving cells away from the axis of rotation and fluid velocity (driving cells toward axis of rotation – “counterflow”). While the rotor is spinning in the centrifuge a suspension of cells is pumped at constant flow rate from outside the centrifuge into the rotor to the narrow end of the elutriation chamber. When suspended cells are inside the chamber they migrate according to their sedimentation rates to the position in the gradient where the effect of those two forces upon them is balanced. For small cells the sedimentation is low and they are quickly washed toward axis of rotation, where they are caught in an increasing flow velocity caused by the rapidly narrowing chamber walls. Cells are washed out of the chamber, up through the rotor, and out into the collection vessel. The larger cells move through chamber more slowly and reaching equilibrium at the elutriation boundary, where the centrifugal force and counter flow were low and the chamber walls are at their widest point. The largest cells remain near the inlets of the chamber where centrifugal force is the highest. By increasing the flow rate in gradual steps, increasingly large cells can be washed out of the rotor and collected (adopted from Beckman elutriation manual).

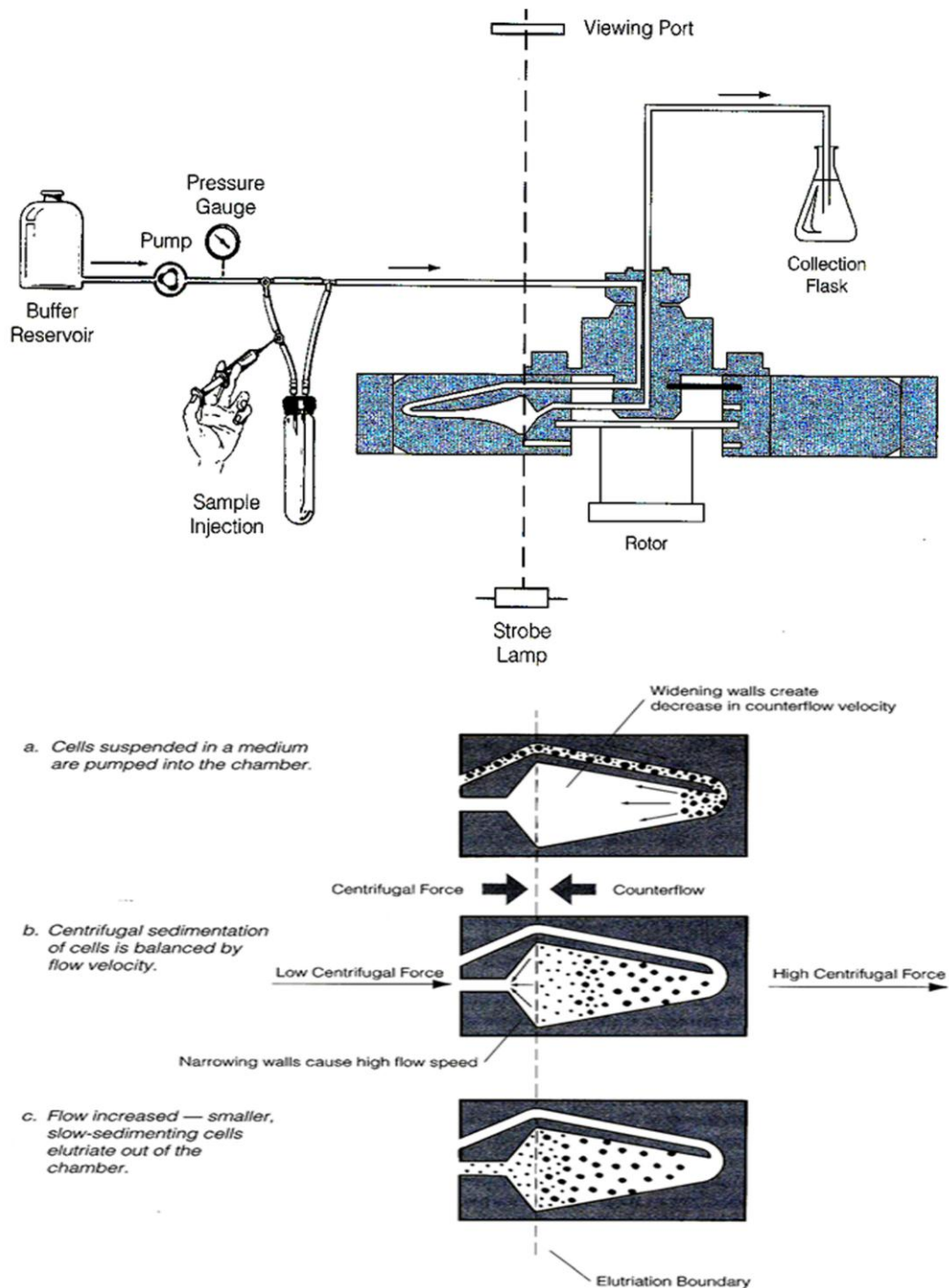


Figure 2. 2. The JE-5.0 elutriation system and process of cells separation inside elutriation chamber (picture from Beckman elutriation manual).

The heart of the elutriation system shown on the top picture is the elutriation chamber positioned in the JE-5.0 rotor that is connected by peristaltic pump with the buffer reservoir using plastic tubing. Cells injected by the valve are moved to the elutriation chamber where they can be viewed at the viewing point. At the elutriation boundary where opposite forces of centrifugal force and contraflow are equal, cells stay inside the chamber. By increasing the flow rate of the buffer, cells can be washed out of the chamber and collected in collection flasks. (adopted from Beckman elutriation manual)

2.6.1. Elutriation of K562 cells.

Before starting the elutriation experiments the following preparation steps were performed. When cells were cultured after elutriation for longer period of time, elutriation was performed in sterile conditions. All external parts of elutriation system were sterilized in 70% ethanol. Before each experiment the centrifuge rotor, tubing, elutriation chamber were disassembled, cleaned with detergent and assembled again. The first run was performed using PBS as an elutriation buffer. This step was performed to verify whether the elutriation system was properly assembled, to confirm that there were no leaks from tubing connections that the stroboscope-lamp is adjusted, and pressure in elutriation chamber is minimal. Next, when the whole system was running, the peristaltic pump was calibrated. This was done automatically by switching the pump to calibration mode in which a known amount of buffer is pumped and collected over period of time. The difference between the volume of buffer that was set up on pump and volume that was collected was used to adjust correct the flow rate.

To conduct sterile elutriation, the chamber and tubing system was sterilized by running 6% H₂O₂ through the system followed by washing in sterile PBS. Cell fractions were collected in 50 ml tubes covered by para-film to keep in sterile condition.

Before loading cells, the elutriation system was filled with flow buffer (RPMI1640 + 10% FBS) and equilibrated by starting and stopping the centrifuge for several times before reaching the final rotor speed (2500 rpm) under minimal pressure. This important step was performed to remove any air bubbles present in the elutriation system, which may increase the pressure or disturb the buffer flow.

For cell cycle separation by elutriation, 2.5-1.5x10⁸ K562 cells were collected by centrifugation and condensed in syringe as a single cell suspension in a small 5 ml volume of medium. Cells were then injected into the elutriation system filled with flow buffer at flow rate 15 ml/min. Cells were then allowed to segregate inside the elutriation chamber for 5-10 min then the flow rate was gradually increased up to 20-28 ml/min (depending on cell number injected into elutriation chamber) and decreased to 15 ml/ml. During this step the behaviour of cells in the elutriation chamber must be verified visually through the stroboscope-window and the pressure level in elutriation system must be constantly monitored. For the first two fractions of K562 cells, 50 ml each were collected under a starting flow rate of 25-30 ml/min, and later fractions of 100 ml each (2x 50 ml) were collected by increasing the flow rate by 5 ml/min for each 100 ml

fraction. Eventually 8 fractions (2x 50 ml each) were collected. The content of each fraction was analysed by flow cytometry as described in section 2.5, and the purest fractions enriched with cells in G1, S and G2 cell cycle phase were selected for subsequent experiments. Using K562 cells it was possible to get fractions of cells that were more than 80% pure in each cell cycle phase. The elutriation protocol used for the K562 cells was adapted from the one used for Lovo cells. Elutriation of Lovo cells was discontinued for the reasons discussed in section 3.3.2.

2.7. Comet assay

Single cell gel electrophoresis, also called the comet assay, is a method used to measure the level of DNA damage in single cells. Cells embedded in agarose on microscope slides are lysed and subjected to electrophoresis. Organisation of damaged DNA is disrupted, therefore individual DNA strands lose their compact structure and relax when the electric field is applied, and the DNA expands out of the nucleus into the agarose. Intact DNA strands are too large to leave the nucleus, whereas the smaller are free to move in a given period of time. The amount of DNA that leaves the nucleus is a measure of DNA damage in the cell. Recently guidelines and technical requirements for this assay were described by (Tice et al., 2000) and assay specificity for detection of SSB or DSB was discussed by (Collins, 2004). It is commonly accepted that procedure of this assay is biased by several sources of variability; therefore, some optimisations of the experimental procedure are usually recommended. Following current and electrophoresis time settings adjustment, the optimal ones were chosen and excluding various electrophoresis tanks and different batches of Comet assay kit were common for all experiments.

The comet assay was performed according to the Trevigen Comet assay protocol (Trevigen Comet Assay Kit, AMS Biotechnologies, Oxford, UK). All preparation was done under dimmed light to avoid additional DNA damage. 5×10^5 cells were suspended in 1 ml PBS. 20 μ l of the cell suspension were combined with 180 μ l of low melting point agarose, at 37 °C, and 75 μ l of this cells – agarose mixture was spread on each well of the 2-well comet slide (Trevigen Comet Assay Kit) which was precoated with a thin agarose layer. Slides were placed flat in the fridge for 20 minutes to allow gelling of the agarose. The slides were then immersed in chilled lysis buffer (Trevigen Comet Assay Kit) and placed in fridge for 30 minutes. After lysis, the assay was adapted

depending on whether the alkaline or neutral version of the comet assay was to be performed.

Alkaline

For the alkaline comet assay comet slides (after lysis) were incubated in chilled alkaline solution (NaOH – 300mM, EDTA – 40mM, pH>13) for 30 min at 4 °C. Treatment of DNA with alkaline solution of pH above 13 results in denaturation of DNA strands therefore allows detection of single as well as double strand breaks. Next, slides were placed flat into large electrophoresis tank (distance between electrode was 20 or 25 cm depending on used tank) filled with the alkaline solution. During electrophoresis the tank was covered with a box to prevent more DNA damage coming from light. The level of electrophoresis solution in tank was adjusted to obtain current of 200-300 mA under applied voltage 0.75V/cm. Electrophoresis was performed for 30min in electrophoresis buffer (NaOH – 300mM, EDTA – 40mM, pH>13).

Neutral

For the neutral comet assay, following the lysis step comet slides were briefly washed in 1xTBE, pH=10 buffer and electrophoresis was carried with 1xTBE, pH=10 buffer at 1V/cm for 30 min. In neutral conditions DNA strands are held together, therefore in this version of comet assay DSB are mainly detected.

After electrophoresis, the slides from both neutral and alkaline were washed in dH₂O, and then placed in 70% (v/v) ethanol for 5 minutes to fix the slides. The slides were then air-dried, and stained with 80 µl SYBR green (Trevigen Comet Assay Kit) diluted 1 to 10,000 in TE buffer for 10 min. After removing the excess of SybrGreen slides were dried again. Slides were imaged using the Leica fluorescent microscope with x10 or x20 magnification, equipped with CCD camera and Spot Advance software. The SpotAdvance software setting was: Exposure time 333 ms, gain 8 or 4 depending on staining efficiency, gamma correction was set to 1, which assures that image grey levels linearly depend on the fluorescent signal emitted from a sample. When 20x magnification was used (section 4.3 and 0 for alkaline comet assay) several random images from each well of comet slide were collected to obtain approximately 100 cells. When magnification 10x (rest of experiments) was used 4 images surrounding centre of each well was recorded. All cells, possible to score were measured, from which a random sample of 100 cells was selected for analysis. Although similar conditions of

electrophoresis were used for all experiments, the source of variation in the range of measurements observed in some experiments is largely unknown. Possibly some variation can be explained by the fact that two different electrophoresis tanks (section 2.1) were used for experiment or by the nature of used cell line. Nevertheless, similar pattern between repeats of single experiment was observed.

Images are displayed with comet tails running from cathode on the left to anode on the right. As the endpoint measurement, the Olive tail moment was chosen. The OTM is expressed as $(\text{tail mean} - \text{head mean}) \times \% \text{ of DNA in the tail}/100$.

2.8. Topoisomerase activity assay

Topoisomerase I (TopoI) is a nuclear enzyme that catalyses the relaxation of DNA supercoils. TopoI activity can be measured by an *in vitro* assay that relies on the ability of TopoI to relax super-coiled plasmid (Figure 2. 3). Super-coiled and relaxed DNA has different mobility in agarose-gel electrophoresis. The super-coiled DNA will travel faster and further down the gel from relaxed DNA. The TopoI activity was performed with K562 cells according TopoGen protocol as described in next section.

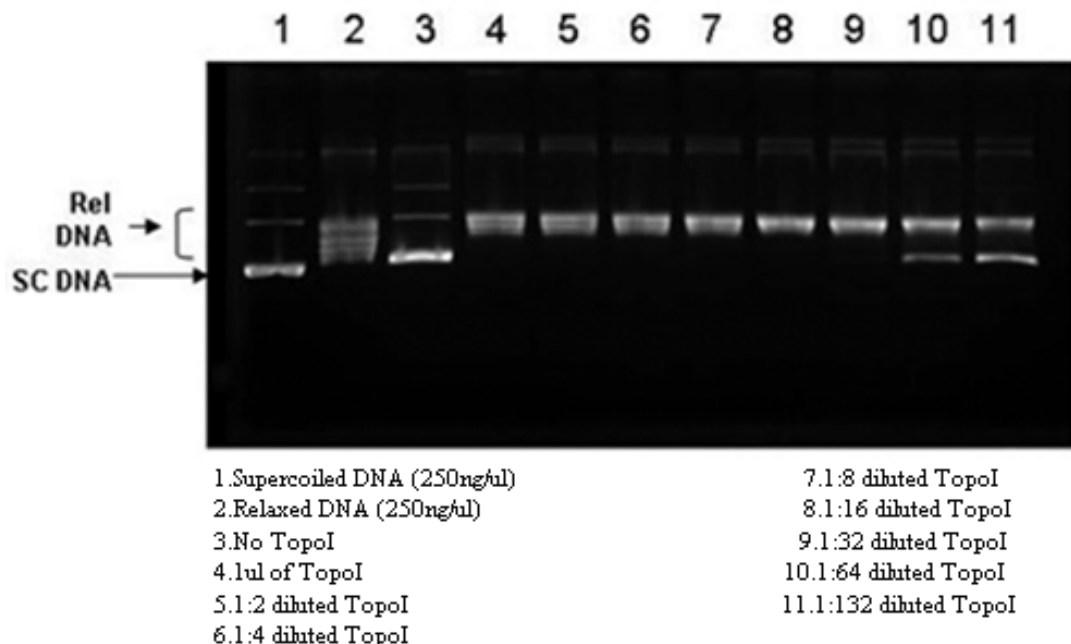


Figure 2. 3. Gel image showing the results of TopoI relaxation activity assay (from www.TopoGen.com)

2.8.1. Lysate preparation.

Following elutriation 5×10^6 – 10^7 of cells in G1, S and G2/M phase were harvested by centrifugation and washed twice in 5 ml of cold TEMP buffer (10 mM Tris-HCL, pH=7.5, 1mM EDTA, 4 mM MgCl₂, 0.5 mM PMSF). Cells were then suspended in 3 ml of cold TEMP buffer and left on ice for 10 min. Next, cells were homogenized in a tight-fitting Dounce homogenizer and checked for nuclei content by phase microscope. The nuclear fraction was then pelleted by centrifugation at 1500 x g for 10 min at 4 °C washed in 1 ml of TEMP buffer and centrifuged at 1500 x g for 2 min (4 °C). The remaining nuclear pellet was suspended in a small volume (3 to 4 pellet volumes) of cold TEP buffer (10 mM Tris-HCL, pH=7.5, 1mM EDTA, 0.5 mM PMSF). An equal volume of 1M NaCl was added and samples were left on ice for 40 min followed by centrifugation at 15000 x g for 30 min (4 °C). The supernatant was then collected and total protein concentration was measured by BCA assay.

2.8.2. TopoI relaxation activity.

Nuclear lysates were diluted in TEP buffer containing 0.5M NaCl, to obtain equal amount of protein per 1 µl. Sample reaction in a volume of 20 µl was assembled by mixing 16 µl of distilled H₂O₂, 2 µl of 10x assay buffer (100 mM Tris-HCL pH 7.9, 10 mM EDTA, 1.5 M NaCl 1% BSA, 1 mM spermidine, 50% glycerol), 1 µl supercoiled DNA and 1 µl of test extract. After incubation at 37 °C for 40 min, the reaction was terminated by adding 5 µl of 5x stop loading buffer (5% sarkosyl, 0.125% bromophenol blue, 25% glycerol). Samples were loaded on to a 1% agarose gel and electrophoresis was run at 2.5 V/cm in TAE buffer (40 mM Tris, pH=8, 20 mM acetic acid, 1 mM EDTA,) until the front of the loading buffer reached the end of the gel. The gel was then stained with 0.5 µg/ml ethidium bromide for 20 min, and briefly washed in distilled water. Images were captured on camera with the GelDoc system and a trans illuminator.

2.9. Parp-1 activity assay

The PARP activity experiments described in section 3.6 were kindly performed by Tomasz Zaremba (an experienced user of this technique) (Zaremba et al., 2011). The activity of PARP was measured by the method validated to GCLP standard that was used as a pharmacodynamics endpoint for clinical trials. This assay measures PARP activity that has been maximally stimulated by a double-stranded oligonucleotide in the presence of excess NAD⁺, therefore eliminating error due to variable activation of the

enzyme by DNA damage accidentally introduced during processing. The PARP activity was measured in asynchronous and elutriated K562 cells in triplicate samples collected from 3 independent experiments. 10^4 cells were permeabilised with digitonin and the PARP activity was stimulated in a reaction mixture containing 350 μ M NAD⁺ and 10 μ g/mL oligonucleotide (CGGAATTCCG) (Europrim, Invitrogen, UK) in a reaction buffer of 100 mM Tris-HCl, 120 mM MgCl₂ (pH 7.8) in a final volume of 100 μ L for 6 min at 26°C. After blotting onto a nitrocellulose membrane (Hybond-N, Amersham, UK), the poly(ADP-ribose) was detected following incubation with the primary anti-PAR 10H antibody (1:1000 diluted) then a HRP-conjugated goat anti-mouse secondary antibody (1:1000 Dako, Ely, UK) and finally ECL reaction and chemiluminescence detection. Results were expressed relative to the number of cells loaded by reference to a purified poly(ADP-ribose) standard curve (0-25 pmol: Enzo Life Sciences).

2.10. γ H2AX detection by immunofluorescence.

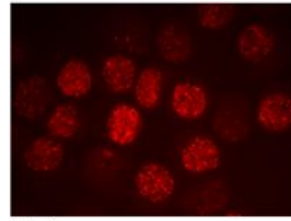
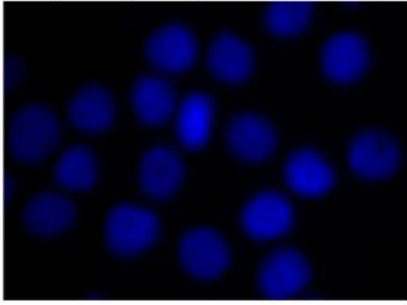
Immunostaining of histone γ H2AX is a sensitive technique used for detection of DNA DSB. This approach was used in this thesis with the K562, EM9 and AA8 cell lines. The adherent EM9 and AA8 cells prior to treatment and staining for γ H2AX were grown onto microscope cover-slips. The suspension K562 cells following treatment were washed with cold PBS, and deposited using cytospin centrifuge onto microscope cover-slips placed on top of microscope glass. Next samples were fixed in cold methanol at -20 °C for 10 min, and re-hydrated with three changes of PBS for 30 min and blocked in blocking buffer (10% milk in PBS) for 1 hour. Cells were then incubated with primary antibody specific to phospho serine 139 of histone H2AX (diluted 1:1000 clone JBW301, mouse monoclonal antibody; Upstate, Millipore Corp which were diluted in blocking buffer containing 0.1% of TritonX-100) for 1h at 37 °C. Cells on covers-slips were washed 3 times for 10 min in PBS with 0,1% TritonX-100, and secondary antibody (goat polyclonal to Mouse IgG antibody Chromeo™ 546) was applied at a dilution of 1:1000 for 1h at 37°C. After the washing step (3x 10 min in PBS) coverslips were mounted onto microscope slides using Vector-shield Mounting Medium (Vector Laboratories, Peterborough, UK). For each sample, two images of DAPI and 2 corresponding images of γ H2AX were recorded on an Epi-fluorescence Microscope using Image Spot Advance software. The exposure time for γ H2AX fluorescence was 1111 ms, with gain 8 and gamma 1. The exposure time and gain was set using sample with expected higher fluorescence signal, so the recorded 8-bit images were not overexposed,

2.10.1. PZFociEZ - ImageJ custom macro.

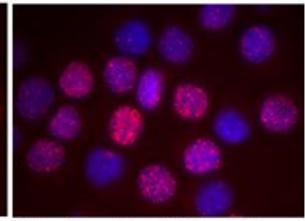
ImageJ is a public image processing program developed at the NIH. In this thesis ImageJ custom macro PZFociEZ was used for the analysis of the γ H2AX foci by measuring foci fluorescence intensity and number of focus within single analysis step. In Appendix possible applications for macro end examples of Image analysis were described.

Some similar macros have been written before, and results were compared with the results obtained by visual scoring and FACS analysis (Kataoka et al., 2006, Cai et al., 2009), The PZFociEZ macro that I have written is a first of this type where a combination of ImageJ built in functions and macros was combined together to provide all necessary tools for analysis of the γ H2AX. The principle of automatic analysis with macro is shown on Figure 2. 4 and Figure 2. 5. Figure 2. 4 shows the sequence of steps applied during creation of nucleus outlines. Figure 2. 5 shows subsequent steps of γ H2AX foci analysis are visualised and described. The basic idea lying behind this analysis is to reduce the image background leaving only the fluorescence signal, which belongs only to single foci. This can be seen in Figure 2. 5 surface plot 2s-5s. The image background (pixels outside the nucleus) and cell non-specific background was reduced with the aid of ImageJ Subtract Background options which uses the rolling ball algorithm. This was achieved by generation of the background image that was later subtracted from original image. After this step it was usually necessary to subtract a constant value from all images to remove any remaining background. For counting foci the Find Maxima option was used.

A. Open Dapi image

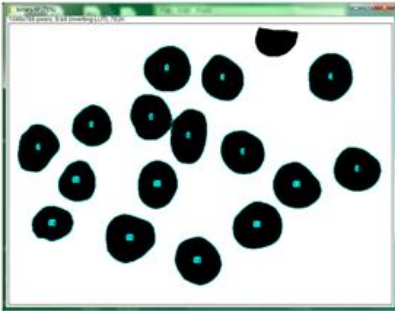


Foci



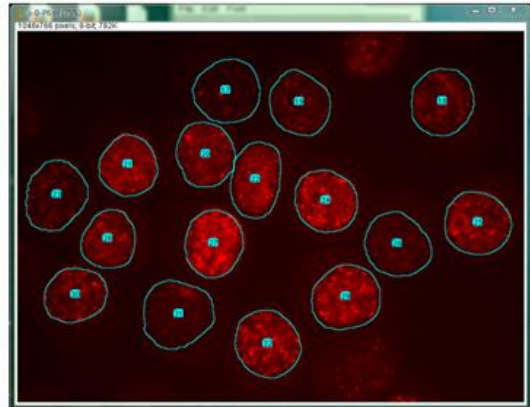
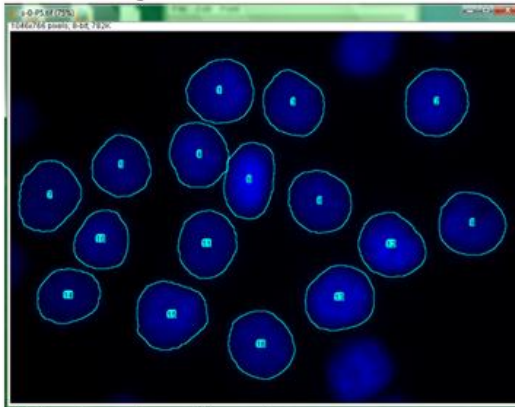
Dapi and Foci Merged

B. Binary image of DAPI.

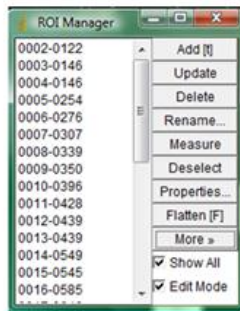


DAPI image (A) was used to obtain nucleus outlines. Following background subtraction DAPI image was smoothed several times and it was converted to binary (B). The watershed algorithm was used to separate adjacent nucleus shapes, and analyse particle options was applied to create mask of nucleus. Created mask was inspected on DAPI and Foci images (C), and saved as sets of nucleus outlines (D) for further analysis.

C. Visual inspection and manual correction of the nucleus outlines.



D. Saving nucleus outlines set



The commands gathered on MaskEZ panel were used to create and correct nucleus outlines. The outline sets were saved into separate folders along with images on which they were displayed using SaveRoi-DAPI option, for DPAI images or SaveRoi-Foci option, for Foci images .

Figure 2. 4. A sequence of operation during generation of the selections for DAPI stained nucleus implemented in MaskEZ panel of the PZFociEZ macro

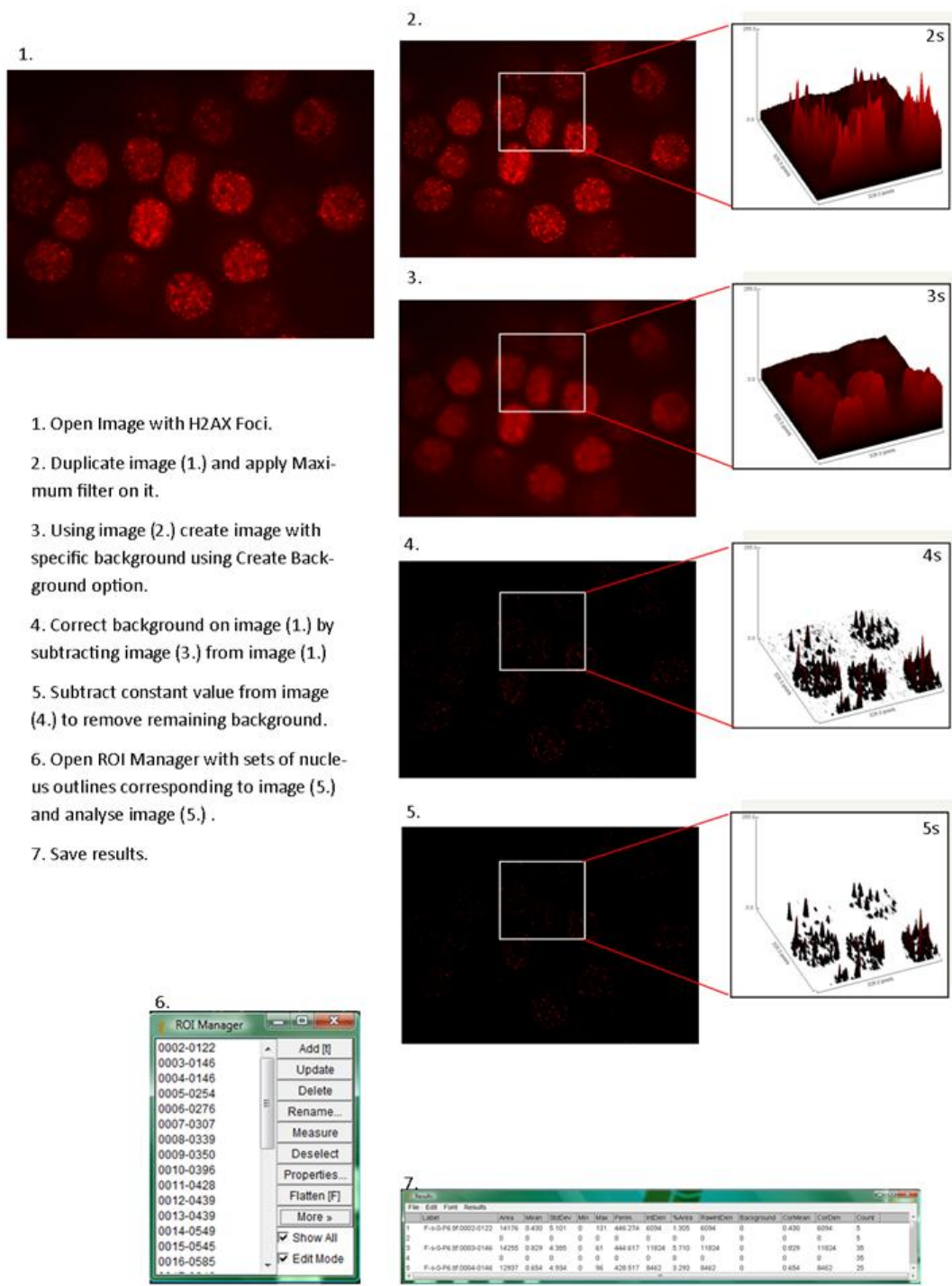


Figure 2. 5. A sequence of operation applied during analysis of images with γ H2AX foci by FociEZ panel

The area in rectangular selections was used to generate a surface plot (images 2s-5s) that illustrates changes of the image during each analysis step.

2.10.2. Comparing image analysis between ImageJ and Image ProPlus software.

To confirm that PZFociEZ macro is working, a comparison of analysis was performed on images recorded on two different fluorescence microscopes and analysed with the aid of PZFociEZ macro and Image ProPlus (commercially available image processing software). The sample cells used for this comparison were prepared as described in section 5.3. Briefly, the EM9 cells were exposed to temozolomide for 4 h and stained for γ H2AX as described in section 2.10. For this comparison images corresponding to control samples (no primary antibody and DMSO) and sample treated with 1000 nM TMZ were recorded on Olympus and Leica fluorescent microscopes. (Figure 2. 6). So far several approaches have been applied for the γ H2AX foci quantification using image analysis reviewed in (Bocker and Iliakis, 2006). Analysis of γ H2AX foci is usually performed by visual counting of foci formed around DNA breaks or by measuring fluorescence intensity for whole nucleus or single foci. To obtain results described in these section 8-bit and 16-bit images were processed using ImageJ software with customized macros and Image ProPlus Software. Using Image ProPlus DAPI images were used to create the nucleus selection and then used for measurement of integrated density of the γ H2AX image. The background was measured at several places on the image and average was subtracted from measurements of foci integrated density. Using PZFociEZ macro images were analysed as described on Figure 2. 5 and Figure 2. 5, by measuring Integrated density and counting foci. First the DAPI Images were used to create outlines for each nucleus. Those outlines were than saved by ImageJ and used later for measurements performed on a second, corresponding image that was recorded for γ H2AX. The γ H2AX images prior to measurements were processed to reduce background and improve resolution of foci, as described in the previous section. The integrated density represents the sum of all pixel intensity values. For counting foci, the Find maxima option was applied. This option with given noise tolerance (10 for 8-bit images and 1000 for 16-bit images) enumerates single foci as pixels with highest value within area specified by noise tolerance value. Maxima are ignored if they do not stand out from the surroundings by more than this value. In other words the threshold is set at the maximum value minus noise tolerance and the contiguous area around the maximum above the threshold is analysed. For accepting a maximum this area must not contain any point with a value higher at than the maximum. Only one maximum within this area is accepted (see Appendix). Figure 2. 7 A and D shows that there that results obtained with Image ProPlus (A, D) are similar to the results obtained with ImageJ

(Figure 2. 7 B,E). A similar pattern was observed when counting of foci on 8- and 16 bit images were performed using ImageJ. A score almost 4 times higher in foci number is seen for 16 bit images resulting from higher resolution of images recorded on Olympus microscope.

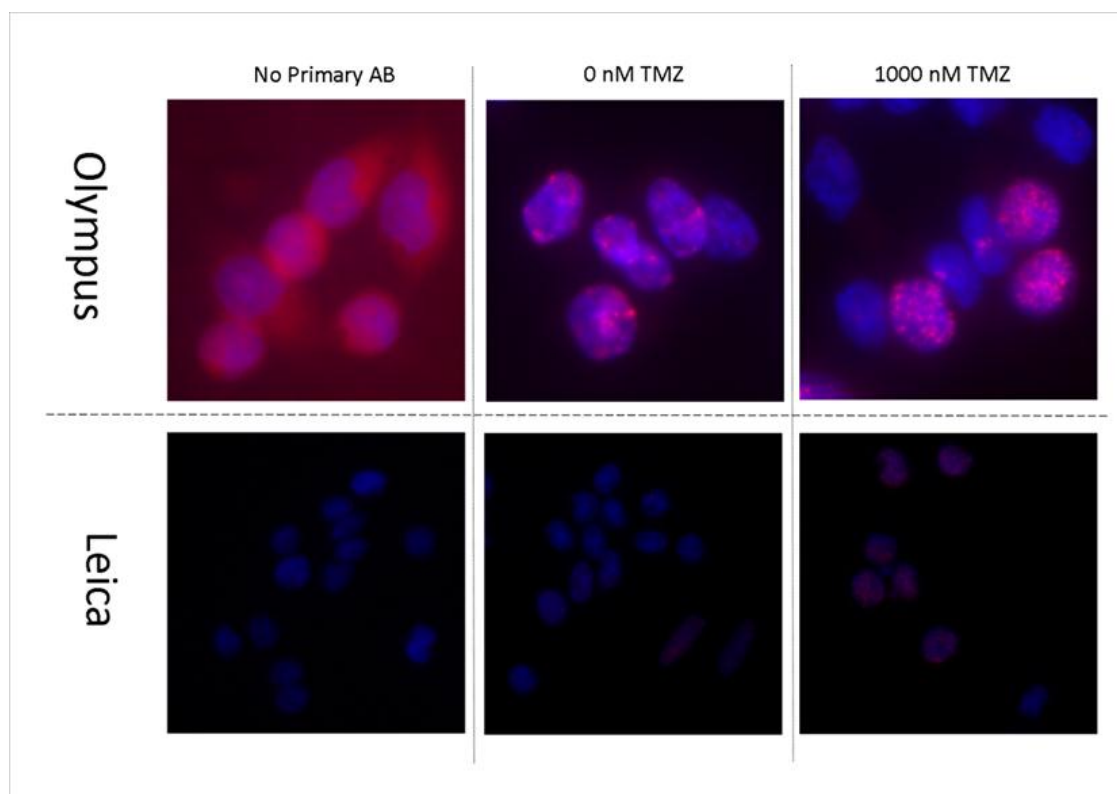


Figure 2. 6. Images of γ H2AX foci obtained using two different microscopes

The EM9 cells seeded on microscope coverslips were treated for 4h with 0 and 1000 nM of temozolomide and the level of DSB was evaluated by γ H2AX immunostaining. Images from the same samples of no primary antibody, untreated (0nM TMZ) or treated (1000nM TMZ) were recorded using Olympus (16-bit) and Leica (8-bit) fluorescent microscopes equipped with Hammamatsu and RTColour SPOT cameras respectively.

Although some differences in absolute values were obtained comparing results of analysis between two-used software's the overall trend in biological meaning is the same. For several reasons the PZFociEZ macro was preferred over ProPlus. The macro provides better flexibility when choosing necessary options for image analysis. Macro reduces time needed for preparing nucleus outlines and for inspection of outlines accuracy. It is also freeware software available to all without any Licencing restriction therefore this may results in more common usage in scientific community.

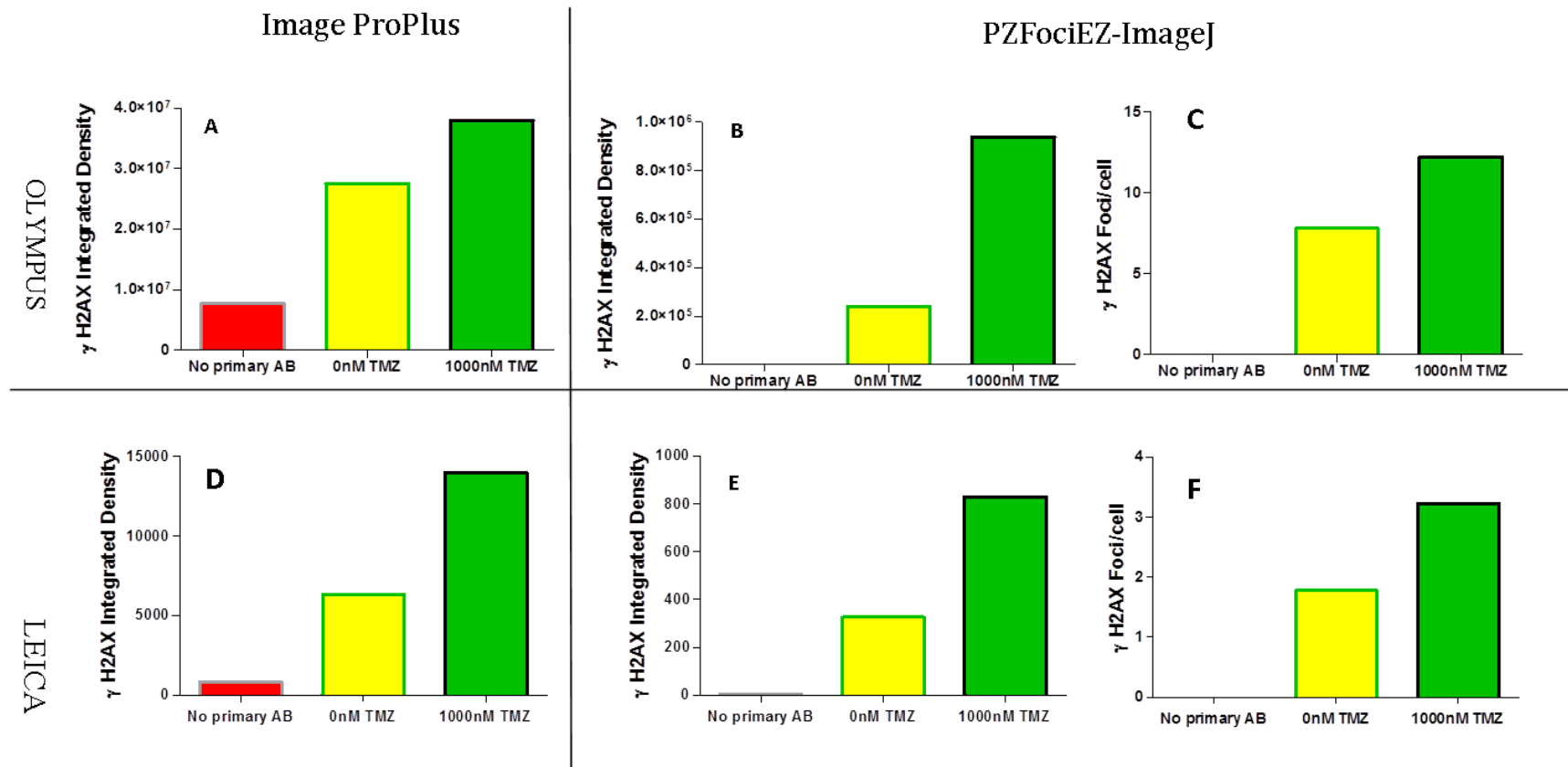


Figure 2. 7. Comparison of the results analysis with the aid of PZFociEZ macro and Image ProPlus softwares of images obtained from Olympus and Leica microscopes

16-bit images recorded on Olympus and 8-bit images recorded on Leica microscope were analysed using PZFociEZ macro and Image ProPlus software. Figure A,D Foci Integrated density measured using Image ProPlus, Figure B,E foci Integrated Density measured using PZFociEZ macro, Figure C, F number of γ H2AX foci counted using PZFociEZ macro.

2.11. Western blotting.

Preparation of protein lysates.

For K562 cells protein lysates were prepared as described in section 2.8.1. For AA8 and EM9 cell lines, cells in exponential growth phase (70% confluence) were trypsinised, washed twice in cold PBS, and equal number of cells (2×10^6) were lysed by addition of ~3x cell pellet volumes of SDS lysis buffer (6.25 mM Tris HCl pH 6.8, 2% SDS, 10% glycerol, 0.125% (w/v) bromophenol blue) and heated to 95°C for 5 min.

BCA protein assay.

To enable an equal amount of protein to be loaded onto the gel, a protein assay was conducted on all samples using Pierce BCA Protein Assay Kit (Pierce, Rockford IL). The assay is based on the reduction of Cu^{2+} to Cu^{1+} by protein in an alkaline medium. In the first reaction step (biuret reaction) peptides, containing three or more amino acid residues chelates copper in an alkaline environment and form a light blue complex.

In the second reaction step, bicinchoninic acid (BCA) reacts with the cations that were formed in step one producing an intense purple-coloured reaction product which results from the chelation of two molecules of BCA with one cuprous ion. The absorbance of this product can be measured on a spectrophotometer at 560 nm.

The amount of protein in samples was evaluated based on standard curve of known BSA concentration range (0.125-2 mg/ml) set in triplicates for each concentration on a 96-well plate. The BCA reagent provided with assay kit was mixed in a ratio of 25:1 reagent A to reagent B and 200 μl added to each well. The plate was incubated at 37 °C for 30 min and the absorbance of solution in each well was measured at 560 nm on a plate reader. The concentration of proteins in protein lysates was calculated by comparison to the standard curve.

The cell lysates of known protein concentration were diluted in the buffer used for lysis to obtain equal volumes of sample with desired protein concentration. Protein dilutions were prepared and mixed with SDS lysis buffer containing 5% β -mercaptoethanol and heated to 90 °C for 5 min.

Protein lysates along with molecular weight markers (MagicMark™ XP Western Protein Standard; Invitrogen, Paisley, UK) were loaded onto NuPAGE® Novex Bis-Tris pre-cast gels (Invitrogen). After electrophoresis, the protein was transferred from

the electrophoresis gel to a nitrocellulose membrane (Hybond C, Amersham, Bucks, UK). The membrane was then blocked in 5% (w/v) dried milk in TBS Tween (50 mM Tris, 150 mM NaCl, with 0.05% Tween 20).

The primary antibody applied to the membrane was diluted 1/1000 in 5% milk in TBS Tween and mixed for at least an hour using a Roller mixer. The membrane was washed three times in TBS Tween before following by application of the appropriate secondary antibody, diluted at 1/1000 dilution, in 5% milk (as above) which was mixed for 1 h as above. The membrane was washed 3 times for 10 min in TBS Tween to reduce non-specific binding of the antibody. Proteins immobilised on membrane were detected using an ECL kit (Amersham) added directly to the membrane for the required length of time.

2.12. Statistical analysis.

Data described in this thesis were analysed using One-way, or N-way analysis of variance depending on experiment design. The results of statistical analysis are given in format *e.g.* $F(n-1, N-1)=f$, where f is the F statistic of the two numbers in parentheses, and n = the number of groups and N =number of cases. This is used to calculate the mean sum of squares for the groups and cases to obtain f . The p value is then calculated for F . When the F statistic was significant at the level of 0.05, comparison between relevant groups was performed using a t-test to compare two samples or Fisher LSD test for multiple comparisons.

Chapter 3. Cell cycle dependent effect of PARP-1 inhibition on topoisomerase I poison-induced cytotoxicity in cells.

3.1. Introduction

As described in the introduction, cell killing by TopoI poisons is thought to be largely due to conversion of TopoI-associated SSB to DSB by collapsed replication forks during S phase (section 1.5.3). It is possible that drug induced potentiation by PARP inhibition is strictly S phase dependent and there is some evidence in the literature to support this hypothesis.

For example, in one of the earliest studies the effect of PARP-1 inhibition on CPT-induced cytotoxicity was demonstrated by Mattern et al. 1987. In this study, inhibition of PARP-1 by 5 mM 3-AB was shown to increase CPT-induced cytotoxicity by 1.5-fold in L1210 mouse lymphocytic leukaemia cell line after 16h exposure, but had no effect when 60 min incubation was applied (Mattern et al., 1987). These authors attributed sensitisation to the direct effect of PARP-1 on the TopoI activity. That is, in the absence of PARP inhibitor TopoI can be constantly poly (ADP-ribosylated) resulting in lower activity. Therefore, inhibition of PARP leads to loss of the inhibition of TopoI. Since the activity of TopoI can be correlated with elevated CPT-induced cytotoxicity because more DNA damage is generated, this can lead to increased sensitivity to TopoI poisons.

In a later study, Smith et al. 2005 demonstrated that CPT-induced cytotoxicity in K562 cells was time-dependent with the GI_{50} being 5 nM for 16h exposure and 30 nM for 30 min. These authors also found that the PARP inhibitor AG14361 (at a concentration of 0.4 μ M) caused 2-fold sensitisation of the 16h exposure to CPT, but no sensitisation of the 30 min CPT exposure, confirming Mattern's observation.

The data described above shows that inhibition of PARP-1 activity during continuous exposure to TopoI poison, for at least one cell doubling time, potentiates TopoI poison-induced cytotoxicity and growth inhibition approximately by 2-fold, in various cellular models. The molecular mechanism behind this phenomenon is poorly understood, and there are some conflicting reports between data obtained with cell free and *in vitro* systems.

For example, Yung *et al.* 2004 used cells co-transfected with fluorescent-tagged PARP-1 and TopoI and demonstrated that unmodified PARP1 co-localizes with TopoI in live

cells, throughout the cell cycle due to direct protein-protein interactions. Following induction of DNA damage, this interaction is disrupted as was demonstrated by the reduced fluorescence signal of the co-localised proteins. Then, using cell free assays these authors demonstrated the interaction of TopoI with unmodified PARP1 was shown to enhance TopoI activity, and increase the TopoI-DNA binding affinity. They also showed that, the poly(ADP-ribosyl)ation of TopoI by PARP-1 regulates their interactions, and reduces TopoI activity. TopoI activity was reduced when the reaction was carried in the presence of automodified PARP-1 or even only with free poly(ADP-ribosyl) polymers. These observations suggest that inhibition of PARP-1 activity will prevent poly(ADP-ribosyl)ation of TopoI that eventually elevates its activity, and on the other hand, DNA repair may be retarded due to PARP-1 inhibition. (Yung et al., 2004).

These findings are in contradiction to results obtained by Smith et al. who investigated effect of PARP inhibition on TopoI activity in K562 cells. TopoI activity was measured in a cell free assay, in a reaction containing supercoiled plasmid and nuclear extract prepared from cells exposed to 0.4 μ M AG14361 for 30 min and 16h. These studies showed that PARP-1 inhibition does not affect TopoI relaxation activity. This was further confirmed by experiments showing that inhibition of PARP-1 activity by AG14361 had no influence on cleavage complex formation induced by 10 μ M CPT after 30 min incubation, These data support the alternative hypothesis, that potentiation of CPT-induced cytotoxicity by PARP inhibitors involves repair of TopoI poison-mediated DNA damage. This hypothesis is also supported by earliest studies of Barrows *et al.* who investigated CPT-induced cytotoxicity using parental AA8 and its BER/SSBR defective derivate EM9 cell line by its mutation of XRCC1. The effect of loss of XRCC1 conferred hypersensitivity to CPT-induced cytotoxicity and is expected to be similar to the effect obtained by PARP-1 inhibition because these two proteins act alongside in BER pathway. Using this model, Barrows demonstrated that 1h exposure to CPT of AA8 cells resulted in specific killing of cells being in S phase, whereas in EM9 cells CPT- caused death both in S phase and non S phase cells. Treatment of AA8 cells with the DNA replication inhibitor aphidicolin protected them from CPT-induced cytotoxicity, but did not have an effect on EM9 cells. This suggests that repair of CPT-induced DNA damage during DNA replication contributes to the cytotoxic effect of TopoI poison, rather than TopoI level or activity which was shown to be similar in both cell lines. (Barrows et al., 1998).

The cytotoxic activity of TopoI poisons is attributed to specific killing of the S phase cells. Nevertheless the consequences of exposure of cells to CPT are more complex and final results of its action depends on the cell line, drug concentration and exposure time, and cell cycle phase during which cells were exposed to drugs. For example, in lymphocytic leukaemia L1210 cells the consequences of exposure to CPT are manifested by delayed progression of cells through G2 phase and increased fraction of cells with aberrant ploidy. Identical treatment condition applied to myelogenous leukaemia HL-60 or KG1 cell lines caused rapid death of S and G2 phases (Del Bino et al., 1990). Goldwasser *et al.* provided another example that supports the complexity of CPT action. In their study, the mechanism of CPT-induced cytotoxicity was investigated in SW620 and KM12 colon carcinoma cell lines, chosen for experiments because of their markedly different sensitivity to CPT, despite similar level of TopoI protein. They showed that after 1h treatment with 1 μ M CPT, the more sensitive SW620 cells showed impaired replication elongation and were irreversibly blocked in S phase, whereas the cells that were resistant to CPT were arrested in G2 phase. Treatment of these cell lines with aphidicolin, resulted in minimal protection from CPT-induced cytotoxicity in KM12 cells and more pronounced protection in SW620 (Goldwasser et al., 1996). These data suggest that DNA replication is a determinant of sensitivity to TopoI poisoning in cells that are inherently sensitive to CPT to a extent in CPT-resistant cells.

Detailed studies, showing the cellular response to 1 hour exposure to topotecan, in the context of the phases of the cell cycle and various concentrations of topotecan, with the IGROVI (ovarian cancer) cell line, was published by (Lupi et al., 2004). Using propidium iodide and BrdU labelling for identification of cells in specific cell cycle phases they showed that the effect of topotecan treatment on cells follows complex dose- and time-dependent cell cycle block, growth delay and cell death scenario depending in which phase of cell cycle cells were exposed to topotecan. For example, cells exposed to topotecan in G1 or G2/M phase underwent a transient block before progressing to S-phase. This block was concentration-dependent and higher concentrations resulted in prolonged arrest and increased rate of cell death. The majority of cells exposed to drug in S-phase were killed or blocked in S or G2/M for prolonged periods (3 days) following exposure to even low drug concentrations (< 1 μ M) of topotecan (Lupi et al., 2004).

In summary, the cellular response to TopoI poisons is complex and drug dosage, duration of treatment and influence of cell cycle phase on drug specificity all need to be taken into account. TopoI poisons have been used in chemotherapy for various types of cancer. Overcoming the commonly observed resistance to TopoI poisons is an aspect currently challenged by many studies. PARP-1 inhibitors are promising agents, which can be used as modifier of this resistance, and this thesis aims to verify their role in potentiation of CPT-induced cytotoxicity.

3.2. Aims

Previous data show in multiple cell systems that the cytotoxic effect of TopoI poisons is selective to S phase cells and that PARP-1 inhibitors potentiate TopoI poison-induced cytotoxicity, however these two observations have not been linked. The question to be answered is: Does the inhibition of PARP activity sensitize cells to CPT at all phases of cell cycle, or is the sensitization cell cycle phase specific?

Therefore, the aim of this chapter was to investigate the effect of PARP1 inhibition on TopoI I poison-induced cytotoxicity in cells that have been separated into different phases of the cell cycle by a non-stressful method. Potentiation of CPT-mediated cytotoxicity by the potent PARP1 inhibitor AG014699 was investigated in Lovo colorectal cancer cells growing asynchronously and after synchronization into G1, S, and G2-phase by centrifugal elutriation. The role of PARP1 inhibition in TopoI poison-induced cytotoxicity was also studied in the K562 cell line. The K562 cell line was chosen due to superior elutriation capability and previously characterised response to CPT and PARP1 inhibitor treatment. The protein levels of TopoI and PARP1, as well as their enzymatic activity were determined for each cell cycle phase.

3.3. Effect of PARP1 inhibition on TopoI poison-induced cell cytotoxicity in elutriated and asynchronously growing Lovo cells.

3.3.1. Effect of AG014699 on CPT induced cytotoxicity in Lovo cells after long and short exposure

TopoI poisons are used clinically to treat colorectal cancer as described in section 1.5.3. Therefore the colorectal cancer cell line Lovo was selected for studies on potentiation of CPT-induced cytotoxicity to PARP inhibitors. To investigate the effect of AG014699 on CPT-induced cytotoxicity in asynchronous cells, survival of cells following a short pulse (1h) and prolonged (24h) exposure to CPT±AG014699 was determined by clonogenic assay.

Asynchronously growing Lovo cells were exposed to increasing CPT concentrations in the presence or absence 0.4 µM AG014699. This concentration was chosen because in previous studies it was shown that the similar, but less potent PARP inhibitor, AG14361 at a concentration of 0.4 µM reduced PARP activity in K562 cells by 90% and was not cytotoxic to cells (Smith et al., 2005). Similarly, AG014699 was shown to be non-toxic (at 0.4µM), inhibiting PARP activity >90% in L1210 cells and was used to chemosensitise at 0.4 µM in SW620 cells (Thomas et al., 2007). The cell cycle doubling time for Lovo cells is approximately 24h. Therefore, cells were exposed to drugs for 24h to cover a complete cell cycle. After the exposure period, cells were trypsinized and plated at known density for colony formation assay. Figure 3.1 A shows the cytotoxicity curve for Lovo cells exposed to CPT±AG014699 for 24h. Treatment of Lovo cells with CPT for 24h induced a sigmoidal concentration-dependent decrease in cell survival (Figure 3.1 A). Co-incubation with AG014699 significantly increased CPT induced cytotoxicity by 2-fold (LC_{50} , camptothecin alone = 0.55 ± 0.033 nM, camptothecin + AG014699 = 0.29 ± 0.024 nM, t-test $p = 0.09$). During 24h exposure the majority of Lovo cells progressed through S-phase where they were exposed to CPT and killed. The survival curve for the 24h exposure reached a plateau phase at the level of 5-6% survival, and this reflects a sub-population of drug-resistant cells. The final aim was to determine the effect of CPT ± AG014699 in Lovo cells separated into different cell cycle fractions. After elutriation, Lovo cells will be in suspension and immediately treated with drugs for a short period (1 h) so that they do not progress to the next cell cycle phase. They therefore will not have enough time to attach to the surface of culture dish. An experiment was performed to investigate whether the cytotoxic effect of the

short pulse of CPT \pm AG14699 treatment has the same effect on cells in suspension and adherent cells (Figure 3.1. B, C). Lovo cells were detached from plate surface by trypsinisation, spun down, re-suspended in fresh medium and exposed to CPT \pm AG014699 for 1h. After the exposure period, cells were centrifuged to remove drug, diluted into desired density and plated in known number for colony formation. In parallel adherent cultures of exponentially-growing Lovo cells were exposed to the same concentrations of CPT \pm AG014699 for 1h. The cytotoxicity curves were obtained by plotting drug concentration versus percentage of cell survival and used to estimate dependency of treatment condition on drug induced-cytotoxicity (Figure 3.1 B, C). A concentration-dependent increase in CPT-induced cytotoxicity was also observed in asynchronous adherent and suspension cells after 1h exposure (Fig. 3.1 B and C) with approximately half the cells being killed at 10 nM and most of the remaining cells being resistant to concentrations as high as 300 nM. Comparing cell cytotoxicity induced by CPT during 1h incubation with 24 h incubation, a maximum of 45% cells were killed by 10 nM CPT after 1h exposure, compared with 95% at 24 hr. The 45% of cells killed in 10 nM CPT for 1h most probably correspond to the fraction of cells that were in S phase. Flow cytometric analysis of asynchronous cells indicated that approximately 40% of cells are in S-phase (data will be shown in next section - Figure 3. 2). However, with prolonged incubation time (24 h) more cells go through S phase are killed, and hence the curve is a typically sigmoidal response. At a concentration of 10 nM, CPT was 10-fold less cytotoxic after 1h exposure than 1nM after 24h exposure.

The survival curves for adherent and suspension Lovo cells treated with CPT \pm AG014699 enter plateau phase around 50-60% of survival, which makes calculation of LC50 very inaccurate, therefore comparisons of LC50 can be misleading. Instead of LC50, survival values taken from individual experiments for specified concentrations were used to compare differences between adherent and suspension cells and verified by t-student test. Results of the survival comparison shown in Table 3. 1 shows that there was no statistically significant differences in the treatment of Lovo adherent versus Lovo suspension cells between 30 nM CPT (p=0.38) and CPT \pm AG014699 (p=0.53). The same was for 100 nM CPT(p=0.23) and CPT \pm AG014699 (p=0.8). The potentiating effect of AG014699 was not significant in both treatment conditions at concentration 30 nM CPT (p=0.28 for adherent; p=0.48 for suspension), but was 1.2-fold (adherent) and 1.4 (suspension) higher when CPT was used at concentration of a 100 nM (p=0.004 for adherent; p=0.0038 for suspension)

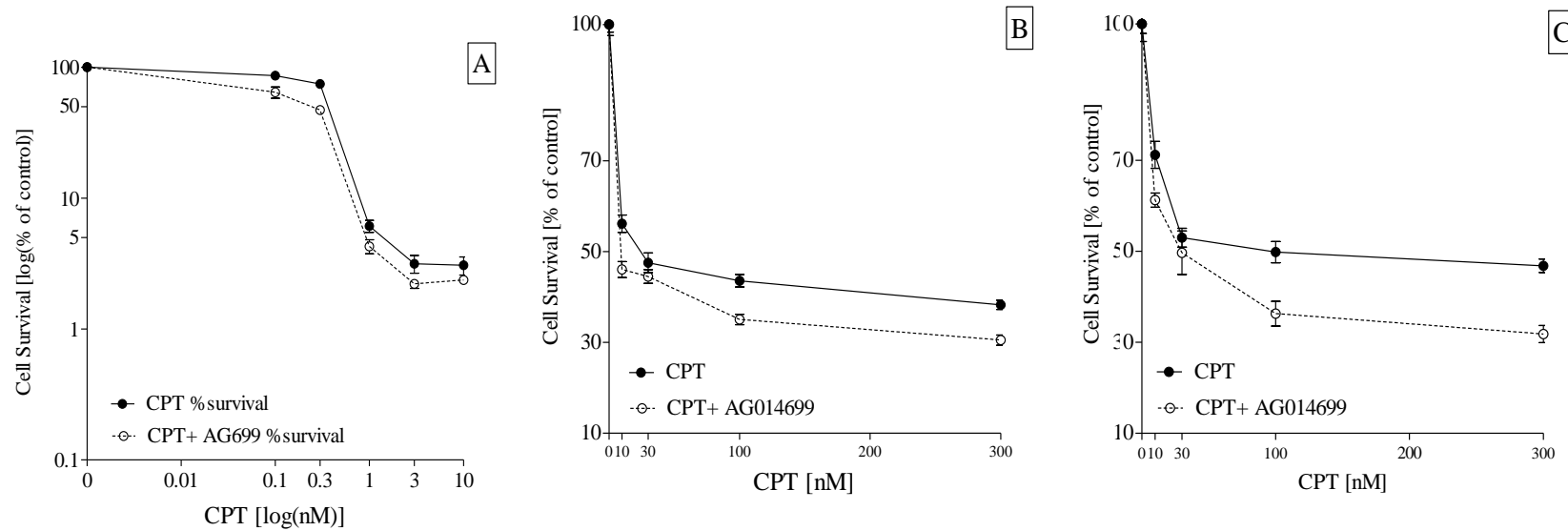


Figure 3. 1. Effect of 0.4 μ M AG014699 on CPT induced cytotoxicity in Lovo cell line.

(A) Lovo cells treated with 0.1, 0.3, 1, 3, and 10 nM CPT \pm AG14699 for 24h. (B) Lovo cells treated with 10, 30 100 and 300 nM CPT \pm AG14699 for 1h. (C) To mimic elutriation outcome where adherent cells have no time to attach to the plate, Lovo cells were trypsinised, re-suspended in fresh medium and treated with 10, 30 100 and 300 nM CPT \pm AG14699 for 1h. Plot shows pooled means from at least 3 independent experiments

	% survival		
	adherent	suspension	adherent/suspension ^{p-value}
30 nM	47.6±2.1	53.0±2.1	0.9 ^{ns}
30 nM + AG14699	44.5±1	49.7±4.8	0.9 ^{ns}
potentiation	<i>1.1^{ns}</i>	<i>1.1^{ns}</i>	
100 nM	43.6±1.4	49.8±2.3	0.9 ^{ns}
100 nM + AG14699	35±1.1	36.3±2.7	1 ^{ns}
potentiation	<i>1.2^{**}</i>	<i>1.4^{**}</i>	

Table 3. 1. Comparison of survival of adherent and suspension Lovo cells.

The values of cell survival obtained from each of 3 independent experiments for 30 and 100 nM CPT±AG014699 were used to determine differences between adherent and suspension Lovo cells using t-student test. Data represent mean ± SEM. Statistically significant differences at level .05 were denoted using *

** - p<0.001, CPT vs. AG014699

ns – Not significant at p=.05

3.3.2. Separation of Lovo cell into different cell cycle fractions by centrifugal elutriation

To obtain significant quantities in different phases of the cell cycle for subsequent experimentation, large quantities of exponentially growing asynchronous cells were required.

Separation of the Lovo cell line into G1, S, and G2 cell cycle phases was performed by centrifugal elutriation as described in section 2.6. Typically, 1.5-2.5x10⁸ cells in exponential growth phase were collected by trypsinisation, spun down, re-suspended, and dispersed into a single cell suspension in 5 ml medium using a syringe with needle. The prepared cell suspension was injected into the elutriation chamber and subsequent fractions were washed out by increasing the flow rate of elutriation buffer. Collected fractions were analysed for the presence of cells in the specific cell cycle phase by flow cytometry.

Figure 3. 2 shows the cell cycle distribution of asynchronous Lovo cells and isolated cell cycle fractions. In exponential growth phase the cell cycle distribution of Lovo, contained 45% cells in G1, 40% in S and 20% in G2-phase. Eventually, elutriation allows separation of Lovo cell into fractions enriched in cell cycle phase specific cells to a maximum of 90% for G1, 55% for S and 65% for G2 cells. The efficiency of

elutriation for Lovo cell line was very poor. The fraction collected during elutriation contains maximally 60% of cells injected into elutriation chamber. The rest of the cells remain in chamber until the end of elutriation process. Despite many attempts, it was problematic to obtain better efficiency and purer cell cycle fractions. Lovo cells are very difficult to disperse into single cell suspension. Additionally, dispersed cells when introduced to the elutriation chamber tend to create multi cellular clumps that disturb buffer flow through the chamber, which significantly reduces resolution of collected fractions. Another disadvantage of the Lovo cell line is the presence of a population of aneuploid cells that contaminates S and G2 fractions.

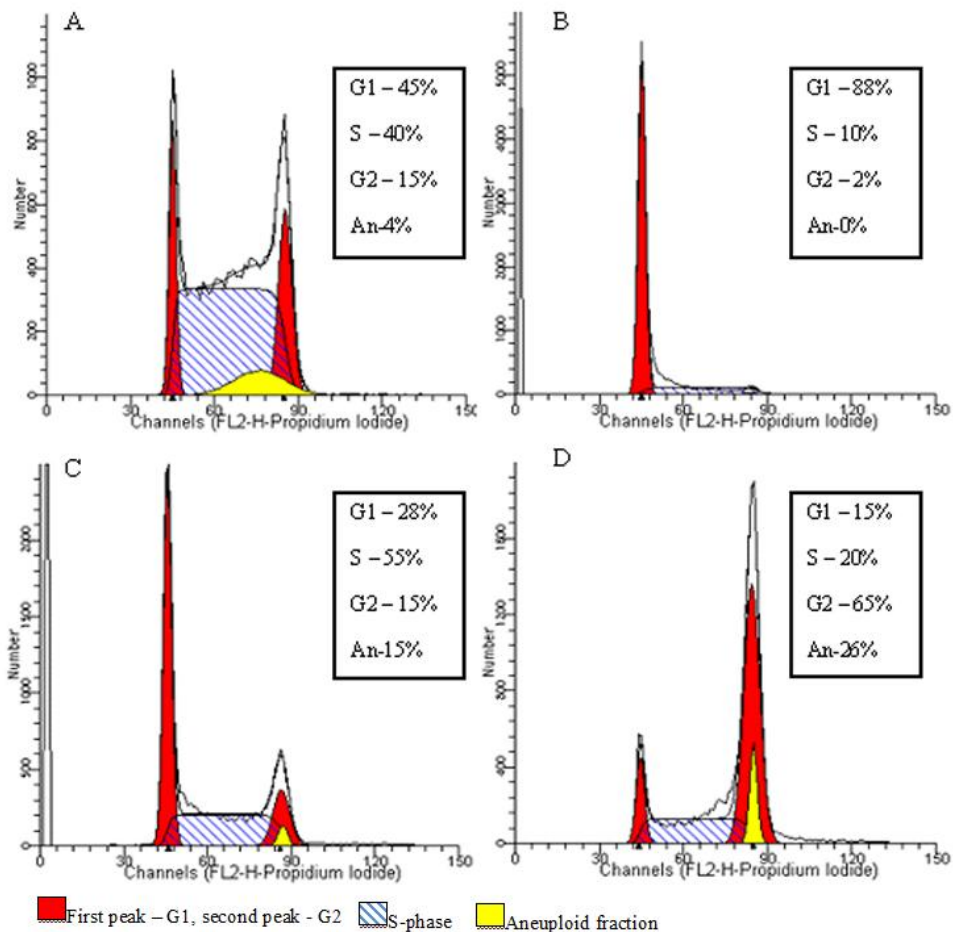


Figure 3. 2. DNA histograms of asynchronous and elutriated Lovo cells.

Asynchronously growing Lovo cells (A) were elutriated into specific cell cycle phase (B – G1, C – S, D – G2) and cell cycle distribution of collected fractions was analysed by flow cytometry. Obtained data were processed with ModFit LT software that allows automatic detection of cell cycle phases and ploidy of analysed cells.

3.3.3. Effect of AG014699 on CPT-induced cytotoxicity in elutriated Lovo cells.

Previous experiments confirmed that CPT±AG014699-induced cytotoxicity in adherent Lovo cells is similar to cytotoxicity in Lovo cells treated in suspension. Therefore, it should be possible to conduct similar experiments on elutriated cells.

The AG014699-induced potentiation of CPT-induced cytotoxicity was investigated by clonogenic assay in Lovo cells synchronised in specific cell cycle phase by elutriation. The content of cell cycle phase specific cells in each collected fraction was determined by flow cytometry and fractions containing 88% of G1, 55% of S and 65% of G2-phase cells were used for cytotoxicity assay.

Table 3. 2 shows data collected from one successful experiment, therefore it should be interpreted with caution. The treatment of cell cycle phase synchronized Lovo cells with CPT at concentration of 30 nM reduced cell survival in all cell cycle fractions, but this was more pronounced in S phase. Increasing the concentration to 100 nM did not cause any further reduction in cell survival of G2 cells, but there was a modest decrease in G1 with a greater effect seen in S phase.

AG014699 potentiated CPT-induced cytotoxicity only in S phase separated cells by 1.6-fold for 30nM CPT and by 1.9-fold for 100 nM CPT. CPT-induced cytotoxicity was unaffected by AG014699 in G1 and G2-phase cells. This most likely suggests that G1 and G2 phase cells are a resistant population found in asynchronous cells (Table 3. 2).

The results presented here cannot be verified, as no other successful experiments were performed, but the data are in agreement with other reports that show S phase specific cytotoxicity of TopoI poisons. The difficulties of trying to obtain pure G1, S, and G2 fractions made Lovo an unsuitable model for these studies; therefore, studies with this cell line were discontinued in favour of cells that grow in suspension.

	% survival		
	G1	S	G2
30 nM	53.2	36.1	57.4
30 nM + AG14699	58.3	21.9	57.5
potentiation	<i>0.9</i>	<i>1.6</i>	<i>1.0</i>
100 nM	45.3	26.0	58.5
100 nM + AG14699	59.3	13.6	53.6
potentiation	<i>0.8</i>	<i>1.9</i>	<i>1.1</i>

Table 3. 2. Effect of AG14699 on TopoI poison (CPT) induced cytotoxicity in Lovo cells elutriated on G1, S, and G2 cell cycle phases.

To confirm the S phase specific cytotoxicity, cells were separated by centrifugal elutriation into G1, S, and G2 phases prior to drug treatment. The table presents data from a single experiment where Lovo cells were elutriated treated for 1h with CPT±AG14699 before plating for colony formation.

3.4. Effect of PARP1 inhibitor on TopoI poison-induced cell cytotoxicity in elutriated and asynchronously growing K562 cells.

Because of the disadvantage of Lovo cells for efficient elutriation, this cell line was replaced by the K562 human myelogenous leukaemia cell line. Several published papers describe usage of various elutriation systems for cell cycle synchronisation of K562 cells confirming excellent predisposition of this cell line for the elutriation process (Kauffman et al., 1990, Banfalvi et al., 2007). The elutriation efficiency reported in those publications corresponds to the efficiency obtained with the protocol applied for experiments performed in this thesis.

The K562 cell line has also been used for the investigation of the effect of PARP1 inhibition on TopoI poison-induced cytotoxicity in earlier studies, where it was reported that K562 cells respond to PARP1 inhibitor-TopoI poison treatment (Smith et al., 2005).

3.4.1. Growth of asynchronous K562 cells.

The purpose of this experiment was to find the optimal seeding density for K562 cells for routine maintenance of cells in culture and preparation of large quantities of exponentially growing cells. The K562 cells were seeded at a density of 1×10^4 cells/ml and allowed to grow to maximal density. The growth was examined by counting of cells at 24h intervals. Two passages were performed using cells taken from the stock culture whose growth curve is shown on Figure 3. 3 Curve A. The first passage, occurred when cells were in exponential growth phase at density of 4.6×10^5 cells/ml (Figure 3. 3 Curve B) and the second, when cells reached confluent phase at a density of 1.5×10^6 cells/ml (Figure 3. 3 Curve C). The growth kinetics of cells taken from an exponentially growing culture was unaffected and rapid. However, when cells were re-seeded from a confluent culture, their growth was markedly reduced. (Figure 3. 3 Curve C). Based on these data, to obtain sufficient numbers of cells, K562 cells were seeded at a density of 1×10^4 cells/ml 3 days before the elutriation experiment. All subsequent experiments were done using cells taken from exponentially growing culture whose density did not exceed 5×10^5 cells/ml.

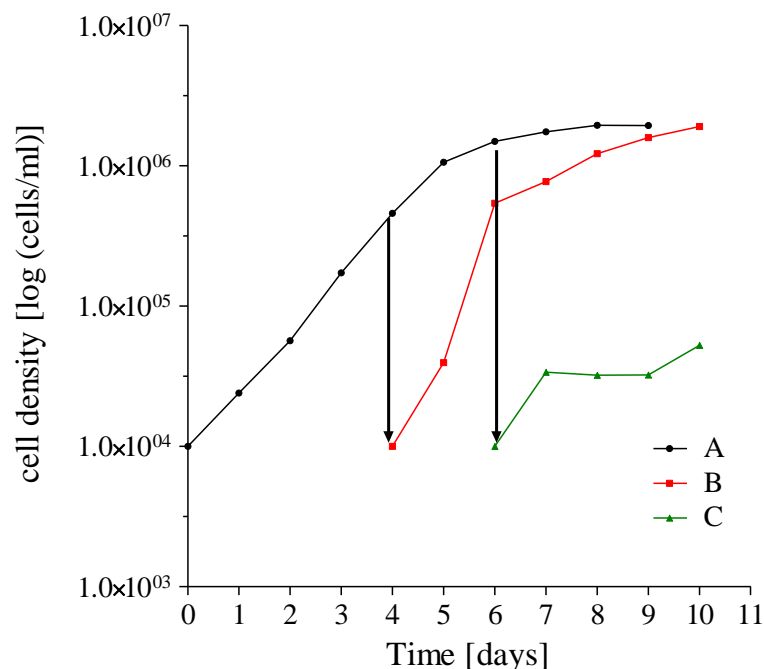


Figure 3. 3. Growth curve for K562 cells

Asynchronous K562 cells were seeded at a density of 1×10^4 (Curve A) cells/ml and counted every 24 hours. After reaching density 5×10^5 (Curve B) and 1.2×10^6 (Curve C) cells/ml cells were re-seeded at a density of 1×10^4 cells/ml and counting was repeated every 24 hours.

3.4.2. Separation of K562 cells into different cell cycle fractions by centrifugal elutriation.

To obtain a sufficient number of cells in each fraction for subsequent experiments, $1.5\text{--}2.5 \times 10^8$ of exponentially growing K562 cells were usually used. Cultured cells were collected by centrifugation, re-suspended in 5 ml medium, and injected into the elutriation system. By increasing stepwise the velocity of buffer flow, 16 fractions were collected and their purity was analysed by flow cytometry and the purest fractions were selected for subsequent experiments. Figure 3. 4 shows a representative analysis of the cell cycle distribution of K562 cells taken from asynchronously growing culture and the distribution of elutriated fraction selected for subsequent experiments. In exponential growth phase, the K562 cell culture consisted of 35% of G1, 54% of S and 11 % of G2-phase cells (Figure 3. 4 A). Depending on the number of cells used for elutriation, it was possible to obtain between 1.5×10^7 and 4×10^7 cells in fractions most enriched (above 85%) with a cell cycle phase specific cells (Figure 3. 4 B, C, D).

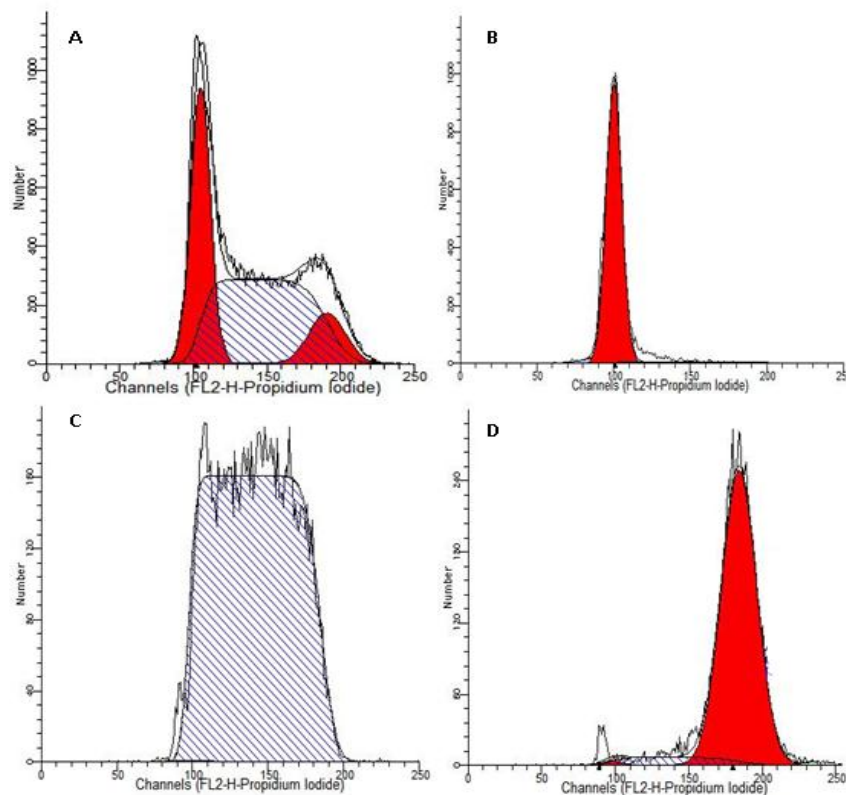


Figure 3. 4. DNA histograms of asynchronous and elutriated K562 cells

K562 cells were subjected to elutriation as described in material and methods. Among 18 collected fractions, fraction enriched with G1, S, and G2 cells were used for subsequent experiments. Representative DNA histograms of asynchronous (A), G1 (B), S (C) and G2 ((D) cell cycle phase are shown.

As the cytotoxicity of TopoI poisons is cell cycle phase-related, determination of the duration of each phase was necessary to ensure that drug-treatment is performed at the appropriate time. To accomplish this, K562 cells synchronized in G1-phase were allowed to grow in an incubator and progression to next cell cycle phase was verified by flow cytometry every 2h (Figure 3. 5). Results presented in Figure 3. 5 show changes in cell cycle distribution of G1 cells over the time and progression to next cell cycle phase. Cells were synchronized in G1-phase and placed in an incubator directly after elutriation (Figure 3. 5 A). Progression to the next phase was almost complete by 4 hours (Figure 3. 5 B, C). At that time more than 90% of synchronised G1 cells moved to S phase. The S phase was lasted for the next 4h (Figure 3. 5 D, E). Between hour 8 and 10 of incubation, S phase cells entered G2-phase (Figure 3. 5 F). These results shows that synchronized cells should be exposed to drug within the first hour after elutriation and this was rigorously applied for all subsequent experiments.

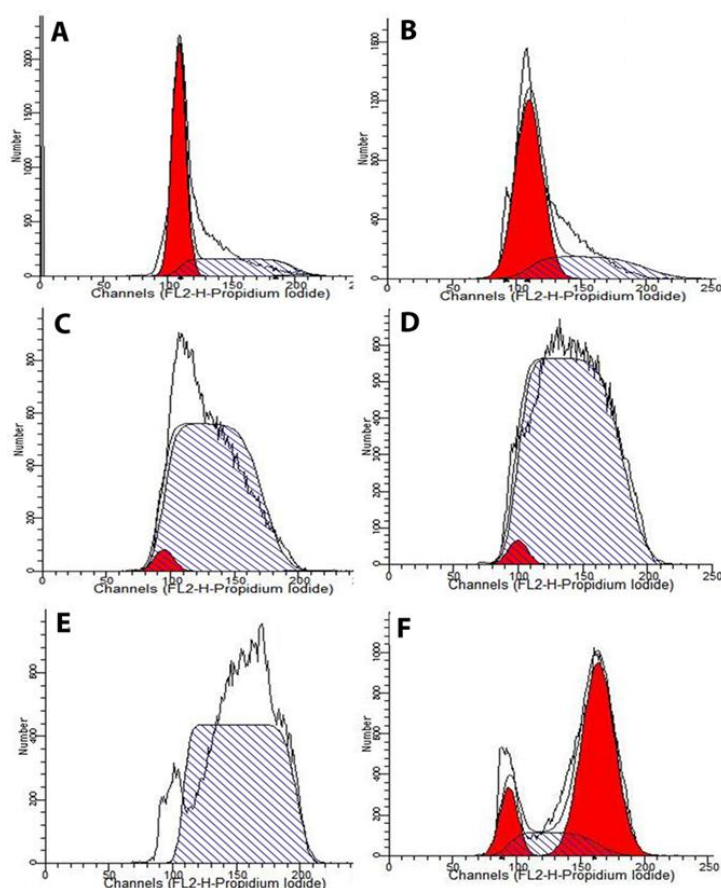


Figure 3. 5. DNA histograms of progression through cell cycle of K562 cells elutriated on G1-phase K652

K562 cells were elutriated and G1 phase cells were seeded and incubated for 0 (A) 2 (B), 4 (C), 6 (D), 8 (E) and 10 (F) hours. Flow cytometry analysis of cell cycle was performed after each time point and DNA histogram was plotted. Representative histograms are shown.

3.4.3. Effect of elutriation process on K562 cell growth.

Within the 2 hours that were required to complete the elutriation process, cells experience various procedures, which can be damaging to them. To ensure that the elutriation process does not have a negative impact on cells, their ability to grow after elutriation was investigated.

Exponentially growing K562 cells were subject to elutriation as described in material and methods (section 2.6.1). Collected fractions were analysed by flow cytometry, and fractions that contained above 85% of cells in G1, S and G2 cell cycle phase were selected for XTT assay, which was performed every 24 hours. The growth curves for K562 cells separated by cell cycle fractions were compared with growth curve of asynchronous un-elutriated cells and are presented in Figure 3. 6. There were no statistically significant differences between the growth rate of asynchronous cells and elutriated cells, which confirms that the elutriation process is not harmful to cells.

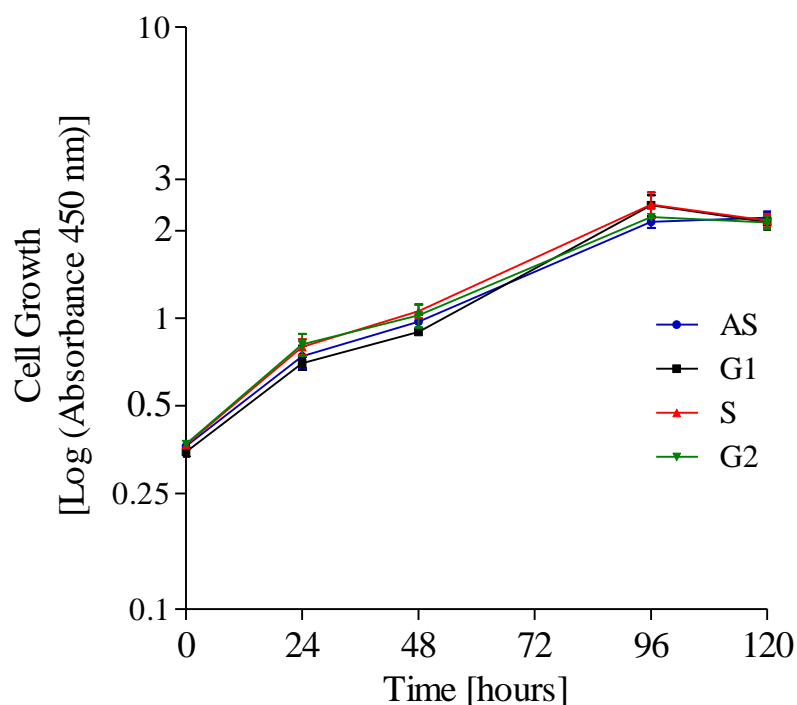


Figure 3. 6. Growth curve for asynchronous and elutriated on G1, S and G2 cell cycle phases K562 cells.

K562 cells were elutriated in sterile condition. Asynchronous, G1, S, and G2 cells were seeded at 2000 cells/well in 96 well plates. The XTT assay was performed at 24-hour intervals. Growth curves represent Mean \pm SEM from 3 independent experiments.

3.4.4. Effect of AG014699 on TopoI poison-mediated growth inhibition in asynchronous and elutriated K562 cells.

As was demonstrated earlier in this chapter, AG014699 potentiated CPT-induced cell cytotoxicity in asynchronous and S phase elutriated Lovo cells. The purpose of this experiment was to ensure that a similar effect could be observed in K562 cells that were chosen as a better model for the elutriation.

The effect of PARP inhibition on CPT-induced cytotoxicity in K562 cells was previously investigated using the PARP inhibitor, AG14361 at a concentration (0.4 μM) that reduced cellular PARP-1 activity by 90%, but did not have a growth inhibitory effect on K562 cells (Smith et al., 2005). Treatment conditions applied in our experiment refer to those used by Smith, where potentiation of AG14361 was investigated in K562 cells exposed to CPT for 30 min. In the growth inhibition experiment here, K562 cells were exposed to 3 nM and 10 nM CPT \pm 0.4 μM AG014699 for 1h to evaluate the effect of the drugs in relation to cell cycle phase.

The K562 cells were separated into cell cycle fractions by centrifugal elutriation. The content of cell cycle specific cells in each collected fraction was evaluated by flow cytometry and fractions containing above 85% cells in specific cell cycle phase were used for growth inhibition experiments. After 1h exposure to CPT \pm AG014699, drugs were removed from the medium by centrifugation and cells were allowed to grow in drug free medium for 5 days. The growth inhibitory effect of CPT \pm AG14599 was determined by XTT assay.

Data presented in Figure 3. 7 shows that CPT has only a modest effect on the growth of asynchronous cells, for which there was no statistically significant differences in growth inhibition caused by 3 nM and 10 nM of CPT. For K562 cells synchronized in G1-phase, 1h incubation with 3 nM CPT decreased cell growth by 4% and with 10 nM CPT by 7%. A similar effect was recorded for G2-phase cells where 3 nM CPT reduced cell growth by 11% and 10 nM CPT by 15% compared to untreated G2-phase cells. The potentiation of CPT-induced growth inhibition by AG014699 was not statistically significant and did not exceed 10% in asynchronous, G1 and G2 cells exposed to 3 nM and 10 nM CPT. In contrast, statistically significant CPT-induced growth inhibition was observed in K562 cells synchronized in S- phase, where incubation with 3 nM CPT reduced cell growth by 17% ($p=0.03$), and with 10 nM CPT by 39% ($p=0.002$) compared to untreated cells. The growth of the S-phase cells exposed to 3 nM CPT was

significantly reduced (by 17%, $p = 0.038$) when cells were incubated simultaneously with CPT and 0.4 μM AG014699. Co-exposure of the S phase K562 to 10 nM CPT and AG014699 for 1h resulted in a further 10% growth reduction compared to cells treated only with 10 nM CPT, but this reduction was not statistically significant ($p=0.09$).

Data obtained in this experiment shows that the growth inhibitory effect of CPT \pm AG014699 in K562 and cytotoxicity induced by those drugs in Lovo cells were S phase specific. K562 cells were exposed to a lower CPT concentration than Lovo cells, which could explain the weaker inhibitory effect of CPT \pm AG014699 in K562 cells. Therefore, subsequent experiments were performed at higher CPT concentrations.

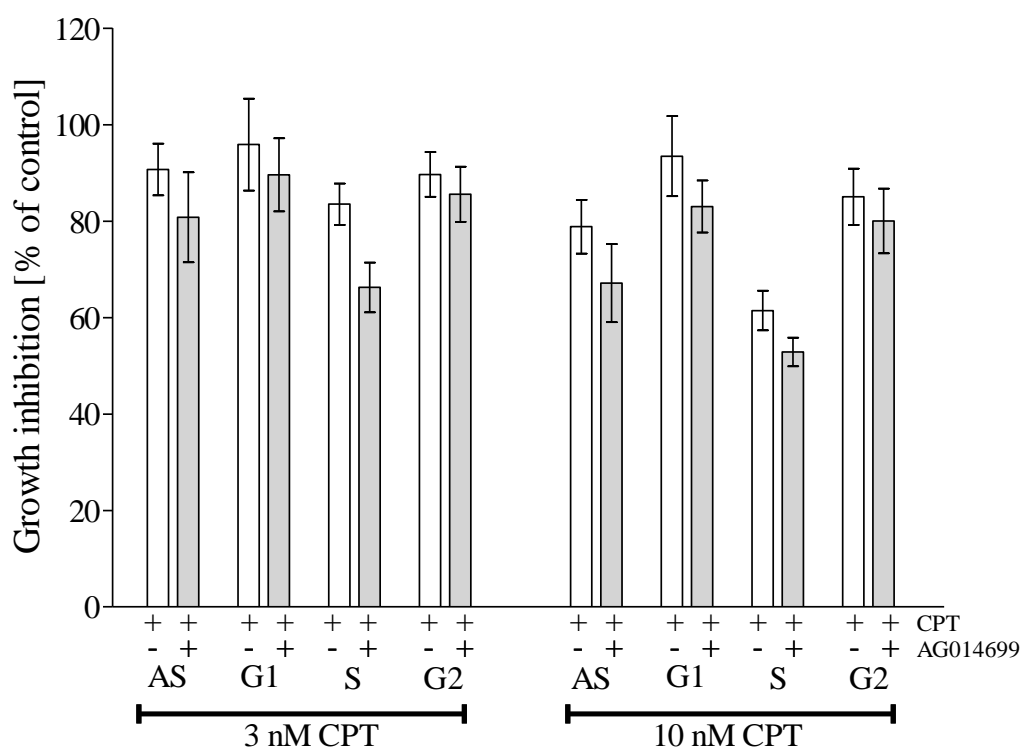


Figure 3. 7. Effect of AG4699 on camptothecin induced growth inhibition in asynchronous and elutriated K652 cells,

Elutriated and asynchronous K562 cells exposed to 3 and 10 nM camptothecin \pm 0.4 μM AG14699 for 1h. After treatment, cells were seeded at 1000 cells/well and XTT assay was performed after 5 days of culturing. Data are the mean of 3 independent experiment \pm SEM.

3.4.5. Effect of PARP1 inhibitor on TopoI poison-induced cell cytotoxicity in elutriated K562 cells.

The effect of anticancer drugs on cells can be measured by inhibition of cell growth and that may not reflect cell killing. The principle of the XTT assay is based on tetrazolium salt reduction by viable cells, and reflects the number of cells remaining after drug treatment. Results obtained from the XTT assay depend on proportional relationship of measured absorbance and the number of viable cell in culture. The measured signal may come from metabolically active cells whose fate is not yet decided. In addition a 50% reduction in XTT readout could represent: a) killing of 50% of the cells, with the remaining 50% growing at the same rate as controls or, b) a reduction of the growth rate of all of the cells such that they underwent one less cell doubling compared to control cells during the culture period, or c) a combination of some cell kill and some reduction in growth rate. For this reason XTT assays should be considered as growth inhibition rather than cytotoxicity assays. To determine how many cells are actually killed a colony forming, or clonogenic, assay must be performed. The clonogenic assay evaluates cell viability based on ability of single cells to re-proliferate and form a colony after exposure to drug. This assay more precisely represents the cytotoxic drug effect as opposed to the cytostatic effect, which can be important in the case of drugs whose activity is time-dependent. The clonogenic survival of K562 cells was investigated for determination of cytotoxic effect of camptothecin and its potentiation by AG14699.

The data presented in section 3.4.4 shows that CPT-induced growth inhibition and its potentiation by AG014699 in KS62 cells is highest in S-phase. To confirm that this represents enhanced cell killing, potentiation of CPT-induced cytotoxicity in KS62 cells by AG014699 was evaluated by clonogenic assay. As the CPT concentration used in growth inhibition experiments appeared to be too low for IC₅₀ determination, the clonogenic assay was done using higher concentrations.

K562 cells were elutriated to obtain fractions enriched in G1, S and G2 cells.

Asynchronous and elutriated cells were then exposed to camptothecin in the presence or absence of 0.4 μ M AG14699 for 1h and plated out at a known density for colony formation.

The result in Figure 3. 8 show that CPT-induced cytotoxicity was concentration-dependent for asynchronous and elutriated cells. CPT (10nM) significantly reduced cell viability in AS ($p=0.034$) and S-phase cells ($p=0.005$), but not in G1 ($p=0.06$) and G2-phase cells ($p=0.069$) when compared to un-treated cells. Incubation of cells with 100 nM CPT was significantly cytotoxic in all assayed cell fractions ($p<0.0006$). Cytotoxicity induced by 10 nM CPT in S-phase cells was significantly 1.4-fold ($p=0.02$) higher than cytotoxicity induced by 10 nM CPT in G1- phase cells, but not significantly different from 10 nM CPT in G2-phase ($p=0.19$). Cytotoxicity induced by 100 nM CPT in S-phase was 2.7-fold higher than in G1-phase ($p=0.0001$) and 3.4-fold greater ($p=0.004$) than in G2-phase. In S-phase cells AG014699 caused a significant 2.4-fold potentiation of the cytotoxicity of 10 nM CPT ($p=0.02$) and 1.9-fold ($p=0.04$) potentiation of 100 nM CPT. AG014699 also potentiated CPT-induced cytotoxicity by 1.3-fold at 100 nM in G2-phase cells. AG014699 did not significantly increase CPT-induced cytotoxicity in G 1 cells.

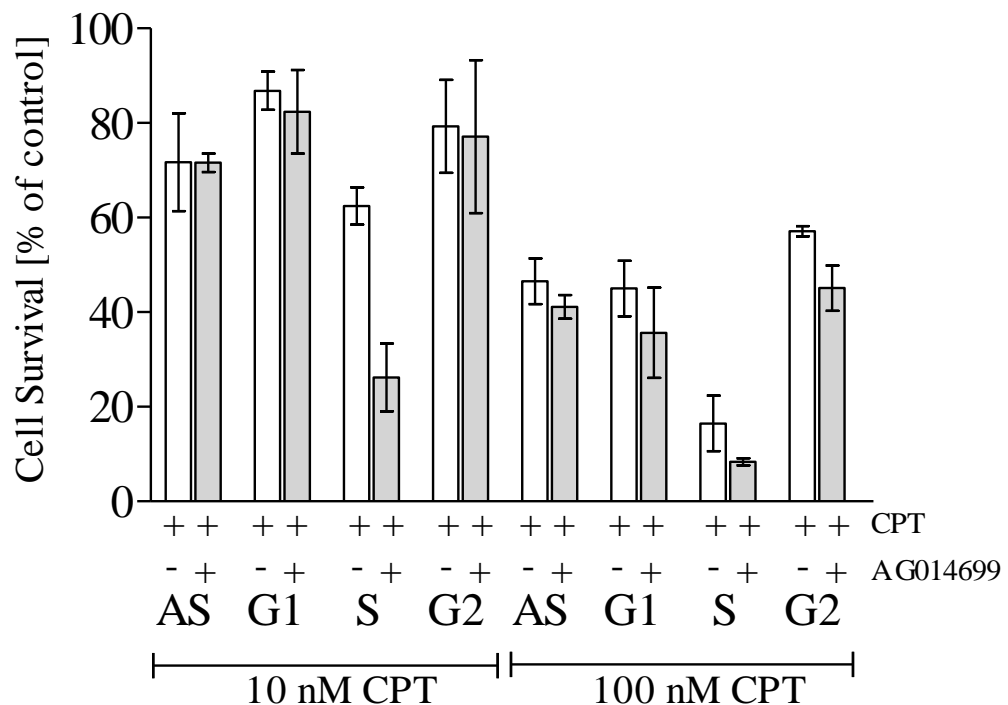


Figure 3. 8. Effect of AG14699 on CPT induced cytotoxicity in asynchronous and elutriated K562 cells.

Asynchronous and elutriated cells in G1, S and G2 cell cycle phases K562 cells were exposed to 10 and 100 nM CPT \pm 0,4 μ M AG14699 for 1 h. Cytotoxicity was measured by sloppy agar clonogenic assay and expressed as percentage of control. Data are mean of 3 independent experiments \pm SEM.

3.5. Variation in TopoI activity in different cell cycle phases

The results presented in the previous section show that AG014699 had the biggest impact on CPT-induced cytotoxicity in K562 cells synchronized in the S phase of the cell cycle. It is also generally known that the cytotoxicity of CPT that is characteristic of S phase cell cycle is associated with the process of DNA replication. As has been described in the introduction of this thesis, one possible mechanism responsible for the resistance of cells to CPT-induced cytotoxicity is *via* reduction of TopoI activity.

According to the hypotheses described in the introduction to this chapter, reduced activity of PARP-1 can re-activate and enhance the ability of TopoI to bind to DNA and thereby increase the amount of DNA damage, however, there is no evidence connecting this observation with TopoI activity in a particular cell cycle phase. Therefore, in this section, the TopoI activity was measured in different phases of the cell cycle in order to correlate the activity of TopoI with the cytotoxicity of CPT and the effect of AG014699 on the cytotoxicity induced by CPT.

TopoI activity was measured for cells in the different phases of the cell cycle that were obtained by the elutriation of asynchronous K562 cells. The method used to measure the activity of TopoI has been described in detail in section 2.8 and is based on the ability of TopoI to relax supercoiled plasmid DNA in the reaction medium, which lacks of ATP thereby preventing TopoII-mediated relaxation.

For this purpose, cells synchronized in G1, S, G2, and asynchronous K562 were used to prepare nuclear extracts, which after measuring the protein concentration were diluted in order to obtain the same amount of protein in an equal volume in order to keep reaction conditions constant. Then, a series of dilutions were prepared so that the lowest (0.01 µg) and highest (0.15 µg) correspond to the concentration of undetectable and detectable activity of TopoI relaxation, respectively. The results of this experiment are shown in Figure 3.9. This figure shows the product of reaction catalysed by TopoI as relaxed and supercoiled plasmid DNA separated on 1% agarose gel (Figure 3.9 A). The results of this reaction were quantitatively measured using the program ImageJ by measuring the integrated density of relaxed and supercoiled plasmid and presented in a graph (Figure 3.9. B and B1) as a percentage of the fraction of relaxed plasmid.

As expected TopoI relaxation activity increases with increased amount of nuclear extract present in the reaction mixture. The activity of TopoI varies between the phases of cell cycle. The largest fractions of relaxed plasmid were observed in the S phase cells, with nearly 100% of supercoiled plasmid being relaxed by 0.15 μg of nuclear extract. In G2 phase the activity of TopoI was approximately 20% lower for all nuclear extract concentrations comparing with TopoI activity in S phase. For 0.15 μg of nuclear extract prepared from G1 and asynchronous cells relaxed less than 40% of supercoiled plasmid.

The high activity of TopoI in G2 phase and residual activity in G1 phase can be possibly explained as a part of the S phase cells which contaminates the G1 and G2 fractions. The TopoI activity observed in G1 fraction may be related to a portion of G1 cells which transverse to S phase after elutriation was completed. The number of S phase cells contaminants in G2 fraction can be estimated approximately at 15% - 20%. This is possible because of the last 3 to 4 fractions of cells collected during elutriation were combined together to obtain enough G2 phase cells for subsequent experiments. Comparing the TopoI activity curves for S and G2 phase in Figure 3. 9 B1, these curves have a similar slope, however, the curve corresponding to G2 phase is shifted to the right. It is therefore possible the activity of TopoI derived from contamination of S phase cells was propagated linearly with increasing concentrations of nuclear extract, and suggests that the activity of TopoI in S phase is not only the main activity of TopoI, but most likely corresponds to the only TopoI activity observed in K562 cells.

These data convincingly correlate with the results obtained in section 3.4.5 and suggest that the highest cytotoxicity induced by CPT in the S phase of cell cycle may be related to highest activity of TopoI in the S phase.

In the next section, this discovery will be juxtaposed with the activity of PARP-1 in the different phases of the cell cycle.

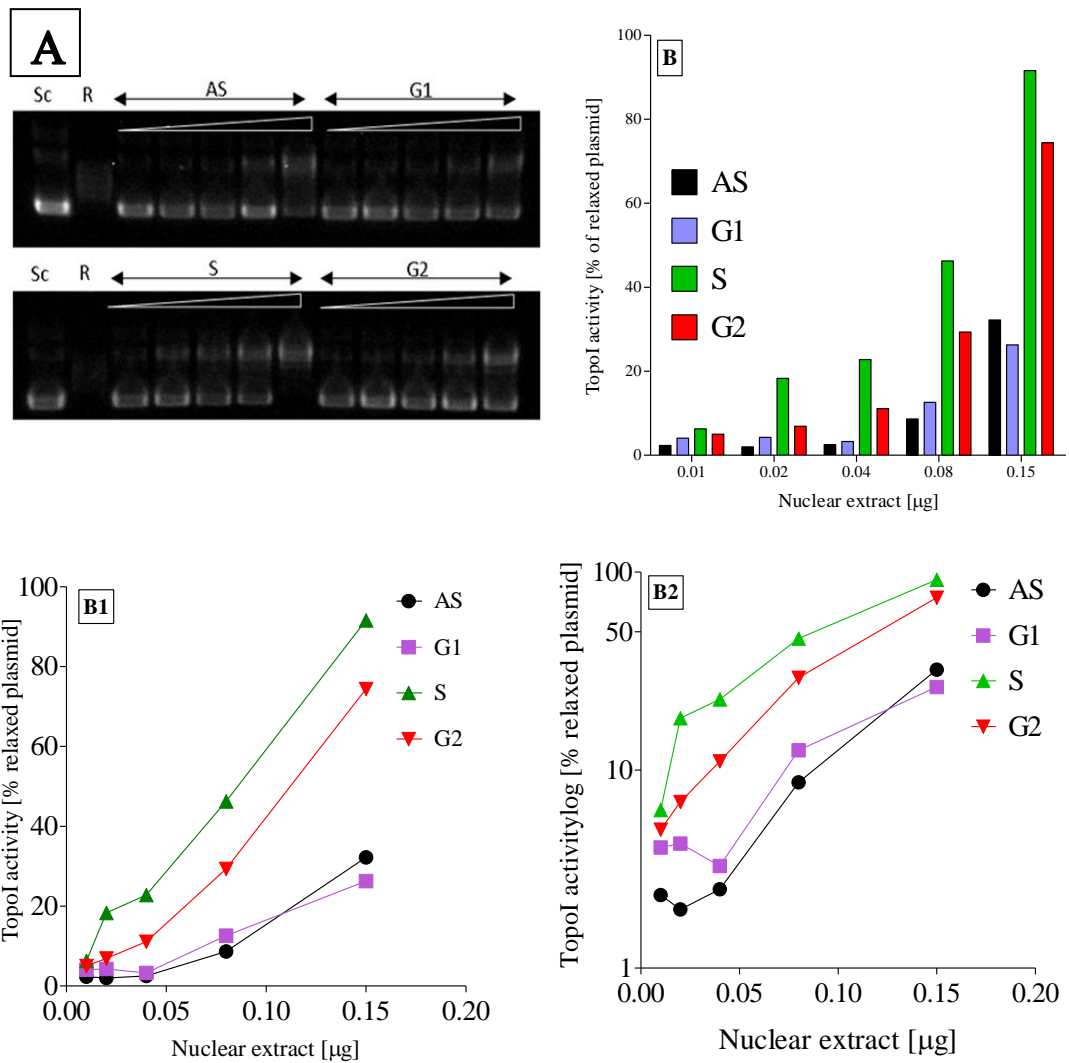


Figure 3. 9. TopoI relaxation activity in asynchronous and elutriated on G1, S and G2 K562 cells.

Nuclear extracts were prepared from asynchronous and elutriated cells. 1 μl of these extracts containing from 0.01 to 0.15 μg protein was incubated with 1 μg of supercoiled plasmid for 40 min. Reaction products were separated on agarose gel. A) Gel image - (Sc) is a negative control and corresponds to supercoiled plasmid, (R) is a positive control corresponding to relaxed plasmid. B, B1, B2) The gel was then quantified using ImageJ gel analysing options as described in section 2.8

3.6. Variation in PARP1 activity in different cell cycle phases.

The results described in the previous section indicate that the cytotoxicity induced by CPT in the different phases of the cell cycle is associated with TopoI activity in these phases. Because inhibition of PARP activity increased the cytotoxicity of CPT mainly in the S phase of the cell cycle it is possible that this is due to PARP being more active in the S phase as compared to other phases of the cell cycle. To investigate this possibility, PARP activity was measured in asynchronous K562 cells, as well as those separated into the G1, S, and G2 cell cycle phase using elutriation. This experiment was carried out exactly as described in section 2.9. Figure 3. 10 shows the activity of PARP is different in phases of the cell cycle. The lowest activity of PARP was observed in the G1 phase. PARP activity increases along with the progression of cells to the next phase of the cell cycle. In comparison to PARP activity in G1 phase the activity of this protein in S phase was significantly 1.6-fold higher ($p < 0.001$, LSD test). PARP1 activity in G2-phase was approximately 2-fold higher than in G1 phase ($p < 0.001$, LSD test) which exactly correlates with the increase in DNA content by cell cycle progression. Since the activity of proteins is often correlated with its expression in a cell, in the next section the level of PARP-1 and TopoI will be examined in elutriated fractions of K562 cells.

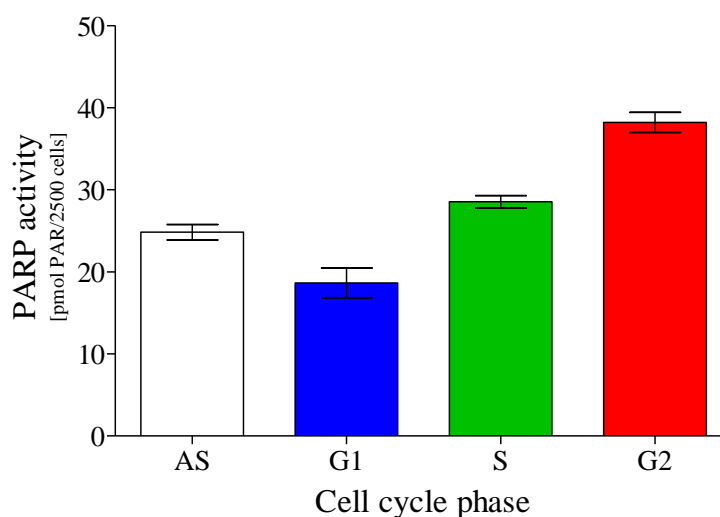


Figure 3. 10. PARP activity.

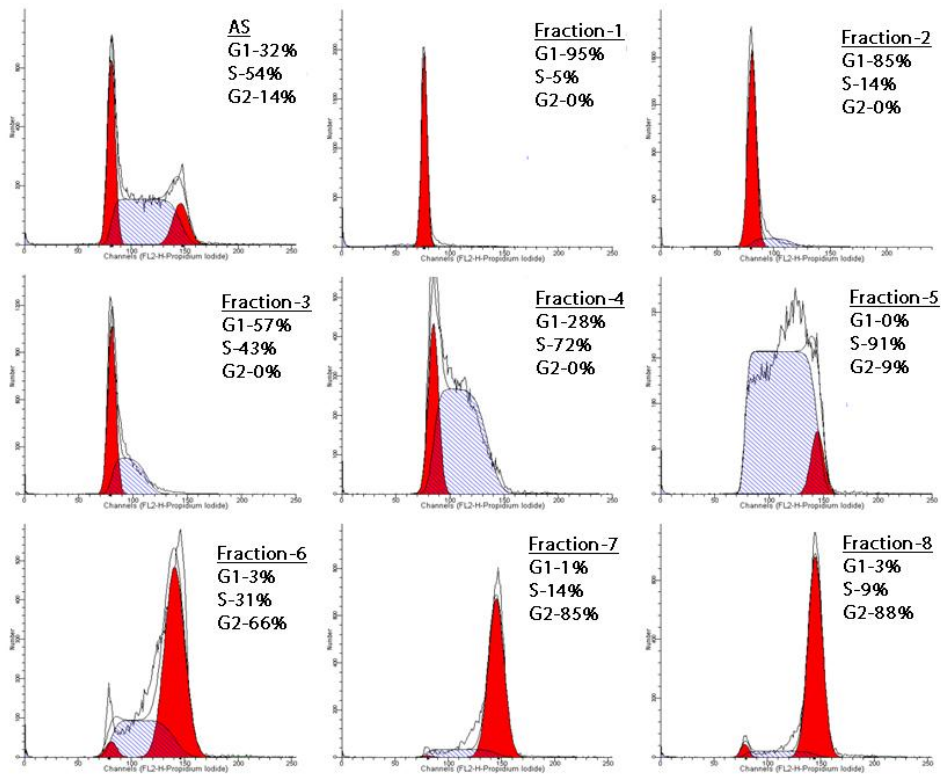
Exponentially growing K562 cells were elutriated and fractions containing >90% cells in G1, S and G2 cell cycle phase were used to measure PARP1 activity as described in section 2.9. Data are the mean \pm SEM of three independent experiments.

3.7. Variation in PARP-1 and TopoI proteins level in different cell cycle phases.

In many types of cancers, elevated levels of TopoI have been observed which is used as a marker for chemotherapeutic efficacy (Pfister et al., 2009). The level of protein in the cells is often correlated with its activity. However, if not, it means that for changes in activity, other factors such as post-translational protein modification may be responsible. The level of protein in K562 cells was measured by Western blot. For this purpose, K562 cells were elutriated and 8 consecutive fractions were collected and used to prepare protein extracts, which was separated by SDS page electrophoresis.

The results of this experiment are shown in Figure 3.11 On these graphs, it can be seen that the level of TopoI seems to increase with the progression of cells through subsequent phases of the cell cycle, even though its activity is higher in S phase than in G2. Therefore, it is possible that TopoI undergoes some post-translational activation in S phase. In contrast, PARP-1 expression showed a peak in S phase, but with otherwise constant levels of expression. Again, this does not correlate with the highest activity being observed in G2. Therefore, based on these data, both proteins are subject to post-translational activation or repressions.

A



B

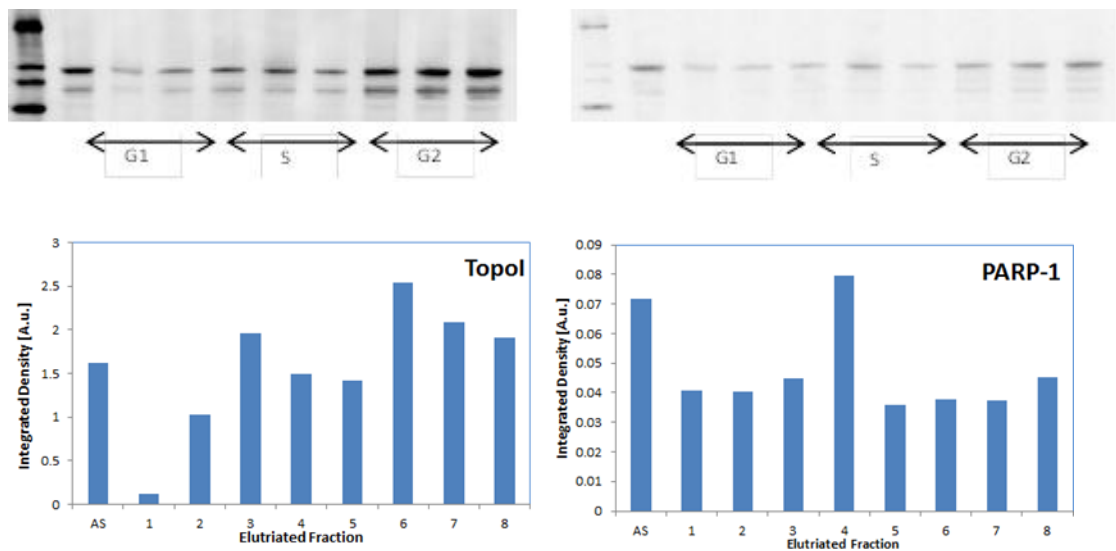


Figure 3. 11. TopoI and PARP-1 protein level in elutriated fractions of K562 cells.

K562 cells were elutriated into 8 subsequent fractions and DNA content was verified using flow cytometry (A). Cells from each fraction were used to obtain total protein extract that was used in Western blots, which were quantified with the aid of ImageJ Analyse Gel option (B). Figure shows data of one experiment. Data on the graphs shows the integrated density values for each band normalized to the integrated density of actin.

3.8. Discussion

The aim of this chapter was to investigate the cell cycle phase-dependence of the potentiation of TopoI poison-induced cytotoxicity by PARP inhibition using centrifugally elutriated cells. Originally, the Lovo colorectal cell line was tested, because TopoI poisons derivatives are used clinically to treat colon cancer (Armand et al., 1995, Magrini et al., 2002).

The data show that CPT-induced cytotoxicity was both time and concentration dependent. The level of cytotoxicity after 24h exposure of Lovo cells to CPT cannot be achieved with a short pulse treatment even for high CPT concentrations. CPT at a concentration of 10nM reduced the survival of cells by 50% after 1h and by 90% after 24h treatment. The shape of survival curves for 1h treatment shows that cytotoxicity reached plateau level at around 50-60% of survival. This indicates a sub population of resistant cells, most likely cell cycle phase-specific because the resistant population is lost when cells are exposed for a whole cell cycle. Based on the literature, this resistant population is likely to be cells that were not in S phase during the incubation period. The S phase selective CPT-induced cytotoxicity is also consistent with reports where CPT-induced cytotoxicity was reduced by the DNA polymerase inhibitor aphidicolin (Goldwasser et al., 1996, Borovitskaya and D'Arpa, 1998, Zhou et al., 2002). The cell cycle distribution analysis by flow cytometry shows that the population of asynchronously growing Lovo cells contains about 40% of cells in S phase (Figure 3. 2 A), which can be related to 50% of cells killed after 1h exposure. The differences can be explained by the fact that cells progressing from G1 to S and S to G2 would also be exposed during the 60 min. Comparing this with 24h exposure during which >90% of cells were killed suggests that virtually all cells will have gone through S phase.

Inhibition of PARP-1 activity by AG014699 in Lovo cells resulted in potentiation of CPT induced cytotoxicity during long and short pulse exposure to CPT. There was a 2-fold sensitization of CPT-induced cytotoxicity during 24h exposure, which supports previous reports (Bowman et al., 2001a, Calabrese et al., 2004, Smith, 2005). It was also observed that AG014699 potentiates CPT-induced cytotoxicity during a short pulse exposure, which appeared to be greater than at 24 hr. This may suggest that potentiation was greater for more sensitive S phase cells. To confirm the hypothesis, that the potentiation of CPT-induced cytotoxicity by AG014699 was S phase-specific CPT cytotoxicity in cell cycle phase synchronized cells was investigated. A cell cycle

block by chemical agents has been criticised because it may have impact on normal cell metabolism (Cooper, 2003). In the experiment here, instead of chemical agents, for cell cycle phase synchronisation, centrifugal elutriation was used, therefore excluding the possibility that the cytotoxic effect may be compromised by the action of a chemical block.

Separation of adherent Lovo cells by elutriation involves different conditions for drug treatment where cells have to be exposed to the cytotoxic agent while being in suspension, which may result in unpredictable response to treatment. To eliminate this possibility, AG014699 potentiation of CPT-induced cytotoxicity was evaluated in Lovo cells that were exposed to drugs in suspension. The data obtained shows that CPT-induced cytotoxicity and its AG014699-mediated potentiation for cells treated in suspension is similar to adherent cells.

During work on the protocol, for optimisation for elutriation of Lovo cells it was found that this cell line was not an ideal model for this technique. For efficient elutriation, the cells have to be dispersed into single cell suspension, which was problematic for Lovo cells, as they tend to aggregate into multicellular clumps. The Lovo cell line is characterised as near diploid cell line with modal number of 49 chromosomes (Ribas et al., 2003). However, a subpopulation of aneuploid cells was shown to overlap with S and G2 fractions and compromise proper evaluation of elutriated fractions by flow cytometry.

Using these conditions, AG014966 potentiation of CPT-induced cytotoxicity was demonstrated for enriched in G1, S, and G2 cell cycle phase cells by clonogenic assay. Although it was only one successful experiment, CPT-induced cytotoxicity was greater for the S phase enriched cells, whereas G1 and G2 cells were 2-fold more resistant. There was a 2-fold sensitization of CPT-induced cytotoxicity by AG014699, which was selective only to S phase fraction.

Lovo cells were replaced by the K562 cell line, because of its better predispositions for elutriation. This cell line was used previously as a model to study TopoI poisons. (Padget et al., 2000).

The elutriation efficiency for K562 was greater than for Lovo cells, and this allowed collection of fractions where content of cell cycle specific cells was usually above 85% (Figure 3. 4). The growth of K562 was unaffected by elutriation procedures and

elutriated cells were able to reach their normal proliferating state directly after elutriation.

After 1h treatment, CPT had a similar effect in asynchronously growing K562 cells as in Lovo cells, with survival around 50% at 100nM in both cell lines. At concentration of 10 nM CPT was less cytotoxic in K562 cells, reducing their survival by 30% compared with a >50% reduction of survival in Lovo cells. AG014699 does not affect the cytotoxicity induced by CPT in asynchronous K562 cells, consistent with previous data showing that the cytotoxicity of short TopoI poison exposures are not increased by PARP inhibition (Smith, 2005). In contrast, there was a modest but significant 20-40% reduction in survival of Lovo cells, suggesting that the effect of AG014699 is cell specific. The differential effect cannot be explained by a higher fraction of S phase cells because the S phase population in Lovo cells is about 10% lower than that in K562 cells.

The results of cytotoxicity experiments with elutriated cells shows that in both Lovo (Table 3. 2) and K562 survival of G1 and G2 phase cells was 1.3 to 2-fold higher than S phase cells following a 1h exposure to CPT. K562 cells were marginally more sensitive than Lovo cells to 100 nM CPT in G1 and G2 and about twice as sensitive in S phase. AG014699 did not significantly enhance the cytotoxicity in either of the cell lines in G1 and G2 phase but there was approximately 2-fold sensitization of 100 nM in S phase of Lovo and K562 cells.

Consistently, S phase K562 and Lovo cells were approximately twice as sensitive to CPT as G1 or G2 cells. In both cell lines, AG014699 caused the greatest enhancement of cytotoxicity in S phase with little or no potentiation in G1 and G2. TopoI poison-induced cytotoxicity is often associated with the level of the TopoI protein in cells, which can be used as a biomarker of clinical efficacy of TopoI poison (Pfister et al., 2009). There is some evidence in the literature that protein levels and activity of TopoI changes during the cell cycle. For example, Tricoli et al. showed that activity of TopoI in synchronized cells of TopoI released from the block in the early G1 phase gradually increased, reaching a maximum in the S phase, and then decreased in the G2 phase at the same time increasing protein levels in this phase (Tricoli et al., 1985).

Meyer et al. also demonstrated cell-cycle phase dependent behaviour of TopoI. According to their research, activity and protein level of TopoI increased, when the cells pass from G1 to G2-M phase (Meyer et al., 1997). These studies support the results

presented here, which show that the level of TopoI in K562 cells increases during the progression from G1 to G2. The possibility that increased level of TopoI observed in G2 phase is caused by decreased binding with DNA during G2 phase and therefore better extraction efficiency cannot be excluded. However, this experiment was performed only once therefore these results should be interpreted with caution.

The very high level of TopoI activity in the S phase (~ 100% relaxation of supercoiled plasmid with 0.15µg nuclear extract – Figure 3.9) was consistent with the greatest level of CPT cytotoxicity in S phase (Figure 3. 8). The highest activity of PARP in G2 phase, but only a moderate effect of AG014699 on CPT-induced cytotoxicity observed in this phase, suggests that the role of PARP-1 plays in the G2 phase is not sufficient to cause cell death.

The highest killing rate in S-phase can be explained by implication of PARP-1 in the repair of CPT-induced DNA breaks. During S-phase the CPT stabilised cleavage complexes can be converted into highly cytotoxic replication-associated double strand breaks. Inhibition of PARP-1 at this point leads to impaired repair that result in the highest killing rate of S-phase cells. The S-phase specific mechanism of cytotoxicity enhancement by PARP-1 inhibitors is not exclusive to TopoI. Similar results were demonstrated by Liu et al, who used a different PARP inhibitor, ABT-888, to enhance temozolomide-induced cell cytotoxicity. Their results show that temozolomide-induced cell cytotoxicity and potentiating effect of ABT-888 was higher for cells synchronized by double thymidine block in S-phase than for cell treated during G1-phase. Increased cytotoxicity in S-phase was correlated with the level of DSB, which resulted from conversion of SSB induced by temozolomide treatment (Liu, Shi et al. 2008).

Here, for the first time cells synchronized without any stressful condition by centrifugal elutriation were used to investigate potentiation of TopoI induced cytotoxicity by inhibitor. S-phase specific AG14699 enhancement of CPT induced cell cytotoxicity implicates inhibition of DNA repair. To verify this hypothesis the level and repair of single and double strand breaks induced by CPT±AG14699 were measured in elutriated K562 cells as described in the next chapter.

Summary

- ✓ AG014699 potentiates TopoI induced cell cytotoxicity in asynchronous Lovo and K562 cells by 2-fold.
- ✓ Elutriation efficiency is better for K562 than Lovo cells
- ✓ Elutriation does not affect the growth of cells.
- ✓ The PARP inhibitor AG014699 potentiates TopoI poison-induced growth inhibition and cell cytotoxicity in K562 cells predominantly in S phase.
- ✓ TopoI activity is highest in S phase and TopoI protein levels increase along with cell cycle progression.
- ✓ PARP1 activity increase with cell cycle progression

Chapter 4. The effect of AG014699 on the formation and repair of CPT-induced DNA damage.

4.1. Introduction

Several lines of evidence in the literature show that inhibition of PARP-1 activity potentiates CPT-induced cytotoxicity. These observations have been connected with higher level of DNA breaks, observed in cells exposed to topoisomerase I poisons and a PARP inhibitor, compared to topoisomerase I poisons alone. One of the first reports providing such evidence came from Mattern *et. al*, who showed that the level of SSB in cells exposed to CPT, was higher when PARP-1 activity was inhibited with 3-AB (Mattern *et al.*, 1987). Other results showing the role of PARP-1 in the repair of TopoI poison-induced SSB include a study by Bowman *et. al*, who demonstrated that the activity of PARP-1 was increased by CPT and that inhibition of PARP-1 activity by a specific inhibitor NU1025, at concentration of 200 μ M, caused 2.5-fold enhancement of CPT-induced DNA breaks and a similar 2.6-fold increase in cytotoxicity in L1210 cells. These results demonstrated that the involvement of PARP-1 in TopoI-induced cytotoxicity is reflected by increasing the level of DNA breaks (Bowman *et al.*, 2001b)

Cleavage complexes stabilized by CPT are usually transient and disappear quickly after the withdrawal of the CPT. Various DNA lesion already present nearby TopoI-processed DNA can convert cleavage complexes into lethal lesions, usually due to collision with the replication fork or during transcription. Different types of TopoI poison-mediated DNA lesions implicate a number of repair pathways (described in section 1.5.4) including BER, NHEJ and HR. The evidence for interaction between TopoI and PARP-1 were described in the recent literature (Malanga and Althaus, 2004, Baumann *et al.*, 2006, Cimmino *et al.*, 2007). The results of cell-free system experiments performed by Malanga and Althaus, where short oligonucleotides and purified proteins were used, shows that poly ADP-ribosylated PARP-1 or free ADP-ribose polymers do not prevent the binding of TopoI to DNA or its dissociation. Poly(ADP-ribosylation) of TopoI resulted in two actions: decreasing DNA cleavage, and, when TopoI was already connected to DNA, increasing the ligation step. This was observed even when formation of cleavage complexes was enhanced by CPT (Malanga and Althaus, 2004). Related results were published by Park and Cheng, but according to those authors PARP-1 itself enhanced the TopoI relegation activity of CPT-stabilized cleavage complexes (Park and Cheng, 2005).

Studies of interactions between TopoI and PARP-1 investigated in intact cells provided conflicting results: Smith et al. 2005 used PARP-1 wt and PARP-1 null cells treated with the TopoI poison, topotecan, in the presence and absence of the potent PARP inhibitor AG14361, to demonstrate a) that PARP-1 was a determinant of sensitivity to topoisomerase I poisons and b) that AG14361 enhanced the TopoI poison-induced cytotoxicity in a PARP-1 dependent manner. These authors investigated the role of PARP inhibition on CPT-mediated TopoI-DNA cleavage complex formation in K562 cells using the TARDIS assay. Exposure of K562 cells to CPT alone in concentrations up to 10 μ M for 30 min showed a dose-dependent increase in the number of cleavage complexes, which was unaffected by co-exposure with 0.4 μ M AG14361. Similarly, AG14361 had no effect on TopoI-mediated relaxation of supercoiled plasmid measured in nuclear extracts from K562 cells treated with 0.4 μ M AG14361 for 30 min and 16h. In contrast, when DNA breaks were measured by alkaline elution, AG14361 was shown to increase the level of CPT-induced breaks. Moreover, AG14361 increased the persistence of DNA breaks at 30 min and 16 h after a 30 min pulse with CPT. These data suggest that PARP-1 activity does not regulate TopoI activity or cleavable complex formation but instead enhances the cytotoxicity of TopoI poisons by inhibiting repair of the DNA damage they induce.

The repair of TopoI poison-induced DNA damage involves several molecular pathways which protein components are common with BER or DSB repair pathways (section 1.5.4). This implicates the role of PARP-1 in DNA repair. With regard to the repair of CPT-induced DNA damage with BER, PARP-1 is proposed to be activated by CPT-induced DNA breaks to recruit XRCC1 (El-Khamisy et al., 2003). XRCC1 was shown to enhance the activity of TDP1 and PNK, which removes the TopoI from DNA leaving SSB behind (Plo et al., 2003). XRCC1 also participates in recruitment and assembly of other BER proteins including DNA polymerase β and DNA ligase III which complete the repair (Cappelli et al., 1997, Dianova et al., 2004).

Involvement of PARP-1 in the repair of CPT-induced DNA breaks is also supported by results obtained using cells defective in one of DNA repair mechanism. Cells defective in HR was shown to be 10-fold more sensitive to CPT, BER-defective cells were 5x more sensitive, but NHEJ-defective cells were only 30% more sensitive to CPT-induced cytotoxicity (Smith et al., 2005). These data suggest that HR is most important and BER next most important pathway involved in the repair of TopoI poisons-induced DNA damage.

The observations suggested by Mattern *et al.*, or by Smith *et al.*, that prolonged exposure to PARP inhibitors is required for its efficient sensitization of CPT-induced cytotoxicity, which is S phase dependent, is more consistent with the role of PARP-1 in DNA double strand break (DSB) repair.

PARP-1 was shown to be involved in DNA DSB repair by NHEJ possibly by involvement in a back-up non-homologous end joining pathway (B-NHEJ) (Audebert *et al.*, 2004, Audebert *et al.*, 2006, Audebert *et al.*, 2008, Iliakis *et al.*, 2008, Iliakis, 2009) and in HRR (Helleday *et al.*, 2005). Some evidence indicates that PARP and components of the NHEJ pathway compete in the repair of DSB (Veuger *et al.*, 2004, Wang *et al.*, 2006) but other evidence suggests they co-operate in the same NHEJ pathway (Mitchell *et al.*, 2009) and yet further evidence indicates that PARP has no role in DSB repair (Noël *et al.*, 2003).

Data from chapter 3 shows that S phase cells were most sensitive to the cytotoxicity of CPT and also that AG014699 had the most pronounced effect on cytotoxicity in S phase cells. Different, cell cycle-dependent, CPT-induced cytotoxicity and sensitization by AG0144699 could not be fully explained by PARP-1 or TopoI activity and protein level in each cell cycle phase. Another possible explanation for the S phase specific effect of AG014699 on CPT-induced cytotoxicity could be related to the role played by PARP-1 during induction or repair of DNA breaks caused by CPT. None of the studies previously conducted had investigated whether the effect of PARP inhibition on DNA breaks induction or repair is also cell cycle-phase specific.

4.2. Aims

The aim of this chapter was to investigate the effect of AG014699 on the formation and repair of CPT-induced DNA breaks in cell cycle-separated K562 cells. The possibility that the S phase-specific enhancement of CPT-induced cytotoxicity by AG014699 was due to S phase-specific inhibition of DNA repair was investigated by measuring the level of single and double strand breaks induced by CPT±AG014699 using alkaline, neutral comet assay and γ H2AX immunofluorescence after short exposure to drugs. The effect of PARP-1 inhibition on the recovery from CPT-induced DNA breaks was also investigated in asynchronous and cell cycle separated K562 cells.

4.3. The level of DNA damage in K562 cells measured directly after elutriation

Elutriation allows the separation of cells into cell cycle specific fractions avoiding usage of chemical compounds *e.g.* aphidicolin. However, during elutriation experiments, cells are exposed to a changing environment that may generate DNA breaks, for example, during sample handling, or when a highly condensed cell suspension is injected into elutriation system. The data presented in section 3.4.3 showed that the elutriation into cell cycle phase enriched fractions does not affect the growth of K562 cells.

Nevertheless, it was important to demonstrate that the elution process does not induce any background DNA breaks.

To exclude this possibility, exponentially growing K562 cells were separated into fractions enriched in G1, S or G2 cells as described in section 2.6.1. Fractions with the highest content of cell cycle phase-specific cells and an asynchronous population of cells were subjected to alkaline comet assay, and the extent of DNA damage was determined by measuring Olive Tail Moment (OTM) (as described in section 2.7).

Two independent experiments were performed and the results are given in Figure 4. 1, which shows a scatter plot of individual OTM values measured for each cell cycle phase-specific cells. Histograms shown in Figure 4. 2 indicate that OTM values of asynchronous as well as G1, S and G2 phase cells does not fit to a normal distribution, however this can be corrected by transforming data by calculation of logarithm or using BoxCox transformation (Box and Cox 1964). Histograms showing data after BoxCox power transformation were shown in Figure 4. 2 on the right panel.

Transformed values of OTM were used in statistical analysis in order to determine if there was a difference in the means of the OTM for two independent variables of the variable level of “cell cycle phase”- (asynchronous (AS), G1, S and G2) and the variable level of “experiment” - (exp1, exp2). For this purpose, variance analysis was applied with OTM as dependent variable and cell cycle phase and experiment as two independent categorical factors.

There were no significant differences among the means of OTM for cell cycle phase separated groups (AS, G1, S and G2) $F(3, 963) = 2.4$, $p = 0.07$ and between two analysed experiments $F(1,3) = 3.1$, $p = 0.08$. This indicates that the mean of OTM is the same between cell cycle phases and that there were no overall divergences between the two analysed experiments. These data conclusively demonstrate that the elutriation

process does not induce DNA strand breaks and that there are no consistent or significant differences between the different cell cycle phases in terms of DNA breakage or fragility.

There is inter assay variation that is commonly observed in comet assay (Tice et al., 2000), and in order to be able to pool experimental data and to compare between experiments, OTM was expressed as % of the asynchronous untreated control.

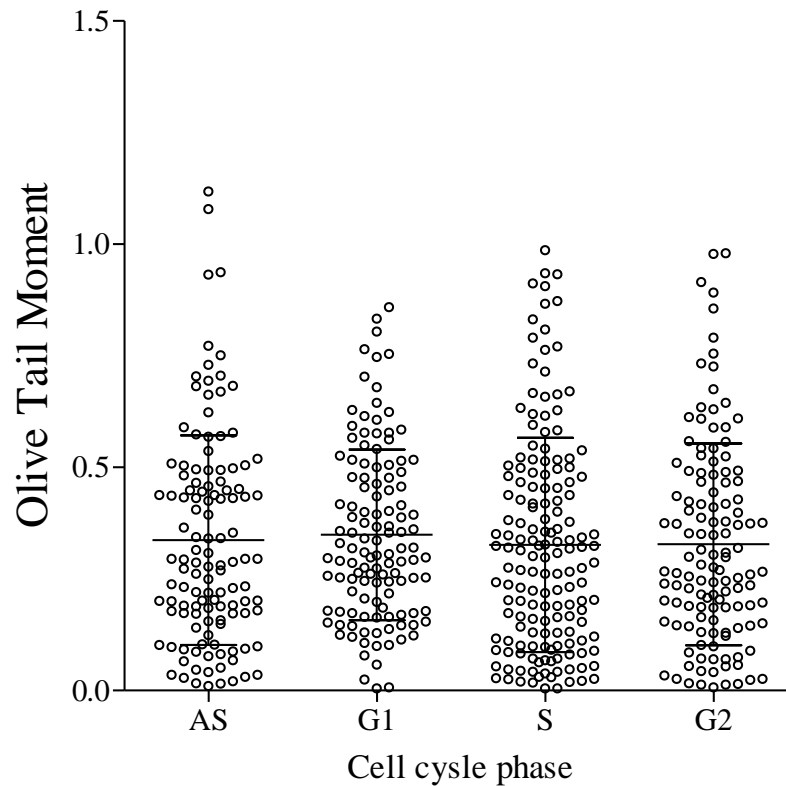


Figure 4. 1. OTM measured in K562 cells directly after elutriation.

Asynchronous K562 cells, and K562 separated into different fractions of cell cycle phases were separated by centrifugal elutriation and the level of total DNA damage was evaluated in these cells using alkaline comet assay. The extent of DNA breaks was given by calculating OTM for more than 100 cells scored in each independent experiment. Horizontal lines denote means and vertical bars denote SD obtained by pooling data from two independent experiments.

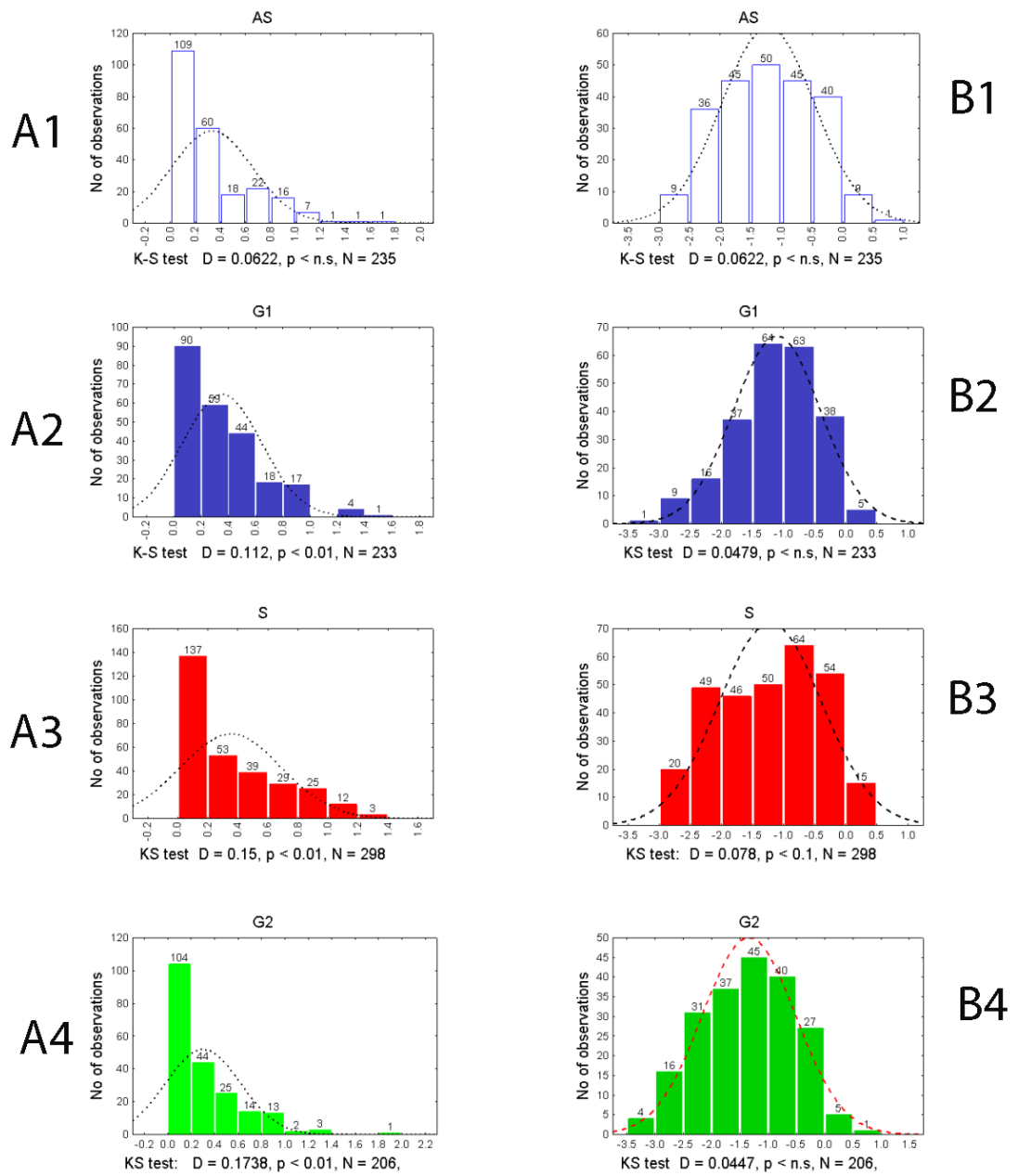


Figure 4. 2. Histograms of the Olive Tail Moment measured in populations of asynchronous and cell cycle separated K562 cells

Asynchronous cells (A1), cells elutriated into G1 (A2), S (A3) and G2 (A4) cell cycle phases. The effect of BoxCox transformation of the OTM is shown on the right (B1-B4), and was applied to correct not-normal distribution. The numbers beneath each figure shows the results of Kolmogorov –Smirnov test.

4.4. The effect of AG14699 on the level of DNA breaks induced by CPT in asynchronous cells and K562 cells separated into cell cycle subpopulations

In the previous chapter, AG014699 was demonstrated to potentiate CPT-induced cytotoxicity by 2-fold in Lovo cells after 1h and 24 h exposures to CPT. The results of clonogenic survival in elutriated populations of Lovo and K562 cells shows that sensitisation of CPT-induced cytotoxicity by AG014699 occurs predominantly in S phase. As described in the introduction, inhibition of PARP-1 sensitizes cells to CPT possibly via the role of PARP-1 in DNA damage repair or via regulation of TopoI activity (Malanga and Althaus, 2004). In this context, the results presented in this chapter were performed to verify the role of PARP inhibition in the generation of DNA breaks induced by CPT in each cell cycle phase.

To investigate the effect of AG014699 on CPT-induced DNA damage in different cell cycle phases, asynchronous K562 cells along with cells separated into specific cell cycle phases were exposed to CPT at concentration of 0, 10, 100 and 300 nM in presence or absence of AG014699 for 30 min. Following incubation, cells were quickly moved to centrifugal tubes, spun down, and re-suspended in cold PBS. All procedures after incubation were performed on ice in subdued light to avoid additional DNA damage. The level of total DNA breaks was evaluated with alkaline comet assay by measuring OTM. The images in Figure 4. 4 show representative comets for each treatment condition applied in this experiment. Comet tails are longer on images recorded for cells treated with CPT and AG014699 than in cells exposed to CPT alone. Data presented in Figure 4. 5 and collated in Table 4. 1 show an increase in the level of breaks with increasing concentration of CPT in all cell cycle phases. The lowest increase was observed in G1 phase cells and the largest increase in the level of DNA damage for all CPT concentration used for treatment was seen in S phase cells. Incubation of cells with AG014699 increased CPT-induced DNA damage in all phases of the cell cycle. The highest level of DNA breaks were seen in S phase cells treated with CPT and AG014699, followed by G2 phase cells (Table 4. 1).

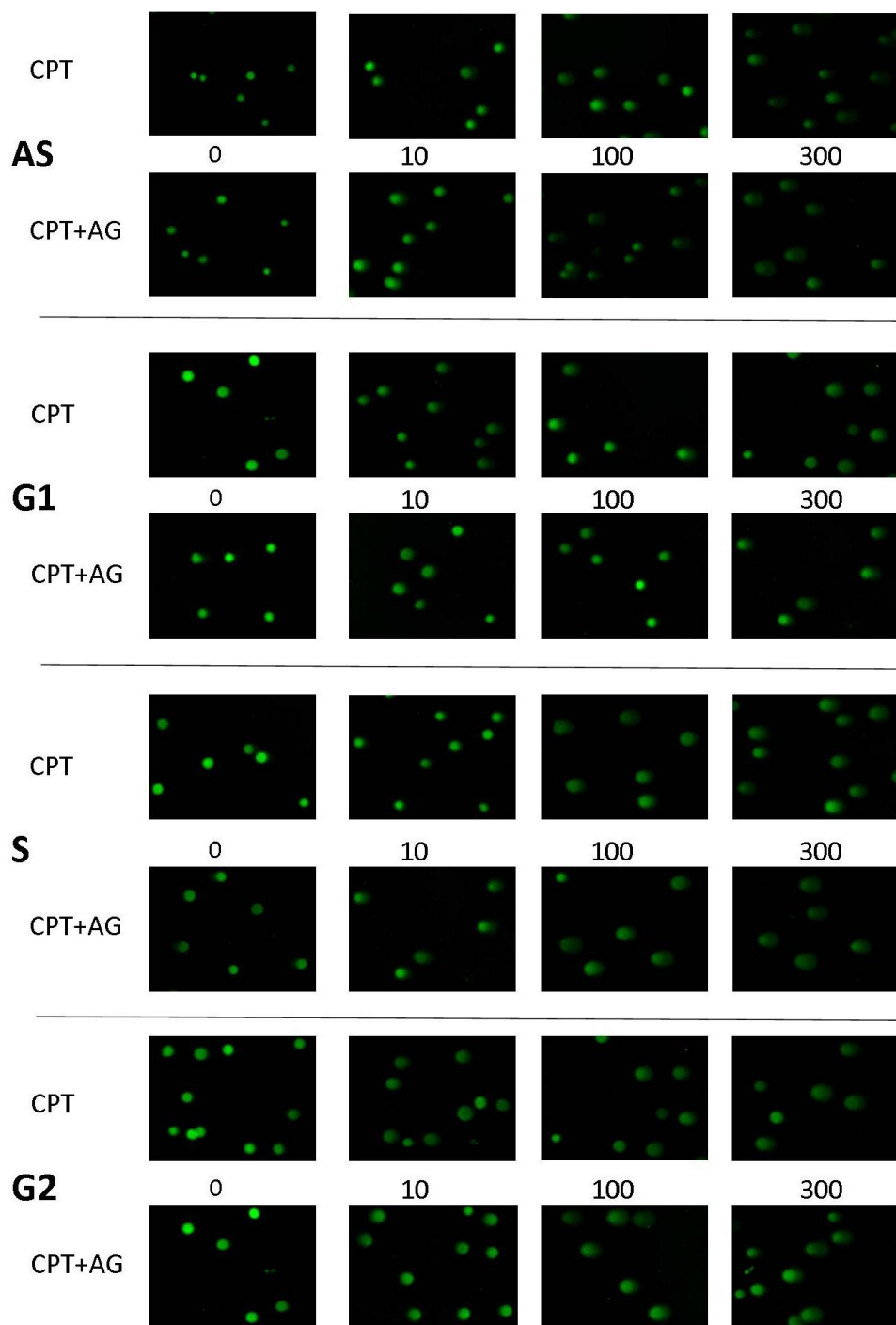


Figure 4. 3. Comets observed after 30 min exposure to CPT \pm 0.4 μ M AG014699 and determined using alkaline comet assay

Asynchronous (AS) and cell cycle phase separated (G1, S, G2) K562 cells were exposed to CPT at concentration of 0 nM (left panel), 10 nM (middle-left panel), 100 nM (middle-right panel) and 300 nM (right panel) with or without 0.4 μ M AG014699 for 30 min and alkaline comet assay was used to evaluate the level of SSB. Conditions - ScottLab electrophoresis tank, 0.75V/cm, 30 min.

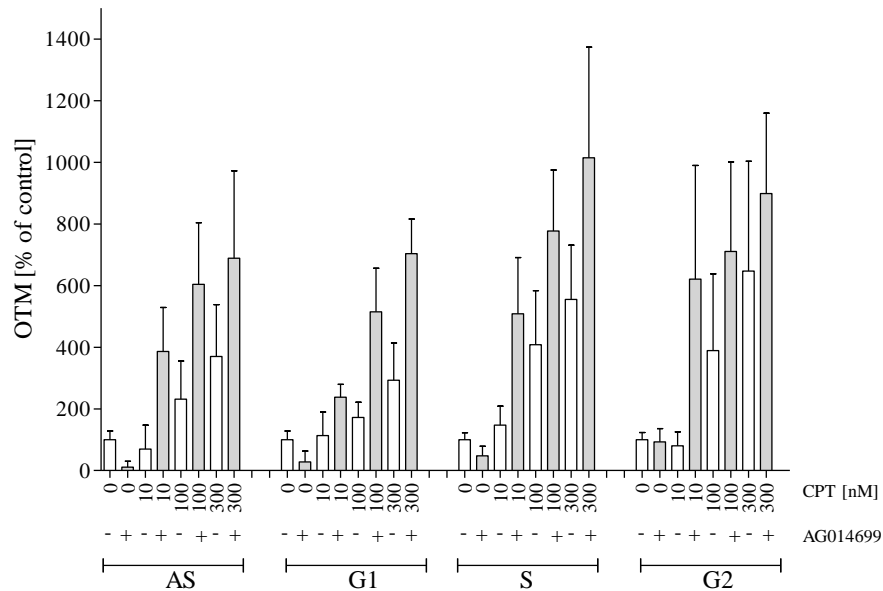


Figure 4. 4. The effect of PARP-1 inhibition on the level of DNA breaks in asynchronous and cell cycle phase separated K562 cells.

Asynchronously growing K562 cells were cell cycle phase separated and exposed to 0, 10, 100 and 300 nM CPT±AG014699 for 30 min following measurement of the level of total DNA breaks by alkaline comet assay. On bar chart: white bars – CPT alone, grey bars – CPT+AG014699. Graphs shows mean of OTM ± SEM of 4 independent experiments expressed as % of control untreated cells.

	CPT [nM]	% increase in OTM CPT	% increase in OTM CPT+ AG	CPT vs CPT+AG p-value
AS	10	-30.1	286.2	0.00
	100	131.2	504.1	0.01
	300	270.0	589.1	0.02
G1	10	13.5	138.2	0.26
	100	72.3	414.8	0.02
	300	193.3	603.9	0.06
S	10	47.5	408.6	0.01
	100	308.4	677.1	0.03
	300	455.1	914.8	0.08
G2	10	-19.5	521.2	0.08
	100	289.3	610.7	0.13
	300	314.9	799.0	0.03

Table 4. 1 Effect of AG014699 on CPT-induced DNA breaks

Data in the table show the increase in OTM above control cells, expressed as % of control untreated cells. The numbers were calculated form values of OTM from 4 independent experiments as shown in Figure 4. 4.

$$\% \text{ increase in OTM} = \left(\frac{\text{OTM CPT} \pm \text{AG}}{\text{OTM control}} \times 100 \right) - 100$$

4.5. Determination of DSB level in K562 cells exposed to CPT± AG014699.

In the previous section, the effect of CPT and AG01499 on DNA breaks was found to be most marked in S and G2 phase cells. The alkaline comet assay allows evaluation of the total level of DNA damage rather than just SSBs, although these will be the majority of the breaks. SSB induced by CPT are not cytotoxic *per se*, but under certain condition, these breaks can be converted to lethal DSB. Therefore, in this section the effect of PARP inhibition by AG014699 on the level of DSB induced by CPT was studied. DSB level can be measured using a variety of techniques including neutral comet assay and γ H2AX immunostaining.

4.5.1. The effect of AG14699 on the DSB level in asynchronous and elutriated K562 cells determined by neutral comet assay.

In this section, the level of DSB was investigated using the neutral comet assay. The drug treatment conditions for these experiments were the same as described in section 0. Representative photomicrographs of the comets for all treatment conditions used in this experiment are shown in

Figure 4. 6 The effect of AG014699 on CPT-induced DSB in asynchronous and elutriated K562 cells.

Images collected in this figure show the variation in the length of comet tails in the cells depending on the concentration of CPT, the phases of the cell cycle and the presence of AG014699. Images collected on the left panel show DNA double strand breaks in the form of comets tails in control cells that were treated with DMSO or with DMSO and AG01499. One can note that the tail length varies depending on the drug treatment conditions used in this experiment. Tail length increases with increasing concentration of CPT (middle and right panel) indicating a concentration-dependent increase in DSBs. The length of the comet tail is greater in pictures showing cells treated with CPT+AG014699. The longest comet tails can be seen on the right panel for S phase cells exposed to 100 nM CPT+AG014699. These images indicate that cells in the S phase of the cell cycle accumulate most DNA DSB.

Images shown in Figure 4.6. were used to measure the OTM and the results were shown in Figure 4. 7. and Table 4. 2. Comparing cells in different phases of the cell cycle, it can be seen that the largest increase in the level of DNA breaks is in S phase, where 10

nM CPT increased the level of the DSB by 58.8% and 100 nM by 134.3% above the level of control cells. AG014699 increased double-strand breakage in S and G2 phases by 1.3 to 1.8-fold. Although an increase in DSBs was also observed with CPT in G1 phase cells (60.9% for 10 nM and 92.2% for 100 nM), incubation with AG014699 did not cause a significant increase. Like the data obtained in the previous section, these results show that the DNA damage caused by CPT is greatest in S phase and G2. The effect of AG014699 is also most evident in the S phase of the cell cycle.

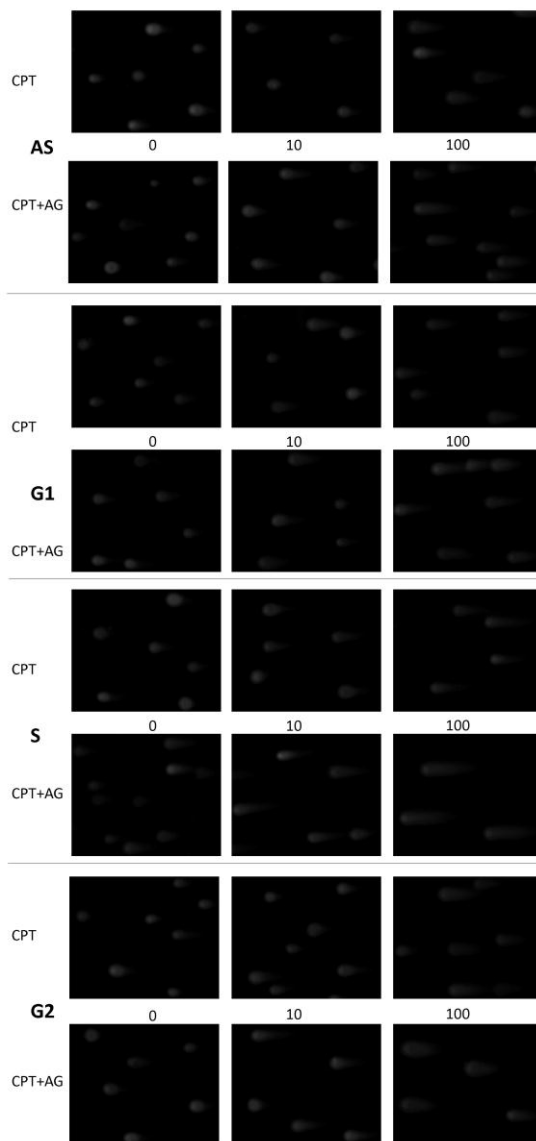


Figure 4. 5. Comets showing the level of DNA double strand breaks in K562 cells

Asynchronous (AS) and cell cycle phase separated (G1, S, G2) K562 cells were exposed to CPT at concentration of 0 nM (left panel), 10 nM (middle panel) and 100 nM CPT (right panel) with or without 0.4 μ M AG014699 for 30 min and neutral comet assay was used to evaluate the level of DSB. Conditions -VWR electrophoresis tank, 1V/cm, 30 min.

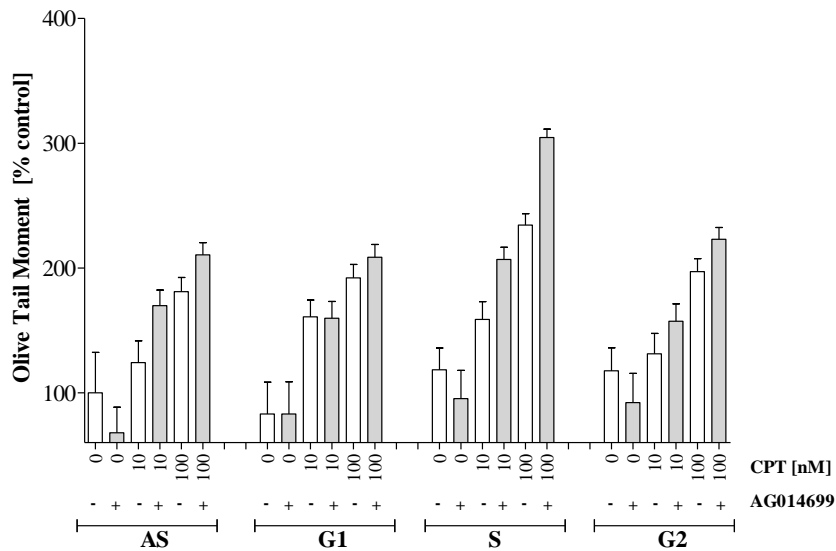


Figure 4. 6 The effect of AG014699 on CPT-induced DSB in asynchronous and elutriated K562 cells.

Asynchronous (AS) and elutriated (G1, S, G2) K562 cells were exposed to 0 nM, 10 nM and 100 nM CPT \pm 0.4 μ M AG014699 for 30 min for evaluation of DSB level by neutral comet assay. Data on bar chart and in table shows mean + SE of single experiment expressed as a % of control with at least 100 cells analysed: White bars – CPT alone, grey bars – CPT+AG014699.

	CPT [nM]	% increase in OTM CPT	% increase in OTM CPT+ AG	CPT vs CPT+AG p-value, LSD	fold increase
AS	10	24.2	69.8	0.01	2.9
	100	81.0	110.6	0.20	1.4
G1	10	60.9	59.8	0.96	1.0
	100	92.2	108.7	0.48	1.2
S	10	58.8	106.8	0.03	1.8
	100	134.3	204.5	0.03	1.5
G2	10	31.2	57.3	0.02	1.8
	100	97.1	123.1	0.29	1.3

Table 4. 2. Effect of AG014699 on CPT-induced DSB

Data in the table show the increase in OTM above control cells, expressed as % of control untreated cells. The numbers were calculated from values of OTM as described in the legend to Table 4. 1 from 4 independent experiments as shown in

Figure 4. 6 The effect of AG014699 on CPT-induced DSB in asynchronous and elutriated K562 cells.

4.5.2. The effect of AG14699 on CPT-induced DSB in asynchronous K562 cells evaluated by γ -H2AX

In the previous section, the effect of AG014699 on CPT-induced DSB level in K562 cells was demonstrated with the neutral comet assay. In this section, the level of DSB was measured by γ H2AX immunostaining and analysed with the aid of custom-created PZFociEZ macro (see also appendix). The macro was validated as described in materials and methods chapter in section 2.10.2 and here more details about analysis are given.

After the exposure of cells to 10 and 1000 nM CPT \pm AG014699 for 30 min, drugs were removed by centrifugation and cells were attached onto microscope cover glass using a cytospin centrifuge. Cells were then stained with antibodies to γ H2AX as described in section 2.10 and mounted on microscope slides with mounting medium that contained DAPI. γ H2AX foci were examined under fluorescence microscope and 8-bit images were recorded, for γ H2AX and DAPI. The sample with the expected highest fluorescence signal was used to adjust the microscope illumination and acquisition settings to avoid sample overexposure so the fluorescence signal did not exceed 8-bit range of record images. This was the critical step for further analysis. Raw images were processed using ImageJ software with customized macros as described in section 2.10.1. Fluorescence of DNA staining with DAPI was used to define the area occupied by DNA of each cells. The outlines created for each nucleus were saved by ImageJ and used later for measurements performed on a second, corresponding image that was recorded for γ H2AX. The γ H2AX images prior to measurements were processed to reduce background using the rolling ball algorithm to reduce uneven picture illumination, and improve resolution of foci, as follows.

Using macros PZFociEZ several measurements can be automatically obtained. First, the *Area* of selection in calibrated units, such as square micrometres was measured. Next, the *Raw Integrated Density* within selection was measured (RawIntDen- the sum of the values of the pixels in the image or selection) and then *Mean Grey Value* (average grey value within the selection: This is the sum of the grey values of all the pixels in the selection divided by the number of pixels) was calculated. Finally, Integrated Density (IntDen) was calculated as the product of *Area* and *Mean Grey Value* which corresponds to foci intensity per nucleus. Finally, the number of foci was counted using

the *options find maxima* at the noise tolerance set to a value of 10 and output set to “count”. The find maxima options determine the local maxima in an image, and under given noise tolerance, maxima are ignored if they do not stand out from the surroundings by more than this value. In other words, a threshold is set at the maximum value minus noise tolerance and the contiguous area around the maximum above the threshold is analysed. For accepting a maximum, this area must not contain any point with a value higher at than the maximum. Only one maximum within this area is accepted. When the output is set to count, the ‘find maxima options displays’ the number of maxima in the Results window.

It should be noted that because of background subtraction using the rolling ball algorithm, the background of the image takes the value 0, therefore remaining pixels with a value above zero correspond only to single foci (Figure 4. 7)

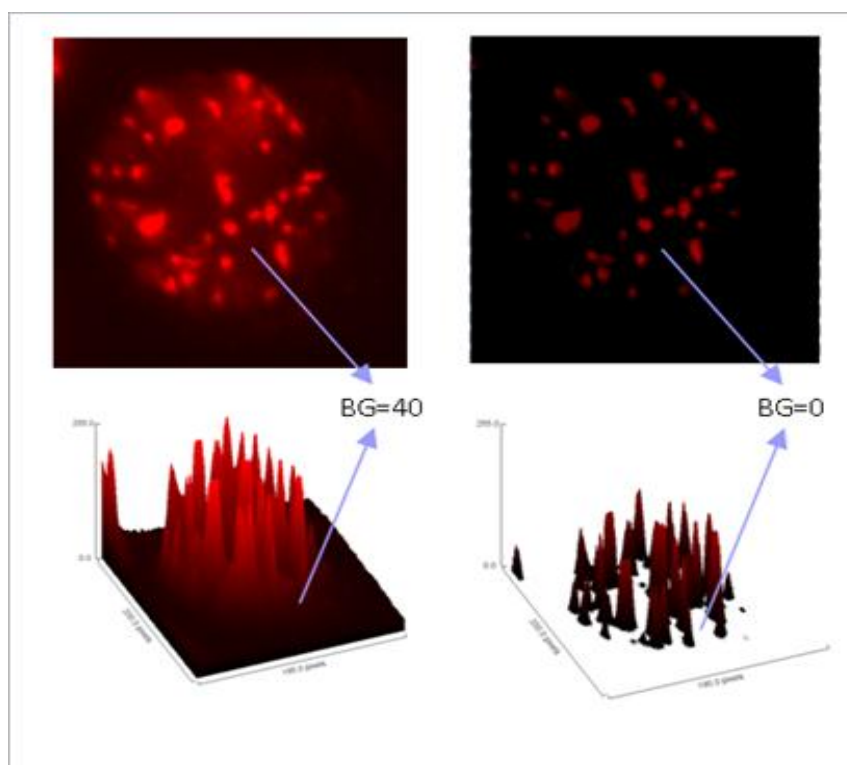


Figure 4. 7. Sample image illustrating background subtractions (BG) using rolling ball algorithm.

Images of γ H2AX foci were recorded using the Leica fluorescence microscope. Images were subjected to corrections for removing background and uneven illumination. As a result under given noise tolerance any background illumination was reduced to 0, leaving signal that is only associated with foci.

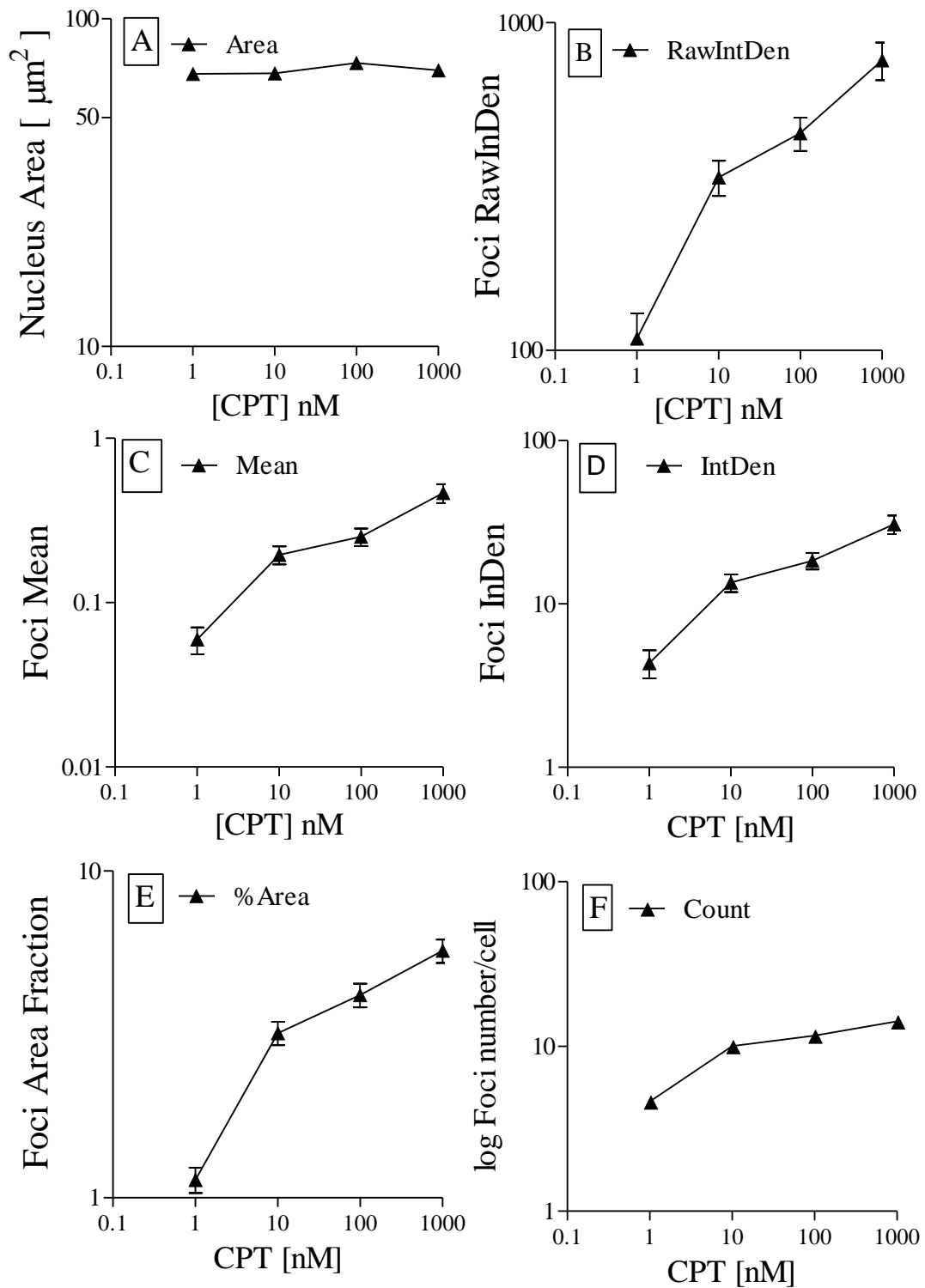


Figure 4. 8. The measurements of H2AX analysis obtained with ImageJ macro.

K562 cells that were exposed to CPT at concentration of 0, 1, 10, 100, 1000 nM for 30 min before staining for γ H2AX foci. Images of foci were scored and analysed with the aid of PZFociEZ macro.

The single focus that is represented by one maxima recognised by software under a noise tolerance possibly may consist of other points that belongs to the area of maxima but are not counted as a maximum due to noise tolerance restriction. This focus can possibly represent additional DNA breaks, e.g. a signal coming from below the focus that represents other DNA break. The option check settings for FociRB serves mainly for visual comparison of the results obtained by Find Maxima option with counting foci by eyes. However, it is possible to apply the lowest possible noise tolerance to count all possible maxima (e.g. compare number of foci counted with noise tolerance 10 – 119 foci, with noise tolerance 50 – 15 foci, Figure A19).

Figure 4. 9 shows photomicrographs of γ H2AX foci. Very weak staining was found in control cells (left panel), in these cells incubated only with DMSO, as well as those that were incubated with DMSO + AG014699. The middle panel of Figure 4. 9 shows examples of γ H2AX foci staining pattern obtained with treatment with 10 nM CPT \pm AG014699. It is obvious that there are more cells expressing a positive coloration. It may be noted that the emergence of a more intense staining of cells with cells incubated with CPT + AG014699. The largest number of cells with most intense staining is visible in the right panel. Particularly intense staining was seen in the S phase cells incubated with 1000 nM CPT + AG014699. The staining pattern in these photos is similar to the pattern that was obtained by staining of comets that is shown in Figure 4. 4 and

Figure 4. 6 The effect of AG014699 on CPT-induced DSB in asynchronous and elutriated K562 cells.

and suggests that the S phase cells treated with CPT and AG014699 are most susceptible to DNA damage. These images were then analysed using a macro PZFociEZ, and the results of this analysis are shown in Figure 4. 10 and Figure 4. 11.

Figure 4. 10 A and B shows a quantitative estimate made by measuring γ H2AX integrated density (IntDen) and the number of Foci. These data show that there was an increase in the amount of DSB with increasing concentrations of camptothecin. For cells in the G1 phase incubation with CPT significantly increased the Integrated Density. There were no significant differences in the number of foci counted for cells in G1 phase between 10 and 1000 nM. In the G1 phase AG014699 only slightly increased the Raw Integrated Density for a concentration of 1000 nM CPT, however, it had no effect on the number of foci. The largest increase following CPT treatment, both in Raw Integrated Density and foci number was observed in S phase cells. A

concentration-dependent increase in the number of foci and Raw Integrated Density was recorded also in G2 phase cells. Data in Figure 4. 10 A and B shows that in the higher CPT concentration (1000 nM), AG014699 did increase both the foci number and integrated density. AG014699 had the biggest impact on the foci number in the S phase of the cell cycle, increasing the number of foci approximately by 2-fold compared to CPT alone. The weakest effect of AG014699 on the number of foci was demonstrated in G1 phase cells. Inhibition of PARP activity in G1 cells resulted in in approximately 1.1-fold increase in the foci number regardless of CPT concentration. These results are consistent with data published previously which show that a high CPT concentration is needed to induce DSBs in non-replicating cells that are in G0/G1 phase. In summary, these data are consistent with the results of neutral comet assays (section 4.5.1), and show that PARP inhibition enhances CPT-induced DNA DSB predominantly in S and G2 phases of the cell cycle

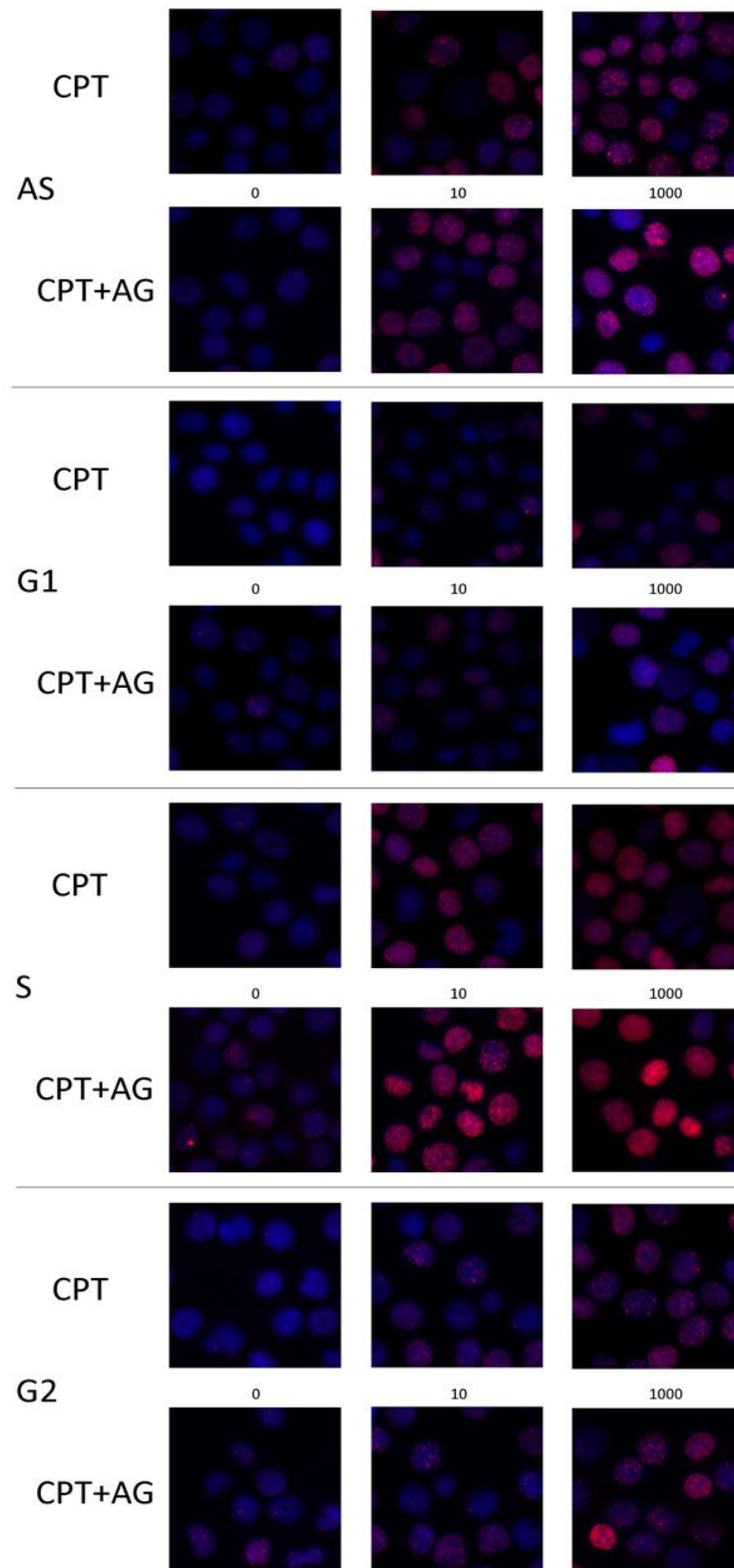


Figure 4. 9. γ H2AX immunostaining pattern found in K562 cells exposed to CPT \pm AG014699

Images of asynchronous (AS) and elutriated K562 cells were exposed to 0 (left panel), 10 nM (middle panel) and 1000 nM (right panel) CPT in the presence or absence of 0.4 μ M AG014699 for 30 min before staining for γ H2AX.

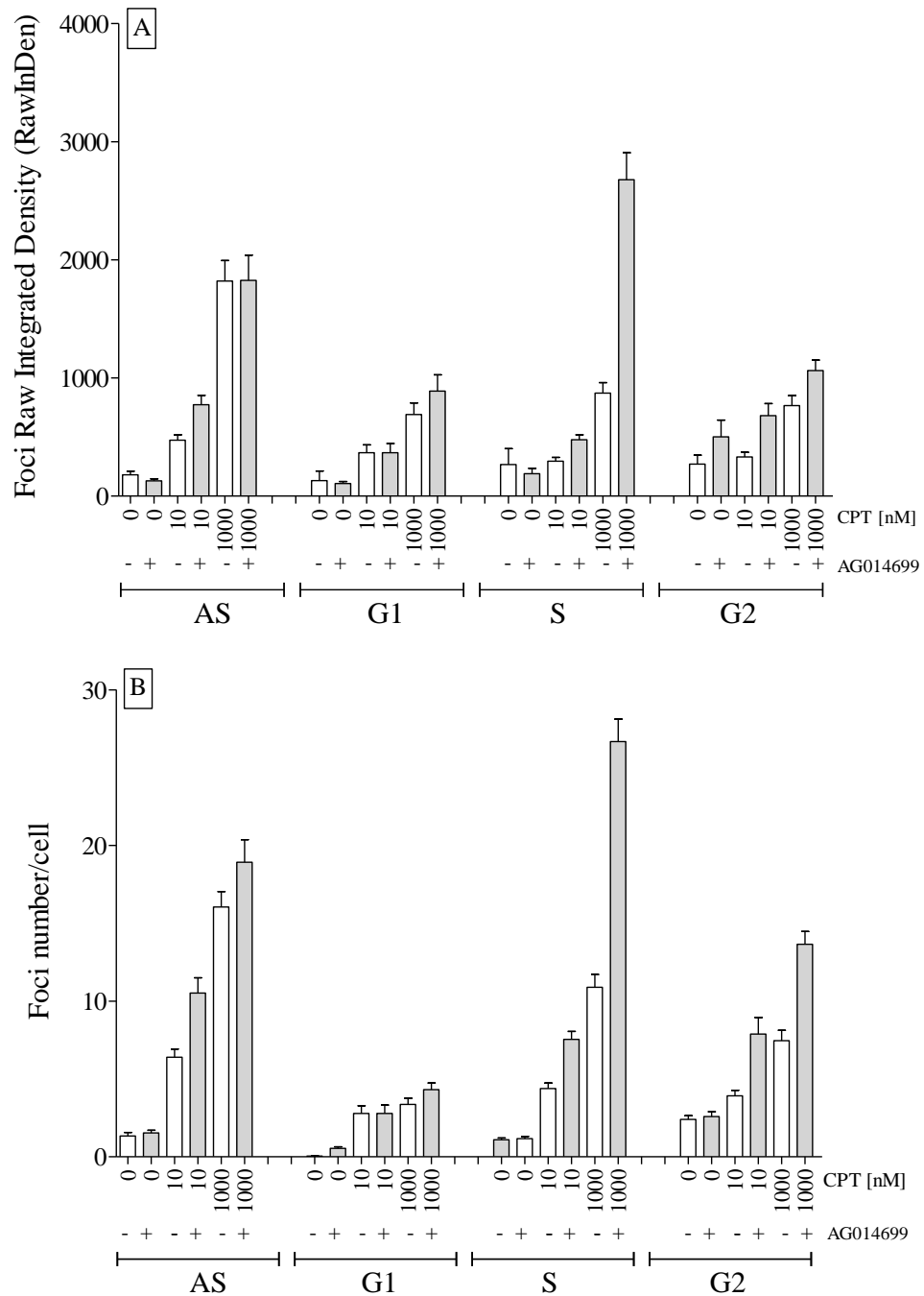


Figure 4. 10. Plot of Foci Raw Integrated Density and Foci number categorised by cell cycle phase, PARP Inhibitor and CPT concentration

K562 cells were separated into individual cell cycle phases using elutriation, after having been treated with CPT for 30 min and then stained for the presence of γ H2AX foci. Using the macro PZFociEZ, Raw Integrated Density was measured (A) and, the number of foci was counted (B) for each cell for the same experiment. Data show results of quantification obtained for one representative experiment. Data shows Mean \pm SEM calculated from at least 100 cells from a single experiment. The white indicates cells exposed to CPT and the grey bars indicates cells exposed to CPT \pm AG014699.

4.6. The effect of AG014699 on the repair of DNA breaks induced by CPT in asynchronous K562 cells

4.6.1. Repair of CPT-induced total DNA breaks in asynchronous K562 cells.

In the previous section, AG014699 was shown to have the most marked effect on CPT-induced DNA break level in S phase cells. This could have been caused by an increase in the number of induced breaks or reduction in their repair during the 30 min exposure period. PARP-1 is considered to promote DNA repair, therefore to clarify whether the accumulation in DNA breaks the presence of AG014699 was due to inhibition of repair, the effect of AG014699 on the repair of breaks was determined following a 30 min pulse of CPT followed by incubation in drug-free medium or medium containing AG014699 for 30 min, 1h and 5h.

Alkaline Comet images presented in Figure 4. 11 show a reduction of comet tails in samples incubated in fresh medium (-AG014699) and after 5h incubation most of the cells do not have any detectable tail, which suggests complete DNA repair. Comparing this to images recorded for samples incubated in medium containing AG014699, the reversal of comet tail is slower and, even after 5h of recovery period, a mixture of cells with small and very long tails can be observed. This suggests that in the asynchronous population some cells repair DNA damage quickly and some cells repair DNA damage more slowly.

Data plotted in Figure 4. 12 and summarised in Table 4. 3 show the kinetics of repair of CPT-induced DNA breaks during incubation in drug free medium or medium containing AG014699. Exposure of the K562 cells to CPT caused a significant increase in DNA breaks by 1.5- fold at 10 nM CPT and by 2-fold at 100 nM.

Incubation of cells in drug-free medium caused rapid reversal of DNA breaks induced by 10 nM and 100 nM CPT, with levels similar to control within 1h of recovery period ($p > 0.07$) (Figure 4. 12 and Table 4. 3). Exposure of cells to AG014699 during the recovery period caused a significant delay in the repair of DNA damage induced by 10 and 100 nM CPT. The most marked effect of AG014699 on DNA damage repair for both CPT concentrations was observed at 30 min recovery period. At this time point, 9% (10 nM) and 41% (100 nM) of DNA breaks remained ($p < 0.01$) in the absence of AG014699 but substantial damage remained in the presence of AG014699. PARP inhibition reduced DNA repair by 96% at 10 nM CPT, and 44% at 100 nM CPT. AG014699 caused 40% reduction in repair of DNA breaks induced by 10 nM CPT and

27% in repair of breaks induced by 100 nM CPT at 1h. At the end of the recovery period treatment with AG014699 had resulted in a 24% inhibition of the repair of damaged DNA at both CPT.

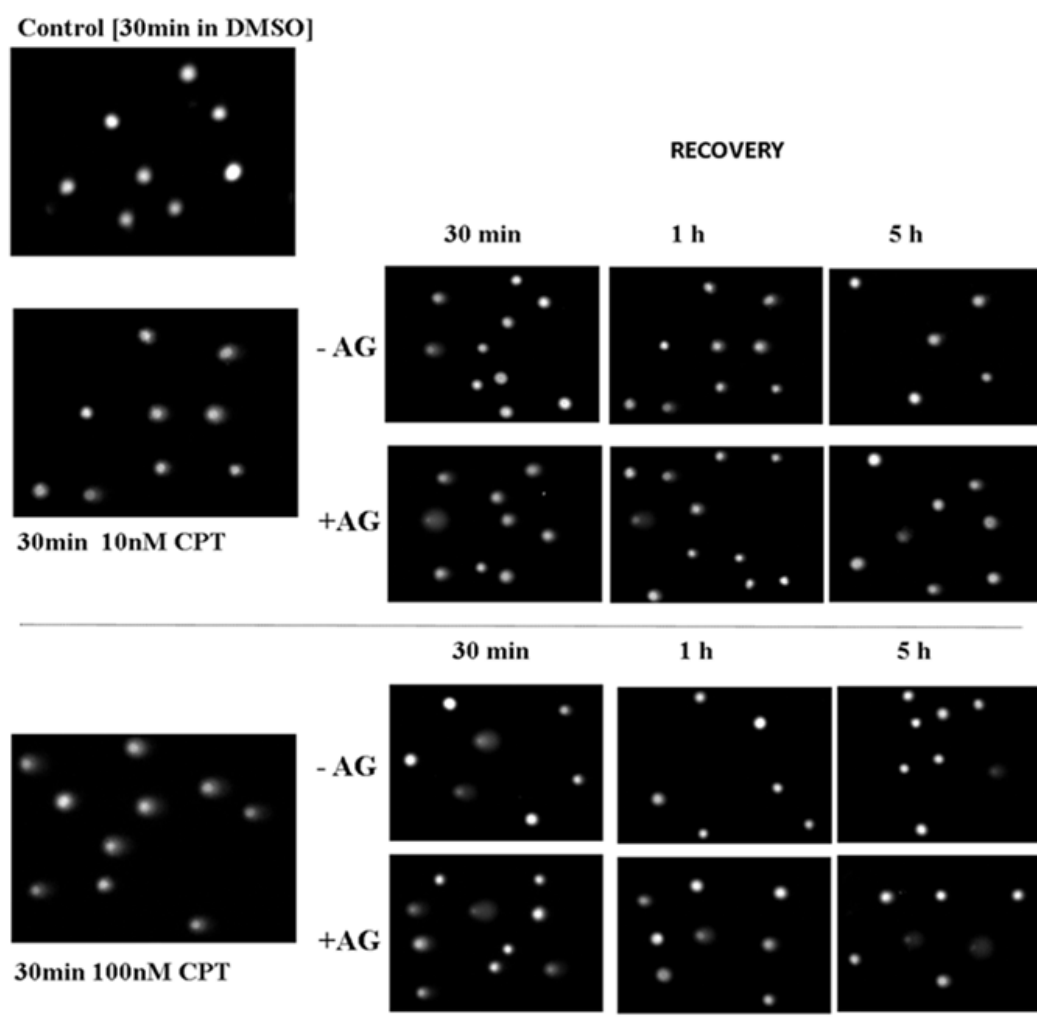


Figure 4. 11. The comets observed after 30 min exposure to 10 and 100 nM CPT followed by incubation in fresh medium \pm 0.4 μ M AG014699 as determined by alkaline comet assay.

K562 cells were exposed to 0, 10 and 100 nM CPT for 30 min. CPT was removed and cells were incubated in fresh medium or medium with AG014699 for up to 5h . The level of remaining DNA breaks was evaluated by alkaline comet assay after 30min, 1h, 5h after CPT removal. VWR electrophoresis tank, 0.75V/cm, 200-300 mA, 30 min.

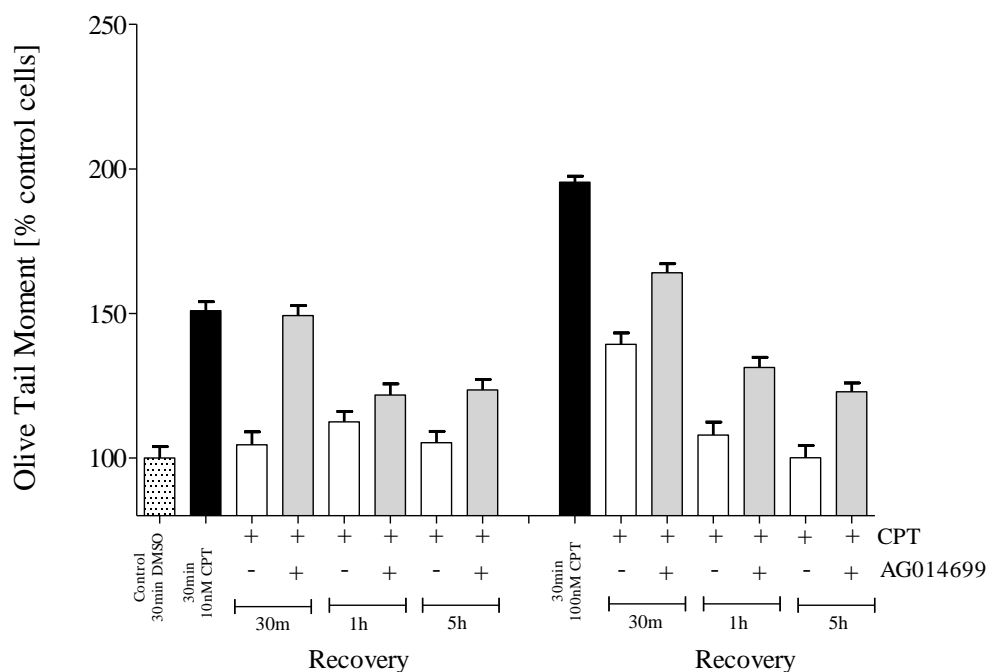


Figure 4. 12. Effect of AG014699 on the repair of total DNA breaks formed during 30 min exposure to 100 nM CPT

K562 cells were incubated with 10 and 100 nM CPT for 30 min following by incubation in drug-free medium or medium with 0.4 μ M AG014699 for 30 min, 1h and 5h. The level of DNA breaks was measured by alkaline comet assay. Data show the average OTM + SEM calculated from the sample of 100 randomly selected cells obtained from two independent experiments. Data, expressed as a percentage of untreated control (speckled bar), are OTM after 30 min exposure to CPT (black bar) followed by recovery in fresh drug-free medium (white bars) or that containing 0.4 μ M AG014699 (grey bars) for the indicated times.

CPT concentration	Recovery time	% Increase in OTM	% Damage remaining	% Damage repair	% Inhibition by AG014699
10 nM	0min	51			
	30min -AG	5	9	91	
	30min +AG	49	97	3	96
	1h -AG	5	10	90	
	1h +AG	24	46	54	40
	5h -AG	13	25	75	
	5h +AG	22	43	57	24
	100 nM	0min	95		
30min -AG		39	41	59	
30min +AG		64	67	33	44
1h -AG		8	8	92	
1h +AG		31	33	67	27
5h -AG		0	0	100	
5h +AG		23	24	76	24

Table 4. 3. The effect of AG014699 on the repair of DNA breaks induced by exposure to CPT for 30 min.

Data in the table show the increase in OTM above control cells, expressed as % of control untreated cells. The numbers were calculated from values of OTM as described in the legend to Table 4.1 from 2 independent experiments as shown in figure 4.12.

$$\% \text{ damage remaining} = \left(\frac{\text{OTM at 30min, 1h or 5h } \pm \text{AG}}{\text{OTM at 0min}} \right) \times 100\%$$

$$\% \text{ damage repair} = 100 - \% \text{ damage remaining}$$

$$\% \text{ inhibition of repair by AG014699} = 100 - \left(100 \times \frac{\% \text{ damage repair } + \text{AG}}{\% \text{ damage repair } - \text{AG}} \right)$$

4.6.2. Effect of AG014699 on the repair of CPT-induced DSB in asynchronous population of K562 cells

4.6.2.1. Neutral comet assay

The reversal of DSB in the presence or absence of AG014699 was studied. K562 cells were treated with CPT ± AG014699 for 30 min, after which the drug was removed and replaced with fresh medium with or without 0.4 µM AG014699 for up to further 5h. Inhibition of the reversal of CPT-induced DNA DSBs by AG014699 during the 5h of recovery period can be clearly observed on images collected in Figure 4. 13 Incubation of cells with CPT results in induction of DNA breaks that is manifested by increased length of comet tail. During the recovery period in drug free medium, the length of comet tail was reduced in all cells. Cells incubated in medium with AG014699 still had a longer tails than controls at the end of recovery period, which suggests that repair of DNA DSBs was inhibited.

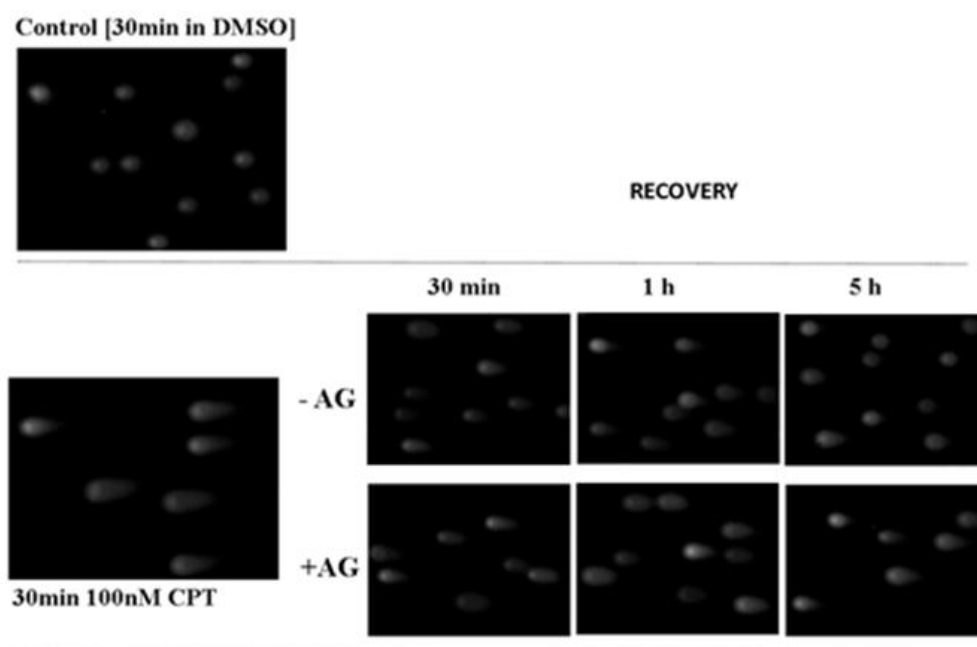


Figure 4. 13. The comets observed after 30 min exposure to 100 nM CPT followed by incubation in fresh medium ± 04 µM AG014699 as determined by neutral comet assay

K562 cells were exposed to 100 nM CPT for 30 min. CPT was removed and cells were incubated in fresh medium or medium with AG014699 for up to 5h. For each time point, the level of remaining DNA DSBs was evaluated by neutral comet assay. Conditions -ScottLab electrophoresis tank, 1V/cm, 30 min.

The results in Figure 4.14 and Table 4. 4 show that there is a time-dependent repair of DSB in the absence of AG014699 but that repair is significantly slower in cells incubated in medium containing AG014699. For example, after incubation for 30 minutes, only 7% of DNA damage was repaired in cells incubated with AG014699, compared to 44% in cells incubated in fresh medium

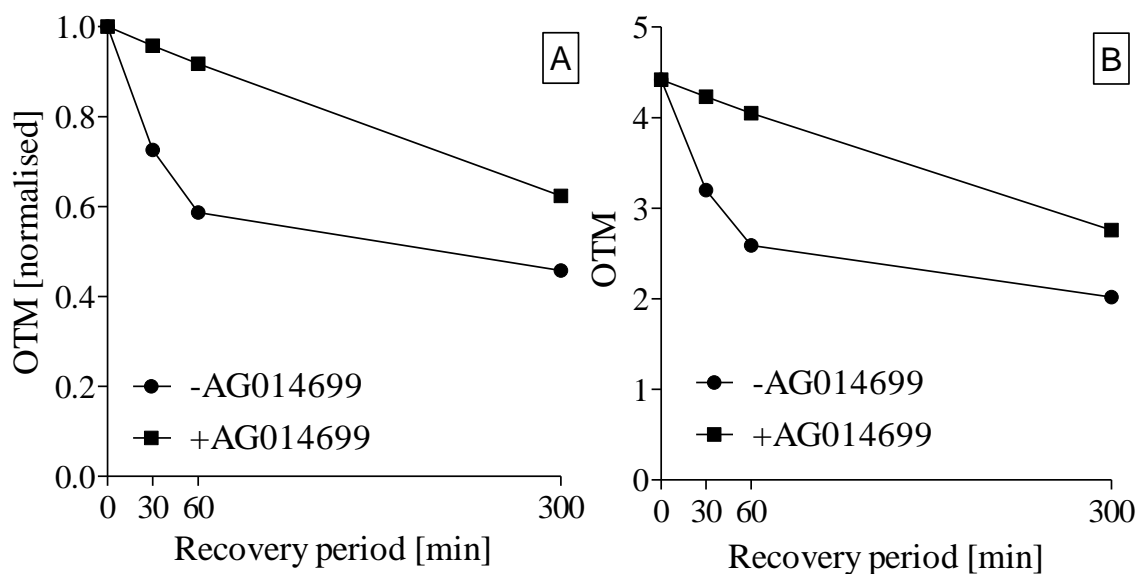


Figure 4. 14. The comets observed after 30 min exposure to 100 nM CPT \pm 04uM AG014699 as determined by neutral comet assay.

Asynchronous K562 cells were exposed to 100 nM CPT for 30 min. CPT was then removed and cells were incubated in fresh medium or fresh medium with AG014699 for up to 5h. The level of DNA breaks was evaluated by neutral comet assay after 30min, 1h, 5h after CPT removal. (A) Data normalised to the value of OTM measured at time 0 min (B) Raw OTM data plotted against recovery time. Data shows OTM mean calculated from a single representative experiment.

Recovery time	% Increase in OTM	% Damage remaining	% Damage repair	Inhibition by AG014699
0 min	166			
30 min	93	56	44	
30 min +AG	155	93	7	85
1h	56	34	66	
1h +AG	144	87	13	80
5h	22	13	87	
5h +AG	66	40	60	31

Table 4. 4. The effect of AG014699 on the repair of DSB induced by exposure to CPT for 30 min

Asynchronous K562 cells were exposed to 100 nM CPT for 30 min. CPT was removed and cells were incubated in fresh medium or medium with AG014699 for up to 5h . The level of remaining DNA breaks was evaluated by neutral comet assay after 30min, 1h, or 5h after CPT removal.

Data was calculated as shown for Table 4. 3

4.6.2.2. *γH2AX immunostaining*

In this section, the effect of 0.4 μM AG014699 on the reversal of DSB induced by 100 nM CPT was investigated, using γH2AX immunostaining with the aid of the PZFociEZ macro. K562 cells were treated with 100 nM CPT \pm AG014699 for 30 min, after which the drug was removed and replaced with fresh medium or fresh medium containing 0.4 μM AG014699 for further 30 min, 1h and 5 h. Representative pictures from this experiment are shown in Figure 4. 15. In this figure, foci fluorescence was barely detected in control DMSO-treated cells, but significant increase in foci intensity, foci number and in the number of foci positive cells was observed following exposure to 100 nM CPT.

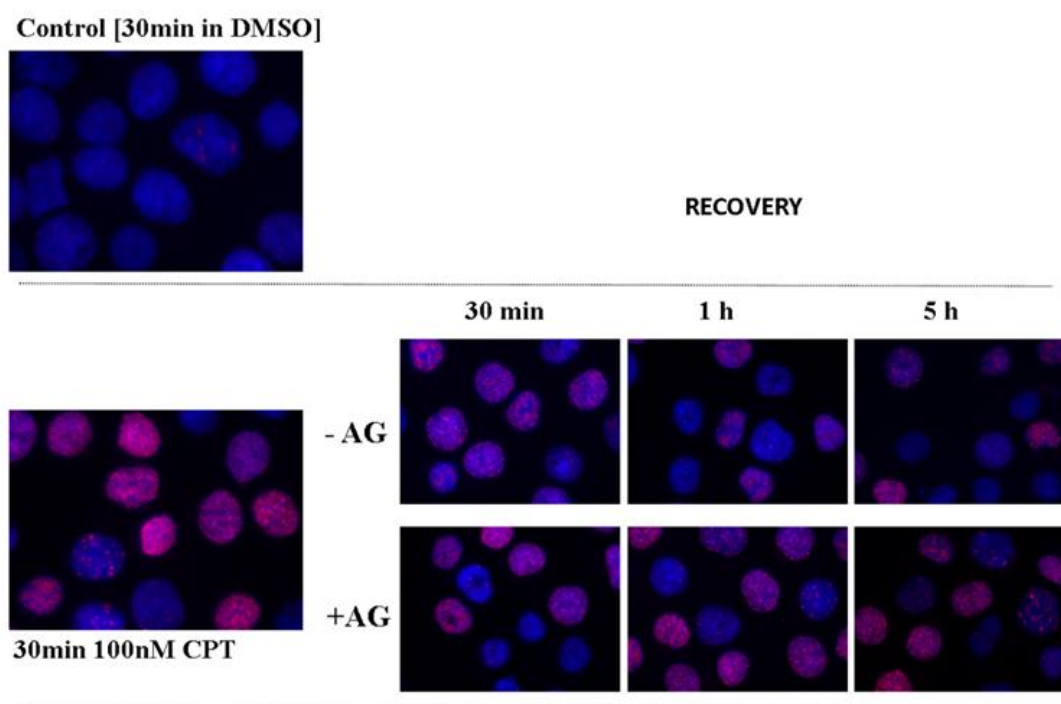


Figure 4. 15. Representative staining of γH2AX foci in K562 cells.

K562 cells were incubated with 100 nM CPT for 30 min. When CPT was removed incubation was continued in fresh medium or medium containing 0.4 μM AG014699 for up to 5h to allow the repair of damaged DNA to take place

The results in

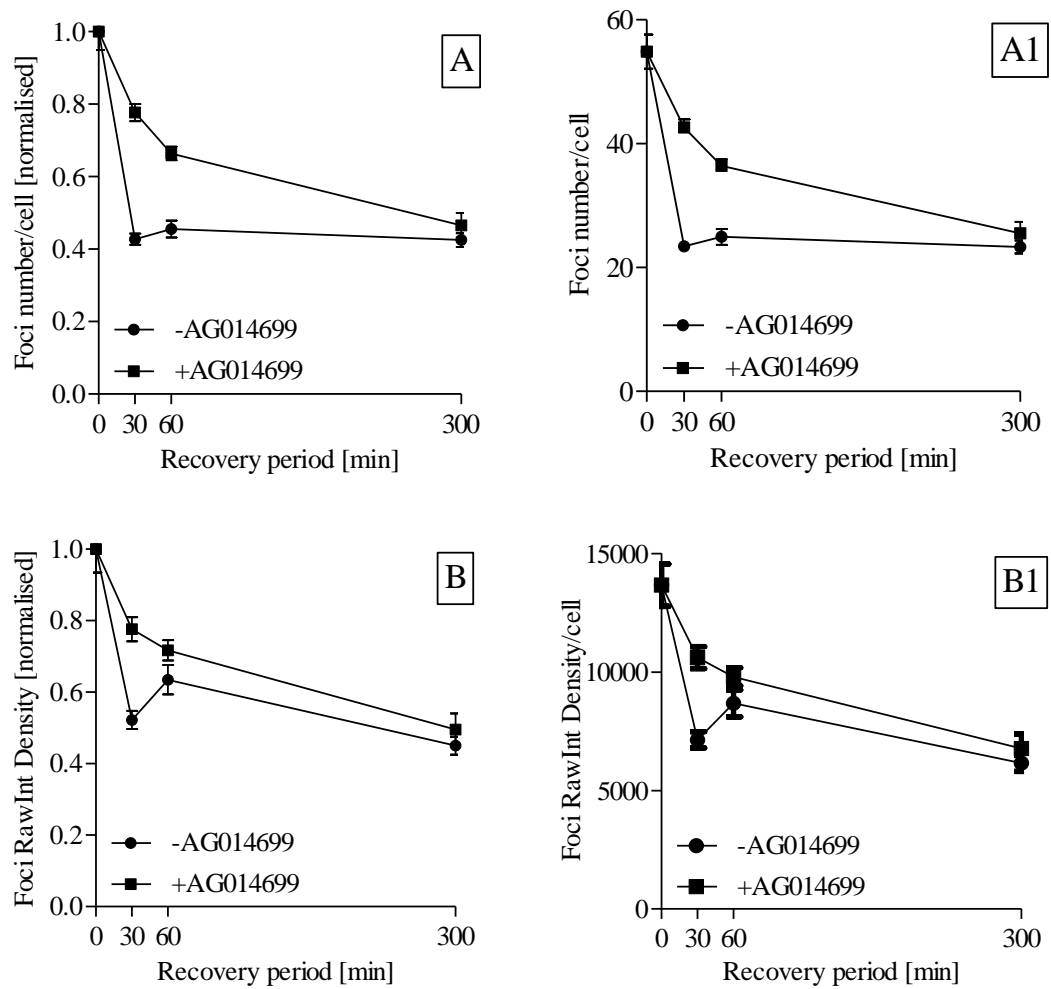


Figure 4. 16 A and B shows that Raw Integrated density induced by 100 nM CPT gradually decreased in cells incubated in fresh recovery medium. Similarly, the average foci number per cell was reduced in fresh medium conditions. The presence of AG014699 over 5h recovery incubation retarded the rate of disappearance of the number of foci.

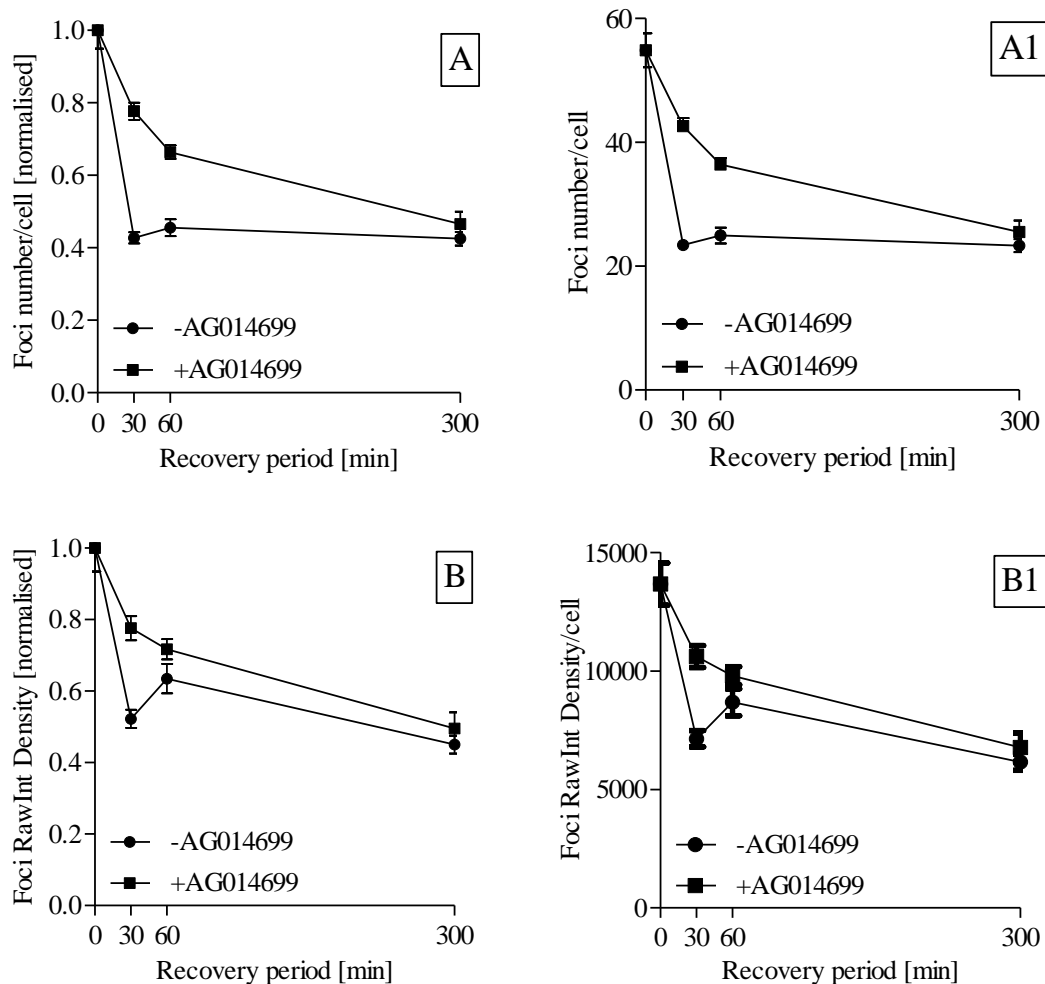


Figure 4. 16. The fluorescence and foci numbers observed after 30 min exposure to 10 and 100 nM CPT \pm 04uM AG014699 as determined by γ H2AX fluorescence.

Asynchronous K562 cells were exposed to 100 nM CPT for 30 min following by CPT removal and incubation in fresh medium or fresh medium with AG014699 for up to 5h. The level of DNA breaks was evaluated by γ H2AX fluorescence after 30min, 1h, 5h after CPT removal. A) Mean foci number normalised to time 0. A1) Mean foci number-raw data. B) Foci Raw integrated density normalised to time 0 B1) Foci Raw integrated density –raw data. Data plotted from a one representative experiment out of 4 performed.

4.7. The effect of AG014699 on the repair of CPT-induced DNA breaks in K562 cells in different phases of the cell cycle.

The previous section showed that AG014699 retarded the repair of CPT-induced DNA breaks. To clarify whether the rate of repair and effect of AG014699 was cell cycle-specific, the reversal of CPT-induced DNA breaks was investigated in cells separated into the different cell cycle phases.

4.7.1. The effect of AG014699 on the repair of total CPT-induced DNA breaks.

K562 cells in exponential growth phase were separated into cell cycle specific fractions using elutriation and along with asynchronous culture were exposed to 100 nM CPT for 30 min. After the incubation period, cells were centrifuged to remove CPT and re-suspended in fresh medium or fresh medium containing 0.4 μ M AG014699 and incubated for further 2h to allow repair of damaged DNA. Immediately after that, cells were collected by centrifugation and subjected to alkaline comet assay. The percentage of DNA damage remaining after a two-hour incubation period was calculated relative to the level of DNA damage in the cells incubated with 100 nM CPT without recovery. The result was later used to calculate the percentage of repaired DNA and the effect of PARP inhibition as described in the equations given in Table 4. 3. The results of these calculations are summarised in Table 4. 5 and Table 4. 6. Representative images of the comets are shown in Figure 4. 17. This figure shows that comet tails observed in cells incubated in 100 nM CPT for 30 min (left panel) are reduced in cells after 2h incubation in fresh medium (middle panel), but at the same time some smaller tails can be seen in cells incubated in medium containing AG014699 (right panel). These images were quantified by measuring OTM and numeric data are shown in Figure 4. 18 and further analysis is shown in Table 4. 5.

Figure 4. 18 shows that the level of DNA damage induced in asynchronous K562 cells, during a 30 min exposure to 100 nM CPT was significantly reduced after the two hour recovery period in fresh medium in asynchronous cells and at all phases of the cell cycle. Repair of DNA breaks was most pronounced in S phase. Incubation with AG014699 consistently inhibited the reduction in DNA breaks at all phases of the cell cycle but the effect was greatest in S and G2-phases.

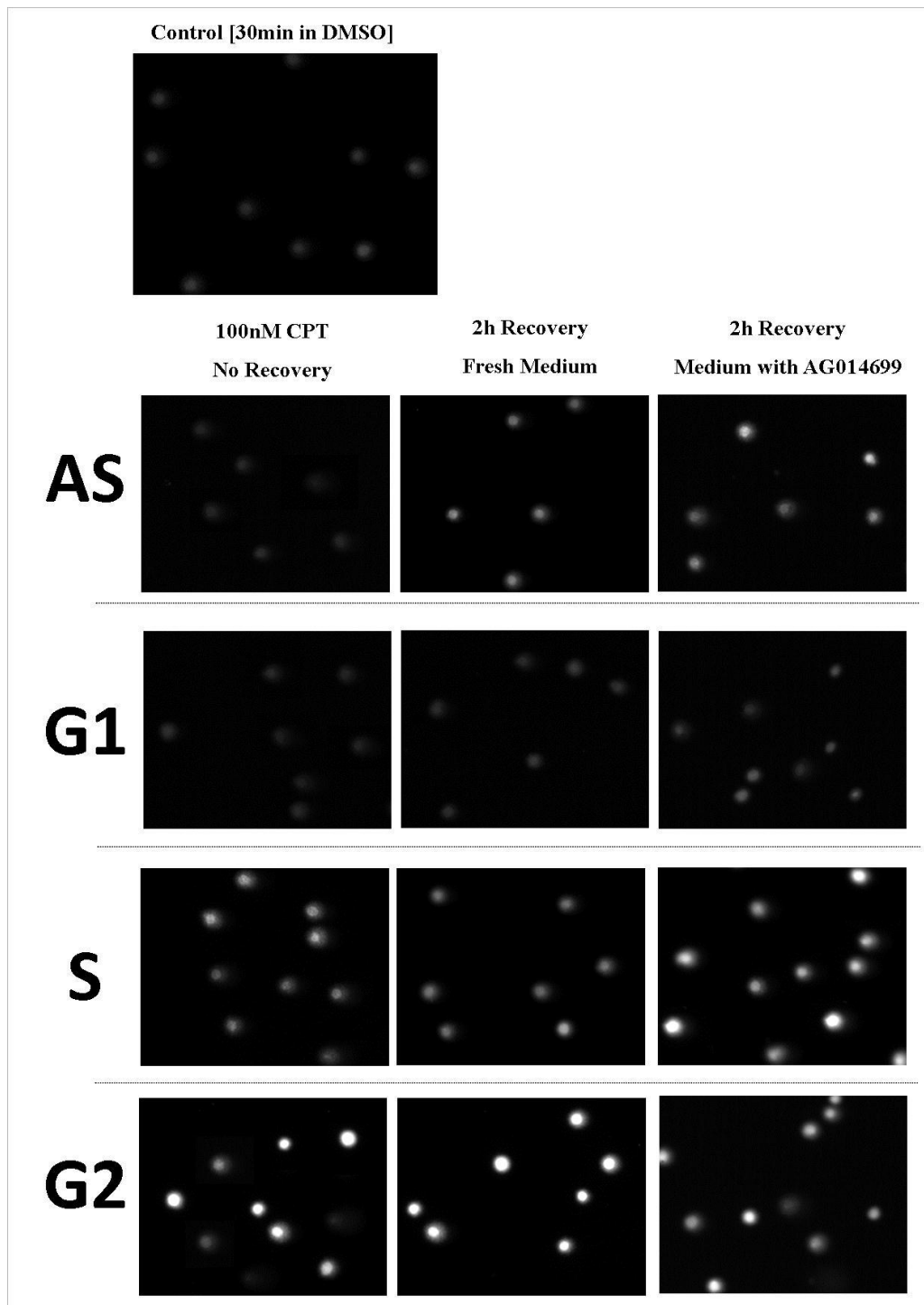


Figure 4. 17. Comets observed in asynchronous and cell cycle separated K562 cells evaluated by alkaline comet assay

Asynchronous (AS) and cell cycle phase separated (G1, S, G2) K562 cells were exposed to 100 nM CPT for 30 min (right panel) following by incubation in fresh medium (middle panel) or with medium containing 0.4 μ M AG14699 (right panel) for further 2h for DNA damage recovery. Control cells were exposed to vehicle [DMSO] for 30min. Conditions -VWR electrophoresis tank, 075V/cm, 200-300 mA, 30 min.

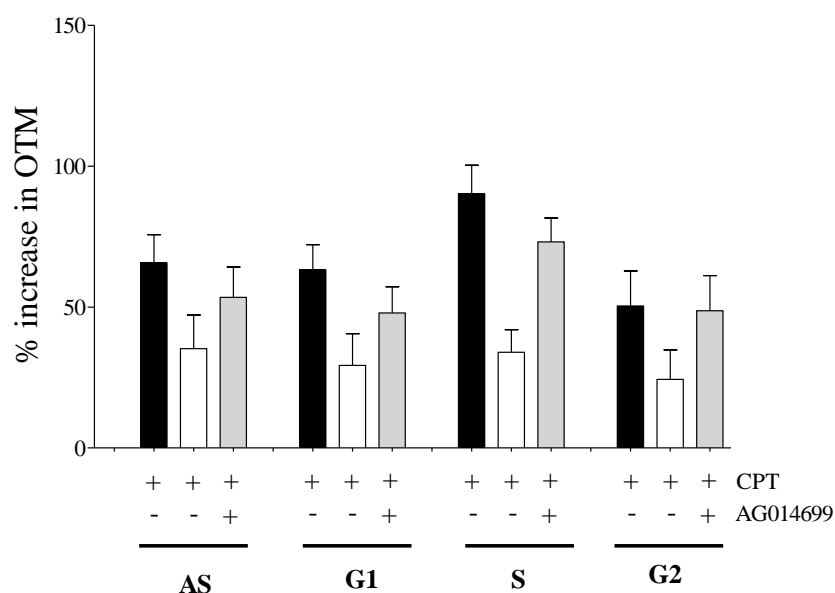


Figure 4. 18. The effect of PARP-1 inhibition on DNA SSB break repair in asynchronous and cell-cycle-phase-separated K562 cells

The level of total DNA breaks at the beginning and at the end of 2h recovery period was evaluated using alkaline comet assay by measuring the Olive Tail Moment, which was expressed as % of the OTM of control cells (asynchronous untreated cells). DNA breaks induced by 100 nM CPT (black bars) and after 2 h incubation in drug-free medium (white bars) or AG014699-containing medium (grey bars) in the K562 cells evaluated by alkaline comet assay. Data shows mean + SEM of 3 independent experiments.

Treatment		% increase in OTM	% Damage remaining	% Damage repair	% inhibition of repair by AG014699
AS	100 nM CPT	66			
	2h recovery -AG	35	54	46	
	2h recovery +AG	53	81	19	60
G1	100 nM CPT	63			
	2h recovery -AG	29	46	54	
	2h recovery +AG	48	76	24	55
S	100 nM CPT	90			
	2h recovery -AG	34	38	62	
	2h recovery +AG	73	81	19	70
G2	100 nM CPT	50			
	2h recovery -AG	24	48	52	
	2h recovery +AG	49	97	3	93

Table 4. 5. The effect of 0.4 μ M AG014699 on the repair of CPT-induced DNA breaks in the K562 cells evaluated by alkaline comet assay

Analysis of data shown in figure 4.18 were calculated as described for Table 4. 3.

4.7.2. The role of PARP inhibition in the repair of CPT-induced DSB.

As demonstrated in previous sections, AG014699 significantly retarded repair of DSB in asynchronous cells and it had greater impact on total DNA repair in S and G2 cell cycle phases of the cell cycle. Since DSB are the most cytotoxic lesion produced by CPT, and sensitization to CPT-induced cytotoxicity was greater in S phase, it was important to determine the effect of AG014699 on the repair of DSB in different phases of cell cycle.

The results in Figure 4. 20 and Table 4. 6 show that 30 min exposure of cells to 100 nM CPT consistently increased the number of DSB in all phases of the cell cycle and in asynchronous cells. As in the previous section (4.5.1, 4.5.2) the greatest induction of DSB compared to DMSO control cells was observed in S phase cells (by 132%; $p=0.03$) and G2 phase cells (by 109%, $p=0.04$) with only a modest, 68% non-significant ($p=0.18$) increase in G1.

Following CPT removal, the level of DSB in asynchronous and phase specific cells incubated in drug free medium was significantly decreased, over the recovery period. Repair of DSB in drug-free medium was greatest in S and G2-phase cells ($p<0.003$) with approximately 75% of breaks being repaired, compared to only 40%-50% in G1 and the asynchronous cells ($p<0.05$). Incubation in AG014699-containing medium retarded repair in all phases of the cell cycle but the effect, compared to DNA damage measured in cells incubated in fresh medium, was only significant in S ($p=0.007$) and G2 ($p=0.01$) with the most profound and significant inhibition being observed in S phase cell.

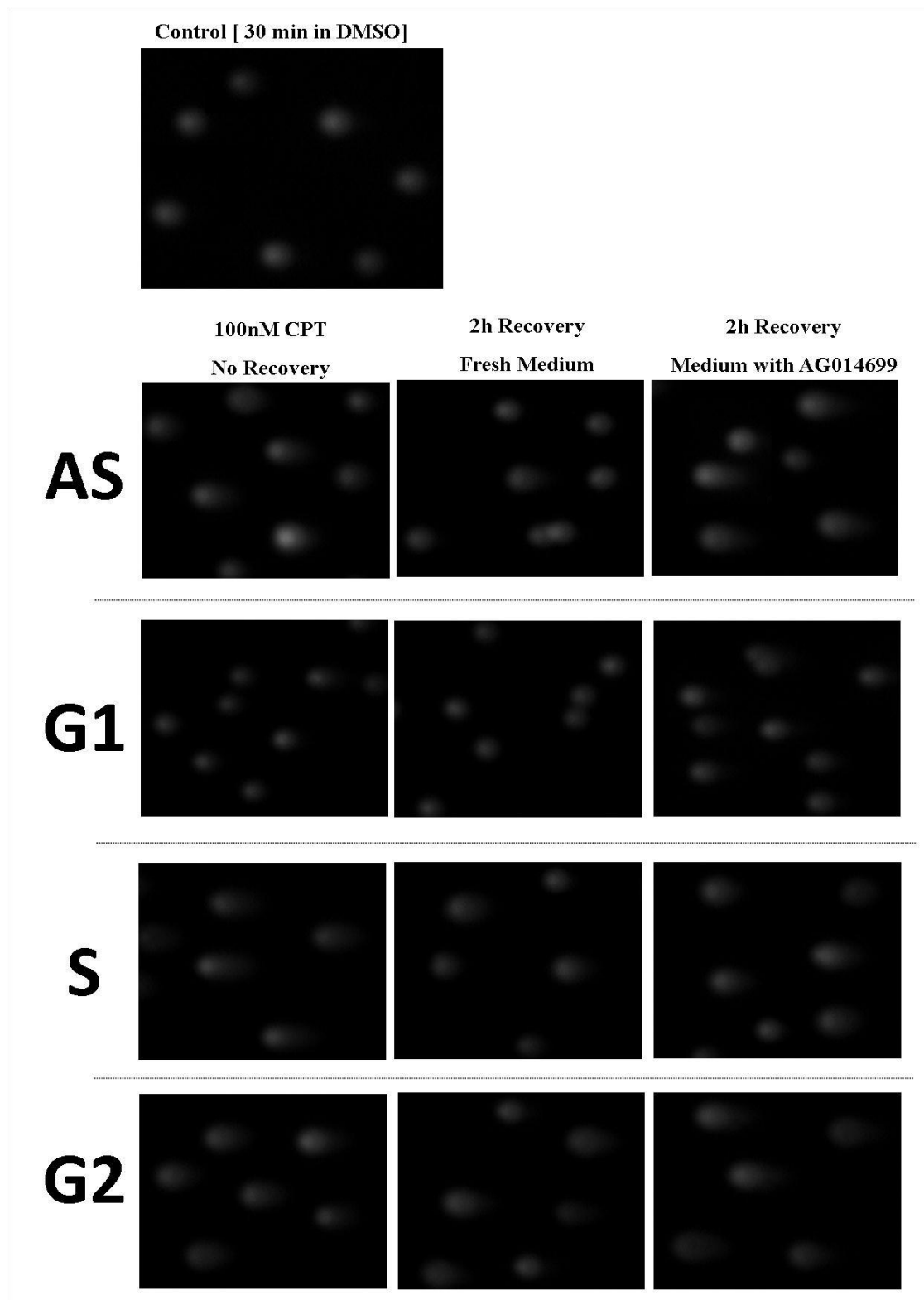


Figure 4. 19. The comets observed after 30 min exposure to 100 nM CPT followed by incubation in fresh medium \pm 04 μ M AG014699 as determined by neutral comet assay

Asynchronous (AS) and cell cycle phase separated (G1, S, G2) K562 cells were exposed to 100 nM CPT for 30 min (right panel) following by incubation in fresh medium (middle panel) or with medium containing 0.4 μ M AG14699 (right panel) for further 2h for DNA damage recovery. Control cells were exposed to vehicle [DMSO] for 30min. Conditions -VWR electrophoresis tank, 1V/cm, 30 min.

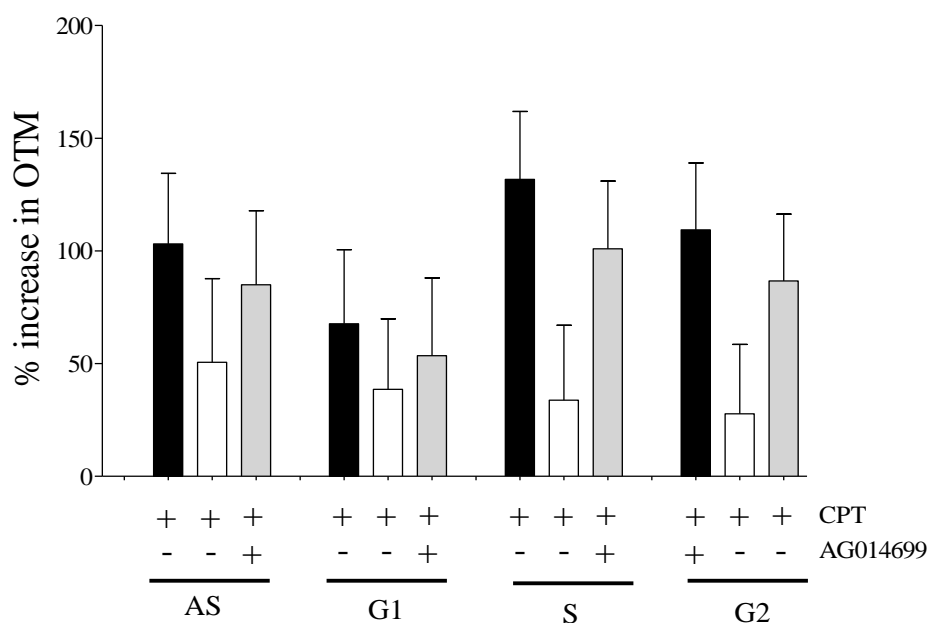


Figure 4. 20. The effect of PARP-1 inhibition on DSB repair in asynchronous and cell cycle phase separated K562 cells

Asynchronous (AS) and populations of cell cycle-phase-separated (G1, S, G2) K562 cells were exposed to 100 nM CPT for 30 min following by incubation in fresh medium or with medium containing 0.4 M AG14699 for further 2h for DNA damage recovery. The level of DSB at the beginning and at the end of 2h recovery period was evaluated using neutral comet assay by measuring the olive tail moment that was expressed as % of the OTM of control cells (asynchronous untreated cells). Data are DNA breaks induced by 100 nM CPT (black bars) and after 2 h incubation in drug-free medium (white bars) or AG014699-containing medium (grey bars) mean + SEM of 3 independent experiments

	Treatment	% Increase in OTM	% damage remaining	% damage repair	% inhibition of repair
AS	100 nM CPT	103			
	2h recovery -AG	51	49	51	
	2h recovery +AG	85	82	18	65
G1	100 nM CPT	68			
	2h recovery -AG	39	57	43	
	2h recovery +AG	54	79	21	51
S	100 nM CPT	132			
	2h recovery -AG	34	26	74	
	2h recovery +AG	101	77	23	69
G2	100 nM CPT	109			
	2h recovery -AG	28	25	75	
	2h recovery +AG	87	79	21	72

Table 4. 6. The effect of 0.4 μ M AG014699 on the repair of CPT-induced DSB in the K562 cells evaluated by neutral comet assay.

Analysis of data shown in Figure 4.20 calculated as described for Table 4.3.

4.8. Discussion

The purpose of this chapter was to examine the impact of inhibition of PARP-1 activity on the amount of DNA damage resulting from exposure of cells to CPT. CPT-induced cytotoxicity is believed to be related to DNA damage. PARP inhibition is reported to increase DNA damage by TopoI poisons and retard the repair of CPT-induced DNA breaks in asynchronous K562 cells (Smith, 2005). In the previous chapter, the greater sensitivity of S phase cells to CPT was demonstrated. In this chapter, the effect of PARP inhibition on the induction of total DNA breaks and the more cytotoxic DSB was investigated after short drug exposures together with the repair of these breaks in different cell cycle phases. The aim was to correlate these findings with the observations made regarding cytotoxicity and PARP-1 and TopoI expression and activity. Since cell elutriation was used to separate cells into different phases of the cell cycle, it was important to demonstrate that this did not introduce DNA breaks. There was no evidence that the elutriation process caused DNA breakage in concordance with the data in Chapter 3 showing that elutriation did not affect cell growth or viability. Surprisingly, there were no cell cycle phase differences in the OTM, indicating that Okazaki fragments formed during S phase do not contribute to comet tails.

In these studies, total DNA breaks were measured by alkaline comet assay. Topoisomerase I poisons, such as CPT, directly introduce DNA SSB, some of which may be converted to DSB through downstream processing or collision with replication forks (Tuduri et al., 2010). Therefore, most of the breaks measured by alkaline comet assay are SSB. As expected, DNA breaks were increased relative to the concentration of CPT administered. The higher levels of DNA breaks observed in S and G2 cells could be related to the higher DNA content in these phases. Induction of DNA breaks could also be related to TopoI activity, which was highest in S phase, and expression, which was highest in G2. AG014699 increased the level of breaks to a similar extent at all phases of the cell cycle so this does not explain the greater sensitisation in S phase. Conversion of SSB to DSB is likely to be the cytotoxic event. Other studies have demonstrated that the potentiation of temozolomide, another DNA SSB-inducing agent, by a PARP inhibitor correlated with DSB, rather than SSB induction. In these studies 17-24 h incubation with the PARP inhibitor, ABT-888, was needed for maximum sensitization of asynchronous cells but only 7h was needed in S phase cells (Liu et al., 2008). Similarly, potentiation of alkylating agent cytotoxicity (MMS) by the PARP inhibitor 4-amino-1,8-naphthalimide was associated with the accumulation of DSBs in S phase (Heacock et al., 2010).

DNA DSB were measured by two methods; neutral comet, which is a direct and physical method, and γ H2AX focus formation, which is an indirect but more sensitive method that depends on DNA damage signalling by ATM/ATR and DNA-PK. These kinases all phosphorylate H2AX in response to DNA DSB or stalled replication fork (Darzynkiewicz et al., 2009). Comparing the data in section 4.5.1 and 4.5.2 it can be seen that the effect of CPT, with or without AG014699, on DSB induction is similar by both methods. In contrast to the alkaline comet data, DSB induction, measured by both neutral comet and γ H2AX focus formation was greatest in S and G2 phases and lowest in G1 phase. This suggests that collision with the replication fork is a major mechanism for the induction of DSB, but that other mechanisms (possibly related to DNA content) may operate in G2. AG014699 consistently increased the level of DSB, with the most marked effect in S phase consistent with the greatest cytotoxic enhancement in this phase.

The mechanism by which DNA breaks were increased was investigated further in terms of measuring whether AG014699 inhibited the repair of these lesions. PARP-1 plays a major and well-documented role in DNA SSB repair with evidence also for a role in DNA DSB repair (Audebert et al., 2006, Wu et al., 2008, Mitchell et al., 2009, Iliakis, 2009). Consistent with previously published data (Padget et al., 2000, Smith, 2005), there was a rapid resolution of total DNA breaks and also specifically DSBs. DSBs were slower to repair than total breaks with only 66% (Table 4. 4) of DSBs resolving 1h after removal of CPT, compared with >90% of total DNA breaks (Table 4. 3),

The role of PARP in the repair of DNA breaks at different phases of the cell cycle has not been reported to date. Therefore the effect of AG014699 on the repair of total and DSB, induced by a 30 min pulse with CPT, was determined at all phases of the cell cycle. Repair of total breaks was marginally faster in S phase cells but broadly similar in all phases of the cell cycle. However, repair of DSBs was more rapid in S and G2 phases than in G1, although this may reflect the lower levels of DNA breaks in G1 phase to start with. AG014699 consistently inhibited the repair of DNA DSB across all phases of the cell cycle but had the most significant effect in S phase cells. Currently there is significant uncertainty about the role of PARP-1 in DNA DSB repair (Veuger et al., 2004, Wang et al., 2005, Mitchell et al., 2009) which may partially be due to the different systems used. Recently PARP-3 has been implicated in DNA DSB repair (Boehler et al., 2011b). There is no data on the inhibition of PARP-3 by AG014699 but

the possibility that the reduction in DNA DSB repair and the enhancement of CPT cytotoxicity by AG014699 is due to inhibition of PARP-3 cannot be excluded.

DNA DSB are repaired by 2 major pathways, non-homologous end joining (NHEJ) and homologous recombination repair (HRR) and both processes involve a cascade of proteins to recognise, signal and repair the breaks, some of which are common to both pathways. HR requires the presence of the complimentary copy of DNA as a template to effect error-free repair and can therefore only take place during S and G2 whereas NHEJ is template independent and can occur at all phases of the cell cycle. The decision of which pathway to employ is cell cycle-dependent (Shrivastav et al., 2008). The faster resolution of DSBs during S and G2 phases suggests that HR may be the predominant mechanism for the repair of CPT-induced DSB consistent with the finding that the HR defective *irs1SF* cells were the most sensitive to CPT (Smith et al., 2005). Likewise, the greatest inhibition of DSB repair by AG014699 during S and G2 may point to a direct role of PARP-1 (or PARP-3) in HR.

In the previous chapter, CPT was shown to be more cytotoxic in S phase cells and AG014699 caused the greatest sensitisation of S phase cells. The observation that DSB induction by CPT is greater in S phase than in G1 explains the greater sensitivity of S phase cells to CPT. However, similarly high levels of DNA DSBs were seen in S and G2 cells, which does not explain why G2 cells are less sensitive to CPT cytotoxicity than S phase cells. Similarly, although AG014699 mediated inhibition of repair was most significant in S phase, there was still a very substantial inhibition in G2 cells. Clearly therefore DNA DSB induced by CPT and inhibition of their repair by AG014699 are major contributors to CPT cytotoxicity. However, the data in this chapter do not entirely explain why S phase cells are so much more sensitive to CPT-induced cytotoxicity than G2 cells.

Summary

- ✓ Elutriation procedures does not introduce DNA damage to processed cells
- ✓ OTM data transformation can overcome some statistical analysis restriction
- ✓ CPT causes concentration dependent increase in total and double stranded DNA breaks
- ✓ AG014699 significantly increased the level of total DNA breaks mostly in synchronous S and G2 phase cells
- ✓ AG014699 significantly increased the level of DSB in synchronous S and G2 phase cells
- ✓ AG015699 significantly retards the repair of total and DSB in asynchronous and elutriated cells K562 cells in all phases of cell cycle, but the most prominent effect of AG014699 is restricted to S phase cells.

Chapter 5. The role of the interaction between PARP and XRCC1 in DSB induction and repair

5.1. Introduction

Previous results chapters show that PARP inhibition results in the greater accumulation of CPT-induced total and DSB, and a slower rate of repair predominantly. The effect of PARP-1 inactivation on increased induction and decreased repair of CPT-induced DNA breaks was observed in all phases of the cell cycle, however the most pronounced effect was seen in S phase enriched K562 cells. The increased persistence of DNA breaks correlates with increased sensitisation to CPT-induced cytotoxicity in the presence of AG014699 also in S phase cells.

As described in the introduction (section 1.6.4) repair of SSB is thought to be dependent on PARP activation recruiting XRCC1. XRCC-1 is a scaffold protein that is necessary for the assembly of other BER/SSBR proteins including Pol β and Ligase III (Almeida and Sobol, 2007). As described in the introduction (section 1.6.4) one hypothesis for the mechanism of PARP-mediated DSB repair also involves XRCC1 and LigIII in a back-up NHEJ (Iliakis, 2009). Thus both PARP-mediated SSB and DSB repair is thought to involve XRCC1 and LigIII. XRCC1 is a necessary partner for PARP-1 and loss of XRCC1 may have the same effect as loss/inhibition of PARP. There are evidences that PARP-1 is required for the assembly or stability of XRCC1 nuclear foci (El-Khamisy et al., 2003).

Chinese hamster ovary AA8 cells, and their XRCC1-defective derivative, EM9 cells (Thompson et al., 1990, Barrows et al., 1998) are excellent tools to investigate if PARP is totally dependent on XRCC1 for its effect or whether it has a role beyond its interaction with XRCC1.

Despite the good pre-clinical data indicating sensitization of TopoI poisons without undue toxicity (Calabrese et al., 2004), the only clinical studies reported to date indicates an increase in topotecan toxicity without any increase in tumour response (Kummar et al., 2011, Samol et al., 2011). Variable data have been obtained clinically with temozolomide (TMZ) and the related DNA alkylating agent, dacarbazine, with regards to efficacy but myelosuppression is a common feature (Plummer et al., 2008, Khan et al., 2011). These results may have beendue to inappropriate dose and/or schedule emphasising the need to thoroughly understand the biology of the drug interactions at the cellular level to aid intelligent drug treatment in patients.

To investigate the mechanisms underlying the chemosensitisation of TopoI poisons and other agents by PARP inhibition, and in particular the dependence on the interaction with XRCC1, the effect of AG014699 on CPT-induced DNA breakage was determined in cells proficient and deficient in XRCC1. In parallel in some of these studies the effect of AG014699 on TMZ and neocarzinostatin (NCS) –induced DSBs and cytotoxicity was determined in the same pair of cell lines by project students Scott Farrenden and Matthias Becker whose were worked under my supervision.

TMZ (brand name - Temadar, Temodal) has been approved for treatment of cancer since early 2000. TMZ (4-methyl-5-oxo-2,3,4,6,8-pentazabicyclo [4.3.0] nona-2 ,7,9-triene-9-carboxamide) is a monofunctional alkylating agent that is an imidazotetrazine derivative of dacarbazine. This product is actively absorbed by cells and under physiological conditions is converted to active MTIC (5-(3-methyl-1-triazeno)imidazole-4-carboxamide) (Chabner i Longo, 1996). As an oral anticancer drug, TMZ slows or stops the growth of cancer cells in the body and is used mainly to treat gliomas and malignant melanoma(Danson and Middleton, 2001)as well as astrocytoma(Hegi et al., 2005). TMZ is usually given once daily for 5 days at a dose of 200 mg/m² and treatment is usually repeated every 28 days, although the length of treatment depends on the patient response. For example, in the treatment of malignant melanoma, there is a response to TMZ in 16 - 31% of treated patients (Stupp et al., 2009). TMZ is a DNA methylating agent causing the formation O⁶-methylguanine (~ 10% of total lesions), N⁷-methylguanine (~ 70%) and N3-methyladenine (~10%) (Newlands et al., 1997). O⁶-methylguanine, which is the most cytotoxic lesion, is repaired by MGMT, and if not repaired it becomes a substrate for MMR. Cells proficient in MMR cells are sensitive to TMZ and loss of MMR confers resistance to it. The most abundant lesions, N⁷-methylguanine and N3-methyladenine, are quickly and efficiently repaired by BER/SSBR. These methylated purines are removed by alkyl adenine glycosylase (AAG) resulting in an AP site. This is then hydrolysed by the endonuclease, APE-1, resulting in a SSB that stimulates PARP-1 activity. As with CPT, unrepaired TMZ-induced lesions obstruct the progression of replication forks and can result in the formation of DSBs at replication (Curtin, 2005, Tentori, 2006, Liu et al., 2008).

Neocarzinostatin (NSC) a macromolecular chromo-protein enediyne antibiotic secreted by *Streptomyces macromomyceticus* with anti-tumour activity. It consists of two parts, the unstable chromophore, and 113 amino acid apoprotein to which the chromophore is

tightly non-covalently bound. The chromophore is a potent DNA damaging agent, it is very unstable and the role of apoprotein is to protect it and release it to the target DNA leading to a di-radical intermediate, and finally cut double-stranded DNA. NCS causes SSB as well as DSB in ratio 6:1. This is a very high frequency of DSB induction, about 3-fold higher than irradiation and unlike CPT or TMZ damage induction is not dependent on replication for their generation.

Therefore in this chapter three agents that induce different types of DNA damage were investigated: CPT, which produces SSB with one end attached to topoisomerase I that may cause replication stalling and associated DSBs; TMZ, which induces base damage that results in DNA SSBs as repair intermediates that may also cause replication stalling and associated DSBs; and NCS which induces both SSB and a high level of DSB directly.

5.2. Aims

The aim of the work described in this chapter was to establish whether inhibition of DNA repair and chemosensitisation by PARP inhibition is dependent on an interaction with XRCC1 or if PARP has a role independent of XRCC1. To verify if the effects of PARP inhibition are mediated by XRCC1 in both SSB and DSB repair, the effects of AG014699 on CPT, TMZ and NCS-induced DNA damage, repair and cytotoxicity in cells with and without XRCC1 was measured.

5.3. Verification of XRCC1 expression in AA8 and EM9 cells by Western blot

Before conducting further experiments, it was important to determine if cells that were used had any possible background expression of XRCC1

The level of XRCC1 was determined in whole cell extracts prepared from AA8 and EM9 cells using anti-XRCC1 monoclonal antibody by Western blotting, as described in section 2.11. To achieve this, an equal number of AA8 and EM9 cells were used to prepare whole protein lysate using Leamlli buffer. Three different volumes of lysates (5, 15, 30 μ l) for each cell line were loaded onto the gel and run on a 4-15% gradient gel and blotted onto nitrocellulose membrane before probing with anti-mouse XRCC1 and later anti actin antibody to verify loading .

Figure 5. 1 shows overlaid images of membrane with protein standard, and bands corresponding to actin and XRCC1. Actin loading control, indicates that more protein extract (approximately two times more) of EM9 cells has been loaded (*e.g.* compare second actin band of EM9 with first actin band of AA8). Despite this no XRCC1 has been found in the EM9 cells but could be seen in AA8 cells.

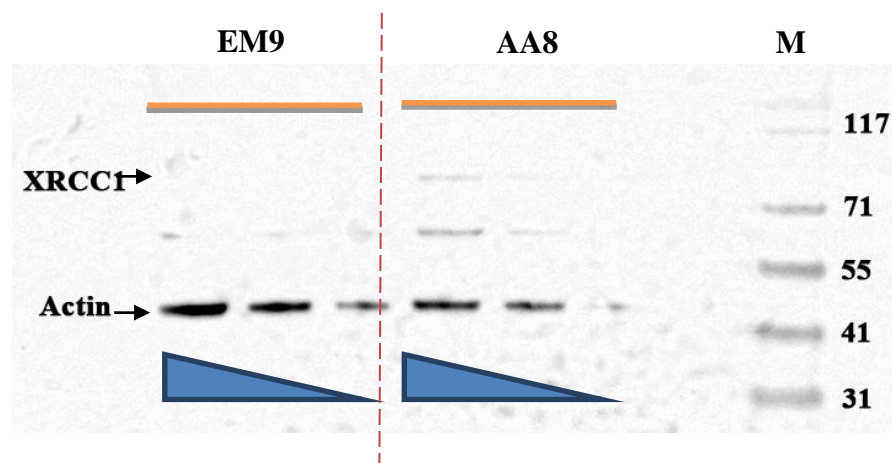


Figure 5. 1. Western blot of XRCC1 in AA8 and EM9 cells

Total cell lysate in the volume of 5, 15, and 30 μ l obtained from AA8 and EM9 cells was loaded per line. Western blotting was performed as described in section 2.11. Blots were probed with anti-XRCC1 monoclonal and antibody and anti-actin monoclonal antibodies and corresponding secondary antibodies.

5.4. Effect of AG014699 on the formation and repair of DNA breaks in EM9 and AA8 cells.

The XRCC1 deficient cells have DNA repair dysfunction (Shen et al., 1998). Because PARP-mediated DNA repair is thought to be dependent on XRCC1 recruitment to the DNA break site, inhibition of PARP activity in EM9 cells should not have marked effects, in contrast to AA8 cells that have normal expression of XRCC1. To clarify this possibility the level of DNA damage (total and DSB) in AA8 and EM9 in cells exposed to TMZ, CPT and NCS were studied. To be comparable to previous data, AG014699 was used at a concentration of 0.4 μ M in all experiments

5.4.1. CPT induced total DNA breaks measured by alkaline comet assay.

AA8 and EM9 cells were incubated with CPT \pm AG014699 for 30 min then subjected to alkaline comet assay in order to determine the induction of total DNA strand breakage. To examine the level of the repair of DNA damage caused by CPT, and the effect of AG014699 on this repair, cells were first incubated with the CPT alone for 30 min and then medium was replaced with fresh medium or medium containing AG014699, and incubations was continued for further 2h. After incubation, the cells were subjected to the alkaline comet assay to investigate the kinetics of DNA damage repair.

Figure 5. 2 shows representative images of comets taken for this experiment. This photomicrograph shows a mixture of cells that differ in the length of the tail. Regardless of experimental conditions, a wide range of DNA damage can be observed, indicated by cells that do not have any tail and cells having very large tails This is because cells were asynchronous and the population of cells with large tails may represent the S phase population. Nevertheless, a tendency to increase the number of cells with large tail can be observed on images taken for 100 nM CPT comparing to control, DMSO treated cells. Both, the number of cells with tails and their comet tail length increases in images taken for the cells incubated with CPT + AG014699.

Control EM9 cells have slightly longer tails than control AA8 cells, which is probably associated with a defective mechanism for BER in these cells leading to an increase in unrepaired endogenous SSBs. However, the mean OTM of comets in control AA8 and control EM9 was 1.1 ± 0.24 and 1.27 ± 0.33 respectively, which was not statistically significant ($p=0.36$, LSD). These values were taken as the 100% baseline control for normalisation of treated cells, which were expressed as a % of these untreated controls.

Quantitative data that were obtained from the analysis of comet images are shown in Figure 5. 3 and Table 5. 1. These data show that AG014699 had a significant impact on DNA breaks in both cell lines. A significant increase in DNA breaks was observed following 100 nM CPT treatment in both cell lines. The percentage increase in DNA damage level induced by CPT in EM9 cells was almost twice that in AA8 cells (119% versus 56% - bars 3 and 9). Exposure of cells to CPT + AG014699 caused a significant increase in the amount of CPT-induced DNA damage in AA8 cells by 2.3-fold compared to CPT alone ($p = 0.02$, LSD). In contrast AG014699 only increased the level of breaks from 119 to 160.5% in EM9 cells (bars 9 and 10).

To examine the repair of DNA damage induced by CPT, EM9 and AA8 cells were first incubated with 100 nM of CPT alone for 30 min and then when CPT was removed incubation was continued in fresh medium or medium containing AG014699 for a further 2h (hatched bars in Figure 5. 3).

In the AA8 cells, all the DNA breaks were repaired during the 2 h incubation in fresh medium and there was no significant difference from baseline [compare bar 1 and 5 in Figure 5. 3]. However, AG014699 completely blocked repair and there was no significant difference at 2 h in AG014699-containing medium from unrepaired CPT-treated cells [bars 3 and 6]. Surprisingly, in EM9 cells repair was also virtually complete after 2 h in fresh medium (being only 8% higher and not significantly different from baseline, $p = 0.16$) [bar 7 and 11]. AG014699 had a significant impact on repair in these cells too, since only 50-60% of breaks had been repaired and the level of breaks was still significantly higher than both baseline ($p = 0.002$) [bar 7 and 12] and cells that repaired in fresh medium ($p = 0.05$) [bar 11 and 12].

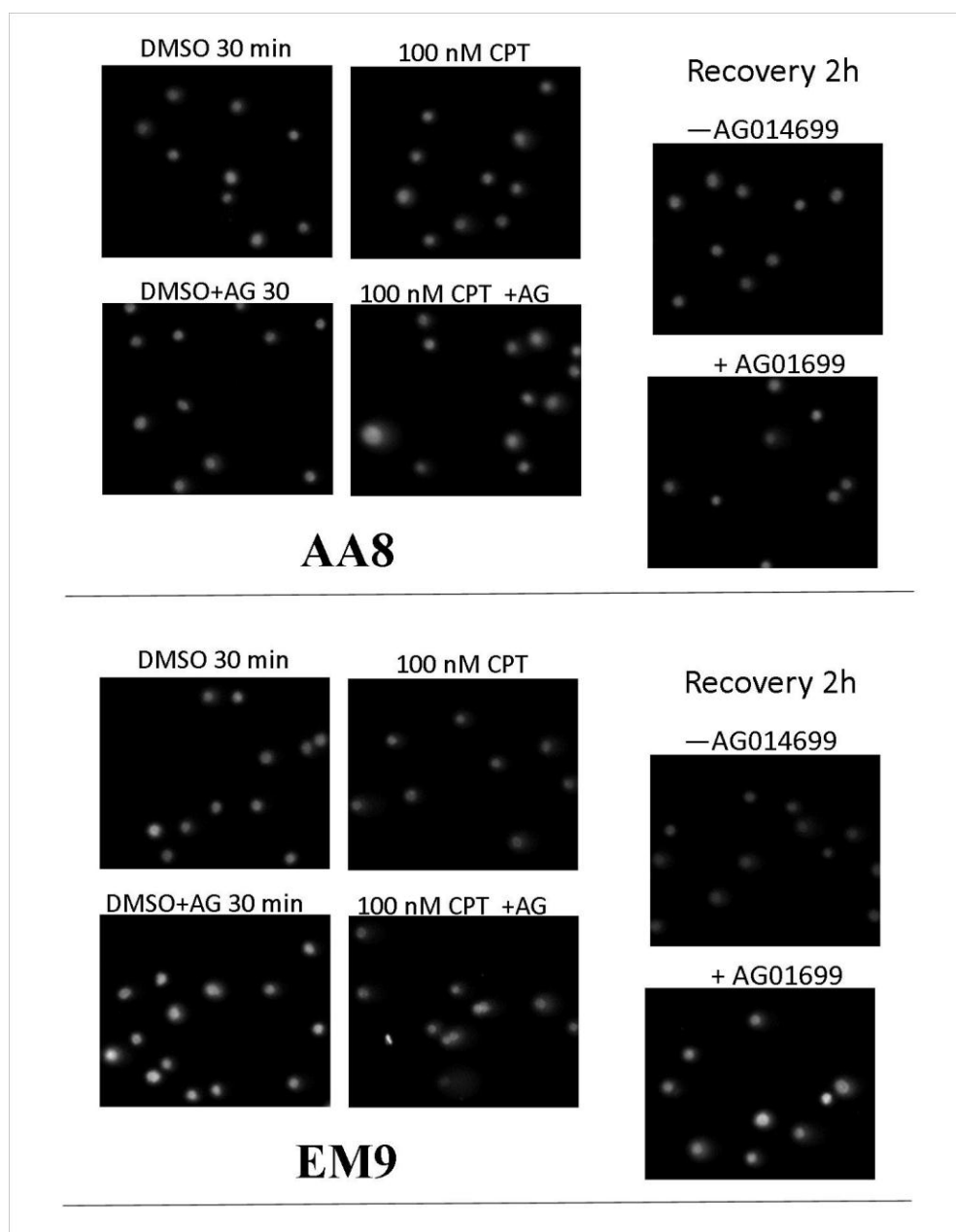


Figure 5. 2. Images of comets showing induction and repair of CPT induced total DNA breaks.

AA8 and EM9 cells were incubated for 30 min with 100 nM CPT \pm 0.4 μ M AG014699. To investigate the repair of CPT-induced DNA breaks following 30min with CPT alone, CPT was removed and incubation of cells was carried on for next 2h in medium without (-AG014699) or with (+AG014699) PARP inhibitor. The alkaline comet assay was performed to evaluate the level of total DNA breaks in these cells Conditions -VWR electrophoresis tank, 0.7V/cm, 200-300 mA, 30 min.

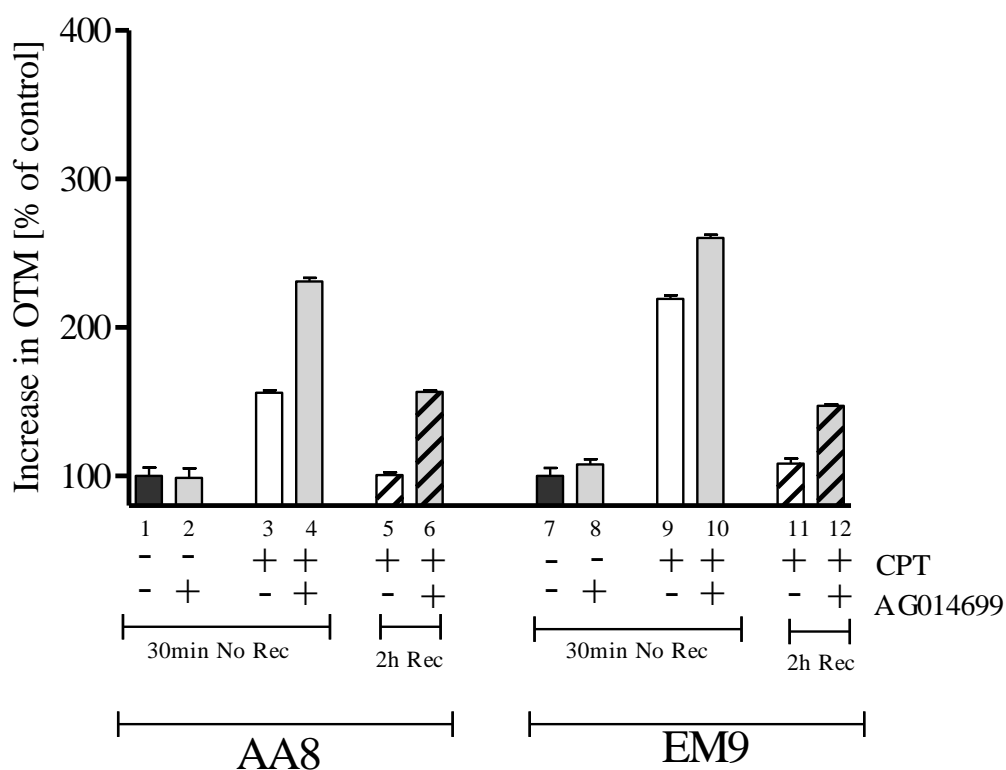


Figure 5. 3. Effect of AG014699 on induction and repair of SSB induced by CPT

Comet images shown in Figure 5. 2 were used to determine DNA damage by measuring the OTM. The Values of OTM from each experiments were expressed as a percentage of CPT alone control. Means of 3 independent experiments+ SEM are shown.

Treatment Conditions		% Increase in OTM CPT	% increase in OTM CPT+ AG
AA8	30 min No Rec	56.0 ³⁾	131.1 ⁴⁾
	2h Recovery	0.7 ⁵⁾	56.6 ⁶⁾
EM9	30 min No Rec	119.4 ⁹⁾	160.5 ¹⁰⁾
	2h Recovery	8.3 ¹¹⁾	47.2 ¹²⁾

Table 5. 1. Formation and repair of total DNA breaks in AA8 and EM9 cells

Analysis of data shown in Figure 5. 3. The % increase in OTM was calculated as described in the legend to Table 4. 1. The partially bracketed superscript numbers refer to the relevant bar in Figure 5. 3.

5.4.2. Effect of AG014699 on the formation and repair of CPT-induced DSB in EM9 and AA8 cells.

The treatment conditions in which the experiment was carried out are the same as described in section 5.4.1. The comets shown in Figure 5. 4 are different from those taken in alkaline comet assay. Comparable to the total DNA breaks the DSB observed in Figure 5. 4 are greater in EM9 cells in both control. The mean OTM of comets in control AA8 and control EM9 was 2.4 ± 0.9 and 2.9 ± 0.9 respectively, which was not statistically significant ($p=0.16$). These values were taken as the 100% baseline control for normalisation of treated cells which were expressed as a % of these untreated controls). Treatment with CPT caused a greater accumulation of DSBs in EM9 compared to AA8. In AA8 cells co-incubation with AG014699 doubled the increase in OTM from 81% to 161% but had only a modest effect in EM9 (Table 5. 2). The data in Figure 5. 5 and in Table 5. 2 show an effect of AG014699 on the repair of CPT-induced DSB. This effect was investigated following 2h recovery period during which cells exposed to CPT were incubated in fresh or AG014699 supplemented medium. Surprisingly in AA8 cells the repair of DSB in fresh medium appeared slower than in EM9 cells. However, after 2 hours incubation in fresh medium the level of DNA damage was not significantly different from the control ($p > 0.1$) in either cell line therefore it can be assumed that both cell lines repaired DSB to similar extent. AG014699 significantly delayed the repair of DSB in both AA8 and EM9. At the end of 2h recovery period there was still 55.% DSB left in AA8 cells and 41% DSB left in EM9 the delay in repair was significant in both cell lines ($P < 0.05$). The data in both these experiments indicate that accumulation of total and DSB is dependent on PARP and XRCC1 together (i.e. AG014699 has no effect on break induction in EM9) but that PARP inhibition has an impact on repair over and above the loss of XRCC1 (i.e. it retards repair in EM9).

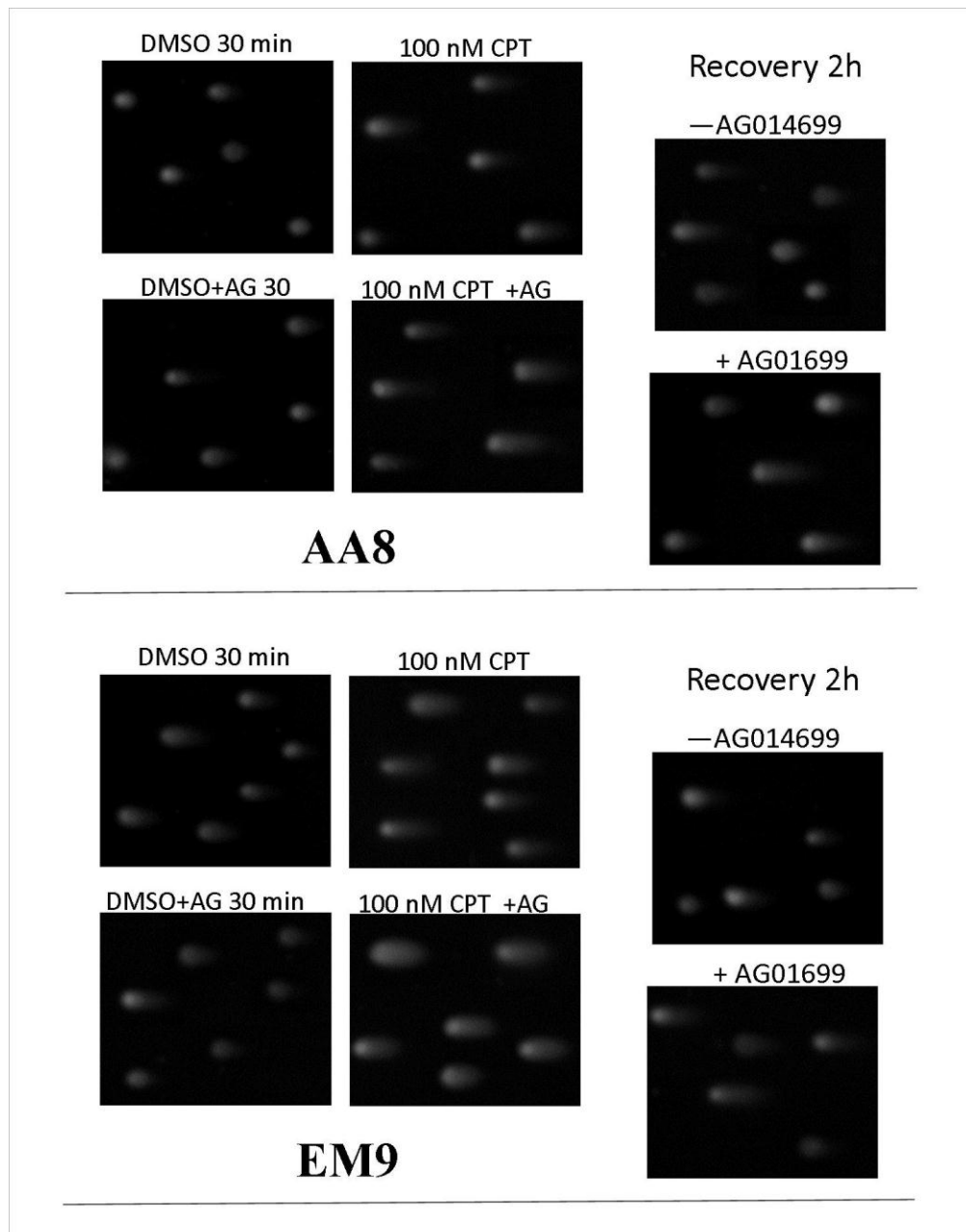


Figure 5. 4. Images of comets showing induction and repair of CPT induced DSB DNA breaks.

The experiment was performed as described in Figure 5. 2 but the neutral comet was used to estimate the level of DNA double strand breaks. Conditions -VWR electrophoresis tank, 1V/cm, 30 min.

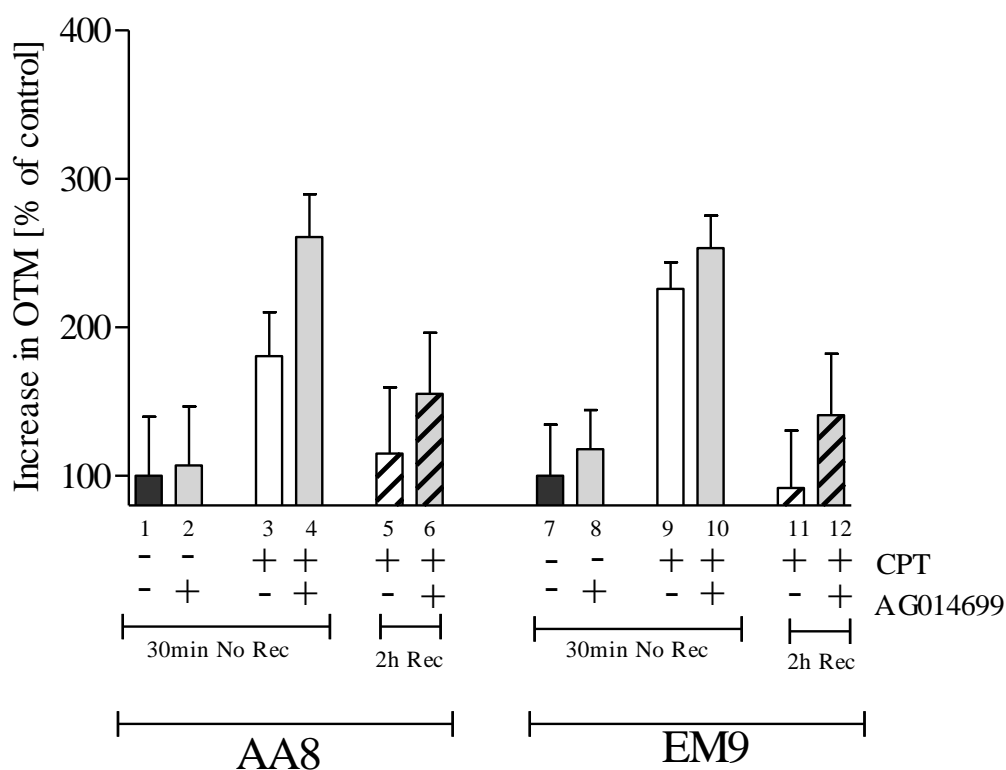


Figure 5. 5. Effect of AG014699 in induction and repair of DSB induced by CPT

Comet images shown in Figure 5. 4 were used to determine DNA damage by measuring the OTM. The Values of OTM from each experiments were expressed as a percentage of CPT alone control. Means of 3 independent experiments+ SEM are shown.

Treatment Conditions		% Increase in OTM CPT	% increase in OTM CPT+ AG
AA8	30 min No Rec	80.7 ³⁾	161.0 ⁴⁾
	2h Recovery	18.8 ⁵⁾	55.3 ⁶⁾
EM9	30 min No Rec	126.1 ⁹⁾	153.4 ¹⁰⁾
	2h Recovery	0.0 ¹¹⁾	41.0 ¹²⁾

Table 5. 2 Effect of AG014699 in induction and repair of DSB induced by CPT.

Analysis of data shown in figure 5.5. The % increase in OTM was calculated as described in the legend to Table 4.1. The partially bracketed superscript numbers refer to the relevant bar in Figure 5.5.

5.4.3. Effect of AG014699 on the formation and repair of CPT-induced DSB in EM9 and AA8 cells determined by H2AX immunofluorescence

Data from the previous section suggest that AG014699 plays role in the induction and repair of DSB induced by 100nM CPT in Chinese hamster ovary as well as K562 cells. In this section these data were confirmed using γ H2AX immunostaining, which is a more sensitive method than the comet assay.

AA8 and EM9 cells were grown on microscope cover slips for 24h before treatment. The treatment with 100 nM CPT was conducted for 30 min in the presence or absence of AG014699. For investigation of the reversal of CPT-induced DNA breaks, cells were first incubated with CPT for 30 min, then medium was replaced with fresh medium or medium containing AG014699, and incubation was continued for further 2h. After the treatment, cells were stained for the presence of γ H2AX and images of foci and DAPI staining in 8-bit grayscale were obtained by Leica fluorescence microscope using the Advanced-SPOT software, as described in section 2.10, because the foci were large and diffuse making them difficult to quantify by counting. Data presented in Figure 5. 6 shows the level of CPT-induced γ H2AX fluorescence in AA8 and EM9. The level of γ H2AX fluorescence in control EM9 cells was slightly higher than in AA8 but this difference was not significant. Also AG014699 alone did not have significant effect on fluorescence intensity. Incubation of cells with CPT caused a similar (approximately 150%) increase in the level of fluorescence intensity in both cell lines Table 5. 2. The presence of AG014699 during 30 min of incubation with CPT caused a further 40% increase in the DSB level in AA8 cells (bar 4) and 100% increase in EM9 cells (bar 10). After the removal of CPT, damage induced in AA8 was decreased by 30% but no apparent repair was observed in EM9 (compare bars 9 with 11). Curiously, in the presence of AG014699 (hatched bars in Figure 5. 6) γ H2AX fluorescence continued to increase in AA8 cells and this increase was even more pronounced in the EM9 cells.

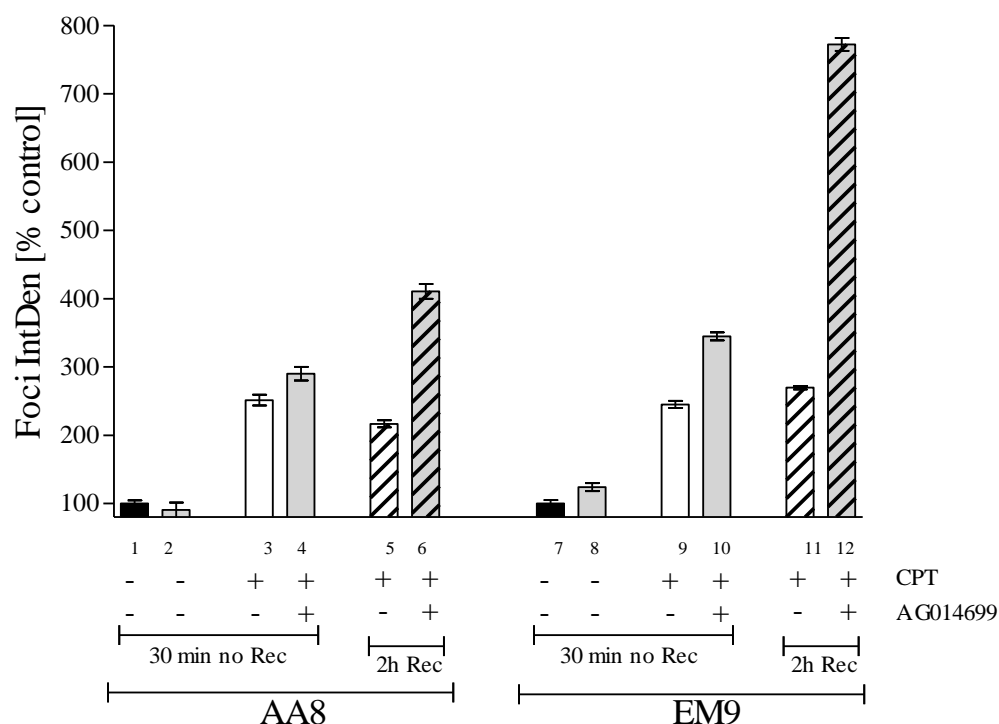


Figure 5. 6 AG014699 effect on induction and repair of CPT-induced DSB

Treatment Conditions		% Increase in OTM CPT	% increase in OTM CPT+ AG
AA8	30 min No Rec	151.3 ³⁾	190.1 ⁴⁾
	2h Recovery	116.7 ⁵⁾	310.5 ⁶⁾
EM9	30 min No Rec	145.2 ⁹⁾	244.8 ¹⁰⁾
	2h Recovery	169.7 ¹¹⁾	672.3 ¹²⁾

Table 5. 3. Effect of AG014699 in induction and repair of DSB induced by CPT

AA8 and EM9 cells were incubated for 30 min with CPT \pm AG014699 and then subjected to staining for the presence of γ H2AX foci. To investigate the repair of DNA damage caused by CPT after 30 min incubation in medium with CPT, the medium was replaced with fresh medium or medium containing AG014699 and incubation was continued for a further 2 hours. Using a macro PZFociEZ integrated fluorescence density of γ H2AX foci per nucleus was measured. Data on the graph shows mean integrated density of three independent experiments \pm SEM expressed as percentage of control (DMSO). The partially bracketed superscript numbers in the Table 5. 3 refer to the relevant bar in Figure 5. 6.

5.4.4. Effect of AG014699 on the formation and repair of TMZ-induced DSB in EM9 and AA8 cells.

Data presented in Figure 5. 7 shows that TMZ increased the level of H2AX phosphorylation in both AA8 and EM9 cells. TMZ alone increased the level of γ H2AX in EM9 cells more than in AA8 cells (white bars). Incubation of cells with TMZ for 4 hours with AG014699 resulted in higher induction of DNA damage in EM9 than in AA8 cells (grey bars). There was 55% increase in the level of DSB caused by AG014699 in AA8 cells and 62% increase in EM9 cells. Figure 5. 7 shows also the repair of TMZ-induced DSB during 2h recovery period in the presence or absence of AG014699 [bars 5, 6 and 7,12]. After 2 h incubation in fresh medium TMZ-induced DSBs in AA8 cells were efficiently repaired (85% reduction in fluorescence intensity – compare bar 3 with 5), while in the EM9 cells there was no reduction in γ H2AX. The presence of AG014699 during the recovery period significantly slowed down the repair of DNA DSB in AA8 cells with only a 23% reduction in γ H2AX (bar 3 and 6), and even increased its level in EM9 cells (bars 9 and 12).

The kinetics of disappearance of H2AX fluorescence after TMZ removal was similar to after CPT removal, i.e. substantial reduction in AA8 but virtually no change in EM9. In the presence of AG014699, the reduction of H2AX fluorescence was minimal in AA8 and actually increased in EM9.

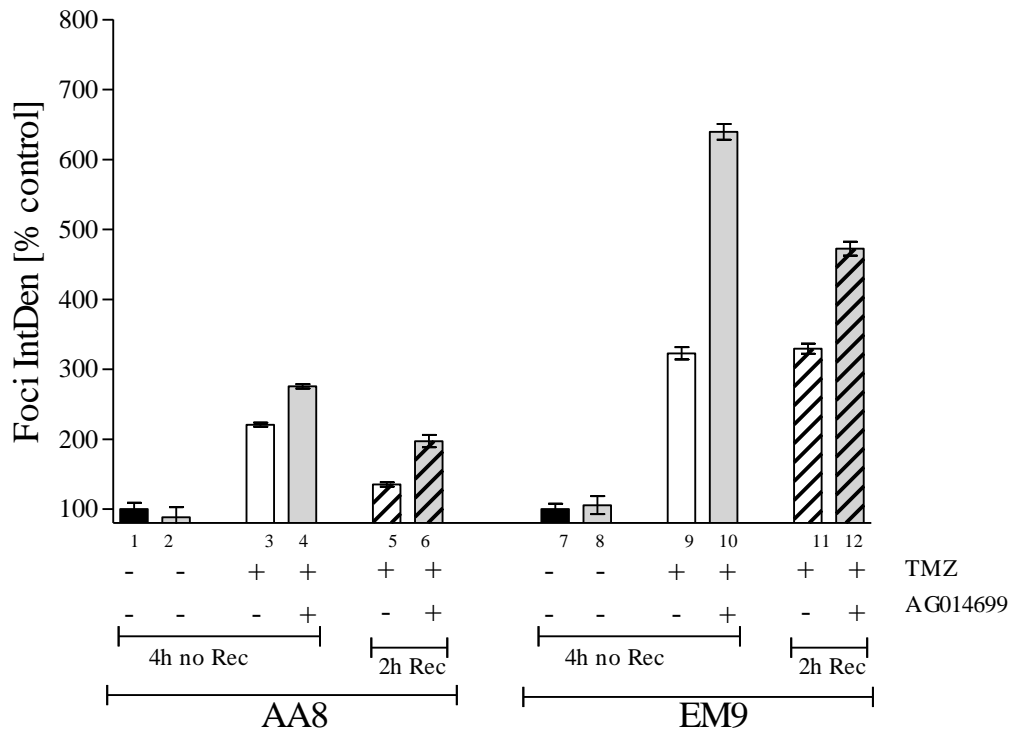


Figure 5. 7. AG014699 effect on induction and repair of TMZ-induced DSB

Treatment Conditions		% Increase in OTM CPT	% increase in OTM CPT+ AG
AA8	4h No Rec	220.7 ³⁾	275.8 ⁴⁾
	2h Recovery	135.3 ⁵⁾	197.3 ⁶⁾
EM9	4h No Rec	322.8 ⁹⁾	639.3 ¹⁰⁾
	2h Recovery	329.4 ¹¹⁾	472.4 ¹²⁾

Table 5. 4. Effect of AG014699 in induction and repair of DSB induced by TMZ

AA8 and EM9 cells were incubated for 4 h with TMZ and AG014699 and then subjected to staining for the presence of γ H2AX foci. To investigate the repair of DNA damage caused by TMZ after 4 hours incubation in medium with TMZ, the medium was replaced with fresh medium or medium containing AG014699 and incubation was continued for a further 2 hours. Using a macro PZFociEZ integrated fluorescence density of γ H2AX foci per nucleus was measured. Data on the graph shows mean integrated density of three independent experiments \pm SEM expressed as percentage of control (DMSO). The partially bracketed superscript numbers in the Table 5. 4 refer to the relevant bar in Figure 5. 7.

5.4.5. Effect of AG014699 on the formation and repair of neocarzinostatin-induced DSB in EM9 and AA8 cells.

CPT and TMZ primarily induce DNA SSB that are converted to stalled replication forks and replication-associated DSBs. To determine the effect of PARP inhibition on the repair of frank DSBs, cells were incubated with NCS. Disappearance of γ H2AX foci formed in cells AA8 and EM9 after exposure to NCS±AG014699 for 1h was measured at 0, 1, 2, 4, and 24 hours after drug removal using the integrated fluorescence to determine the kinetics of DSB repair in the absence and presence of 0.4 μ M AG014699.

Figure 5. 8 shows a decrease in the integrated fluorescence integrated over time and is a measure of the rate of disappearance of DSBs. Both in AA8 cells and EM9 in the initial phase of incubation (1h after removal of the NCS medium) there is an increase of fluorescence intensity in all tested conditions. After 1h, the fluorescence intensity decreases with the progressive repair of damaged DNA.

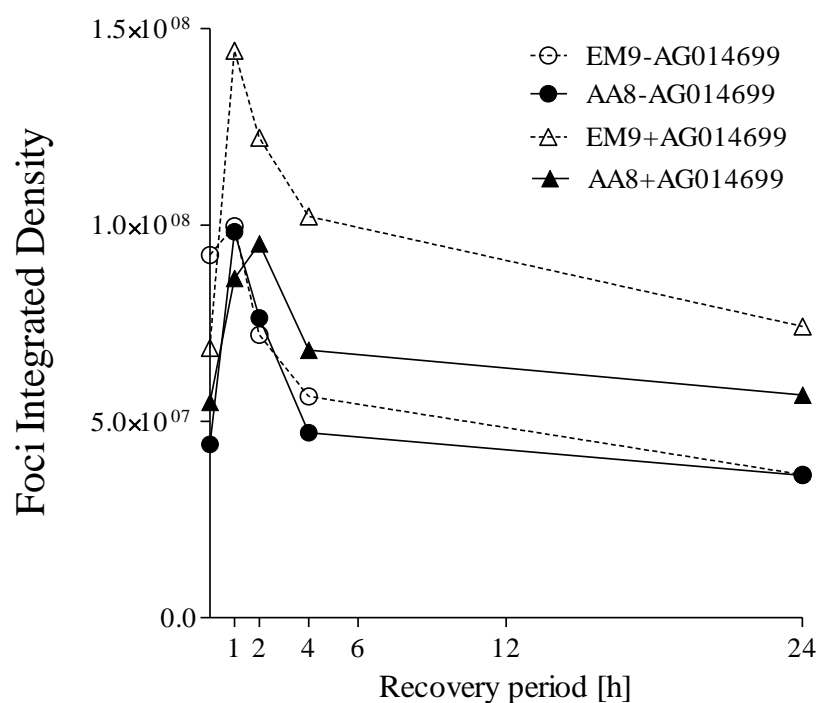


Figure 5. 8. The effect of AG014699 on neocarzinostatin-induced DSB

AA8 and EM9 cells were exposed to neocarzinostatin for 1h and drug was replaced with fresh medium or medium containing AG014699 and incubation was carried on for up to 24 hours.

NCS causes a profound increase in γ H2AX fluorescence intensity in both cell lines to an approximately equal amount at 1h. AG014699 caused a substantial increase in the level of γ H2AX at this time in EM9 cells but delayed the peak in AA8 cells. In the AA8 cells H2AX phosphorylation had returned to baseline 4 h after NCS removal, but was still elevated in the presence of AG014699 at 24 h. Repair was slightly slower in EM9 cells and very substantially retarded by AG014699. By 24 h γ H2AX levels had returned to baseline in both AA8 and EM9 cultured in drug-free medium but was still substantially elevated in the presence of AG014699, indicating compromised DSB repair, in both cell lines.

5.5. The effect of PARP-1 inhibition on CPT, TMZ and neocarzinostatin induced cell cytotoxicity.

DNA damage induction and repair data in previous section of this chapter indicates that AG014699 increased the level and reduced the rate of repair of DNA breaks in both AA8 and EM9 cells. To strengthen these data the effect of AG014699 on cytotoxicity mediated by CPT, TMZ and NSC was also examined.

The effect of PARP inhibition on the cytotoxicity caused by exposure to CPT, TMZ and NSC was studied using clonogenic assay. AG014699-mediated potentiation of the cytotoxicity caused by CPT and TMZ in EM9 and AA8 cell lines, was evaluated in parallel experiment, by seeding AA8 and EM9 cells in 6 well plates in different densities (125, 250, 500, 1000, 2500, 5000 cells) per well, in 2 ml of medium at the day before treatment with CPT or TMZ. The next day, medium was replaced with 2 ml of medium with an appropriate dose of CPT or TMZ \pm AG014699 and incubated for 30 min or 4 h (control- 0.5% DMSO \pm AG014699 medium) and then replaced with fresh medium without drugs and incubation was continued for 7 days to allow the creation of colonies. When colonies were visible, plates were stained with crystal violet, and colonies were counted by eye. This method differs from that described in the section 2.4.2 however, is less complicated, therefore results can be obtained faster.

The effect of PARP inhibition on the cytotoxicity caused by exposure to CPT, TMZ and NSC was studied using clonogenic assay. AG014699-mediated potentiation of the cytotoxicity caused by CPT and TMZ in EM9 and AA8 cell lines, was evaluated in parallel experiment, by seeding AA8 and EM9 cells in 6 well plates in different densities (125, 250, 500, 1000, 2500, 5000 cells) per well, in 2 ml of medium at the day before treatment with CPT or TMZ. The next day, medium was replaced with 2 ml of medium

with an appropriate dose of CPT or TMZ \pm AG014699, incubated for 30 min (control-0.5% DMSO \pm AG014699 medium), and then replaced with fresh medium without drugs and incubation was continued for 7 days to allow the creation of colonies. On day, plates were stained with crystal violet, and colonies were counted by eye. This method differs from that described in the section 2.4.2 however, is less complicated, allowing to obtain the results shorter.

For the NSC-induced cytotoxicity, cells were maintained in exponential growth phase before dosing with drug. Following the treatment, cells were trypsinized and plated in known densities in 90 mm petri dish and left to grow and form colonies allowing to obtain the results shorter.

For the NSC-induced cytotoxicity, cells were maintained in exponential growth phase before dosing with drug. Following the treatment, cells were trypsinized and plated in known densities in 90 mm petri dish and left to grow and form colonies (section 2.4.2).

Because of insufficient time most of these data are for a single experiment, so statistical analysis cannot be performed. However, the results obtained were consistent with predicted results. First, the cytotoxicity induced by CPT was studied in AA8 and EM9 cells exposed to CPT for 30 min. The 30 min exposure was chosen to be able to compare these data with data from previous chapters where the same exposure time was used. Data in Figure 5. 9 shows that EM9 cells were more sensitive to CPT (estimated LC50 between 1 and 10 nM) than AA8 cells (LC50>100 nM). Nevertheless, sensitisation by AG was similar in both cell lines *e.g.* at 1 nM CPT AG reduced survival from 104% to 84% in AA8 and from 75% to 52% in EM9.

Figure 5. 10 shows the results of the cytotoxicity experiment for AA8 and EM9 cells exposed to TMZ \pm AG014699 for 4h. In both cell lines TMZ reduced survival, which was concentration-dependent at least in AA8 cells. However the concentrations of TMZ were too low to have a marked effect on cell survival. AG014699 caused a further reduction in survival, which was more marked in the EM9 cells. Clearly, these data, based on a single experiment are insufficiently robust to draw major conclusions but taken together these results were consistent with data obtained for CPT, and indicates that PARP inhibition sensitises cells to TMZ irrespective of XRCC1 status

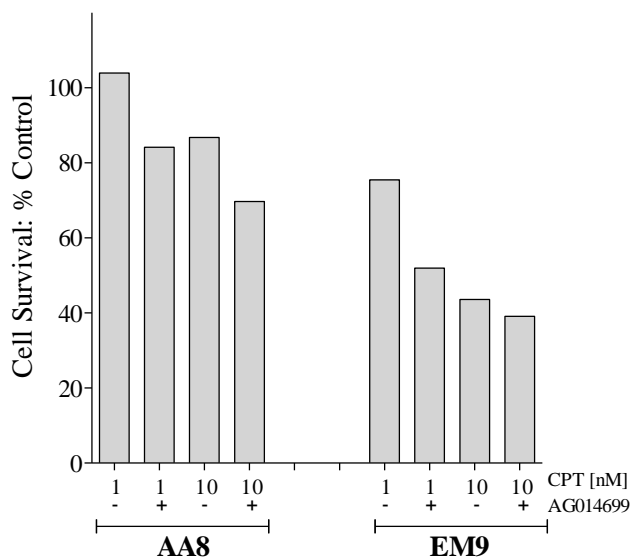


Figure 5. 9. Survival of AA8 and EM9 cells following increasing concentration of CPT±AG014699

AA8 and EM9 cells were incubated with CPT ± AG014699 for 30 min and cell survival was evaluated by colony forming assay. Graph shows data for one experiment.

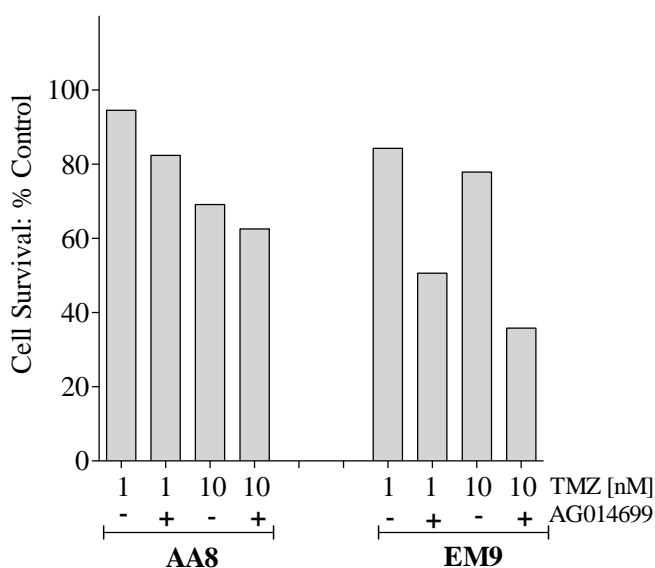


Figure 5. 10. Survival of AA8 and EM9 cells exposed to TMZ±AG014699.

AA8 and EM9 cells were exposed to 0, 1, 10 μM TMZ for 4h and its survival was evaluated by clonogenic assay. Graph plotted using data from one experiment.

To investigate the role of PARP and XRCC1 in the survival of cells treated with a DSB-inducing agent AA8 and EM9 cells were exposed to range concentrations of NCS \pm 0.4 μ M AG014699 for 1h. Following incubations drugs was removed, cells were diluted and plated in desired density in fresh medium for colony formation assay.

Figure 5. 11 shows that cytotoxicity caused by NCS in AA8 and EM9 cells is similar to cytotoxicity caused in these cells by CPT and TMZ. Neocarzinostatin causes more cell death in EM9 cells than in AA8 cells. For example, after incubation of AA8 cells with 10 nM NCS 7.8% cells survived, whereas the same dose resulted in the 2.8% survival in EM9 cells. In AA8 cells co-incubation AG014699 reduced survival to 2.6% (a 3-fold reduction compared to NCS alone) and in EM9 cells survival was reduced to 0.8% (a 3.5-fold reduction compared to NCS alone). Thus, AG014699 seems to have a similar effect in both cell lines.

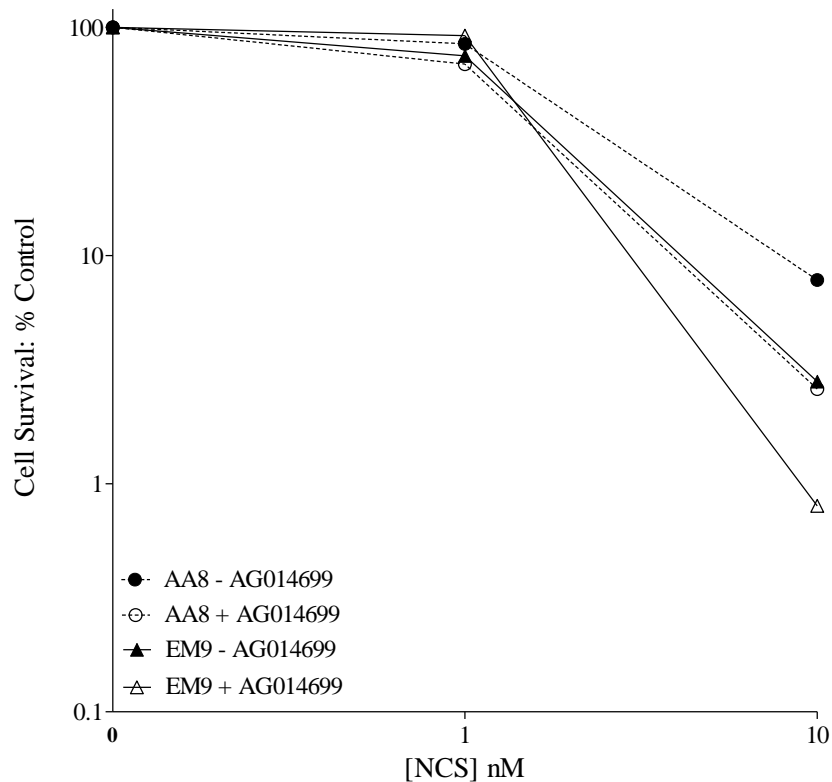


Figure 5. 11. Effect of AG014699 on neocarzinostatin-induced cell cytotoxicity.

The AA8 and EM9 cells were incubated with NCS \pm AG014699 for 1h and survival in response to treatment was evaluated by colony forming assay. Data show a representative experiment out of 3 that were performed.

5.6. Discussion.

Investigations described in this chapter aimed to determine and describe the interaction of XRCC1 and PARP-1 in both SSB repair and DSB repair, and the effect of this interaction on cell cytotoxicity. To achieve this, the formation of DNA damage by CPT, TMZ and NCS, DNA repair and cell cytotoxicity by these agents was investigated in cells with (AA8) and without (EM9) functional XRCC1. The level of XRCC1 expression in both cell lines was verified by western blot and these data show that XRCC1 level was not detected in EM9 cells (Figure 5. 1) confirming previously reported data (Shen et al., 1998). As was demonstrated by measurement of OTM using alkaline and neutral comet assay, CPT causes a greater accumulation of total and DSBs in EM9 compared to AA8, implicating a role for XRCC1 in both processes which is in line with other reports showing the hypersensitivity of EM9 cells to TopoI poisons (Barrows et al., 1998).

AG014699 caused a significant increase in the induction of CPT-induced DNA breaks in AA8 (~2-fold), but not EM9 cells, indicating that XRCC1 and PARP are epistatic. However, repair of both total and double strand breaks in both cell lines was retarded by AG014699 implicating an independent role for PARP (Figure 5. 3, Figure 5. 3) Surprisingly, the comet data suggest that DNA damage was repaired to a similar extent in EM9 and AA8 cells during the recovery period. This is in direct contrast to research published by Plo *et al.* 2003, in which the repair of CPT-induced DNA damage was compared between XRCC1 deficient and XRCC1-complemented EM9 cells, and the XRCC1-complemented EM9 cells repaired CPT-induced damage faster. (Plo et al., 2003). However, the results obtained by measuring γ H2AX integrated fluorescence using the same experimental conditions, in cells exposed to CPT (Figure 5. 6) or TMZ (Figure 5.7), indicates slower DNA repair in the XRCC1 mutant EM9 cells, and supports previous observation. γ H2AX measured in CTP-treated AA8 cells then incubated in fresh medium was lower compared to EM9 cells, which shows more efficient repair of DNA damage. The same effect was even more pronounced for repair of DNA damage induced by TMZ. γ H2AX integrated density measured after 2-hour recovery period in fresh medium was almost three times lower in AA8 cells compared to cells EM9. Additionally, γ H2AX immunofluorescence continued to accumulate in the presence of AG014699 even after removal of CPT, especially in the EM9 cells, where they also apparently continued to accumulate after removal of TMZ as well. These studies suggest that the observed DNA repair depends on the activity of PARP-1.

γ H2AX accumulates at stalled replication forks as well as DSBs. The persistence of γ H2AX staining after the removal of CPT and TMZ (compare last bars of Figure 5.6 and Figure 5.7) may be related to replication fork arrest associated with accumulation of unrepaired endogenous SSBs. This hypothesis is supported by the greater accumulation and persistence of DSBs observed in CPT-treated S-phase cells as described in Chapter 4. Increased γ H2AX was also observed at early time-points following recovery from NCS-induced DSBs. Multiple mechanisms for eliminating γ H2AX as DNA repair completes are possible, including removal by histone exchange followed potentially by degradation, or, alternatively, dephosphorylation. Studies where parallel measurements of DSB by neutral comet and γ H2AX foci counting show that γ H2AX foci appearance and disappearance lags behind that of neutral comet DSB measurements (Mitchell et al., 2009). Integrated fluorescence increase as measured in this chapter may be as a result of greater phosphorylation or reduced dephosphorylation of γ H2AX at foci rather than an increase in the number of foci. This might explain the increase during repair incubation in the presence of AG014699 as these data are different from data in chapter 4 where the number of foci were counted.

In contrast to the results of Smith et al. 2005 data in this chapter as well as in chapter 4 show that 30 min incubation of K562, AA8 and EM9 cells with CPT+AG014699 is sufficient to increase the level of DNA breaks. Although, longer exposure was not investigated here, a substantial increase in induction of DNA breaks was observed after 30 min exposure.

The data presented in this chapter show that AG014699 increases the persistence of DNA DSBs in cells treated with 2 types of DNA SSB-inducing agent (CPT and TMZ) and also a direct DSB-inducing agent (NCS) in both XRCC1 proficient and deficient cells. Furthermore, this was associated with an increase in cytotoxicity in both cell lines. Similar data have also been observed with paired XRCC1^{+/+} and XRCC1^{-/-} mouse embryonic fibroblasts in which the PARP inhibitor, 4-AN, increased MMS-induced DNA damage and increased the cytotoxicity of TMZ and CPT in XRCC1^{-/-} as well as XRCC1^{+/+} cells (Horton et al., 2008a). This may indicate a role for PARP-1 independent of XRCC1. However, it could be argued that inhibition of PARP activity will not prevent PARP binding to DNA but will prevent PAR formation that is needed not only for XRCC1 recruitment but also chromatin relaxation and PARP-1 dissociation. Thus, in the presence of an inhibitor the chromatin is not relaxed and PARP-1 remains bound to the break, which may hinder repair of the break (by either

BER/SSBR or back-up NHEJ) to a greater extent than loss of XRCC1. In support of this hypothesis is the recent observation that PARP inhibition increases the persistence of SSBs induced by dimethyl sulphate in EM9 leading to the suggestion that PARP inhibitors trap PARP at SSBs hindering their repair (Ström et al., 2011). It is likely that the unrepaired SSBs will ultimately be repaired at replication by other repair pathways, particularly homologous recombination repair (HRR) and it is also likely that those bound to inactive PARP-1 (and PARP-2) are more difficult to repair than those without PARP-1 or -2 attached. Further experiments in HRR competent and dysfunctional cells and using knockdown of PARP-1 as well as PARP inhibitors would be needed to confirm these hypotheses.

The comparison of cytotoxicity results in this chapter has to be considered with caution because of insufficient amount of time meant that mostly single experiments were performed. Despite incomplete data, a similar effects of CPT TMZ and NCS cytotoxicity in EM9 and AA8 cells was observed. That is, in general, EM9 cells were more sensitive to the DNA damaging agent and that AG014699 increased the cytotoxicity of all agents in XRCC1-deficient EM9 cells as well as XRCC1 proficient AA8 cells. This supports previous reports showing role of PARP-1 in an alternative form of DNA repair, independent of XRCC1 probably B-NHEJ and /or HR. PARP-1 can also be linked to replication fork restart (Bryant et al., 2009b)

It is difficult to draw conclusions from these data whether this is the result of BER deficiency or loss of DSB repair mechanism such as B-NHEJ that depends on PARP-1. In some models the proposed mechanism of DNA repair by B-NHEJ can proceed without the requirement of BER scaffold protein XRCC1. Repair of DNA DSBs within 2 hours after exposure is more dominated by D-NHEJ. Later, during repair inactivity of PARP-1 is more pronounced when it comes to repair the DSB. This indicates the data from the γ H2AX immunostaining of NSC treated AA8 and EM9 cells where after the initial rapid recovery phase a long period of the plateau followed, which was significantly greater for cells incubated with AG014699. These data suggest the role of PARP-1 in DSB repair could be more complex.

Summary

- ✓ CPT, TMZ and neocarzinostatin induced cytotoxicity is potentiated by the PARP inhibitor AG014699 in AA8 and EM9 cells suggesting that the effect of PARP inhibition is greater than loss of signalling SSBR or back-up NHEJ *via* XRCC1.
- ✓ AG014699 increased the level of total and DSB induced by CPT, TMZ and NSC
- ✓ Repair of Total and DSB is quick without inhibitor but significantly retarded by AG014699.

Chapter 6. Summary and final discussion.

TopoI poisons have been in clinical use for several years, however resistance and side effect to them is common. One of the promising new solutions to improve the effectiveness of TopoI poison anticancer therapy, is the use of PARP inhibitors. PARP inhibitors are an exciting new class of anticancer drug, of which nine are currently undergoing clinical trial. Numerous laboratory, pre-clinical data indicate that the use of PARP inhibitors improve the anticancer activity of TopoI poisons and there are several different mechanisms that have been proposed. TopoI poisons exert their cytotoxicity largely during S phase of the cell cycle but it is not clear if potentiation by PARP inhibitors is also cell cycle phase-specific.

Therefore, the hypothesis tested in this thesis is as follows: the potentiation of TopoI poison-induced cytotoxicity by PARPi is specific to S phase and the effect of PARP inhibitors on repair of TopoI poison-induced DNA damage (total or DSB) occurs preferentially in S-phase. Also, this thesis determined whether the variations in PARP and TopoI expression/activity in different phases of cell cycle are related to sensitisation effect of PARPi.

Initially to test this hypothesis the Lovo colon cancer cells were used, because the TopoI poisons are clinically used to treat colon cancer. The effect of AG014699 on CPT-induced cytotoxicity investigated during short (1 h) revealed a large (approx. 50%) resistant population that was reduced to $\leq 5\%$ by longer exposure (24 h) that equates to approximately 1 cell cycle (

Figure 3. 1) This suggests that only some phases of the cell cycle are sensitive to treatment. Supporting this hypothesis, flow cytometric analysis of asynchronous Lovo cells showed that ~40% of cell population is in S-phase and, most likely, this corresponds to the sensitive population (Figure 3. 2.). The study of CPT cytotoxicity using Lovo cells separated into cell cycle phase specific fractions by cell elutriation confirmed that the CPT-induced cytotoxicity and its sensitisation was S phase specific. The sensitisation by AG014699 seen in the asynchronous Lovo population was shown to be greatest during S-phase (Table 3. 2.).

Because of difficulties in obtaining pure cell cycle specific fractions of Lovo cells due to the presence of an aneuploid sub- population of cells (Figure 3. 2) and problems with dispersion of the cells into a single cell suspension, Lovo cells were replaced with K562 leukemic cells. Separation of cells by centrifugal elutriation did not affect the growth kinetics of K562 cells (Figure 3. 6) neither did it introduce DNA breaks (Figure 4. 1) and therefore is not harmful to the cells. Studies in K562 cells confirmed that CPT-induced growth inhibition and cytotoxicity is greatest in S phase and also the potentiation by AG014699 is also greatest in S phase (Figure 3. 7 and Figure 3. 8).

Increased sensitivity to TopoI poisons has been related to elevated levels of TopoI (Husain et al., 1994, Pfister et al., 2009). Data in this thesis shows that TopoI activity is highest in S phase cells and perhaps taking into account possible contamination of G1 and G2 phases by S phase cells, only specific to S phase cells (Figure 3.9), which corresponds well with higher sensitivity to camptothecin of S phase cells (Figure 3. 7 and Figure 3. 8). In contrast, PARP activity (Figure 3. 10) increased throughout cell cycle, which may be related to DNA content. Cell cycle phase changes in PARP-1 and TopoI activity was not related to the levels of PARP-1 or TopoI expression suggesting that both proteins are regulated by posttranslational modification. If the mechanism of potentiation of TopoI poisons-induced cytotoxicity by PARP inhibition is *via* modulation of TopoI activity one would expect the greatest effect to be observed in G2 phase, when the PARP activity is highest. However, this was not the case, suggesting that PARP-1 does not modulate TopoI activity, confirming data provided earlier by Smith et al, 2005.

Topoisomerase I poisons introduce DNA SSB, some of which may be converted to DSB through downstream processing or collision with replication forks (Tuduri et al., 2010). Therefore the formation of SSB and DSB following short exposures (30 min) to CPT±AG014699 was studied using the comet assay (alkaline and neutral), and histone

γ H2AX immunostaining, in asynchronous and separated into different phases of the cell cycle K562 cells.

Using alkaline comets assay, which detect both single and double strand breaks, the greatest number of total CPT-related DNA breaks were shown to be induced in the S phase, however co-incubation of K562 cells with AG014699 increased the number of breaks in all phases of cell cycle to similar extent. Previous reports Smith et al, 2005 indicated that PARP-1 promotes the repair of TopoI poison-induced DNA breaks, but did not investigate repair in different phases of the cell cycle. The possibility that the observed increase in DNA breaks was due to inhibition of their repair was investigated. Repair was most rapid in S-phase and AG014699 virtually abolished repair in all phases of cell cycle (Figure 4. 12, Table 4. 3, Figure 4. 18, Table 4. 5). Therefore, the effect of AG014699 on total (mostly SSB) breaks does not explain the greater chemosensitisation in S-phase.

The hypothesis that DNA DSB were more closely associated with chemosensitisation was investigated. DNA DSB were measured using two methods; neutral comet assay and γ H2AX focus formation. γ H2AX is used as a marker of DNA damage but most currently used detection methods are laborious. The software I wrote (Appendix) provides an efficient automated analysis of images acquired by immunofluorescence microscopy of nuclei. The data obtained using the PZFociEZ macro is comparable with the data obtained using other software (Figure 2. 6). The macro as an open source project is freely available, highly efficient (thousands of cells in several different pictures can be measured within a few minutes) and provides several analysis methods with different endpoint measurements.

The investigation of the induction of DSB by both neutral comets and γ H2AX showed that they were highest in S-phase and this was further increased by co-incubation with AG014699 (

Figure 4. 6 The effect of AG014699 on CPT-induced DSB in asynchronous and elutriated K562 cells.

The overall conclusion from these data is that inhibition of DNA break repair by AG014699 leads to massive accumulation of DSB and stalled replication forks in S-phase and that this is largely responsible for the cytotoxic potentiation.

Interestingly, the lack of potentiation in G1 phase suggest that DNA breaks was repaired prior entry into S phase, despite PARP inhibition. Possibly, K562 cells were able to engage G1 checkpoint, despite mutant p53 such that repair of CPT-induced SSB is completed prior to progression into S phase such that cytotoxic DSB and stalled replication forks do not accumulate. However, this was not tested experimentally to confirm this hypothesis. There are limitation to this experiments. The DNA induction experiments were performed directly after elutriation, therefore most of cleavage complexes is likely to be persist at the time when experiment was performed. In the cytotoxicity assays, due to size of the experiment, only two concentrations of CPT were used, therefore there is possibility that with wider range of CPT concentrations the potentiation of G1 phase cells may be detectable.

Both the repair of DNA SSB and repair of DSB *via* back-up NHEJ is thought to involve recruitment of XRCC1 to the damage site by PARP-1 activation. An investigation of whether PARP-dependent repair and cell survival following exposure to camptothecin was dependent on XRCC1 was investigated in isogenic cells with (AA8) and without (EM9) XRCC1. In parallel, similar investigations were conducted to determine the dependence of PARP-XRCC1 interactions in the response to temozolomide (which causes base modification that is repaired by BER/SSBR) and neocarzinostatin, a radio-mimetic that causes a high level of DSBs. Curiously, although CPT-induced DNA breaks were higher in EM9 cells they were repaired at same rate as in AA8 cells and AG014699 inhibited repair in both cells to similar extent (Figure 5. 3, Figure 5. 4, and Figure 5. 5 and Table 5. 1 and Table 5. 2). γ H2AX foci measurement suggested that stalled replication forks continued to accumulate even after removal of CPT in EM9 cells with a further increase in the presence of AG014699. Similar to CPT-induced DNA breaks, more TMZ-induced breaks accumulated in the EM9 cells and repair was slower, but again, AG014699 slowed repair in both AA8 and EM9 cell lines. These data suggest that PARP-1 has a role over and above its interaction with XRCC1 in the repair of TopoI poison, DNA methylating agent induced DNA damage, and this was further supported by cytotoxicity assays showing that AG014699 enhanced CPT and TMZ cytotoxicity in both XRCC1 functional and dysfunctional cells.

The induction of DSBs by neocarzinostatin was similar in both AA8 and EM9 cells and so were their repair kinetics (Figure 5. 8.). Again, AG014699 inhibited repair in cells lacking XRCC1 as well as XRCC1 functional cells. Effects of AG014699 on DNA repair in both cell types correlated with the observed chemosensitisation to

neocarzinostatin in both AA8 and EM9 cells (Figure 5. 11). These data suggest that PARP has a function independent of XRCC1 in the repair of DNA DSBs. They also cast doubt on the role of PARP and XRCC1 in back-up NHEJ.

An alternative hypothesis is that inhibition of PARP, which does not prevent it binding to DNA but does inhibit its dissociation, results in PARP causing an obstruction at the break that hinders repair irrespective of XRCC1 status.

To summarise the investigations carried out in this thesis and the overall conclusions: CPT-induced breaks are highest in S-phase, possibly related to higher TopoI activity in this phase (Figure 3.9), and this results in greater sensitivity of S-phase cells to CPT-induced cytotoxicity. PARP inhibition leads to greater accumulation of SSBs in S-phase but has a similar impact on repair in all phases. PARP inhibition preferentially increases stalled replication forks/DSBs in S-phase and almost completely blocks their repair. The accumulation of these lesions is greatest in S-phase cells treated with CPT and AG014699 correlating with cytotoxic potentiation. Chemosensitisation and inhibition of DNA repair by AG014699 is independent of XRCC1, possibly due to an independent role of PARP in repair or an obstruction formed by inactive PARP at the site of the break.

The data presented in this thesis are the first demonstration that potentiation of CPT-induced cytotoxicity by PARP inhibition is S phase-specific and closely linked to the accumulation of stalled replication forks/DSBs through inhibition of their reactivation/repair. The major strengths of the work are: **(i)** Use of potent and specific PARP inhibitor that is undergoing clinical evaluation, **(ii)** use of a method to separate the cells into different cell cycle phases that does not impact on DNA integrity or cell viability, **(iii)** the ability to directly correlate DNA breakage and repair to cytotoxicity by virtue of using exactly the same experimental conditions and **(iv)** the investigation of the role of XRCC1 in isogenically paired cell lines is valuable as it suggests that PARP inhibitors will be effective in tumours that have compromised XRCC1 function due to well-documented polymorphisms that are associated with cancer.

However due to time limitations there are some weaknesses: The data in the XRCC1 wild-type and mutant cells were not repeated a sufficient number of times to be sufficiently robust for publication. Similarly, the evaluation of PARP-1 and TopoI expression and activity assays requires further repetition to validate the data presented here. The kinetics of the removal of γ H2AX foci in different phases of cell cycle remains to be determined.

The results presented in this thesis provide a number of opportunities, which possibly can be applied in clinical trials. The data presented here indicate that PARP inhibitors preferentially sensitize S-phase cells to TopoI poisons. Patients with rapidly growing tumors, with a high S-phase fraction would therefore be predicted to benefit most from the combination of PARP inhibitors with TopoI poisons. Staining the diagnostic biopsy for Ki67 may identify such tumors. It will be also important to identify how fast, following a drug dose the tumor cells will recycle entering another cell cycle and what will be the fraction of S-phase cells in repopulating tumor before applying next dose of drug.

Slow growing tumors may be less responsive to ensure that all tumor cells pass through S-phase exposure to both drugs would need to be sustained. Data in this thesis indicates that PARP-1 inhibitor was able to increase SSBs levels up to 5-fold in G1 phase cells but was ineffective on DSB formation in this phase. TopoI poisons are less cytotoxic for G1 phase cells, which are somewhat similar to the quiescent tumor cell population, which can regenerate the tumor after therapy withdrawal. A clinical trial that can address this problem, probably requiring several cycles of therapy to kill the reactivated tumor would be required. A careful balance is needed to avoid toxicity to proliferative normal tissues, such as the bone marrow and gut mucosa.

The data in Figure 3. 1 shows that only a small fraction of the tumor cells (presumed the S phase fraction) would be killed by a single dose of a TopoI poison that persisted in the circulation for a short time. Repeated dosing for the patient would be required to kill remaining tumor cells as they entered S phase. The schedule would be dependent on the fraction of cells in S phase, the half-life of the drug and the rate of re-entry into S-phase of remaining quiescent cells. Assuming 40% of tumor cells are in S phase and that drug concentration to kill S phase cells persist for 1h and that 72 hours are required for the remaining 60% of cells to enter cycle (again with 40% in S phase) then a modest dose of drug given every 3 days might prove more efficient than a most common current topotecan (half –life = 2-3 hours) and camptosar (half –life = 6-12 hours) dosing schedules: once daily dosing for 3 to 5 consecutive days repeated every 21 days, and once weekly for 3 or 6 weeks, respectively.

One of the reason for the resistance to TopoI poisons in tumor cells is lower TopoI expression/activity with TopoI activity reported to be correlated with its expression (Holden, 2001, Pfister et al., 2009). The data obtained in this work suggest than the activity of TopoI in S phase is much greater than would appear from its expression.

Therefore, it may be possible to use PARP inhibitors to potentiate TopoI poison-induced anticancer activity in rapidly growing cancers predicted to be resistant by virtue of low TopoI expression. Survival of the cells exposed to PARP-1 and TopoI will depend on DNA repair capacity (in particular DSB) by tumor cells and thereby the factor limiting the use of PARP-1 and TopoI in the treatment of particular type of cancer. The data presented in this thesis suggest that the polymorphisms in XRCC1 that are associated with cancer will not affect the ability of PARP inhibitors to improve TopoI poison therapy.

A number of further studies are indicated to follow on from the work presented here: Firstly, the weaknesses described above should be addressed. The possibility that inactivated PARP, bound to the DNA break formed a physical obstruction to the repair of the DNA could be investigated by comparing the data obtained here with similar studies knocking down PARP-1 (by siRNA or shRNA). The data described here should be confirmed in different cell lines, particularly in those with defects in DNA repair such as DNA PolB, which is commonly altered in tumours (Horton et al., 2008b).

PARP inhibition had a major impact on the repair of DNA DSBs and it is possible that stalled replication forks continued to accumulate in the presence of AG014699 even after CPT withdrawal. It has been proposed that PARP is necessary to reactivate stalled replication forks and PARP inhibitors are selectively cytotoxic to cells lacking homologous recombination repair (HRR) (Bryant et al., 2009a). It would therefore be interesting to investigate how the CPT-induced DNA DSB are repaired at different phases of the cell cycle and the impact of PARP inhibition compared with PARP knockdown on the repair pathways. Apart from a plasmid-based assay, which is not appropriate for these studies due to lack of histones, there is no way to determine non-homologous end-joining activity. However, there are sufficiently potent and specific DNA-PK inhibitors to address whether NHEJ is important. The more likely scenario in S and G2 cells is that HRR is the predominant pathway. Assembly of Rad51 foci detected by immunofluorescence can be applied as an indicator of HRR function. This latter assay has been applied to primary cultures of tumour tissue (Mukhopadhyay et al., 2010) so it may be possible to predict which patients will benefit most from this therapy. The PZFociEZ macro can be applied for efficient analysis of Rad51 foci, which would make this analysis quicker.

It is clear from the data presented in this thesis that PARP inhibition causes S-phase-specific chemosensitisation of TopoI poisons that is related to the impact of PARP

inhibition on DNA breaks. This has clinical implications suggesting rapidly growing tumours would be most sensitive. Identification of patients with tumours that have a high proliferative fraction may be possible using the diagnostic biopsy. As with most research, the data presented here have thrown up as many questions as answers. It is now important to identify how CPT-induced DNA damage is repaired in the presence of a PARP inhibitor, if inhibited PARP-1 is equivalent to lack of PARP-1 or whether it forms a physical obstruction at the site of the break and on the basis of these data can we predict whether defects in specific DNA repair pathways would render cells exquisitely sensitive to PARP-inhibitor-TopoI poison combinations that could be exploited clinically.

A. APPENDIX - PZFociEZ, ImageJ macro for γ H2AX foci analysis - documentation.

A.1. Introduction

Immunodetection of the γ H2AX histone using fluorescence microscope has been applied as a biomarker for monitoring drug response in clinical trials before (Redon et al., 2010). The methods for analysing γ H2AX emitted fluorescence signal are laborious and involves counting by eye the γ H2AX corresponding dots, or measurements of fluorescence signal from whole cells as an integrated density. On top of that before any measurements applied each image usually requires to be processed (e.g. background correction). There is a lack of methods allows effective analysis of γ H2AX immunofluorescence and minimizing the researcher's participation.

The purpose for writing PZFociEZ macro was to fill this gap and provides at least semi-automatic methods for analysis γ H2AH foci fluorescence.

The macro significantly reduces time needed for analysis and increases the number of scored cell. It also provides several analysis methods that can be easily applied to various experimental conditions. The PZFociEZ macro is an application written in ImageJ macro language. ActionBar plugin written by plugin Jerome Mutterer (http://imagejdocu.tudor.lu/doku.php?id=plugin:utilities:action_bar:start) was used to create GUI. The macro has a collection of most frequently used options for analysing pictures with γ H2AX foci made with the aid of fluorescence microscope.

The PZ-FociEZ panel (Figure A2) is a main control panel which provides an access to most option applied at the beginning of image analysis. These options were divided into two sets. First, is a collection of the necessary options predisposed to create outlines of nuclei, inspection and corrections of these outlines and for preparation of images for the batch analysis. The second set of options is available as a panel FociEZ and includes several different options for a comprehensive measurement of γ H2AX foci. Figure A 1 show the structure of folders in which macro is organized. All of these options with examples of application were described in following sections.

In this Appendix the whole functional software is provided. To make it running one needs to copy the source code from section A5 and save it as a text file in PZFociEZ folder (Figure A 1). Next, the ActionBar plugin must be installed.

PZFociEZ macro is free to use for everybody -

For support or questions write to author [-pawel.znojek@pzfociez.com](mailto:pawel.znojek@pzfociez.com).

A.2. Folder map

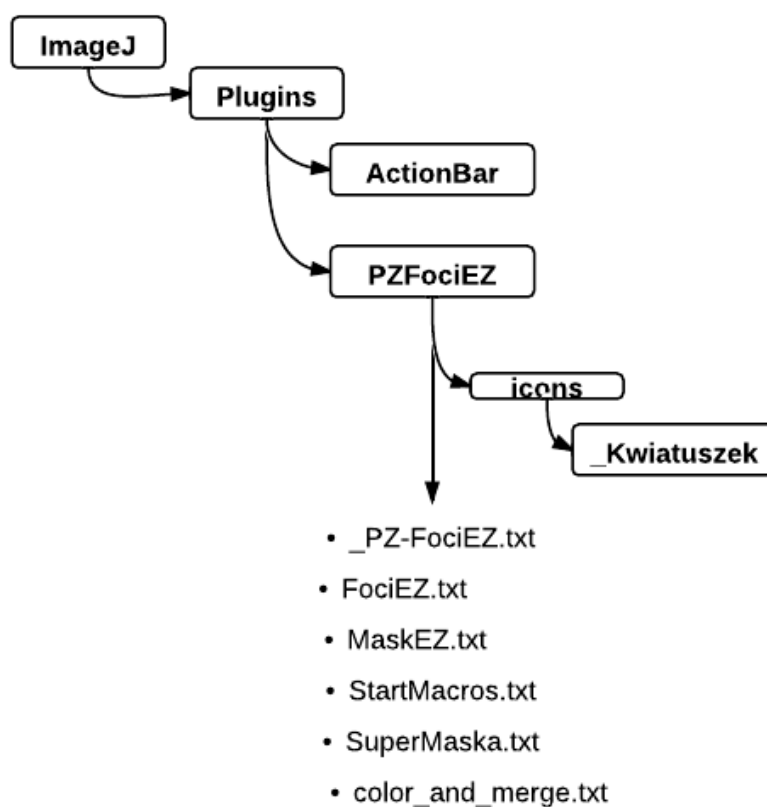


Figure A 1. Schematic of folder structure in macro PZFociEZ


Folder map for PZFociEZ macro. Within ImageJ folder the icons pictures (section A3) shall be copied and saved as PNG format using given name in the directory: Plugins/PZFociEZ/icons/ _Kwiatuszek. Each part of source code (section A5) should be saved as txt file in folder PZFociEZ .

A.3. PZ-FociEZ



Figure A 2. PZFociEZ macro graphical user interface.

A.3.1  **Open Image – Access to images**

A.3.2  **Open ROI for this Image –** When ROI set for given image is saved in the same folder as the image, pressing this button opens and displays nucleus outlines on the image.

A.3.3  **Create ROI Mask –** (see section A3)

A.3.4  **Fluorescence Intensity Measurement And Foci Counting –** (See section A4)

A.3.5  **Merging Dapi With Foci Images –** applies pseudo colour (Red, Blue or Green) colour on greyscale image and merges two images with different colour (written by Jerome Mutterer).

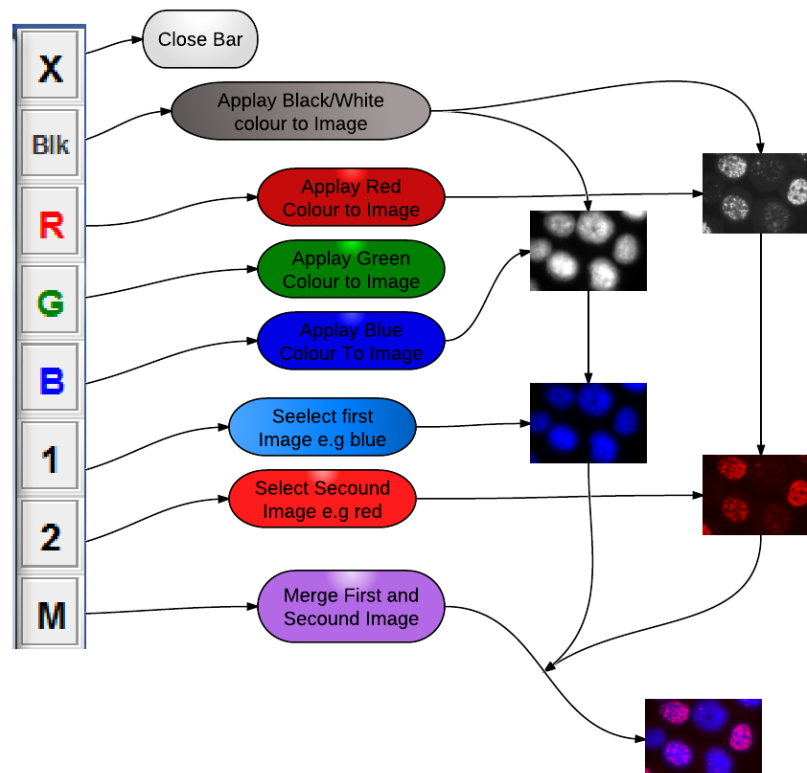

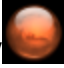




Figure A 3. Diagram illustrating steps applied when merging two images.


A.3.6  **ZoomTool** –Allows to increase or decrease the magnification of the image.

A.3.7  **OvalROI [x]** – Switching to ImageJ drawing mode allows to draw an ovals on the image. [x] indicates keyboard shortcut available when Start-up Macros (A2.12.) option is initiated.

A.3.8  **Free Hand ROI [c]** - Switching to ImageJ drawing mode allows to draw an lines in various directions on the image

A.3.9  **Set Scale** – shortcut to ImageJ Set Scale command (Analyse/Set Scale...) This dialog allowsto define the spatial scale of the active image so measurement results can be presented in calibrated units, such as mm or μm .

(See more in ImageJ Documentation - <http://imagej.nih.gov/ij/docs/guide/userguide-27.html#toc-Subsection-27.8>).

A.3.8  **Set Measurements** - shortcut to ImageJ Set Measurements command (Analyse/Set Measurements).

See more in ImageJ Documentation -

<http://imagej.nih.gov/ij/docs/menus/analyze.html#set>

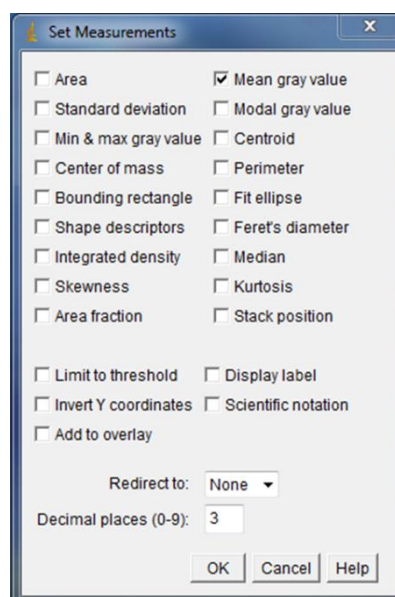



Figure A 4. Set Measurements dialog window.

This dialog window allows choosing several options, which can be used as endpoint measurements.

 **A.3.10 Start-up Macros** – Clicking this button installs several macros to provide handy keyboard shortcuts applicable during edition of nucleus outlines.

 **A.3.11 Close All Windows** – pressing this button closes all open images

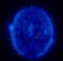

 **A.3.12 Files Log** – Allows displaying in Log window a list of files in selected folder.



Figure A 5. Displaying files using Log Files option.

Files Log returns a list of files in selected directory or subdirectory. By clicking on the path to file in the Log windows, it is possible to open an Image or ROI set

 **A.3.13 Help-** Help and documentation to PZ-FociEZ macro available at www.pzfociez.com.

 **A.3.14 Hide IJ** - allows to hide/unhide ImageJ panel

A.4. MaskEZ Panel

A.4.1. OpenImage - Access to images

A.4.2. OpenNext-opens subsequent images from selected folder

A.4.3. Make Mask – Automatically creates nucleus outlines and display them on the image.

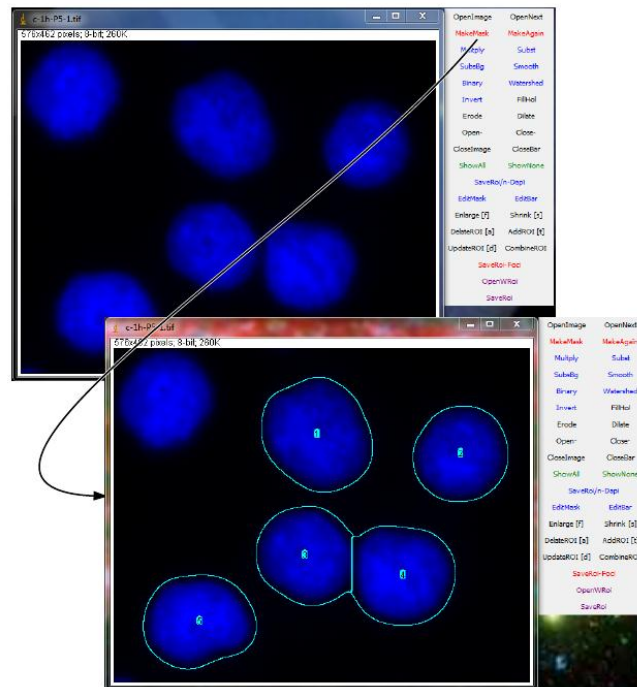


Figure A 6. Results of Make Mask option

After opening Dapi image and choosing MakeMask option nucleus outlines will appear on the image. To save outlines one can either choose SaveRoi (see A.4.15) or SaveRoi/n-Dapi (see A.4.14) options. Using OpenNext (see A.4.2.) option will open corresponding foci image on which outlines will be also displayed. After applying any required corrections, one can use SaveRoi-Foci (see A.4.15) option to save ROI set assigned for foci image. Notice that one nucleus outlines is missing. This may happen depending on image quality and can be quickly corrected using MakeAgain option.

A.4.4. Binary – create binary (black and white) images (shortcut to Process/Binary/Make Binary)

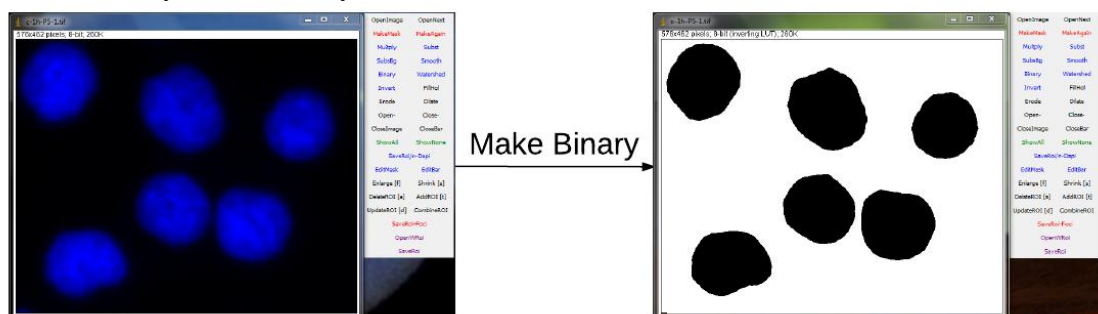


Figure A 7. Greyscale and binary images.

The binary option is used before MakeAgain (A.4.5.) option.

A.4.5. MakeAgain – Creates nucleus outlines using binary image

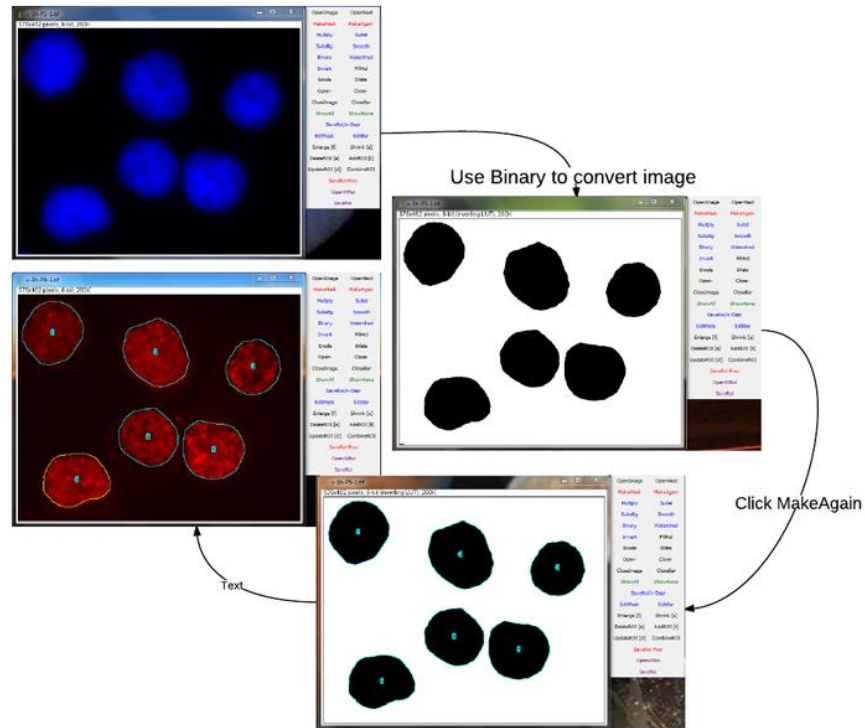


Figure A 8. Example of making nucleus outlines on more demanding images.

The MakeMask options sometimes is insufficient, however it is possible to easily create nucleus outlines using MakeAgain option in combination with options described in next sections.

A.4.6. Multiply – multiplies image by given number.

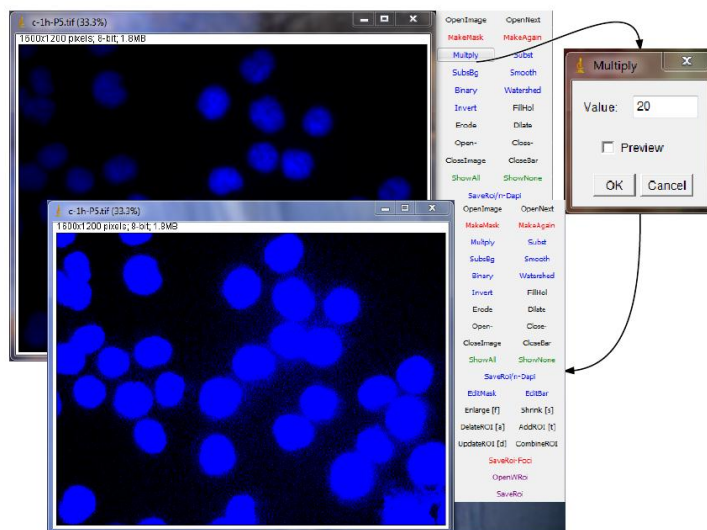


Figure A 9. Example of Multiply option usage.

The multiply, subtract (A.4.7.) or smooth (A.4.10.) options can be used to increase image contrast and prepare image for making nucleus outlines.

A.4.7. Subtract – subtract constant value from the image

A.4.8. Watershed – automatic separation or cutting apart particles that touch each other

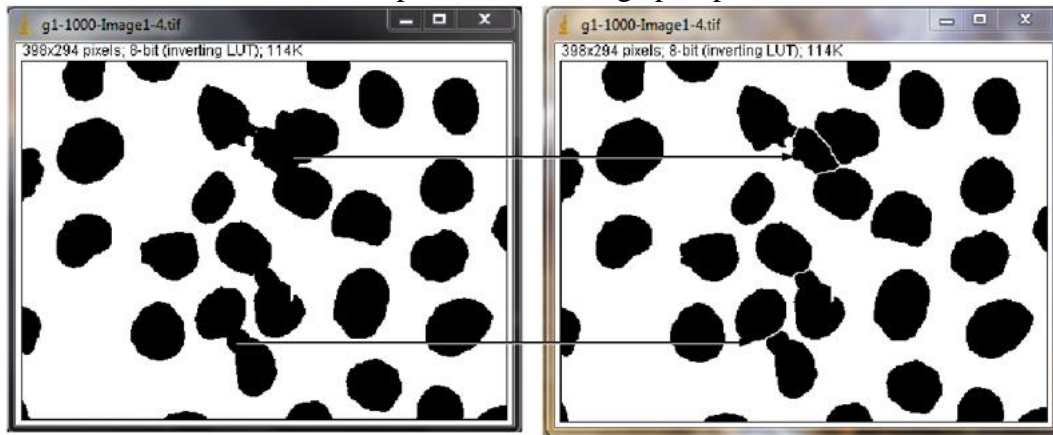


Figure A 10. Graphical example of watersheding binary image

The watershed algorithm is used to separate particles on the binary image.

A.4.9. Invert

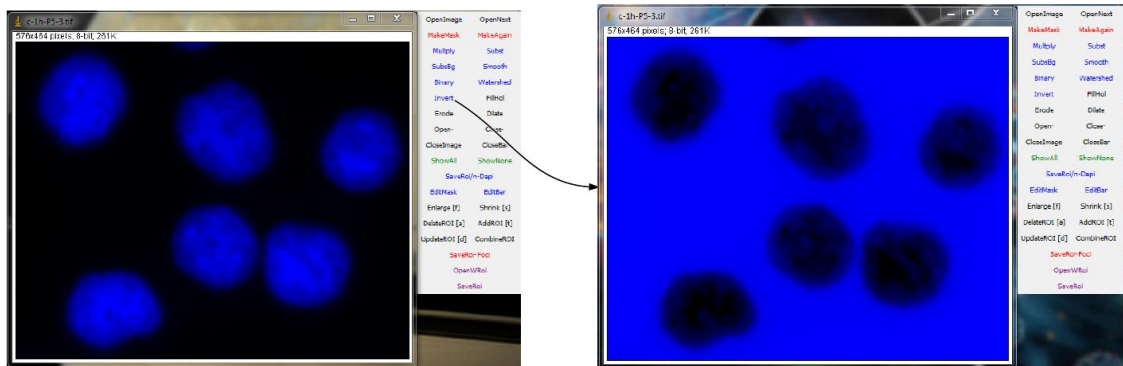


Figure A 11. Illustration showing results of inverting image

The invert option reverts colors on the image.

A.4.10. Smooth – makes images looking smooth using gaussian blur option.

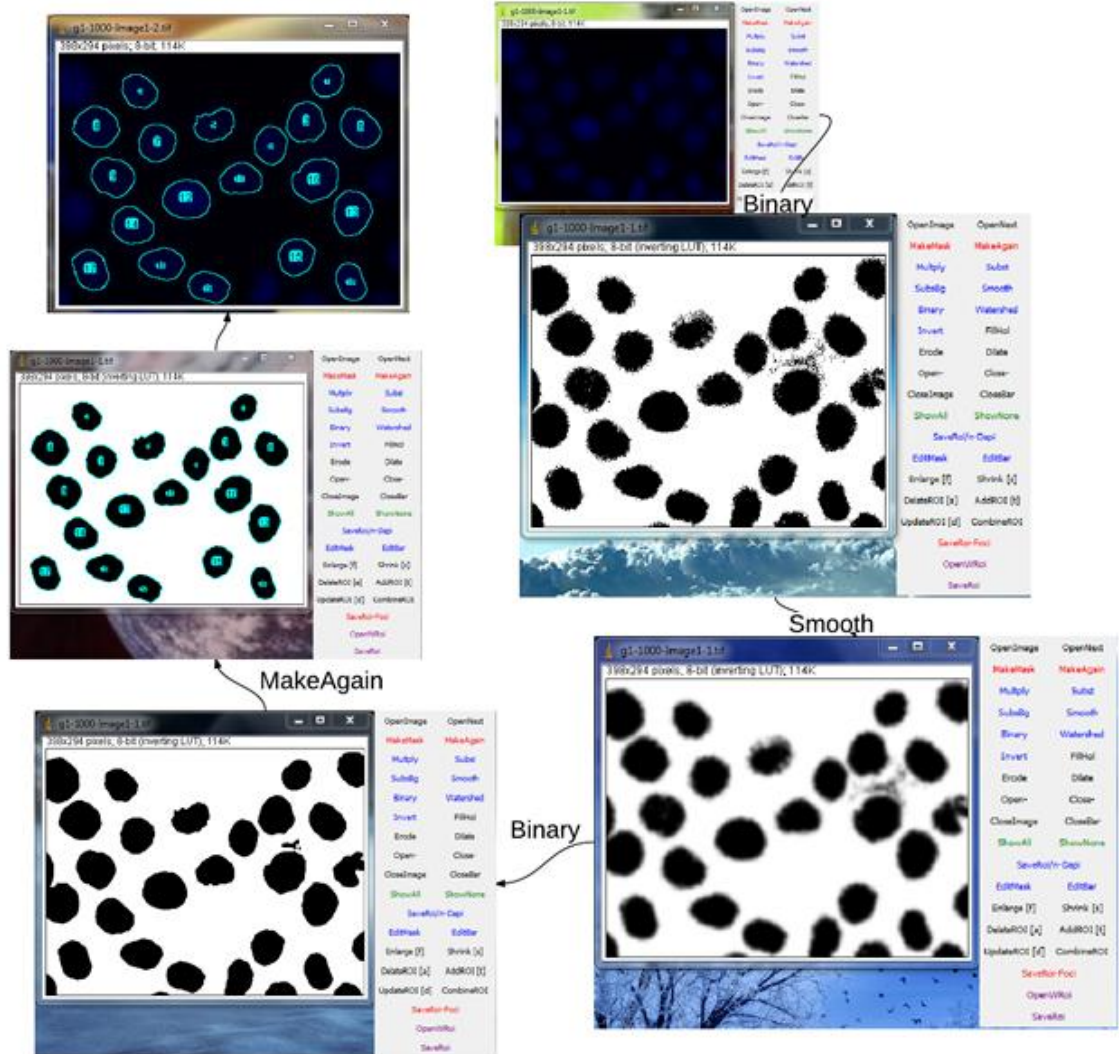


Figure A 12. The "smooth" option applied to create the outlines of nuclei

A combination of Binary and smooth options used to create nucleus outlines.

A.4.10. FillHol - This command fills holes (four connected background elements) in objects by filling the background

A.4.10. Erode - Removes pixels from the edges of objects in a binary image

A.4.11. Dilate - Adds pixels to the edges of objects in a binary image.

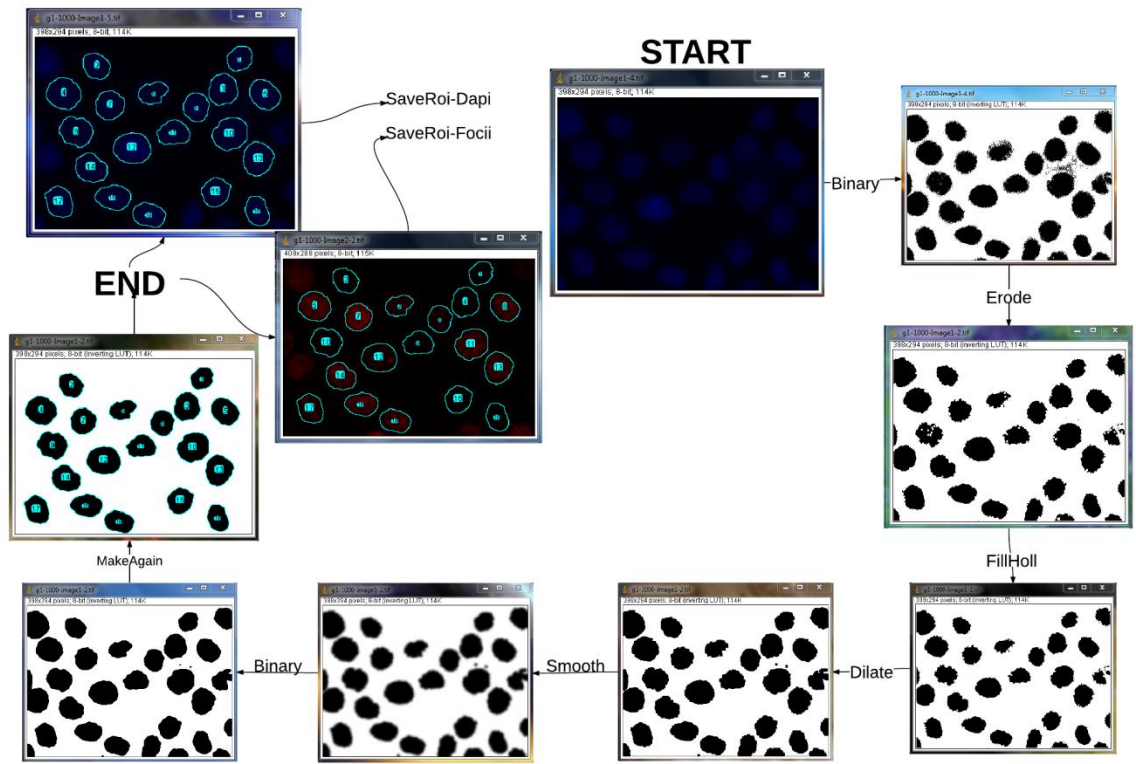
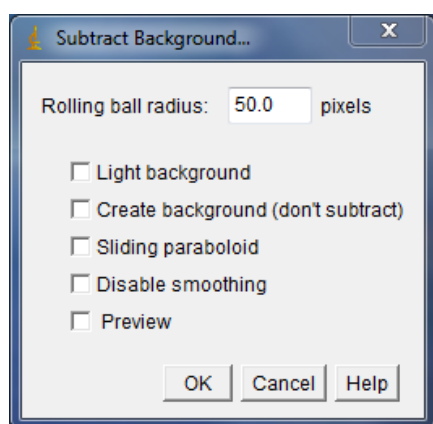


Figure A 13. Example of Erode, Dilate, FillHoll, Smooth, Binary and MakeAgain option usage.

Due to poor staining or insufficient image quality the option MakeMask sometimes gives unsatisfactory results. In this case the contrast of Dapi image can be improved by conversion of the image to binary and applying a sequence of options (Erode, Dilate, FillHoll, Smooth, Binary and MakeAgain - the order might be different) ending with binary conversion following by MakeAgain option.

A.4.12. SubsBG - Subtract background

A standard ImageJ method for correcting uneven background on the image.



Based on the ‘rolling ball’ algorithm by Stanley Sternberg (*see* Sternberg S, Biomedical image processing, *IEEE Computer*, Jan 1983). Imagine a 3D surface with the pixel values of the image being the height, then a ball rolling over the back side of the surface creates the background.

Rolling Ball Radius - The radius of curvature of the paraboloid. As a rule of thumb, for 8-bit or RGB images it should be at least as large as the radius of the largest object in the image that is not part of the background. Larger values will also work unless the background of the image is too uneven. For 16-bit and 32-bit images with pixel value ranges different from 0—255, the radius should be inversely proportional to the pixel value range (e.g., for 16-bit images (pixel values 0—65535), typical values of the radius are around 0.2 to 5).

Light Background - Allows the processing of images with bright background and dark objects.

Create Background (Don't Subtract) - If checked, the output is not the image with the background subtracted but rather the background itself. This option is useful for examining the background created (in conjunction with the *Preview* option).

Create Background can be also used for custom background subtraction algorithms where the image is duplicated and filtered (e.g. removing ‘holes’ in the background) before creating the background and finally subtracting it with Process>Image Calculator...

Sliding Paraboloid If checked, the ‘rolling ball’ is replaced by a paraboloid that has the same curvature at the apex as a ball of that radius. This option allows any value of the radius > 0.0001 (The ‘rolling ball’ algorithm requires a radius of at least 1). The ‘sliding paraboloid’ typically produces more reliable corrections since the ‘rolling ball’, a legacy algorithm, is prone to edge artifacts. E.g., to reduce the computing time the ‘rolling ball’ algorithm downscapes the image in a way that is not consistent. The ‘sliding paraboloid’ algorithm does not use downscaling and thus produces no downscaling artifacts. Nevertheless, the ‘sliding paraboloid’ is also an approximation, since it does not really use a paraboloid (an exact implementation would require a great computing effort) but it rather slides in different directions over the image.

Disable Smoothing For calculating the background (‘rolling the ball’), images are maximum-filtered (3×3 pixels) to remove outliers such as dust and then smoothed to reduce noise (average over (3×3) pixels). With *Disable Smoothing* checked, the unmodified image data are used for creating the background. Check this option to make sure that the image data after subtraction will never be below the background.

Adopted exactly from

<http://imagej.nih.gov/ij/docs/menus/process.html#background>

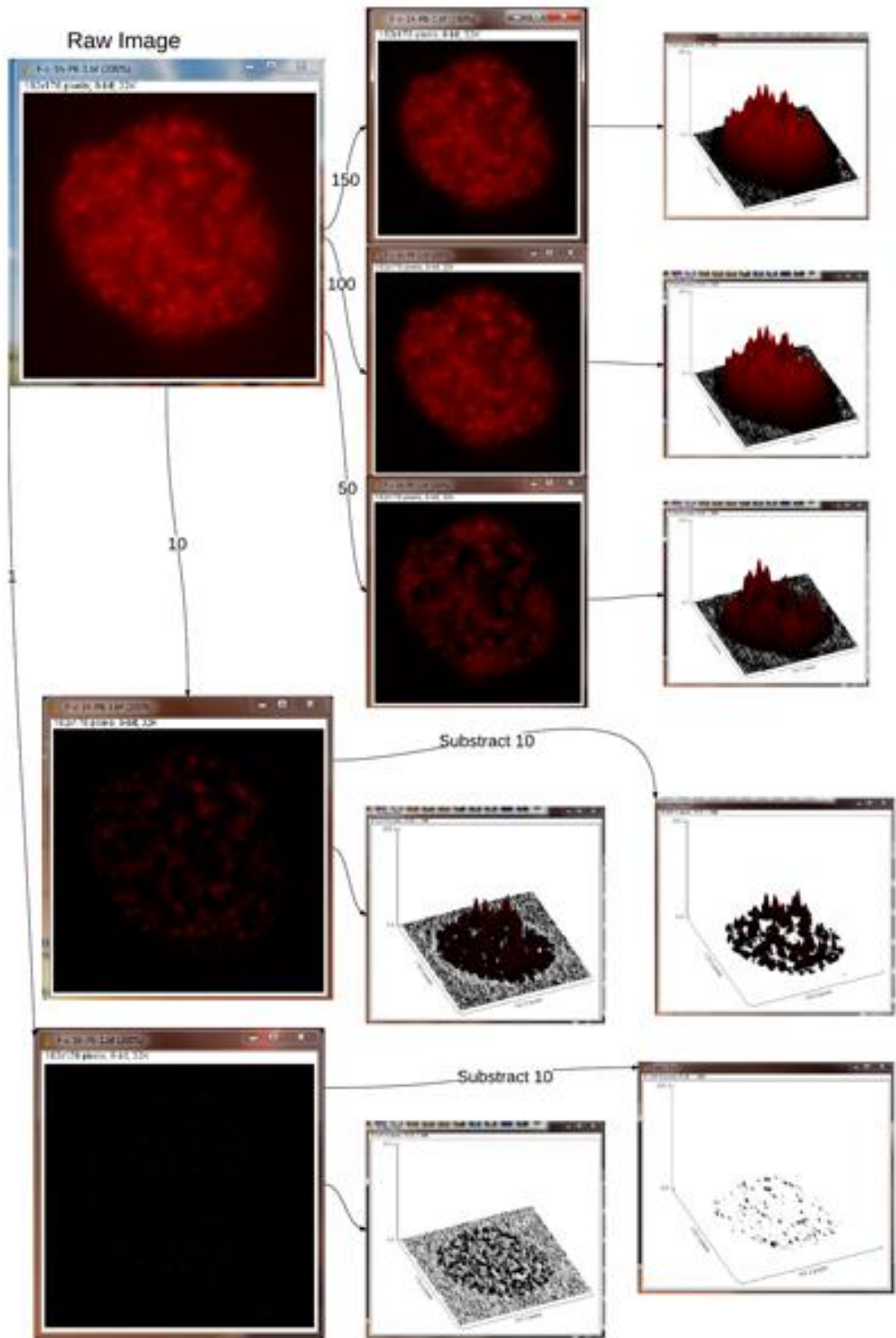


Figure A 14. Subtract background examples.

The numbers crossing the arrows indicates rolling ball radius. “Subtract 10” indicates that a value of 10 was subtracted from the image.

A.4.12 ShowAll - displays all outlines on the image

A.4.13 ShowNone –removes outlines from image

Correcting Nucleus outlines on Foci image.

Options **Enlarge [f]** (make bigger) **Shrink [s]** (make smaller), **DeleteROI [a]** (remove outline from image, **AddROI [t]** (adding new outline to image), **UpdateROI [d]** (updates ROI set in ROI Manager when outlines was modified, **CombineROI [f]** (connects single separate outlines) can be applied to correct nucleus outlines on the foci image. These options are also available as a keybord shortcuts when StartUp =macros

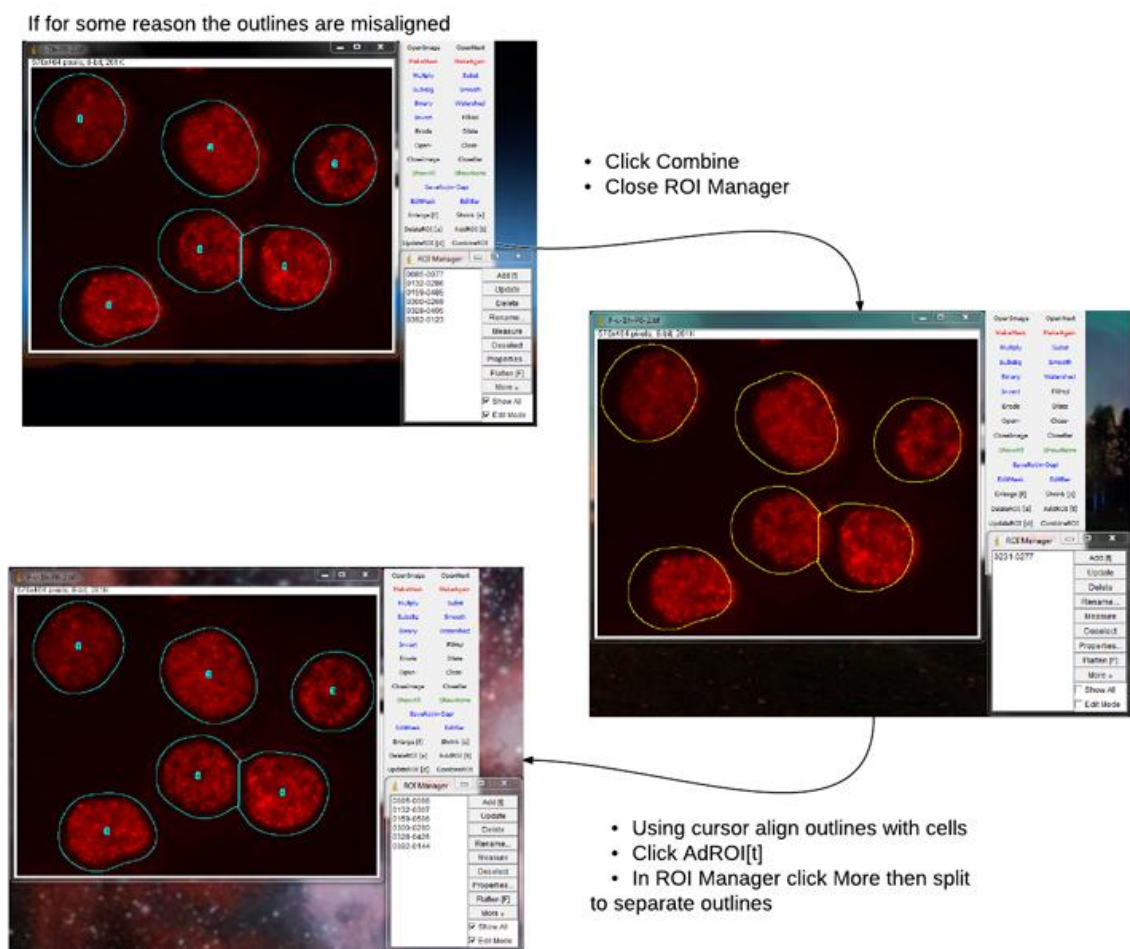


Figure A 15. Example of correcting misaligned nucleus outlines on foci image.

Misaligned Dapi mask with corresponding Foci Image can be corrected as follow

A.4.14 SaveRoi/n-Dapi- automatically creates new folder called DAPI and saves the active image with corresponding ROI set in this folder. This option is used with Batch analysis and allows collecting all images for the analysis in a single folder.

A.4.15 SaveRoi-Foci- automatically creates new folder called Foci and saves the active image with corresponding ROI set in this folder. This option is used with Batch analysis and allows collecting all images for the analysis in a single folder.

A.4.16 OpenWRoi – option similar to OpenNext. It opens subsequent images with corresponding ROI.

A.4.17 SaveRoi – saves ROI set of nucleus outlines in the same folder as the image for which outlines was created

A.5. FociEZ panel

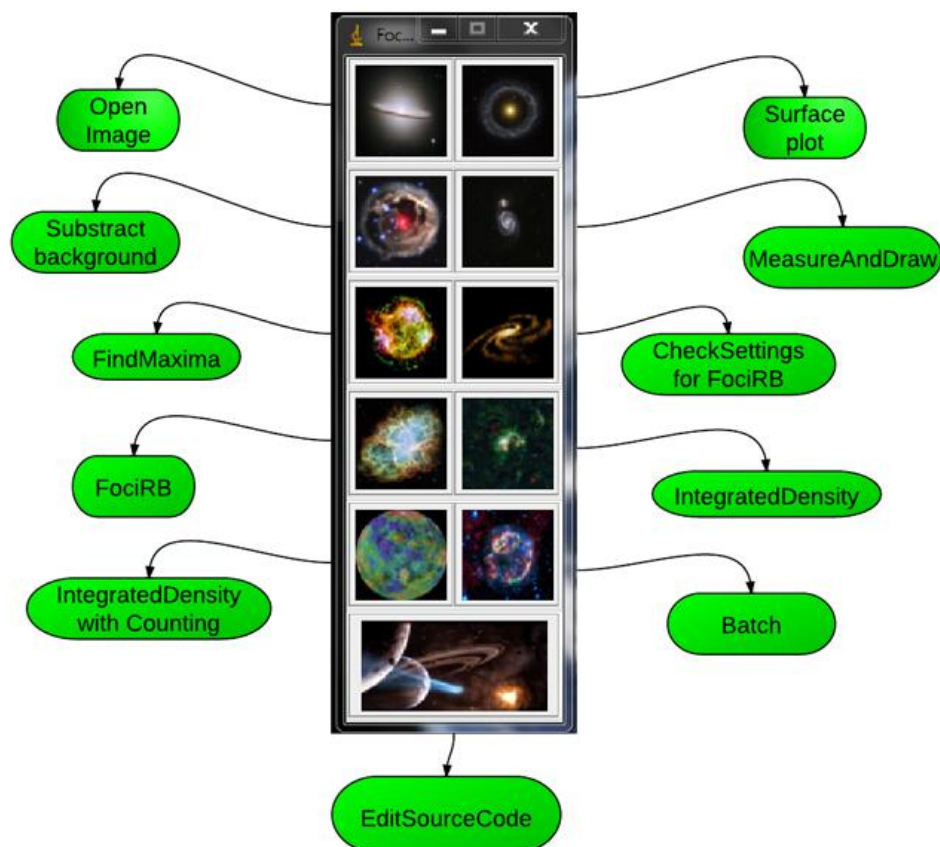


Figure A 16 FociEZ graphical user interface.



A.5.1 **Open** – Access to image or ROI



A.5.2 **SurfacePlot** – Displays a three-dimensional graph of the intensities of pixels in a grayscale or pseudo colour image (non-RGB images). The plot is based on the existing selection or on the entire image. A stack of plots can be produced when the source image is a stack or hyperstack. In this case, closing the plot stack window will abort the plotting process (adopted from ImageJ user guide)

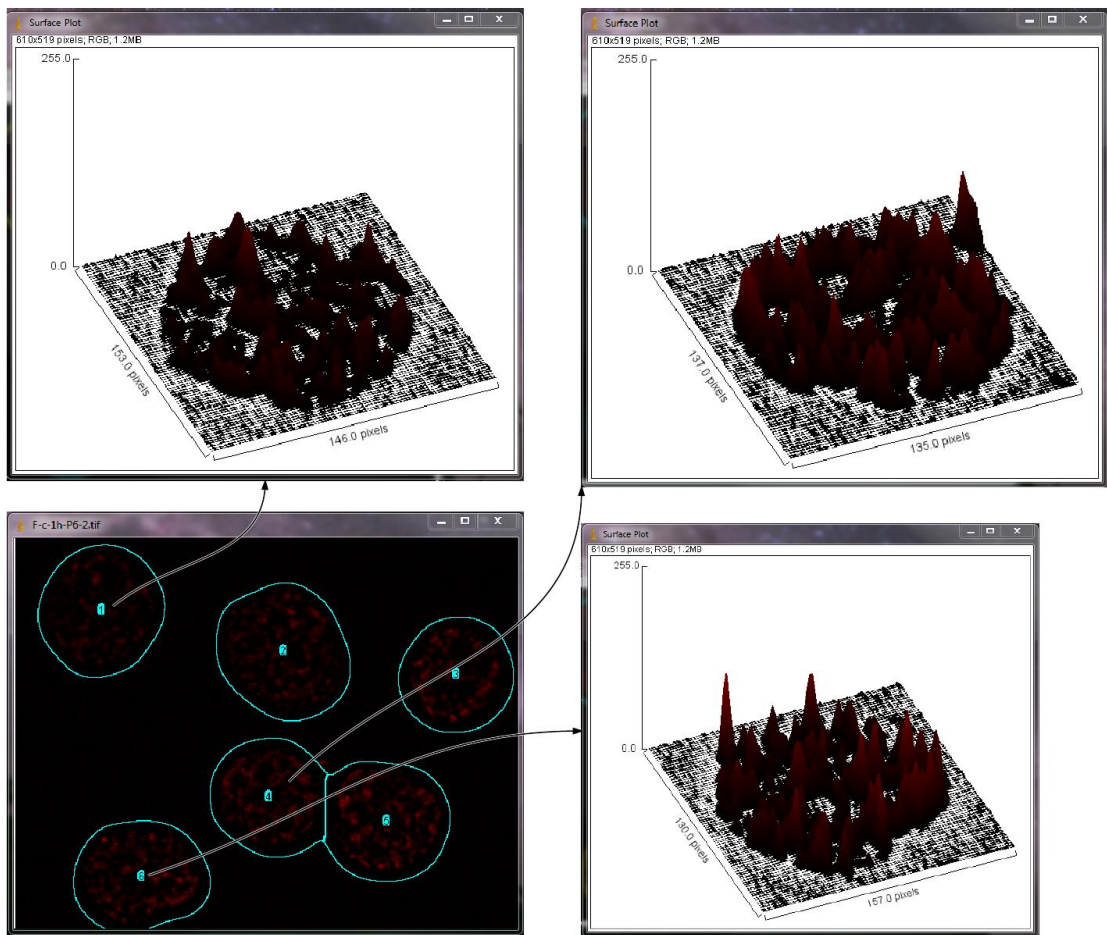


Figure A 17. Examples of the surface plots created for single cells.

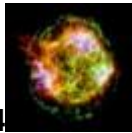
Surface plot options can be used to estimate the accuracy of background subtraction



A.5.3 Subtract Background - see section A.4.12.



A.5.4 MeasureAndDraw – this macro was adopted form (Katoka, Bindokas et al. 2006) with some modification applied. It does not require a stack image consisted of DAPI/Foci. Instead requires to open DAPI image first and then Foci Image.



A.5.4 FindMaxima – Determines the local maxima in an image based on given Noise tolerance.

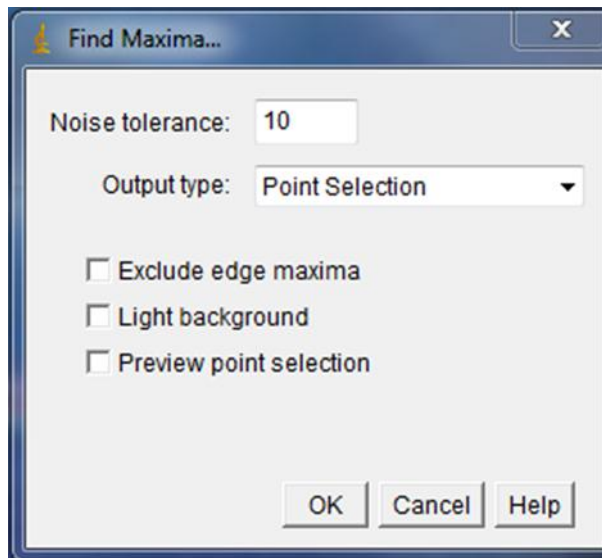


Figure A 18. Find Maxima dialog window

Detailed information available in
(<http://imagej.nih.gov/ij/docs/menus/process.html#find-maxima>)

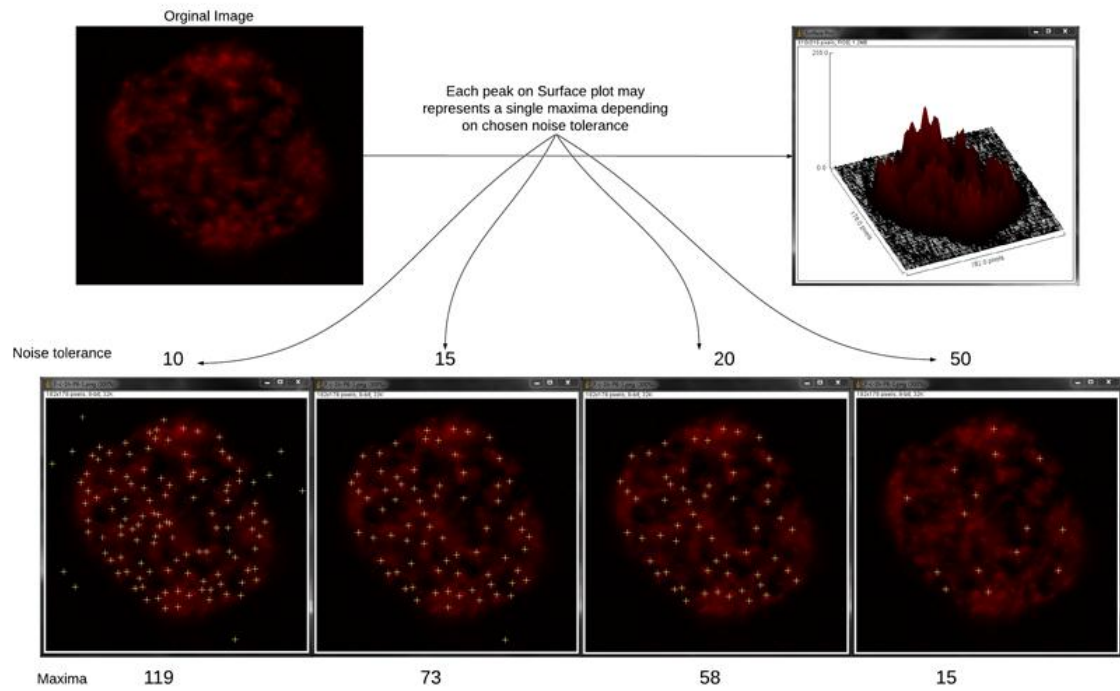


Figure A 19. Example of application of the find maxima option for γ H2AX foci counting.

Choosing different maxima noise tolerance one can adjust automatic foci counting much counting by eye.



A.5.5 Check Settings For FociRB - This allows to choose settings for processing the image with FociRB macro which uses the rolling ball algorithm for the background subtraction to provide a clean image for counting the foci. By changing the available parameters, one can select the appropriate settings so that the automatic counting of foci corresponded to the counting of foci by eye.

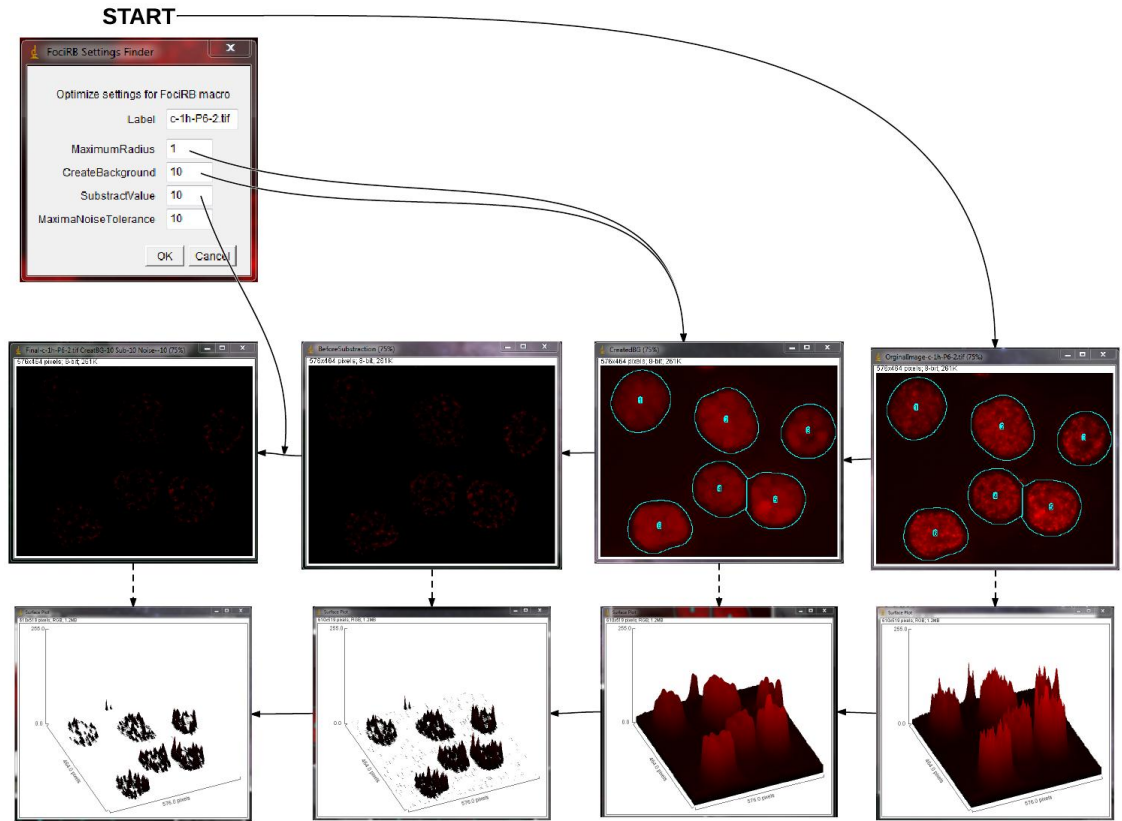


Figure A 20. A method applied for background subtraction with FociRB option.



A.5.6 FociRB - macro for analysing foci. It uses rolling ball algorithm to subtract background from image (A.4.12), and find maxima option to count foci number (A.5.4). Use Check settings option (A.5.5) first to adjust settings so the score of foci counting be equal visual scoring.

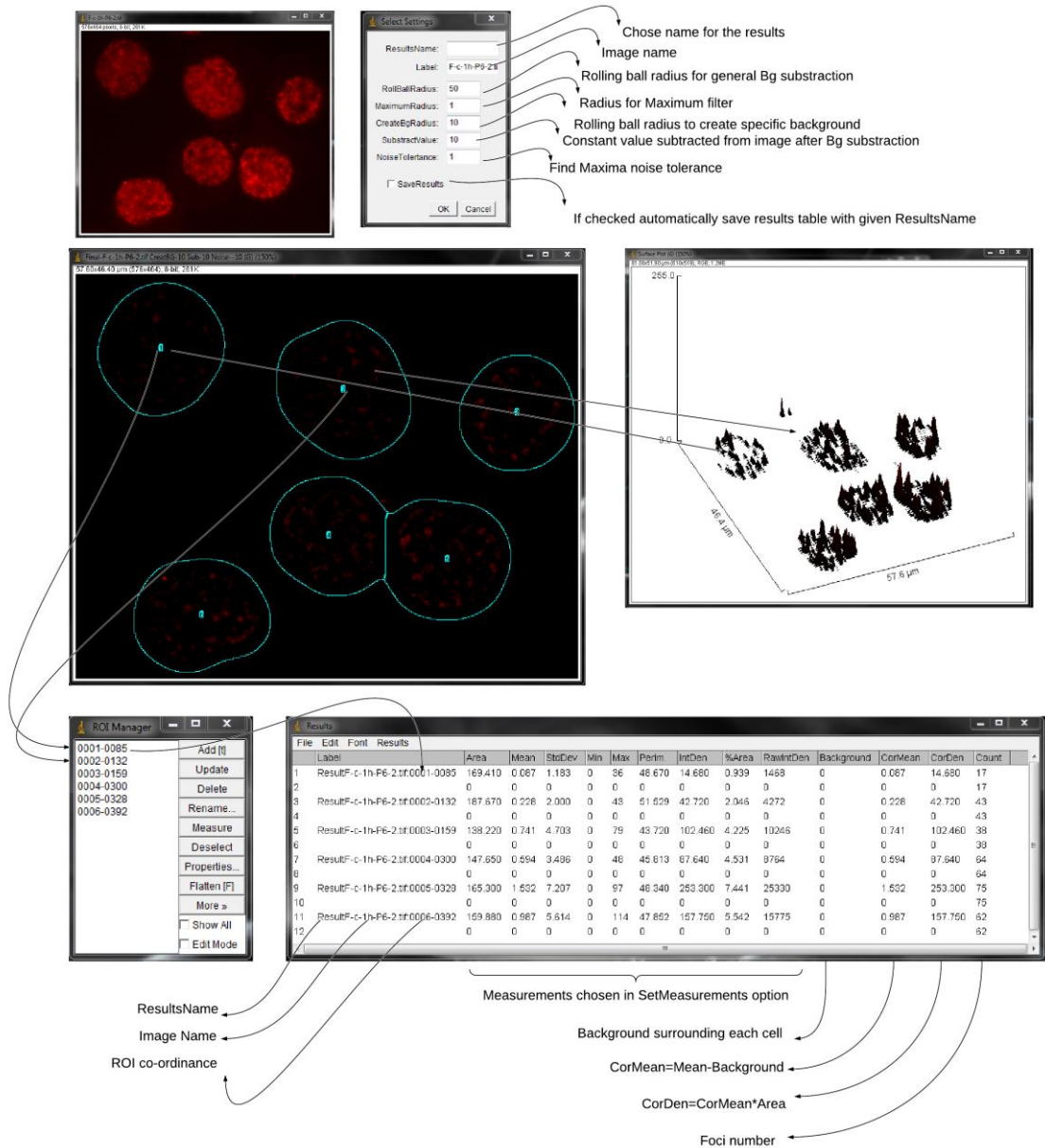


Figure A 21. Analysis of H2AX foci using FociRB option.

When running FociRB macro, the dialog window will appear first. In this window, the settings selected by Check Settings For FociRB (A.5.5) has to be entered. Following background subtraction, the image background should be reduced to 0 as shown on surface plot above. Obtained results will indicate a unique Label for each cell, which consists of chosen results name, image name, and cell coordinates followed by chosen endpoint measurements. CorDen and CorMean are options which uses for subtraction background calculated from first layer of pixels outside the outlines. If the outline is crossing the several bright points which belongs to nucleolus this CorDen and Cor Mean becomes negative and outlines for such nucleus shall be corrected (using one of options designed for Correcting Nucleus outlines).



A.5.7 IntegratedDensity- macro for measuring foci integrated density.

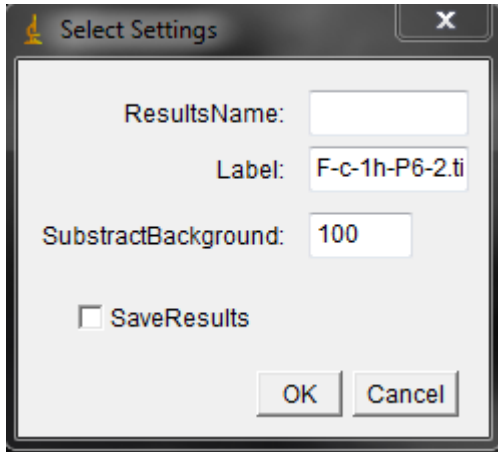
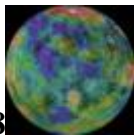


Figure A 22. Dialog window for settings selection for IntegratedDensity macro.

This macro uses global background subtraction (A.4.12) and measures total Integrated Density for each selected nucleus and saves results for single image.



A.5.8 IntegratedDensity with Counting- macro for measuring foci integrated density along with counting foci.

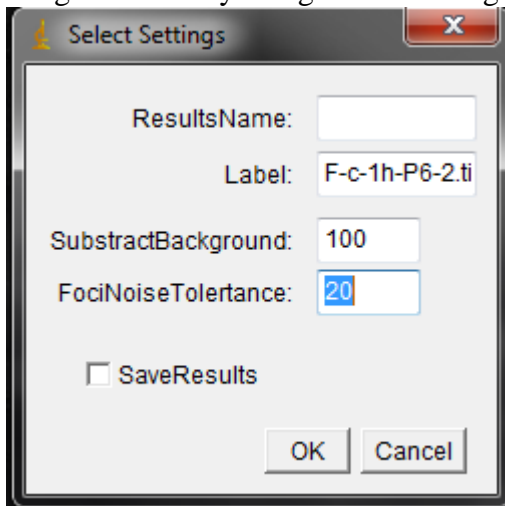


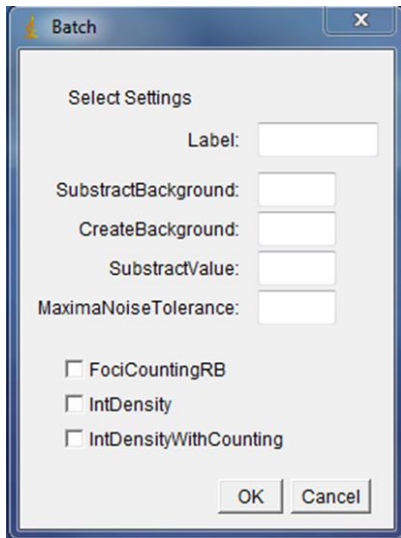
Figure A 23. Dialog window for settings selection for IntegratedDensity with Counting

This macro works as macro above but additionally counts foci number.

Scattered foci or foci beyond the resolution are treated as a part of the background. The option IntegratedDensity with Counting allows to count foci using images without background subtraction. This analysis may provide additional information if the background inside the cell nucleus is considerable.



A.5.9 Batch- allows automatic analysis of all images using one of selected method (IntegratedDensity with Counting, IntegratedDensity or FociRB).



Label – allows to add additional label to results label.

SubtractBackground – Rolling ball radius for general background subtraction (available for all types of analysis)

CreateBackground - Rolling Ball radius for creating an image with specific background that is later subtracted from original image (available only for FociCountingRB options)

SubtractValue – constant value that will be subtracted from image to remove any remaining

background (see A.4.12.), (available for all types of analysis)

MaximaNoiseTolerance – Noise tolerance used by Find Maxima options to count foci.

To run the Batch analysis:

All images about to be analysed has to be placed in one folder along with corresponding ROI set.

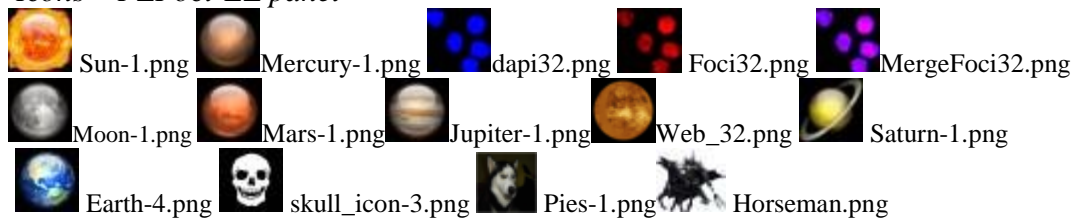
- a. Open ROI set from the folder where image about to be analysed are collected
- A.5.1
- b. Click Batch icon (A.5.9) and enter settings into dialog window
- c. Choose one of the available analysis
 1. FociCountingRB – See A.5.6
 2. IntDensity – See A.5.7
 3. IntDensityWirhCounting- See A.5.9
- d. OK



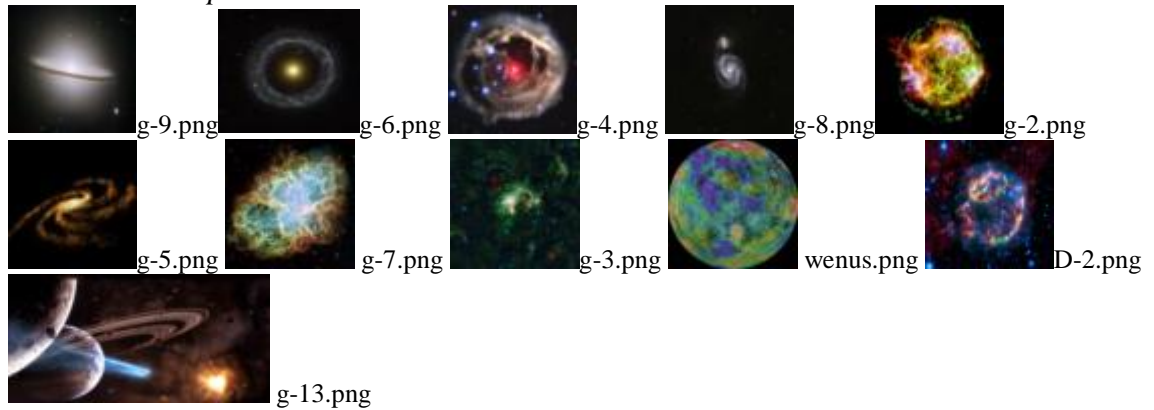
A.5.10 Edit Source Code – allows access to source code for this panel

A.6. Icons

Icons – PZFoci-EZ panel



Icons - FociEZ panel



Images adopted from NASA.

A.7. Source code.

A.7.1. _PZ-FociEZ.txt

```
run("Action Bar", "/plugins/PZFociEZ/_PZ-FociEZ.txt");
exit();
open();
<Grid>
<line>
<button>
label=<html><font color=blue size=+1>Open Image</font></html>
icon=_Kwiatuszek/Sun-1.png
arg=open();
<line>
<button>
label=<html><font color=blue size=+1>Open ROI for this Image</font></html>
icon=_Kwiatuszek/Mercury-1.png
arg=<macro>
d = getInfo("image.directory");
f = getInfo("image.filename");
t=getTitle();
roiManager("reset");
roiManager("Open" d+" "+f+".zip");
roiManager("Show All");
</macro>
<button>
label=<html><font color=blue size=+1>Create ROI Mask</font></html>
icon=_Kwiatuszek/dapi32.png
```

```

arg=run("Action Bar", "/plugins/PZFociEZ/MaskEZ.txt");
<button>
label=<html><font color=blue size=+1>Fluorescence Intensity Measurement And Foci
Counting</font></html>
icon=_Kwiatuszek/Foci32.png
arg=run("Action Bar", "/plugins/PZFociEZ/FociEZ.txt");
<button>
label=<html><font color=blue size=+1>Merging Dapi With Foci
Images</font></html>
icon=_Kwiatuszek/MergeFoci32.png
arg=run("Action Bar", "/plugins/PZFociEZ/color_and_merge.txt");
<button>
label=<html><font color=blue size=+1>Zoom [z]</font></html>
icon=_Kwiatuszek/Moon-1.png
arg=setTool("zoom");
<button>
label=<html><font color=blue size=+1>OvalROI [x]</font></html>
icon=_Kwiatuszek/Mars-1.png
arg=setTool("oval");
<button>
label=<html><font color=blue size=+1>Free Hand ROI [c]</font></html>
icon=_Kwiatuszek/Jupiter-1.png
arg=setTool("freehand");
<button>
label=<html><font color=blue size=+1>Set Scale</font></html>
icon=_Kwiatuszek/Web_32.png
arg=run("Set Scale...");
<button>
label=<html><font color=blue size=+1>Set Measurements</font></html>
icon=_Kwiatuszek/Saturn-1.png
arg=run("Set Measurements...");
<button>
label=<html><font color=blue size=+1>Start up Macros</font></html>
icon=_Kwiatuszek/Earth-4.png
arg=run("Install...", "install=plugins/PZFociEZ/StartMacros.txt");
<button>
label=<html><font color=blue size=+1>Close All Windows</font></html>
icon=_Kwiatuszek/skull_icon-3.png
arg=while (nImages >0) close();
<button>
label=<html><font color=blue size=+1>Files Log</font></html>
icon=_Kwiatuszek/info_32.png
arg=<macro>
dir = getDirectory("Choose a Directory ");
count = 1;
listFiles(dir);
function listFiles(dir) {
list = getFileList(dir);
for (i=0; i<list.length; i++) {
if (endsWith(list[i], "."))
listFiles(""+dir+list[i]);
else

```

```

        print((count++) + ": " +dir + list[i]);
    }
}
</macro>
<button>
label=<html><font color=blue size=+1>HELP</font></html>
icon=_Kwiatuszek/Pies-1.png
arg= run("URL...", "url=file:///E:/PZFociEZSite/index.html");
<button>
label=<html><font color=blue size=+1>Hide IJ</font></html>
icon=_Kwiatuszek/Horseman.png
arg=<hide>
</line>
<codeLibrary>
</codeLibrary>
<startupAction>
</startupAction>
//<main>
//<DnD>

```

A.7.2. MaskEZ.txt

```

//Action Bar description file : MaskEZ
run("Action Bar", "/plugins/PZFociEZ/MaskEZ.txt");
exit();
</noGrid>
<sticky>
<line>
<button>
label=<html><font color=magenta size=2>OpenImage</font></html>
icon=noicon
arg=<macro>
open();
t=getTitle();
print(t);
</macro>
<line>
<line>
<button>
label=<html><font color=magenta size=2>OpenNext</font></html>
icon=noicon
arg=<macro>
dir=getInfo("image.directory");
nam=getInfo("image.filename");
run("Open Next", "/"+"".tif");
</macro>
</line>
<line>
<button>
label=<html><font color=red size=2>MakeMask</font></html>
icon=noicon
arg=<macro>

```

```

run("Run...", "run=plugins/PZFociEZ/SuperMaska.txt");
</macro>
<line>
<line>
<button>
label=<html><font color=red size=2>MakeAgain</font></html>
icon=noicon
arg=<macro>
run("Analyze Particles...", "size=500-Infinity circularity=0.01-1.00 show=Masks
exclude clear include record add in_situ");
</macro>
</line>
<line>
<button>
label=<html><font color=blue size=2>Multiply</font></html>
icon=noicon
arg=<macro>
run("Multiply...");
</macro>
</line>
<line>
<button>
label=<html><font color=blue size=2>Subst</font></html>
icon=noicon
arg=<macro>
run("Subtract...");
</macro>
</line>
<line>
<button>
label=<html><font color=blue size=2>SubsBg</font></html>
icon=noicon
arg=<macro>
run("Subtract Background...");
</macro>
</line>
<line>
<button>
label=<html><font color=blue size=2>Smooth</font></html>
icon=noicon
arg=<macro>
run("Gaussian Blur...", "sigma=2");
</macro>
</line>
<line>
<button>
label=<html><font color=blue size=2>Binary</font></html>
icon=noicon
arg=<macro>
run("Make Binary");
</macro>
</line>

```

```

<line>
<button>
label=<html><font color=blue size=2>Watershed</font></html>
icon=noicon
arg=<macro>
run("Watershed");
</macro>
</line>
<line>
<button>
label=<html><font color=blue size=2>Invert</font></html>
icon=noicon
arg=<macro>
run("Invert");
</macro>
<line>
<line>
<button>
label=<html><font color=black size=2>FillHol</font></html>
icon=noicon
arg=<macro>
run("Fill Holes");
</macro>
</line>
<line>
<button>
label=<html><font color=magenta size=2>Erode</font></html>
icon=noicon
arg=<macro>
run("Erode");
</macro>
<line>
<line>
<button>
label=<html><font color=magenta size=2>Dilate</font></html>
icon=noicon
arg=<macro>
run("Dilate");
</macro>
</line>
<line>
<button>
label=<html><font color=magenta size=2>Open-</font></html>
icon=noicon
arg=<macro>
run("Open");
</macro>
</line>
<line>
<button>
label=<html><font color=magenta size=2>Close-</font></html>
icon=noicon

```

```

arg=<macro>
run("Close-");
</macro>
</line>
<line>
<button>
label=<html><font color=black size=2>CloseImage</font></html>
icon=noicon
arg=<macro>
close();
</macro>
</line>
<button>
label=<html><font color=magenta size=2>CloseBar</font></html>
icon=noicon
arg=<close>
</line>
<button>
label=<html><font color=green size=2>ShowAll</font></html>
icon=noicon
arg=<macro>
roiManager("Show All");
</macro>
</line>
<button>
label=<html><font color=green size=2>ShowNone</font></html>
icon=noicon
arg=<macro>
roiManager("Show None");
</macro>
</line>
<button>
label=<html><font color=blue size=2>SaveRoi/n-Dapi</font></html>
icon=noicon
arg=<macro>
t=getTitle();
f = getInfo("image.filename");
d=getInfo("image.directory") ;
run("Duplicate...", "title=temp");
rename(""+ t + "");
t1=getTitle();
File.makeDirectory(d+"Dapi");
roiManager("Save", d+"Dapi/"+ "D-" + t1 + ".zip");
saveAs("tif", d+"Dapi/"+ "D-" + t1);
close();
</macro>
</line>
</line>

```

```

<button>
label=<html><font color=blue size=2>EditMask</font></html>
icon=noicon
arg=<macro>
run("Edit...", "open=plugins/PZFociEZ/SuperMaska.txt");
</macro>
<line>
<line>
<button>
label=<html><font color=blue size=2>EditBar</font></html>
icon=noicon
arg=<macro>
run("Edit...", "open=plugins/PZFociEZ/MaskEZ.txt");
</macro>
</line>
<line>
<button>
label=<html><font color=magenta size=2>Enlarge [f]</font></html>
icon=noicon
arg=<macro>
macro "enlarge [f]" {
run("Enlarge...", "enlarge=1");
}
</macro>
<line>
<line>
<button>
label=<html><font color=magenta size=2>Shrink [s]
icon=noicon
arg=<macro>
macro "shrink [s]" {
pixels = 1;
saveSettings();
rectOrOval = selectionType==0 || selectionType==1;
getPixelSize(unit, pixelWidth, pixelHeight);
n = 1;
decimalPlaces = 0;
if (floor(n)!=n) decimalPlaces = 2;
pixels = round(n/pixelWidth);
if (rectOrOval)
shrinkRectOrOval(pixels);
else
shrink(pixels);
restoreSettings();
function shrinkRectOrOval(n) {
getBoundingRect(x, y, width, height);
x += n;
y += n;
width = width - 2*n;
height = height - 2*n;
if (width>0 && height>0) {
if (selectionType==0)

```



```

        makeRectangle(x, y, width, height);
    else
        makeOval(x, y, width, height);
    }
}
function shrink(n) {
    if (pixels>255)
        exit("Cannot shrink by more than 255 pixels");
    id = getImageID();
    setBatchMode(true);
    width = getWidth();
    height = getHeight();
    run("Options...", "iterations=1 count=1");
    run("Create Mask");
    run("Distance Map");
    setThreshold(n+1, 255);
    run("Create Selection");
    close();
    selectImage(id);
    run("Restore Selection");
}
}
</macro>
</line>
<line>
<button>
label=<html><font color=magenta size=2>DeleteROI [a]</font></html>
icon=noicon
arg=<macro>
macro "DeleteROI [a]" {
roiManager("Delete");
}
</macro>
</line>
<line>
<button>
label=<html><font color=magenta size=2>AddROI [t]</font></html>
icon=noicon
arg=<macro>
roiManager("Add");
</macro>
</line>
<line>
<button>
label=<html><font color=magenta size=2>UpdateROI [d]</font></html>
icon=noicon
arg=<macro>
macro "update [d]" {
roiManager("Update");
}
</macro>
</line>

```

```

<line>
<button>
label=<html><font color=magenta size=2>CombineROI</font></html>
icon=noicon
arg=<macro>
macro "Combine" {
roiManager("Select All");
roiManager("Combine");
}
</macro>
</line>
<line>
<button>
label=<html><font color=red size=2>SaveRoi-Foci</font></html>
icon=noicon
arg=<macro>
t=getTitle();
f = getInfo("image.filename");
d=getInfo("image.directory") ;
run("Duplicate...", "title=temp");
rename(""+ t + "");
t1=getTitle();
File.makeDirectory(d+"Foci");
roiManager("Save", d+"Foci/"+ "F-" + t1+".zip");
saveAs("tif", d+"Foci/"+ "F-" +t1);
close();
</macro>
</line>
<line>
<button>
label=<html><font color=purple size=2>OpenWRoi</font></html>
icon=noicon
arg=<macro>
run("Open Next");
d = getInfo("image.directory");
f = getInfo("image.filename");
roiManager("reset");
roiManager("Open" d+""+f+".zip");
roiManager("Show All");
</macro>
</line>
<line>
<button>
label=<html><font color=purple size=2>SaveRoi</font></html>
icon=noicon
arg=<macro>
d = getDirectory("current");
f = getInfo("image.filename");
roiManager("Save", d+""+f+".zip");
</macro></line>

```

A.7.3. *FociEZ.txt*

```
// Action Bar description file :FociEZ
run("Action Bar", "/plugins/PZFociEZ/FociEZ.txt");
exit();
//<sticky>
<Grid>
<line>
<button>
label=<html><font color=purple size=+1>Open Image</font></html>
icon=_Kwiatuszek/g-9.png
arg=<macro>
run("Open...");
</macro>
<line>
<line>
<button>
label=<html><font color=red size=+1>Surface Plot</font></html>
icon=_Kwiatuszek/g-6.png
arg=<macro>
run("Surface Plot...", "polygon=100 shade draw_axis smooth");
</macro>
</line>
<line>
<button>
label=<html><font color=purple size=+1>Subtract Background</font></html>
icon=_Kwiatuszek/g-4.png
arg=<macro>
run("Subtract Background...");
</macro>
<line>
<line>
<button>
label=<html><font color=green size=+1>MeasureAndDraw</font></html>
icon=_Kwiatuszek/g-8.png
arg=<macro>
macro "FociDraw" {
open();
t=getTitle();
t2= t +' ROI.tif';
setFont("SansSerif", 14);
run("Out");
run("Brightness/Contrast...");
run("Enhance Contrast", "saturated=0.5");
rename("dapi");
run("Out");
run("Duplicate...", "title=dapicopy");
open();
run("Out");
rename("FITC");
selectWindow("dapi");
run("Subtract Background...", "rolling=60");
run("Gaussian Blur...", "radius=4");
```

```

selectWindow("dapi");
setThreshold(10, 200);
run("Threshold", "thresholded remaining black");
run("Watershed");
selectWindow("dapi");
run("Colors...", "foreground=black background=white selection=yellow");
run("Analyze Particles...", "minimum=300 maximum=15000 show=Nothing record
exclude");
o = nResults;
for (i=0; i<o; i++) {
x = getResult('XStart', i);
y = getResult('YStart', i);
doWand(x,y);
roiManager("add");
}
selectWindow('FITC');
run("Set Measurements...", "area mean limit display redirect=None decimal=4");
n = roiManager("count");
run("Colors...", "foreground=white background=black selection=yellow");
roiManager("deselect");
for (i=0; i<n; i++) {
if (i==1) {
write(" " +t);
write("found " +n);
}
run("Set Measurements...", "area mean centroid limit display redirect=None
decimal=4");
setThreshold(0, 40);
roiManager("select", i);
write("foci for nucleus "+i);
run("Analyze Particles...", "minimum=3 maximum=999999 show=Nothing display ");
run("Colors...", "foreground=white background=black selection=yellow");
write("FITC intensity for nucleus: " +i);
resetThreshold();
run("Set Measurements...", "area mean centroid display redirect=None decimal=4");
run("Measure");
x = getResult('X');
y = getResult('Y');
L = toString(i);
getVoxelSize(width, height, depth, unit);
drawString(L, x/width, y/height);
roiManager("draw");
roiManager("deselect");
}
selectWindow("dapicopy");
write("integrated DAPI intensity per nucleus ");
setThreshold(30, 255);
for (i=0; i<n; i++) {
roiManager("select", i);
run("Analyze Particles...", "minimum=30 maximum=15000 bins=20 show=Nothing
display");
roiManager("deselect");
}

```

```

}
resetThreshold();
selectWindow("ROI Manager");
run("Close");
selectWindow("dapi");
run("Close");
run("RGB Merge...", "green=*None* red=FITC blue=dapicopy");
rename(t2);
selectWindow("Results");
}
</macro>
</line>
<line>
<button>
label=<html><font color=red size=+1>FindMaxima</font></html>
icon=_Kwiatuszek/g-2.png
arg=<macro>
run("Find Maxima...");
</macro>
</line>
<line>
<button>
label=<html><font color=red size=+1>Check settings for FociRB</font></html>
icon=_Kwiatuszek/g-5.png
arg=<macro>
macro "SettingsFinder" {
open();
getRawStatistics(area, mean, min, max, std, h);
    label = getTitle();
    radius= 1;
    background = 10;
    subtract = 10;
    noise = 10;
    Dialog.create('FociRB Settings Finder');
Dialog.addMessage('Optimize settings for FociRB macro');
Dialog.addString('Label', label);
Dialog.addNumber('MaximumRadius', radius);
Dialog.addNumber('CreateBackground', background);
Dialog.addNumber('SubtractValue', subtract);
Dialog.addNumber('MaximaNoiseTolerance', noise);
Dialog.show();
label1 = Dialog.getString();
radius = Dialog.getNumber();
background1 = Dialog.getNumber();
subtract1 = Dialog.getNumber();
noise1 = Dialog.getNumber();
    print(label);
    a = 0 + mean;
    b = 0 + std;
    print("Image mean");
    print(a);
    print("Image StdDev");
}
}

```

```

        print(b);
        rename("OrginalImage-"+label1+"");
        t1=getTitle();
        selectWindow(""+t1+"");
        run("Duplicate...", "title=CreatedBG");
        run("Maximum...", "radius="+ radius + "");
run("Subtract Background...", "rolling="+ background1 + " create");
    print("Background" +background1);
    print(background1);
    imageCalculator("Subtract create", ""+t1+"", "CreatedBG");
        t2=getTitle();
        run("Duplicate...", "title=BeforeSubstraction");
        selectWindow(""+t2+"");
        run("Subtract...", "value="+ subtract1 + "");
            print("Subtract");
            print(subtract1);

                selectWindow(""+t2+"");
                rename("Final-"+label1+"
CreatBG-"+ background1 + " Sub-"+ subtract1 + " Noise--"+ noise1 + "");
                t3=getTitle();
                run("Tile");

        open();
        selectWindow(t3);
        n = roiManager("count");
        for (i=0; i<n; i++) {
            roiManager("select", i);
            run("Find Maxima...", "noise="+ noise1 + " output=Count");
            roiManager("Measure");
                }
                    print("Noise");
                    print(noise1);
                print("*****");
    }
</macro>
</line>
<line>
<button>
label=<html><font color=blue size=+1>FociRB</font></html>
icon=_Kwiatuszek/g-7.png
arg=<macro>
macro "CountFoci" {
run("ROI Manager...");
open();
t=getTitle();
roiManager("reset");
open(t+".zip");
foci = getInfo("image.filename");
curr=getDirectory("current");
default= " ";
macro "Get Time" {

```

```

MonthNames =
newArray("Jan","Feb","Mar","Apr","May","Jun","Jul","Aug","Sep","Oct","Nov","Dec"
);
DayNames = newArray("Sun","Mon","Tue","Wed","Thu","Fri","Sat");
getDateAndTime(year, month, dayOfWeek, dayOfMonth, hour, minute, second,
msec);
TimeString = "Date: "+DayNames[dayOfWeek]+" ";
if (dayOfMonth<10) {TimeString = TimeString+"0";}
TimeString = TimeString+dayOfMonth+"-"+MonthNames[month]+"-
"+year+"\nTime: ";
if (hour<10) {TimeString = TimeString+"0";}
TimeString = TimeString+hour+":";
if (minute<10) {TimeString = TimeString+"0";}
TimeString = TimeString+minute+":";
if (second<10) {TimeString = TimeString+"0";}
TimeString = TimeString+second;
print(TimeString);
getRawStatistics(area, mean, min, max, std, h);
print("File Path");
print(curr);
print("ImageName");
print(foci);
print("Image mean");
print(mean);
print("Image StDev");
print(std);
print("Minimum Pixel Value");
print(min);
print("Maximum Pixel Value");
print(max);
Dialog.create("Select Settings");
title = ""+default+"";
label1 = ""+foci+"";
Dialog.addString("ResultsName:", title);
Dialog.addString("Label:", label1);
Dialog.addNumber("RollBallRadius:", 50);
Dialog.addNumber("MaximumRadius:", 1);
Dialog.addNumber("CreateBgRadius:", 10);
Dialog.addNumber("SubstractValue:", 10);
Dialog.addNumber("NoiseTolertance:", 1);
Dialog.addCheckbox('SaveResults',false);
Dialog.show();
title = Dialog.getString();
label1 = Dialog.getString();
rollingb = Dialog.getNumber();
maximum = Dialog.getNumber();
background = Dialog.getNumber();
subtract = Dialog.getNumber();
noise = Dialog.getNumber();
res=Dialog.getCheckbox();
rename("copy");
run("Subtract Background...", "rolling="+ rollingb + "");

```

```

run("Duplicate...", "title=BG");
selectWindow("BG");
run("Maximum...", "radius="+ maximum + "");
run("Subtract Background...", "rolling="+ background + " create");
imageCalculator("Subtract create", "copy", "BG");
    selectWindow("BG");
    close();
    selectWindow("copy");
    close();

    selectWindow("Result of copy");

rename("" + title + "" + label1 + "");
run("Subtract...", "value="+ subtract + "");
sum=0;
coun=0;
s = roiManager("count");
for (l=0;l<s; l++) {
    roiManager("Select", l);
    getSelectionCoordinates(x,y);
    for (i=0;i<x.length;i++) {
        if (i<x.length-1) {
            dx=x[i+1]-x[i];
            dy=y[i+1]-y[i];
        } else {
            dx=x[0]-x[i];
            dy=y[0]-y[i];
        }
        n=round(sqrt(dx*dx+dy*dy));
        xinc=dx/n;
        yinc=dy/n;
        xx=x[i];
        yy=y[i];
        for (j=0;j<n;j++) {
            sum+=calibrate(getPixel(round(xx),round(yy)));
            xx+=xinc;
            yy+=yinc;
            coun++;
        }
    }
    roiManager("Measure");
    background=sum/coun;
    area=getResult('Area',nResults-1);
    mean=getResult('Mean',nResults-1);
    if (isNaN(area)||isNaN(mean))
        exit("Area and Mean must be selected in Analyze>Set Measurements");
    cormean=mean-background;
    corden=area*cormean;
    setResult('Background',nResults-1,background);
    setResult('CorMean',nResults-1,cormean);
    setResult('CorDen',nResults-1,corden);
    run("Find Maxima...", "noise="+ noise + " output=Count");

```



```

focii=getResult('Count', nResults-1);
setResult('Count',nResults-2,focii);
updateResults();
}

print("Number of Cells");
print(s);
print("*****");
print("
");
selectWindow("Results");
if (res==true) {
saveAs("txt",
curr+"FociRB"+label1+title);
run("Close");
}
if (res==false);
selectWindow(""+title+""+label1+"");
close();
selectWindow("ROI Manager");
run("Close");

}
</macro>
<line>
<line>
<button>
label=<html><font color=blue size=+1>Integrated Density</font></html>
icon=_Kwiatuszek/g-3.png
arg=<macro>
macro "BackgroundCorrected" {
run("ROI Manager...");
open();
t = getTitle();
curr=getDirectory("current");
roiManager("reset");
open(t+".zip");
foci = getInfo("image.filename");
default = " ";
macro "Get Time" {
MonthNames =
newArray("Jan","Feb","Mar","Apr","May","Jun","Jul","Aug","Sep","Oct","Nov","Dec"
);
DayNames = newArray("Sun", "Mon", "Tue", "Wed", "Thu", "Fri", "Sat");
getDateAndTime(year, month, dayOfWeek, dayOfMonth, hour, minute, second,
msec);
TimeString = "Date: "+DayNames[dayOfWeek]+" ";
if (dayOfMonth<10) {TimeString = TimeString+"0";}
TimeString = TimeString+dayOfMonth+"-"+MonthNames[month]+"-
"+year+"\nTime: ";
if (hour<10) {TimeString = TimeString+"0";}
TimeString = TimeString+hour+":";
if (minute<10) {TimeString = TimeString+"0";}
TimeString = TimeString+minute+":";
if (second<10) {TimeString = TimeString+"0";}
}
}

```

```

TimeString = TimeString+second;
print(TimeString);
    getRawStatistics(area, mean, min, max, std, h);
    print("File Path");
    print(curr);
    print("ImageName");
    print(foci);
    print("Image mean");
    print(mean);
    print("Image StDev");
    print(std);
    print("Minimum Pixel Value");
    print(min);
    print("Maximum Pixel Value");
    print(max);
        Dialog.create("Select Settings");
        title = ""+default+"";
        label1 = ""+foci+"";
        rb= " ";
        Dialog.addString("ResultsName:", title);
        Dialog.addString("Label:", label1);
        Dialog.addNumber("SubstractBackground:", 255);
        Dialog.addCheckbox('SaveResults',false);
        Dialog.show();
        title = Dialog.getString();
        label1 = Dialog.getString();
        rollingb = Dialog.getNumber();
        res=Dialog.getCheckbox();
selectWindow("" + label1 + "");
rename("" +title+"" +label1+ "");
run("Subtract Background...", "rolling="+ rollingb + "");
sum=0;
coun=0;
s = roiManager("count");
for (l=0;l<s; l++) {
    roiManager("Select", l);
    getSelectionCoordinates(x,y);
for (i=0;i<x.length;i++) {
setBatchMode(true);
    if (i<x.length-1) {
        dx=x[i+1]-x[i];
        dy=y[i+1]-y[i];
    } else {
        dx=x[0]-x[i];
        dy=y[0]-y[i];
    }
    n=round(sqrt(dx*dx+dy*dy));
    xinc=dx/n;
    yinc=dy/n;
    xx=x[i];
    yy=y[i];
    for (j=0;j<n;j++) {

```

```

        sum+=calibrate(getPixel(round(xx),round(yy)));
        xx+=xinc;
        yy+=yinc;
        coun++;
    }
}
roiManager("Measure");
background=sum/coun;
area=getResult('Area',nResults-1);
mean=getResult('Mean',nResults-1);
if (isNaN(area)||isNaN(mean))
    exit("Area and Mean must be selected in Analyze>Set Measurements");
    cormean=mean-background;
    corden=area*cormean;
setResult('Background',nResults-1,background);
setResult('CorMean',nResults-1,cormean);
setResult('CorDen',nResults-1,corden);
updateResults();
}

        print("Number of Cells");
        print(s);
        print("*****");
        print("                ");

selectWindow("Results");
if (res==true) {
saveAs("txt", curr+"IntDen-"+label1+title);
run("Close");
}
if (res==false);
selectWindow(""+title+""+label1+"");
close();
selectWindow("ROI Manager");
roiManager("Delete");
run("Close");
}
</macro>
</line>
<line>
<button>
label=<html><font color=blue size=+1>Integrated Density with
Counting</font></html>
icon=_Kwiatuszek/Pies-3.png
arg=<macro>
macro "BackgroundCorrectedVmaxima" {
run("ROI Manager...");
open();
t = getTitle();
curr=getDirectory("current");
roiManager("reset");
open(t+".zip");
foci = getInfo("image.filename");
default = " ";

```

```

macro "Get Time" {
    MonthNames =
newArray("Jan", "Feb", "Mar", "Apr", "May", "Jun", "Jul", "Aug", "Sep", "Oct", "Nov", "Dec"
);
    DayNames = newArray("Sun", "Mon", "Tue", "Wed", "Thu", "Fri", "Sat");
    getDateAndTime(year, month, dayOfWeek, dayOfMonth, hour, minute, second,
msec);
    TimeString = "Date: "+DayNames[dayOfWeek]+" ";
    if (dayOfMonth<10) {TimeString = TimeString+"0";}
    TimeString = TimeString+dayOfMonth+"-"+MonthNames[month]+"-
"+year+"\nTime: ";
    if (hour<10) {TimeString = TimeString+"0";}
    TimeString = TimeString+hour+": ";
    if (minute<10) {TimeString = TimeString+"0";}
    TimeString = TimeString+minute+": ";
    if (second<10) {TimeString = TimeString+"0";}
    TimeString = TimeString+second;
    print(TimeString);
    getRawStatistics(area, mean, min, max, std, h);
    print("File Path");
    print(curr);
    print("ImageName");
    print(foci);
    print("Image mean");
    print(mean);
    print("Image StDev");
    print(std);
    print("Minimum Pixel Value");
    print(min);
    print("Maximum Pixel Value");
    print(max);
    Dialog.create("Select Settings");
    title = ""+default+"";
    label1 = ""+foci+"";
    rb= " ";
    Dialog.addString("ResultsName:", title);
    Dialog.addString("Label:", label1);
    Dialog.addNumber("SubstractBackground:", 666);
    Dialog.addNumber("FociNoiseTolertance:", 10);
    Dialog.addCheckbox('SaveResults',false);
    Dialog.show();
    title = Dialog.getString();
    label1 = Dialog.getString();
    rollingb = Dialog.getNumber();
    noise = Dialog.getNumber();
    res=Dialog.getCheckbox();
selectWindow("" + label1 + "");
rename("" +title+""+label1+"");
run("Subtract Background...", "rolling="+ rollingb + "");
sum=0;
coun=0;
s = roiManager("count");

```

```

for (l=0;l<s; l++) {
    roiManager("Select", l);
    getSelectionCoordinates(x,y);
    for (i=0;i<x.length;i++) {
        if (i<x.length-1) {
            dx=x[i+1]-x[i];
            dy=y[i+1]-y[i];
        } else {
            dx=x[0]-x[i];
            dy=y[0]-y[i];
        }
        n=round(sqrt(dx*dx+dy*dy));
        xinc=dx/n;
        yinc=dy/n;
        xx=x[i];
        yy=y[i];
        for (j=0;j<n;j++) {
            sum+=calibrate(getPixel(round(xx),round(yy)));
            xx+=xinc;
            yy+=yinc;
            coun++;
        }
    }
    roiManager("Measure");
    background=sum/coun;
    area=getResult('Area',nResults-1);
    mean=getResult('Mean',nResults-1);
    if (isNaN(area)||isNaN(mean))
        exit("Area and Mean must be selected in Analyze>Set Measurements");
    cormean=mean-background;
    corden=area*cormean;
    setResult('Background',nResults-1,background);
    setResult('CorMean',nResults-1,cormean);
    setResult('CorDen',nResults-1,corden);
    run("Find Maxima...", "noise="+ noise +" output=Count");
    foci=getResult('Count', nResults-1);
    setResult('Count',nResults-2,foci);
    updateResults();
}

        print("Number of Cells");
        print(s);
        print("*****");
        print("                ");

selectWindow("Results");
if (res==true) {
    saveAs("txt", curr+"IntCnt-"+label1+title);
    run("Close");
}
if (res==false)
selectWindow(""+title+""+label1+"");
close();
selectWindow("ROI Manager");

```

```

roiManager("Delete");
run("Close");
}
</macro>
<line>
<line>
<button>
label=<html><font color=black size=+1>Batch Devil</font></html>
icon=_Kwiatuszek/D-2.png
arg=<macro>
macro "batch" {
default=" ";
Dialog.create('Batch');
Dialog.addMessage('Select Settings');
Dialog.addString("Label:", default);
Dialog.addNumber("SubstractBackground:", 666);
Dialog.addNumber("CreateBackground:", 10);
Dialog.addNumber("SubstractValue:", 10);
Dialog.addNumber("MaximaNoiseTolerance:", 10);
Dialog.addCheckbox('FociCountingRB',false);
Dialog.addCheckbox('IntDensity',false);
Dialog.addCheckbox('IntDensityWithCounting',false);
Dialog.show();
default=Dialog.getString();
subbackground = Dialog.getNumber();
background = Dialog.getNumber();
substract = Dialog.getNumber();
noise = Dialog.getNumber();
a=Dialog.getCheckbox();
b=Dialog.getCheckbox();
c=Dialog.getCheckbox();
setBatchMode(true);
if (a==0 && b==0 && c==0)
    exit("Select a Method You must");
if (a==1 && b==1 && c==1)
    exit("An Idiot You are");
if (a==0 && b==1 && c==1)
    exit("HWDP");
if (a==1 && b==0 && c==1)
    exit("Tempy Chuj??");
if (a==1 && b==1 && c==0)
    exit("A stupid choise You made");
if (a==1 && b==0 && c==0) {
start = getTime;
dir = getDirectory("current");
list = getFileList(dir);
h=list.length;
g=(h/2);
k=1;
for (r=0; k<=list.length; r++) {
if (endsWith(list[r], ".tif")) {
w=File.getName(list[r]);

```

```

print(w);
selectWindow("ROI Manager");
roiManager("reset");
open(list[r]+".zip");
setBatchMode(true);
open(w);
    selectWindow(w);
    rename("copy");
    run("Subtract Background...", "rolling="+ subbackground + "");
    run("Duplicate...", "title=BG");
    run("Maximum...", "radius=1");
    run("Subtract Background...", "rolling="+ background + " create");
    imageCalculator("Subtract create", "copy", "BG");
        selectWindow("BG");
        close();
        selectWindow("copy");
        close();

        selectWindow("Result of copy");

        rename(""+default+""+w+"");
        run("Subtract...", "value="+ subtract + "");
sum=0;
coun=0;
s = roiManager("count");
for (l=0;l<s; l++) {
    roiManager("Select", l);
    getSelectionCoordinates(x,y);
    for (i=0;i<x.length;i++) {
        if (i<x.length-1) {
            dx=x[i+1]-x[i];
            dy=y[i+1]-y[i];
        } else {
            dx=x[0]-x[i];
            dy=y[0]-y[i];
        }
        n=round(sqrt(dx*dx+dy*dy));
        xinc=dx/n;
        yinc=dy/n;
        xx=x[i];
        yy=y[i];
        for (j=0;j<n;j++) {
            sum+=calibrate(getPixel(round(xx),round(yy)));
            xx+=xinc;
            yy+=yinc;
            coun++;
        }
    }
}
roiManager("Measure");
backgroun=sum/coun;
area=getResult('Area',nResults-1);
mean=getResult('Mean',nResults-1);

```

```

    if (isNaN(area)||isNaN(mean))
        exit("Area and Mean must be selected in Analyze>Set Measurements");
        cormean=mean-background;
        corden=area*cormean;
    setResult('Background',nResults-1,background);
    setResult('CorMean',nResults-1,cormean);
    setResult('CorDen',nResults-1,corden);
    run("Find Maxima...", "noise="+ noise +" output=Count");
    focii=getResult('Count', nResults-1);
    setResult('Count',nResults-2,focii);
    updateResults();
}
selectWindow(""+default+""+w+"");
close();
setBatchMode(false);
end=getTime;
e=(end - start)/1000;
}
if (r==h-1)
    exit("Congratulations! With the speed of "+ e++/g +"sec/Image "+ g +" pictures were
    successfully analysed. ImageJ wish you breaktrough results. Have a Nice Day -:");
}
}
if (a==0 && b==1 && c==0) {
    start=getTime;
    dir=getDirectory("current");
    list = getFileList(dir);
    h=list.length;
    g=(h/2);
    k=1;
    for (r=0; k<=list.length; r++) {
        if (endsWith(list[r], ".tif")) {
            w=File.getName(list[r]);
            selectWindow("ROI Manager");
            roiManager("reset");
            open(list[r]+".zip");
            setBatchMode(true);
            open(w);
            rename(""+default+""+w+"");
            run("Run...", "run=plugins/PZFociEZ/BackgroundCorrectedBatch");
            selectWindow(""+default+""+w+"");
            close();
            setBatchMode(false);
            end=getTime;
            e1=(end - start)/1000;
        }
    }
    if (r==h-1)
        exit("Congratulations! With the speed of "+ e1++/g +"sec/Image "+ g +" pictures were
        successfully analysed. ImageJ wish you breaktrough results. Have a Nice Day -:");
}
}
if (a==0 && b==0 && c==1) {

```



```

start = getTime;
dir = getDirectory("current");
list = getFileList(dir);
h=list.length;
g=(h/2);
k=1;
for (r=0; k<=list.length; r++) {
if (endsWith(list[r], ".tif")) {
w=File.getName(list[r]);
selectWindow("ROI Manager");
roiManager("reset");
open(list[r]+".zip");
print(w);
setBatchMode(true);
open(w);
rename(""+default+""+w+"");
run("Subtract Background...", "rolling="+ subbackground + "");
sum=0;
coun=0;
s = roiManager("count");
for (l=0;l<s; l++) {
roiManager("Select", l);
getSelectionCoordinates(x,y);
for (i=0;i<x.length;i++) {
if (i<x.length-1) {
dx=x[i+1]-x[i];
dy=y[i+1]-y[i];
} else {
dx=x[0]-x[i];
dy=y[0]-y[i];
}
n=round(sqrt(dx*dx+dy*dy));
xinc=dx/n;
yinc=dy/n;
xx=x[i];
yy=y[i];
for (j=0;j<n;j++) {
sum+=calibrate(getPixel(round(xx),round(yy)));
xx+=xinc;
yy+=yinc;
coun++;
}
}
roiManager("Measure");
backgroun=sum/coun;
area=getResult('Area',nResults-1);
mean=getResult('Mean',nResults-1);
if (isNaN(area)||isNaN(mean))
exit("Area and Mean must be be selected in Analyze>Set Measurements");
cormeans=mean-backgroun;
corden=area*cormeans;
setResult('Background',nResults-1,backgroun);

```

```

setResult('CorMean',nResults-1,cormean);
setResult('CorDen',nResults-1,corden);
run("Find Maxima...", "noise="+ noise + " output=Count");
foci=getResult('Count', nResults-1);
setResult('Count',nResults-2,foci);
updateResults();
}
selectWindow(""+default+""+w+"");
close();
setBatchMode(false);
end=getTime;
z=(end - start)/1000;
}
if (r==h-1)
exit("Congratulations! With the speed of "+ z++/g +"sec/Image "+ g +" pictures were
successfully analysed. ImageJ wish you breaktrough results. Have a Nice Day -:");
}
setBatchMode(false);
</macro>
</line>
<line>
<button>
label=<html><font color=purple size=+1>Edit FociEZ</font></html>
icon=_Kwiatuszek/g-13.png
arg=<macro>
run("Edit...", "open=plugins/PZFociEZ/FociEZ.txt");
</macro>
</line>

```

A.7.4. StartMacros.txt

```

macro "DelateROI [a]" {
roiManager("Delete");
}
macro "update [d]" {
roiManager("Update");
}
macro "enlarge [f]" {
run("Enlarge...", "enlarge=1");
}
macro "Zoom [z]" {
setTool("zoom"); z
}
macro "FreeHandRoi [c]" {
setTool("freehand");
}
macro "OvalRoi [x]" {
setTool("oval");
}
}

```

A.7.5. SuperMaska.txt

```
macro "SuperMaska [1]" {
//open();
t = getTitle();
f = getInfo("image.filename");
dir=getInfo("image.directory");
print(t);
//print(dir);
run("Subtract Background...", "rolling=50");
run("Enhance Contrast", "saturated=0.35");
currwa = getDirectory("current");
run("Gaussian Blur...", "sigma=10");
run("Smooth");
run("Smooth");
//run("Smooth");
run("Subtract...", "value=5");
//run("Subtract Background...", "rolling=10 create");
run("Multiply...", "value=3.000");
//run("Subtract...", "value=11");
//run("Gaussian Blur...", "sigma=4");
//run("Multiply...", "value=4.000");
//run("Minimum...", "radius=1")
//run("Subtract Background...", "rolling=60");
//run("Smooth");
run("Make Binary");
run("Dilate");
run("Watershed");
run("Analyze Particles...", "size=20-Infinity circularity=0.01-1.00 show=Masks clear
include record add in_situ");
run("Analyze Particles...", "size=30-Infinity circularity=0.01-1.00 show=Masks exclude
clear add in_situ");
run("Analyze Particles...", "size=40-Infinity circularity=0.01-1.00 show=Masks exclude
include add in_situ");
run("Analyze Particles...", "size=50-Infinity circularity=0.01-1.00 show=Masks exclude
include add in_situ");
run("Analyze Particles...", "size=500-Infinity circularity=0.01-1.00 show=Masks
exclude clear include record add in_situ");
id=getImageID();
d=0-id;
print("*****");
t=getTitle();
selectWindow(t);
close();
open(dir+f);
id1=getImageID;
rename(f);
roiManager("Show All");
}
```

A.7.6. BackgroundCorrectedBatch.txt

```
macro "BackgroundCorrectedBatch" {
```

```

sum=0;
coun=0;
s = roiManager("count");
for (l=0;l<s;l++) {
  roiManager("Select", l);
  getSelectionCoordinates(x,y);
  for (i=0;i<x.length;i++) {
    setBatchMode(true);
    if (i<x.length-1) {
      dx=x[i+1]-x[i];
      dy=y[i+1]-y[i];
    } else {
      dx=x[0]-x[i];
      dy=y[0]-y[i];
    }
    n=round(sqrt(dx*dx+dy*dy));
    xinc=dx/n;
    yinc=dy/n;
    xx=x[i];
    yy=y[i];
    for (j=0;j<n;j++) {
      sum+=calibrate(getPixel(round(xx),round(yy)));
      xx+=xinc;
      yy+=yinc;
      coun++;
    }
  }
  roiManager("Measure");
  background=sum/coun;
  area=getResult('Area',nResults-1);
  mean=getResult('Mean',nResults-1);
  if (isNaN(area)||isNaN(mean))
    exit("Area and Mean must be selected in Analyze>Set Measurements");
  cormean=mean-background;
  corden=area*cormean;
  setResult('Background',nResults-1,background);
  setResult('CorMean',nResults-1,cormean);
  setResult('CorDen',nResults-1,corden);
  updateResults();
}
}

```

A.7.7. color_and_merge.txt

```

// Action Bar description file :color_and_merge
run("Action Bar","/plugins/PZFociEZ/color_and_merge.txt");
exit();
<sticky>
<line>
<button>
label=<html><font color=black size=+1>X</font></html>
icon=noicon
arg=<close>

```

```

</line>
<line>
<button>
label=Blk
icon=noicon
arg=<macro>
run("Grays");
</macro>
</line>
<line>
<button>
label=<html><font color=red size=+1>R</font></html>
icon=noicon
arg=<macro>
run("Red");
</macro>
</line>
<line>
<button>
label=<html><font color=green size=+1>G</font></html>
icon=noicon
arg=<macro>
run("Green");
</macro>
</line>
<line>
<button>
label=<html><font color=blue size=+1>B</font></html>
icon=noicon
arg=<macro>
run("Blue");
</macro>
</line>
<line>
<button>
label=<html><font color=black size=+1>1</font></html>
icon=noicon
arg=<macro>
id = getImageID();
set("image1",id);
</macro>
</line>
<line>
<button>
label=<html><font color=black size=+1>2</font></html>
icon=noicon
arg=<macro>
id = getImageID();
set("image2",id);
</macro>
</line>
<line>

```

```

<button>
label=<html><font color=black size=+1>M</font></html>
icon=noicon
arg=<macro>
id1 = parseInt(get("image1"));
id2 = parseInt(get("image2"));
setBatchMode(true);
selectImage(id1);
run("Duplicate...", "title=temp");
run("RGB Color");
id1 = getImageID();
selectImage(id2);
run("Duplicate...", "title=temp");
run("RGB Color");
id2 = getImageID();
imageCalculator("Add create", id1,id2);
rename("Merge");
setBatchMode(false);
</macro>
</line>
<codeLibrary>
function get(s) (return parseInt(call("ij.Prefs.get", "JMAB."+s,0));)
function set(s,v) (call("ij.Prefs.set", "JMAB."+s,v); return;)</codeLibrary>

```

References

- Affar, E. B., Germain, M., Winstall, E., Vodenicharov, M., Shah, R. G., Salvesen, G. S. and Poirier, G. G. (2001) 'Caspase-3-mediated processing of poly(ADP-ribose) glycohydrolase during apoptosis', *J Biol Chem*, 276, (4), pp. 2935-42.
- Almeida, K. H. and Sobol, R. W. (2007) 'A unified view of base excision repair: lesion-dependent protein complexes regulated by post-translational modification', *DNA Repair (Amst)*, 6, (6), pp. 695-711.
- Alvarez-Gonzalez, R. and Mendoza-Alvarez, H. (1995) 'Dissection of ADP-ribose polymer synthesis into individual steps of initiation, elongation, and branching', *Biochimie*, 77, (6), pp. 403-7.
- Alvarez-Gonzalez, R., Pacheco-Rodriguez, G. and Mendoza-Alvarez, H. (1994) 'Enzymology of ADP-ribose polymer synthesis', *Mol Cell Biochem*, 138, (1-2), pp. 33-7.
- Ame, J. C., Rolli, V., Schreiber, V., Niedergang, C., Apiou, F., Decker, P., Muller, S., Hoger, T., Menissier-de Murcia, J. and de Murcia, G. (1999) 'PARP-2, A novel mammalian DNA damage-dependent poly(ADP-ribose) polymerase', *J Biol Chem*, 274, (25), pp. 17860-8.
- Ame, J. C., Spenlehauer, C. and de Murcia, G. (2004) 'The PARP superfamily', *Bioessays*, 26, (8), pp. 882-93.
- Armand, J. P., Cunningham, D., van Cutsem, E., Misset, J. L. and Kohne, C. H. (1999) 'Clinical advances with topoisomerase I inhibitors in gastrointestinal malignancies', *Anticancer Drugs*, 10 Suppl 1, pp. S5-12.
- Armand, J. P., Ducreux, M., Mahjoubi, M., Abigeres, D., Bugat, R., Chabot, G., Herait, P., de Forni, M. and Rougier, P. (1995) 'CPT-11 (irinotecan) in the treatment of colorectal cancer', *Eur J Cancer*, 31A, (7-8), pp. 1283-7.
- Arundel-Suto, C. M., Scavone, S. V., Turner, W. R., Suto, M. J. and Sebolt-Leopold, J. S. (1991) 'Effect of PD 128763, a new potent inhibitor of poly(ADP-ribose) polymerase, on X-ray-induced cellular recovery processes in Chinese hamster V79 cells', *Radiat Res*, 126, (3), pp. 367-71.
- Audebert, M., Salles, B. and Calsou, P. (2004) 'Involvement of poly(ADP-ribose) polymerase-1 and XRCC1/DNA ligase III in an alternative route for DNA double-strand breaks rejoining', *J Biol Chem*, 279, (53), pp. 55117-26.
- Audebert, M., Salles, B. and Calsou, P. (2008) 'Effect of double-strand break DNA sequence on the PARP-1 NHEJ pathway', *Biochem Biophys Res Commun*, 369, (3), pp. 982-8.
- Audebert, M., Salles, B., Weinfeld, M. and Calsou, P. (2006) 'Involvement of polynucleotide kinase in a poly(ADP-ribose) polymerase-1-dependent DNA double-strand breaks rejoining pathway', *J Mol Biol*, 356, (2), pp. 257-65.
- Augustin, A., Spenlehauer, C., Dumond, H., Menissier-De Murcia, J., Piel, M., Schmit, A. C., Apiou, F., Vonesch, J. L., Kock, M., Bornens, M. and De Murcia, G. (2003) 'PARP-3 localizes preferentially to the daughter centriole and interferes with the G1/S cell cycle progression', *J Cell Sci*, 116, (Pt 8), pp. 1551-62.
- Banasik, M., Komura, H., Shimoyama, M. and Ueda, K. (1992) 'Specific inhibitors of poly(ADP-ribose) synthetase and mono(ADP-ribosyl)transferase', *J Biol Chem*, 267, (3), pp. 1569-75.
- Banfalvi, G., Klaisz, M., Ujvarosi, K., Trencsenyi, G., Rozsa, D. and Nagy, G. (2007) 'Gamma irradiation induced apoptotic changes in the chromatin structure of human erythroleukemia K562 cells', *Apoptosis*, 12, (12), pp. 2271-83.
- Barrows, L. R., Holden, J. A., Anderson, M. and D'Arpa, P. (1998) 'The CHO XRCC1 mutant, EM9, deficient in DNA ligase III activity, exhibits hypersensitivity to camptothecin independent of DNA replication', *Mutat Res*, 408, (2), pp. 103-10.

- Bauer, P. I., Chen, H. J., Kenesi, E., Kenessey, I., Buki, K. G., Kirsten, E., Hakam, A., Hwang, J. I. and Kun, E. (2001) 'Molecular interactions between poly(ADP-ribose) polymerase (PARP I) and topoisomerase I (Topo I): identification of topology of binding', *FEBS Lett*, 506, (3), pp. 239-42.
- Baumann, C., Boehden, G. S., Burkle, A. and Wiesmuller, L. (2006) 'Poly(ADP-RIBOSE) polymerase-1 (Parp-1) antagonizes topoisomerase I-dependent recombination stimulation by P53', *Nucleic Acids Res*, 34, (3), pp. 1036-49.
- Baylin, S. B. and Jones, P. A. (2011) 'A decade of exploring the cancer epigenome — biological and translational implications', *Nat Rev Cancer*, 11, (10), pp. 726-734.
- Beidler, D. R. and Cheng, Y. C. (1995) 'Camptothecin induction of a time- and concentration-dependent decrease of topoisomerase I and its implication in camptothecin activity', *Mol Pharmacol*, 47, (5), pp. 907-14.
- Benjamin, R. C. and Gill, D. M. (1980) 'ADP-ribosylation in mammalian cell ghosts. Dependence of poly(ADP-ribose) synthesis on strand breakage in DNA', *J Biol Chem*, 255, (21), pp. 10493-501.
- Berger, W., Steiner, E., Grusch, M., Elbling, L. and Micksche, M. (2009) 'Vaults and the major vault protein: novel roles in signal pathway regulation and immunity', *Cell Mol Life Sci*, 66, (1), pp. 43-61.
- Blenn, C., Wyrsh, P. and Althaus, F. R. (2011) 'The ups and downs of tannins as inhibitors of poly(ADP-ribose) glycohydrolase', *Molecules*, 16, (2), pp. 1854-1877.
- Bocker, W. and Iliakis, G. (2006) 'Computational Methods for analysis of foci: validation for radiation-induced gamma-H2AX foci in human cells', *Radiat Res*, 165, (1), pp. 113-24.
- Boehler, C., Gauthier, L., Yelamos, J., Noll, A., Schreiber, V. and Dantzer, F. (2011a) 'Phenotypic Characterization of Parp-1 and Parp-2 Deficient Mice and Cells', *Methods Mol Biol*, 780, pp. 313-336.
- Boehler, C., Gauthier, L. R., Mortusewicz, O., Biard, D. S., Saliou, J. M., Bresson, A., Sanglier-Cianferani, S., Smith, S., Schreiber, V., Boussin, F. and Dantzer, F. (2011b) 'Poly(ADP-ribose) polymerase 3 (PARP3), a newcomer in cellular response to DNA damage and mitotic progression', *Proc Natl Acad Sci U S A*, 108, (7), pp. 2783-8.
- Borovitskaya, A. E. and D'Arpa, P. (1998) 'Replication-dependent and -independent camptothecin cytotoxicity of seven human colon tumor cell lines', *Oncol Res*, 10, (5), pp. 271-6.
- Boulares, A. H., Yakovlev, A. G., Ivanova, V., Stoica, B. A., Wang, G., Iyer, S. and Smulson, M. (1999) 'Role of poly(ADP-ribose) polymerase (PARP) cleavage in apoptosis. Caspase 3-resistant PARP mutant increases rates of apoptosis in transfected cells', *J Biol Chem*, 274, (33), pp. 22932-40.
- Bowman, A., Rye, T., Ross, G., Wheatley, A. and Smyth, J. F. (2001a) 'Effective dosing of topotecan with carboplatin in relapsed ovarian cancer: a phase I/II study', *J Clin Oncol*, 19, (13), pp. 3255-9.
- Bowman, K. J., Newell, D. R., Calvert, A. H. and Curtin, N. J. (2001b) 'Differential effects of the poly (ADP-ribose) polymerase (PARP) inhibitor NU1025 on topoisomerase I and II inhibitor cytotoxicity in L1210 cells in vitro', *Br J Cancer*, 84, (1), pp. 106-12.
- Bryant, H. E., Petermann, E., Schultz, N., Jemth, A.-S., Loseva, O., Issaeva, N., Johansson, F., Fernandez, S., McGlynn, P. and Helleday, T. (2009a) 'PARP is activated at stalled forks to mediate Mre11-dependent replication restart and recombination', *Embo J*, 28, (17), pp. 2601-2615.
- Box, G.E.P. and Cox, D.R. (1964) An analysis of transformations. *J.R. Stat. Soc., Series B (Methodological)*, 26, 211–252.

- Bryant, H. E., Petermann, E., Schultz, N., Jemth, A. S., Loseva, O., Issaeva, N., Johansson, F., Fernandez, S., McGlynn, P. and Helleday, T. (2009b) 'PARP is activated at stalled forks to mediate Mre11-dependent replication restart and recombination', *EMBO Journal*, 28, (17), pp. 2601-2615.
- Burkle, A. (2000) 'Poly(ADP-ribosyl)ation: a posttranslational protein modification linked with genome protection and mammalian longevity', *Biogerontology*, 1, (1), pp. 41-6.
- Busk, P. K., Hinrichsen, R., Bartkova, J., Hansen, A. H., Christoffersen, T. E., Bartek, J. and Haunso, S. (2005) 'Cyclin D2 induces proliferation of cardiac myocytes and represses hypertrophy', *Exp Cell Res*, 304, (1), pp. 149-61.
- Cadet, J., Douki, T. and Ravanat, J. L. (2011) 'Measurement of oxidatively generated base damage in cellular DNA', *Mutat Res*, 711, (1-2), pp. 3-12.
- Cai, Z., Vallis, K. A. and Reilly, R. M. (2009) 'Computational analysis of the number, area and density of γ -H2AX foci in breast cancer cells exposed to ^{111}In -DTPA-hEGF or γ -rays using Image-J software', *Int J Radiat Biol*, 85, (3), pp. 262-271.
- Calabrese, C. R., Almassy, R., Barton, S., Batey, M. A., Calvert, A. H., Canan-Koch, S., Durkacz, B. W., Hostomsky, Z., Kumpf, R. A., Kyle, S., Li, J., Maegley, K., Newell, D. R., Notarianni, E., Stratford, I. J., Skalitzky, D., Thomas, H. D., Wang, L. Z., Webber, S. E., Williams, K. J. and Curtin, N. J. (2004) 'Anticancer chemosensitization and radiosensitization by the novel poly(ADP-ribose) polymerase-1 inhibitor AG14361', *J Natl Cancer Inst*, 96, (1), pp. 56-67.
- Caldecott, K. and Jeggo, P. (1991) 'Cross-sensitivity of gamma-ray-sensitive hamster mutants to cross-linking agents', *Mutat Res*, 255, (2), pp. 111-21.
- Cappelli, E., Taylor, R., Cevasco, M., Abbondandolo, A., Caldecott, K. and Frosina, G. (1997) 'Involvement of XRCC1 and DNA ligase III gene products in DNA base excision repair', *J Biol Chem*, 272, (38), pp. 23970-5.
- Chabner, B. A. and Roberts, T. G., Jr. (2005) 'Timeline: Chemotherapy and the war on cancer', *Nat Rev Cancer*, 5, (1), pp. 65-72.
- Chambon, P., Weill, J. D. and Mandel, P. (1963) 'Nicotinamide mononucleotide activation of a new DNA-dependent polyadenylic acid synthesizing nuclear enzyme', *Biochemical and Biophysical Research Communications*, 11, (1), pp. 39-43.
- Champoux, J. J. (2001a) 'DNA topoisomerase I-mediated nicking of circular duplex DNA', *Methods Mol Biol*, 95, pp. 81-7.
- Champoux, J. J. (2001b) 'DNA topoisomerases: structure, function, and mechanism', *Annu Rev Biochem*, 70, pp. 369-413.
- Chatterjee, S., Cheng, M. F., Trivedi, D., Petzold, S. J. and Berger, N. A. (1989) 'Camptothecin hypersensitivity in poly(adenosine diphosphate-ribose) polymerase-deficient cell lines', *Cancer Commun*, 1, (6), pp. 389-94.
- Cimmino, G., Pepe, S., Laus, G., Chianese, M., Prece, D., Penitente, R. and Quesada, P. (2007) 'Poly(ADPR)polymerase-1 signalling of the DNA damage induced by DNA topoisomerase I poison in D54(p53wt) and U251(p53mut) glioblastoma cell lines', *Pharmacol Res*, 55, (1), pp. 49-56.
- Cline, S. D. and Hanawalt, P. C. (2003) 'Who's on first in the cellular response to DNA damage?', *Nat Rev Mol Cell Biol*, 4, (5), pp. 361-72.
- Collins, A. R. (2004) 'The comet assay for DNA damage and repair: principles, applications, and limitations', *Mol Biotechnol*, 26, (3), pp. 249-61.
- Cooper, S. (2003) 'Rethinking synchronization of mammalian cells for cell cycle analysis', *Cell Mol Life Sci*, 60, (6), pp. 1099-106.
- Creemers, G. J. (1997) 'Topotecan in advanced colorectal cancer', *Semin Oncol*, 24, (6 Suppl 20), pp. S20-42-S20-48.

- Creemers, G. J., Bolis, G., Gore, M., Scarfone, G., Lacave, A. J., Guastalla, J. P., Despax, R., Favalli, G., Kreinberg, R., Van Belle, S., Hudson, I., Verweij, J. and Ten Bokkel Huinink, W. W. (1996) 'Topotecan, an active drug in the second-line treatment of epithelial ovarian cancer: results of a large European phase II study', *J Clin Oncol*, 14, (12), pp. 3056-61.
- Curtin, N. J. (2005) 'PARP inhibitors for cancer therapy', *Expert Rev Mol Med*, 7, (4), pp. 1-20.
- D'Amours, D., Desnoyers, S., D'Silva, I. and Poirier, G. G. (1999) 'Poly(ADP-ribose)ylation reactions in the regulation of nuclear functions', *Biochem J*, 342 (Pt 2), pp. 249-68.
- D'Arpa, P., Beardmore, C. and Liu, L. F. (1990) 'Involvement of nucleic acid synthesis in cell killing mechanisms of topoisomerase poisons', *Cancer Res*, 50, (21), pp. 6919-24.
- Danson, S. J. and Middleton, M. R. (2001) 'Temozolomide: a novel oral alkylating agent', *Expert Rev Anticancer Ther*, 1, (1), pp. 13-9.
- Dantzer, F., Ame, J., Schreiber, V., Nakamura, J., Menissierdemurcia, J. and Demurcia, G. (2006a) 'Poly(ADP-ribose) Polymerase-1 Activation During DNA Damage and Repair', *Methods Enzymol*, 409, pp. 493-510.
- Dantzer, F., Ame, J. C., Schreiber, V., Nakamura, J., Menissier-de Murcia, J. and de Murcia, G. (2006b) 'Poly(ADP-ribose) polymerase-1 activation during DNA damage and repair', *Methods Enzymol*, 409, pp. 493-510.
- Darzynkiewicz, Z., Halicka, D. H. and Tanaka, T. (2009) 'Cytometric assessment of DNA damage induced by DNA topoisomerase inhibitors', *Methods Mol Biol*, 582, pp. 145-53.
- Davidovic, L., Vodenicharov, M., Affar, E. B. and Poirier, G. G. (2001) 'Importance of poly(ADP-ribose) glycohydrolase in the control of poly(ADP-ribose) metabolism', *Exp Cell Res*, 268, (1), pp. 7-13.
- de Murcia, G., Schreiber, V., Molinete, M., Saulier, B., Poch, O., Masson, M., Niedergang, C. and Menissier de Murcia, J. (1994) 'Structure and function of poly(ADP-ribose) polymerase', *Mol Cell Biochem*, 138, (1-2), pp. 15-24.
- de Murcia, J. M., Niedergang, C., Trucco, C., Ricoul, M., Dutrillaux, B., Mark, M., Oliver, F. J., Masson, M., Dierich, A., LeMeur, M., Walztinger, C., Chambon, P. and de Murcia, G. (1997) 'Requirement of poly(ADP-ribose) polymerase in recovery from DNA damage in mice and in cells', *Proc Natl Acad Sci U S A*, 94, (14), pp. 7303-7.
- Del Bino, G., Skierski, J. S. and Darzynkiewicz, Z. (1990) 'Diverse effects of camptothecin, an inhibitor of topoisomerase I, on the cell cycle of lymphocytic (L1210, MOLT-4) and myelogenous (HL-60, KG1) leukemic cells', *Cancer Res*, 50, (18), pp. 5746-50.
- Delaney, C. A., Wang, L. Z., Kyle, S., White, A. W., Calvert, A. H., Curtin, N. J., Durkacz, B. W., Hostomsky, Z. and Newell, D. R. (2000) 'Potentiation of temozolomide and topotecan growth inhibition and cytotoxicity by novel poly(adenosine diphosphoribose) polymerase inhibitors in a panel of human tumor cell lines', *Clin Cancer Res*, 6, (7), pp. 2860-7.
- DeVita, V. T., Jr. and Chu, E. (2008) 'A history of cancer chemotherapy', *Cancer Res*, 68, (21), pp. 8643-53.
- Dianova, II, Sleeth, K. M., Allinson, S. L., Parsons, J. L., Breslin, C., Caldecott, K. W. and Dianov, G. L. (2004) 'XRCC1-DNA polymerase beta interaction is required for efficient base excision repair', *Nucleic Acids Res*, 32, (8), pp. 2550-5.
- Ding, R. and Smulson, M. (1994) 'Depletion of nuclear poly(ADP-ribose) polymerase by antisense RNA expression: influences on genomic stability, chromatin organization, and carcinogen cytotoxicity', *Cancer Res*, 54, (17), pp. 4627-34.

- Durkacz, B. W., Omidiji, O., Gray, D. A. and Shall, S. (1980) '(ADP-ribose)n participates in DNA excision repair', *Nature*, 283, (5747), pp. 593-6.
- Durkacz, B. W., Shall, S. and Irwin, J. (1981) 'The effect of inhibition of (ADP-ribose)n biosynthesis on DNA repair assayed by the nucleoid technique', *Eur J Biochem*, 121, (1), pp. 65-9.
- Eker, A. P., Quayle, C., Chaves, I. and van der Horst, G. T. (2009) 'DNA repair in mammalian cells: Direct DNA damage reversal: elegant solutions for nasty problems', *Cell Mol Life Sci*, 66, (6), pp. 968-80.
- El-Khamisy, S. F., Masutani, M., Suzuki, H. and Caldecott, K. W. (2003) 'A requirement for PARP-1 for the assembly or stability of XRCC1 nuclear foci at sites of oxidative DNA damage', *Nucleic Acids Res*, 31, (19), pp. 5526-33.
- Elias, E., Lalun, N., Lorenzato, M., Blache, L., Chelidze, P., O'Donohue, M. F., Ploton, D. and Bobichon, H. (2003) 'Cell-cycle-dependent three-dimensional redistribution of nuclear proteins, P 120, pKi-67, and SC 35 splicing factor, in the presence of the topoisomerase I inhibitor camptothecin', *Exp Cell Res*, 291, (1), pp. 176-88.
- Eng, W. K., McCabe, F. L., Tan, K. B., Mattern, M. R., Hofmann, G. A., Woessner, R. D., Hertzberg, R. P. and Johnson, R. K. (1990) 'Development of a stable camptothecin-resistant subline of P388 leukemia with reduced topoisomerase I content', *Mol Pharmacol*, 38, (4), pp. 471-80.
- Ferro, A. M., Higgins, N. P. and Olivera, B. M. (1983) 'Poly(ADP-ribosylation) of a DNA topoisomerase', *J Biol Chem*, 258, (10), pp. 6000-3.
- Fiorani, P., Bruselles, A., Falconi, M., Chillemi, G., Desideri, A. and Benedetti, P. (2003) 'Single mutation in the linker domain confers protein flexibility and camptothecin resistance to human topoisomerase I', *J Biol Chem*, 278, (44), pp. 43268-75.
- Flatten, K. (2005) 'The Role of Checkpoint Kinase 1 in Sensitivity to Topoisomerase I Poisons', *Journal of Biological Chemistry*, 280, (14), pp. 14349-14355.
- Furuta, T., Takemura, H., Liao, Z. Y., Aune, G. J., Redon, C., Sedelnikova, O. A., Pilch, D. R., Rogakou, E. P., Celeste, A., Chen, H. T., Nussenzweig, A., Aladjem, M. I., Bonner, W. M. and Pommier, Y. (2003) 'Phosphorylation of histone H2AX and activation of Mre11, Rad50, and Nbs1 in response to replication-dependent DNA double-strand breaks induced by mammalian DNA topoisomerase I cleavage complexes', *J Biol Chem*, 278, (22), pp. 20303-12.
- Giovanella, B. C., Stehlin, J. S., Wall, M. E., Wani, M. C., Nicholas, A. W., Liu, L. F., Silber, R. and Potmesil, M. (1989) 'DNA topoisomerase I-targeted chemotherapy of human colon cancer in xenografts', *Science*, 246, (4933), pp. 1046-8.
- Goldblatt, E. M. and Lee, W. H. (2010) 'From bench to bedside: the growing use of translational research in cancer medicine', *Am J Transl Res*, 2, (1), pp. 1-18.
- Goldwasser, F., Shimizu, T., Jackman, J., Hoki, Y., O'Connor, P. M., Kohn, K. W. and Pommier, Y. (1996) 'Correlations between S and G2 arrest and the cytotoxicity of camptothecin in human colon carcinoma cells', *Cancer Res*, 56, (19), pp. 4430-7.
- Goto, T. and Wang, J. C. (1985) 'Cloning of yeast TOP1, the gene encoding DNA topoisomerase I, and construction of mutants defective in both DNA topoisomerase I and DNA topoisomerase II', *Proc Natl Acad Sci U S A*, 82, (21), pp. 7178-82.
- Griffin, R. J., Pemberton, L. C., Rhodes, D., Bleasdale, C., Bowman, K., Calvert, A. H., Curtin, N. J., Durkacz, B. W., Newell, D. R., Porteous, J. K. and et al. (1995) 'Novel potent inhibitors of the DNA repair enzyme poly(ADP-ribose)polymerase (PARP)', *Anticancer Drug Des*, 10, (6), pp. 507-14.

- Hakme, A., Huber, A., Dolle, P. and Schreiber, V. (2008) 'The macroPARP genes Parp-9 and Parp-14 are developmentally and differentially regulated in mouse tissues', *Dev Dyn*, 237, (1), pp. 209-15.
- Hanahan, D. and Weinberg, R. A. (2000) 'The hallmarks of cancer', *Cell*, 100, (1), pp. 57-70.
- Hanahan, D. and Weinberg, R. A. (2011) 'Hallmarks of cancer: the next generation', *Cell*, 144, (5), pp. 646-74.
- Heacock, M. L., Stefanick, D. F., Horton, J. K. and Wilson, S. H. (2010) 'Alkylation DNA damage in combination with PARP inhibition results in formation of S-phase-dependent double-strand breaks', *DNA Repair (Amst)*, 9, (8), pp. 929-36.
- Hegde, M. L., Hazra, T. K. and Mitra, S. (2008) 'Early steps in the DNA base excision/single-strand interruption repair pathway in mammalian cells', *Cell Res*, 18, (1), pp. 27-47.
- Helleday, T., Bryant, H. E. and Schultz, N. (2005) 'Poly(ADP-ribose) polymerase (PARP-1) in homologous recombination and as a target for cancer therapy', *Cell Cycle*, 4, (9), pp. 1176-8.
- Hohegger, H., Dejsuphong, D., Fukushima, T., Morrison, C., Sonoda, E., Schreiber, V., Zhao, G. Y., Saberi, A., Masutani, M., Adachi, N., Koyama, H., de Murcia, G. and Takeda, S. (2006) 'Parp-1 protects homologous recombination from interference by Ku and Ligase IV in vertebrate cells', *Embo J*, 25, (6), pp. 1305-14.
- Hoeijmakers, J. H. (2001) 'Genome maintenance mechanisms for preventing cancer', *Nature*, 411, (6835), pp. 366-74.
- Holden, J. A. (2001) 'DNA topoisomerases as anticancer drug targets: from the laboratory to the clinic', *Curr Med Chem Anticancer Agents*, 1, (1), pp. 1-25.
- Hollstein, M., Hergenhahn, M., Yang, Q., Bartsch, H., Wang, Z. Q. and Hainaut, P. (1999) 'New approaches to understanding p53 gene tumor mutation spectra', *Mutat Res*, 431, (2), pp. 199-209.
- Horton, J. K., Watson, M., Stefanick, D. F., Shaughnessy, D. T., Taylor, J. A. and Wilson, S. H. (2008a) 'XRCC1 and DNA polymerase beta in cellular protection against cytotoxic DNA single-strand breaks', *Cell Res*, 18, (1), pp. 48-63.
- Horton, J. K., Watson, M., Stefanick, D. F., Shaughnessy, D. T., Taylor, J. A. and Wilson, S. H. (2008b) 'XRCC1 and DNA polymerase β in cellular protection against cytotoxic DNA single-strand breaks', *Cell Res*, 18, (1), pp. 48-63.
- Horton, M. A., Cedar, S. H. and Edwards, P. A. (1981) 'Expression of red cell specific determinants during differentiation in the K562 erythroleukaemia cell line', *Scand J Haematol*, 27, (4), pp. 231-40.
- Hottiger, M. O., Hassa, P. O., Luscher, B., Schuler, H. and Koch-Nolte, F. (2010) 'Toward a unified nomenclature for mammalian ADP-ribosyltransferases', *Trends Biochem Sci*, 35, (4), pp. 208-19.
- Hsiang, Y. H., Lihou, M. G. and Liu, L. F. (1989) 'Arrest of replication forks by drug-stabilized topoisomerase I-DNA cleavable complexes as a mechanism of cell killing by camptothecin', *Cancer Res*, 49, (18), pp. 5077-82.
- Husain, I., Mohler, J. L., Seigler, H. F. and Besterman, J. M. (1994) 'Elevation of topoisomerase I messenger RNA, protein, and catalytic activity in human tumors: demonstration of tumor-type specificity and implications for cancer chemotherapy', *Cancer Res*, 54, (2), pp. 539-46.
- Ikeguchi, M., Arai, Y., Maeta, Y., Ashida, K., Katano, K. and Wakatsuki, T. (2011) 'Topoisomerase I expression in tumors as a biological marker for CPT-11 chemosensitivity in patients with colorectal cancer', *Surg Today*, 41, (9), pp. 1196-9.

- Ikejima, M., Noguchi, S., Yamashita, R., Ogura, T., Sugimura, T., Gill, D. M. and Miwa, M. (1990) 'The zinc fingers of human poly(ADP-ribose) polymerase are differentially required for the recognition of DNA breaks and nicks and the consequent enzyme activation. Other structures recognize intact DNA', *J Biol Chem*, 265, (35), pp. 21907-13.
- Iliakis, G. (2009) 'Backup pathways of NHEJ in cells of higher eukaryotes: cell cycle dependence', *Radiother Oncol*, 92, (3), pp. 310-5.
- Iliakis, G., Wu, W. and Wang, M. (2008) 'DNA double strand break repair inhibition as a cause of heat radiosensitization: re-evaluation considering backup pathways of NHEJ', *Int J Hyperthermia*, 24, (1), pp. 17-29.
- Ireton, G. C., Stewart, L., Parker, L. H. and Champoux, J. J. (2000) 'Expression of human topoisomerase I with a partial deletion of the linker region yields monomeric and dimeric enzymes that respond differently to camptothecin', *J Biol Chem*, 275, (33), pp. 25820-30.
- Isabelle, M., Moreel, X., Gagné, J., Rouleau, M., Ethier, C., Gagné, P., Hendzel, M. J. and Poirier, G. G. (2010) 'Investigation of PARP-1, PARP-2, and PARG interactomes by affinity-purification mass spectrometry', *Proteome Science*, 8.
- Jagtap, P. G., Baloglu, E., Southan, G. J., Mabley, J. G., Li, H., Zhou, J., van Duzer, J., Salzman, A. L. and Szabo, C. (2005) 'Discovery of potent poly(ADP-ribose) polymerase-1 inhibitors from the modification of indeno[1,2-c]isoquinolinone', *J Med Chem*, 48, (16), pp. 5100-3.
- Jaxel, C., Capranico, G., Kerrigan, D., Kohn, K. W. and Pommier, Y. (1991) 'Effect of local DNA sequence on topoisomerase I cleavage in the presence or absence of camptothecin', *Journal of Biological Chemistry*, 266, (30), pp. 20418-20423.
- Kataoka, Y., Bindokas, V. P., Duggan, R. C., Murley, J. S. and Grdina, D. J. (2006) 'Flow cytometric analysis of phosphorylated histone H2AX following exposure to ionizing radiation in human microvascular endothelial cells', *J Radiat Res (Tokyo)*, 47, (3-4), pp. 245-57.
- Kauffman, M. G., Noga, S. J., Kelly, T. J. and Donnenberg, A. D. (1990) 'Isolation of cell cycle fractions by counterflow centrifugal elutriation', *Anal Biochem*, 191, (1), pp. 41-6.
- Kaufmann, S. H., Desnoyers, S., Ottaviano, Y., Davidson, N. E. and Poirier, G. G. (1993) 'Specific proteolytic cleavage of poly(ADP-ribose) polymerase: an early marker of chemotherapy-induced apoptosis', *Cancer Res*, 53, (17), pp. 3976-85.
- Khan, O. A., Gore, M., Lorigan, P., Stone, J., Greystoke, A., Burke, W., Carmichael, J., Watson, A. J., McGown, G., Thorncroft, M., Margison, G. P., Califano, R., Larkin, J., Wellman, S. and Middleton, M. R. (2011) 'A phase I study of the safety and tolerability of olaparib (AZD2281, KU0059436) and dacarbazine in patients with advanced solid tumours', *Br J Cancer*, 104, (5), pp. 750-5.
- Kickhoefer, V. A., Siva, A. C., Kedersha, N. L., Inman, E. M., Ruland, C., Streuli, M. and Rome, L. H. (1999) 'The 193-kD vault protein, VPARP, is a novel poly(ADP-ribose) polymerase', *J Cell Biol*, 146, (5), pp. 917-28.
- Koh, D. W., Dawson, T. M. and Dawson, V. L. (2005) 'Mediation of cell death by poly(ADP-ribose) polymerase-1', *Pharmacol Res*, 52, (1), pp. 5-14.
- Krishan, A. (1975) 'Rapid flow cytofluorometric analysis of mammalian cell cycle by propidium iodide staining', *J Cell Biol*, 66, (1), pp. 188-93.
- Kummar, S., Chen, A., Ji, J., Zhang, Y., Reid, J. M., Ames, M., Jia, L., Weil, M., Speranza, G., Murgo, A. J., Kinders, R., Wang, L., Parchment, R. E., Carter, J., Stotler, H., Rubinstein, L., Hollingshead, M., Melillo, G., Pommier, Y., Bonner, W., Tomaszewski, J. E. and Doroshow, J. H. (2011) 'Phase I study of PARP inhibitor ABT-888 in combination with topotecan in adults with refractory solid tumors and lymphomas', *Cancer Res*, 71, (17), pp. 5626-34.

- Kunze, N., Klein, M., Richter, A. and Knippers, R. (1990) 'Structural characterization of the human DNA topoisomerase I gene promoter', *Eur J Biochem*, 194, (2), pp. 323-30.
- Kurosawa, A. and Adachi, N. (2010) 'Functions and regulation of artemis: A goddess in the maintenance of genome integrity', *Journal of Radiation Research*, 51, (5), pp. 503-509.
- Kysela, B., Doherty, A. J., Chovanec, M., Stiff, T., Ameer-Beg, S. M., Vojnovic, B., Girard, P. M. and Jeggo, P. A. (2003) 'Ku stimulation of DNA ligase IV-dependent ligation requires inward movement along the DNA molecule', *J Biol Chem*, 278, (25), pp. 22466-74.
- Lagerwerf, S., Vrouwe, M. G., Overmeer, R. M., Fouteri, M. I. and Mullenders, L. H. F. (2011) 'DNA damage response and transcription', *DNA Repair*, 10, (7), pp. 743-750.
- Larsen, A. K. and Gobert, C. (1999) 'DNA topoisomerase I in oncology: Dr Jekyll or Mr Hyde?', *Pathol Oncol Res*, 5, (3), pp. 171-8.
- Lindahl, T. (1993) 'Instability and decay of the primary structure of DNA', *Nature*, 362, pp. 709-715.
- Liu, L., Lee, J. and Zhou, P. (2010) 'Navigating the nucleotide excision repair threshold', *J Cell Physiol*, 224, (3), pp. 585-9.
- Liu, L. F., Desai, S. D., Li, T. K., Mao, Y., Sun, M. and Sim, S. P. (2000) 'Mechanism of action of camptothecin', *Ann N Y Acad Sci*, 922, pp. 1-10.
- Liu, X., Shi, Y., Guan, R., Donawho, C., Luo, Y., Palma, J., Zhu, G. D., Johnson, E. F., Rodriguez, L. E., Ghoreishi-Haack, N., Jarvis, K., Hradil, V. P., Colon-Lopez, M., Cox, B. F., Klinghofer, V., Penning, T., Rosenberg, S. H., Frost, D. and Giranda, V. L. (2008) 'Potentiation of temozolomide cytotoxicity by poly(ADP)ribose polymerase inhibitor ABT-888 requires a conversion of single-stranded DNA damages to double-stranded DNA breaks', *Mol Cancer Res*, 6, (10), pp. 1621-9.
- Lozzio, C. B. and Lozzio, B. B. (1975) 'Human chronic myelogenous leukemia cell-line with positive Philadelphia chromosome', *Blood*, 45, (3), pp. 321-34.
- Lukas, C., Sørensen, C. S., Kramer, E., Santoni-Ruglu, E., Lindeneg, C., Peters, J. M., Bartek, J. and Lukas, J. (1999) 'Accumulation of cyclin B1 requires E2F and cyclin-A-dependent rearrangement of the anaphase-promoting complex', *Nature*, 401, (6755), pp. 815-818.
- Lukas, J. and Bartek, J. (2004) 'Cell division: the heart of the cycle', *Nature*, 432, (7017), pp. 564-7.
- Lupi, M., Matera, G., Branduardi, D., D'Incalci, M. and Ubezio, P. (2004) 'Cytostatic and cytotoxic effects of topotecan decoded by a novel mathematical simulation approach', *Cancer Res*, 64, (8), pp. 2825-32.
- Magrini, R., Bhonde, M. R., Hanski, M.-L., Notter, M., Scherobl, H., Boland, C. R., Zeitz, M. and Hanski, C. (2002) 'Cellular effects of CPT-11 on colon carcinoma cells: Dependence on p53 and hMLH1 status', *Int J Cancer*, 101, (1), pp. 23-31.
- Malanga, M. and Althaus, F. R. (2004) 'Poly(ADP-ribose) reactivates stalled DNA topoisomerase I and Induces DNA strand break resealing', *J Biol Chem*, 279, (7), pp. 5244-8.
- Marchand, C., Antony, S., Kohn, K. W., Cushman, M., Ioanoviciu, A., Staker, B. L., Burgin, A. B., Stewart, L. and Pommier, Y. (2006) 'A novel norindenoisoquinoline structure reveals a common interfacial inhibitor paradigm for ternary trapping of the topoisomerase I-DNA covalent complex', *Mol Cancer Ther*, 5, (2), pp. 287-95.
- Masson, M., Niedergang, C., Schreiber, V., Muller, S., Menissier-de Murcia, J. and de Murcia, G. (1998) 'XRCC1 is specifically associated with poly(ADP-ribose)

- polymerase and negatively regulates its activity following DNA damage', *Mol Cell Biol*, 18, (6), pp. 3563-71.
- Masson, M., Rolli, V., Dantzer, F., Trucco, C., Schreiber, V., Fribourg, S., Molinete, M., Ruf, A., Miranda, E. A., Niedergang, C. and et al. (1995) 'Poly(ADP-ribose) polymerase: structure-function relationship', *Biochimie*, 77, (6), pp. 456-61.
- Masutani, M., Nozaki, T., Nakamoto, K., Nakagama, H., Suzuki, H., Kusuoka, O., Tsutsumi, M. and Sugimura, T. (2000) 'The response of Parp knockout mice against DNA damaging agents', *Mutat Res*, 462, (2-3), pp. 159-66.
- Mattern, M. R., Mong, S. M., Bartus, H. F., Mirabelli, C. K., Crooke, S. T. and Johnson, R. K. (1987) 'Relationship between the intracellular effects of camptothecin and the inhibition of DNA topoisomerase I in cultured L1210 cells', *Cancer Res*, 47, (7), pp. 1793-8.
- McClendon, A. K., Rodriguez, A. C. and Osheroff, N. (2005) 'Human topoisomerase IIalpha rapidly relaxes positively supercoiled DNA: implications for enzyme action ahead of replication forks', *J Biol Chem*, 280, (47), pp. 39337-45.
- Menear, K. A., Adcock, C., Boulter, R., Cockcroft, X. L., Copsey, L., Cranston, A., Dillon, K. J., Drzewiecki, J., Garman, S., Gomez, S., Javaid, H., Kerrigan, F., Knights, C., Lau, A., Loh, V. M., Jr., Matthews, I. T., Moore, S., O'Connor, M. J., Smith, G. C. and Martin, N. M. (2008) '4-[3-(4-cyclopropanecarbonylpiperazine-1-carbonyl)-4-fluorobenzyl]-2H-phth alazin-1-one: a novel bioavailable inhibitor of poly(ADP-ribose) polymerase-1', *J Med Chem*, 51, (20), pp. 6581-91.
- Menissier-de Murcia, J., Molinete, M., Gradwohl, G., Simonin, F. and de Murcia, G. (1989) 'Zinc-binding domain of poly(ADP-ribose)polymerase participates in the recognition of single strand breaks on DNA', *J Mol Biol*, 210, (1), pp. 229-33.
- Merkle, D., Douglas, P., Moorhead, G. B., Leonenko, Z., Yu, Y., Cramb, D., Bazett-Jones, D. P. and Lees-Miller, S. P. (2002) 'The DNA-dependent protein kinase interacts with DNA to form a protein-DNA complex that is disrupted by phosphorylation', *Biochemistry*, 41, (42), pp. 12706-14.
- Meyer, K. N., Kjeldsen, E., Straub, T., Knudsen, B. R., Hickson, I. D., Kikuchi, A., Kreipe, H. and Boege, F. (1997) 'Cell cycle-coupled relocation of types I and II topoisomerases and modulation of catalytic enzyme activities', *J Cell Biol*, 136, (4), pp. 775-88.
- Miknyoczki, S., Chang, H., Grobelny, J., Pritchard, S., Worrell, C., McGann, N., Ator, M., Husten, J., Deibold, J., Hudkins, R., Zulli, A., Parchment, R. and Ruggeri, B. (2007) 'The selective poly(ADP-ribose) polymerase-1(2) inhibitor, CEP-8983, increases the sensitivity of chemoresistant tumor cells to temozolomide and irinotecan but does not potentiate myelotoxicity', *Mol Cancer Ther*, 6, (8), pp. 2290-302.
- Milam, K. M., Thomas, G. H. and Cleaver, J. E. (1986) 'Disturbances in DNA precursor metabolism associated with exposure to an inhibitor of poly(ADP-ribose) synthetase', *Exp Cell Res*, 165, (1), pp. 260-8.
- Mitchell, J., Smith, G. C. and Curtin, N. J. (2009) 'Poly(ADP-Ribose) polymerase-1 and DNA-dependent protein kinase have equivalent roles in double strand break repair following ionizing radiation', *Int J Radiat Oncol Biol Phys*, 75, (5), pp. 1520-7.
- Molinete, M., Vermeulen, W., Burkle, A., Menissier-de Murcia, J., Kupper, J. H., Hoeijmakers, J. H. and de Murcia, G. (1993) 'Overproduction of the poly(ADP-ribose) polymerase DNA-binding domain blocks alkylation-induced DNA repair synthesis in mammalian cells', *Embo J*, 12, (5), pp. 2109-17.

- Morgan, W. F. and Cleaver, J. E. (1982) '3-Aminobenzamide synergistically increases sister-chromatid exchanges in cells exposed to methyl methanesulfonate but not to ultraviolet light', *Mutat Res*, 104, (6), pp. 361-6.
- Morham, S. G., Kluckman, K. D., Voulomanos, N. and Smithies, O. (1996) 'Targeted disruption of the mouse topoisomerase I gene by camptothecin selection', *Molecular and Cellular Biology*, 16, (12), pp. 6804-6809.
- Morrow, D. A., Brickman, C. M., Murphy, S. A., Baran, K., Krakover, R., Dauerman, H., Kumar, S., Slomowitz, N., Grip, L., McCabe, C. H. and Salzman, A. L. (2009) 'A randomized, placebo-controlled trial to evaluate the tolerability, safety, pharmacokinetics, and pharmacodynamics of a potent inhibitor of poly(ADP-ribose) polymerase (INO-1001) in patients with ST-elevation myocardial infarction undergoing primary percutaneous coronary intervention: results of the TIMI 37 trial', *J Thromb Thrombolysis*, 27, (4), pp. 359-64.
- Mukhopadhyay, A., Elattar, A., Cerbinskaite, A., Wilkinson, S. J., Drew, Y., Kyle, S., Los, G., Hostomsky, Z., Edmondson, R. J. and Curtin, N. J. (2010) 'Development of a functional assay for homologous recombination status in primary cultures of epithelial ovarian tumor and correlation with sensitivity to poly(ADP-ribose) polymerase inhibitors', *Clin Cancer Res*, 16, (8), pp. 2344-51.
- Newlands, E. S., Stevens, M. F., Wedge, S. R., Wheelhouse, R. T. and Brock, C. (1997) 'Temozolomide: a review of its discovery, chemical properties, pre-clinical development and clinical trials', *Cancer Treat Rev*, 23, (1), pp. 35-61.
- Noël, G., Giocanti, N., Fernet, M., Mégnin-Chanet, F. and Favaudon, V. (2003) 'Poly(ADP-ribose) polymerase (PARP-I) is not involved in DNA double-strand break recovery', *BMC Cell Biology*, 4.
- O'Leary, J. and Muggia, F. M. (1998) 'Camptothecins: a review of their development and schedules of administration', *Eur J Cancer*, 34, (10), pp. 1500-8.
- Oei, S. L. and Ziegler, M. (2000) 'ATP for the DNA ligation step in base excision repair is generated from poly(ADP-ribose)', *J Biol Chem*, 275, (30), pp. 23234-9.
- Padget, K., Carr, R., Pearson, A. D., Tilby, M. J. and Austin, C. A. (2000) 'Camptothecin-stabilised topoisomerase I-DNA complexes in leukaemia cells visualised and quantified in situ by the TARDIS assay (trapped in agarose DNA immunostaining)', *Biochem Pharmacol*, 59, (6), pp. 629-38.
- Park, S. Y. and Cheng, Y. C. (2005) 'Poly(ADP-ribose) polymerase-1 could facilitate the religation of topoisomerase I-linked DNA inhibited by camptothecin', *Cancer Res*, 65, (9), pp. 3894-902.
- Patel, C. N., Koh, D. W., Jacobson, M. K. and Oliveira, M. A. (2005) 'Identification of three critical acidic residues of poly(ADP-ribose) glycohydrolase involved in catalysis: determining the PARG catalytic domain', *Biochem J*, 388, (Pt 2), pp. 493-500.
- Petrucco, S. (2003) 'Sensing DNA damage by PARP-like fingers', *Nucleic Acids Res*, 31, (23), pp. 6689-99.
- Pfister, T. D., Reinhold, W. C., Agama, K., Gupta, S., Khin, S. A., Kinders, R. J., Parchment, R. E., Tomaszewski, J. E., Doroshow, J. H. and Pommier, Y. (2009) 'Topoisomerase I levels in the NCI-60 cancer cell line panel determined by validated ELISA and microarray analysis and correlation with indenoisoquinoline sensitivity', *Mol Cancer Ther*, 8, (7), pp. 1878-84.
- Pleschke, J. M., Kleczkowska, H. E., Strohm, M. and Althaus, F. R. (2000) 'Poly(ADP-ribose) binds to specific domains in DNA damage checkpoint proteins', *J Biol Chem*, 275, (52), pp. 40974-80.
- Plo, I., Liao, Z. Y., Barcelo, J. M., Kohlhagen, G., Caldecott, K. W., Weinfeld, M. and Pommier, Y. (2003) 'Association of XRCC1 and tyrosyl DNA

- phosphodiesterase (Tdp1) for the repair of topoisomerase I-mediated DNA lesions', *DNA Repair (Amst)*, 2, (10), pp. 1087-100.
- Plummer, E. R., Middleton, M. R., Jones, C., Olsen, A., Hickson, I., McHugh, P., Margison, G. P., McGown, G., Thorncroft, M., Watson, A. J., Boddy, A. V., Calvert, A. H., Harris, A. L., Newell, D. R. and Curtin, N. J. (2005) 'Temozolomide pharmacodynamics in patients with metastatic melanoma: dna damage and activity of repair enzymes O6-alkylguanine alkyltransferase and poly(ADP-ribose) polymerase-1', *Clin Cancer Res*, 11, (9), pp. 3402-9.
- Plummer, R., Jones, C., Middleton, M., Wilson, R., Evans, J., Olsen, A., Curtin, N., Boddy, A., McHugh, P., Newell, D., Harris, A., Johnson, P., Steinfeldt, H., Dewji, R., Wang, D., Robson, L. and Calvert, H. (2008) 'Phase I study of the poly(ADP-ribose) polymerase inhibitor, AG014699, in combination with temozolomide in patients with advanced solid tumors', *Clin Cancer Res*, 14, (23), pp. 7917-23.
- Pommier, Y. (2004) 'Camptothecins and topoisomerase I: a foot in the door. Targeting the genome beyond topoisomerase I with camptothecins and novel anticancer drugs: importance of DNA replication, repair and cell cycle checkpoints', *Curr Med Chem Anticancer Agents*, 4, (5), pp. 429-34.
- Pommier, Y. (2006) 'Topoisomerase I inhibitors: camptothecins and beyond', *Nat Rev Cancer*, 6, (10), pp. 789-802.
- Pommier, Y. (2009) 'DNA topoisomerase I inhibitors: chemistry, biology, and interfacial inhibition', *Chem Rev*, 109, (7), pp. 2894-902.
- Pommier, Y., Leo, E., Zhang, H. and Marchand, C. (2010) 'DNA Topoisomerases and Their Poisoning by Anticancer and Antibacterial Drugs', *Chemistry & Biology*, 17, (5), pp. 421-433.
- Purdy, J. A. (2008) 'Dose to normal tissues outside the radiation therapy patient's treated volume: a review of different radiation therapy techniques', *Health Phys*, 95, (5), pp. 666-76.
- Redon, C. E., Nakamura, A. J., Zhang, Y. W., Ji, J., Bonner, W. M., Kinders, R. J., Parchment, R. E., Doroshow, J. H. and Pommier, Y. (2010) 'Histone γ H2AX and poly(ADP-ribose) as clinical pharmacodynamic biomarkers', *Clinical Cancer Research*, 16, (18), pp. 4532-4542.
- Ribas, M., Masramon, L., Aiza, G., Capella, G., Miro, R. and Peinado, M. A. (2003) 'The structural nature of chromosomal instability in colon cancer cells', *Faseb J*, 17, (2), pp. 289-91.
- Riley, T., Sontag, E., Chen, P. and Levine, A. (2008) 'Transcriptional control of human p53-regulated genes', *Nature Reviews Molecular Cell Biology*, 9, (5), pp. 402-412.
- Rouleau, M., El-Alfy, M., Levesque, M. H. and Poirier, G. G. (2009) 'Assessment of PARP-3 distribution in tissues of cynomolgous monkeys', *J Histochem Cytochem*, 57, (7), pp. 675-85.
- Ruf, A., Rolli, V., de Murcia, G. and Schulz, G. E. (1998) 'The mechanism of the elongation and branching reaction of poly(ADP-ribose) polymerase as derived from crystal structures and mutagenesis', *J Mol Biol*, 278, (1), pp. 57-65.
- Rulten, S. L., Fisher, A. E. O., Robert, I., Zuma, M. C., Rouleau, M., Ju, L., Poirier, G., Reina-San-Martin, B. and Caldecott, K. W. (2011) 'PARP-3 and APLF function together to accelerate nonhomologous end-joining', *Molecular Cell*, 41, (1), pp. 33-45.
- Samol, J., Ranson, M., Scott, E., Macpherson, E., Carmichael, J., Thomas, A. and Cassidy, J. (2011) 'Safety and tolerability of the poly(ADP-ribose) polymerase (PARP) inhibitor, olaparib (AZD2281) in combination with topotecan for the

- treatment of patients with advanced solid tumors: a phase I study', *Invest New Drugs*.
- Schreiber, V., Ame, J. C., Dolle, P., Schultz, I., Rinaldi, B., Fraulob, V., Menissier-de Murcia, J. and de Murcia, G. (2002) 'Poly(ADP-ribose) polymerase-2 (PARP-2) is required for efficient base excision DNA repair in association with PARP-1 and XRCC1', *J Biol Chem*, 277, (25), pp. 23028-36.
- Schreiber, V., Dantzer, F., Ame, J.-C. and de Murcia, G. (2006a) 'Poly(ADP-ribose): novel functions for an old molecule', *Nature Reviews Molecular Cell Biology*, 7, (7), pp. 517-528.
- Schreiber, V., Dantzer, F., Amé, J. C. and De Murcia, G. (2006b) 'Poly(ADP-ribose): Novel functions for an old molecule', *Nature Reviews Molecular Cell Biology*, 7, (7), pp. 517-528.
- Schreiber, V., Hunting, D., Trucco, C., Gowans, B., Grunwald, D., De Murcia, G. and De Murcia, J. M. (1995) 'A dominant-negative mutant of human poly(ADP-ribose) polymerase affects cell recovery, apoptosis, and sister chromatid exchange following DNA damage', *Proc Natl Acad Sci U S A*, 92, (11), pp. 4753-7.
- Shall, S. and de Murcia, G. (2000) 'Poly(ADP-ribose) polymerase-1: what have we learned from the deficient mouse model?', *Mutat Res*, 460, (1), pp. 1-15.
- Shen, M. R., Zdzienicka, M. Z., Mohrenweiser, H., Thompson, L. H. and Thelen, M. P. (1998) 'Mutations in hamster single-strand break repair gene XRCC1 causing defective DNA repair', *Nucleic Acids Res*.
- Shiloh, Y. (2001) 'ATM and ATR: networking cellular responses to DNA damage', *Curr Opin Genet Dev*, 11, (1), pp. 71-7.
- Shrivastav, M., De Haro, L. P. and Nickoloff, J. A. (2008) 'Regulation of DNA double-strand break repair pathway choice', *Cell Res*, 18, (1), pp. 134-47.
- Smith, L. M. (2005) 'The Novel Poly(ADP-Ribose) Polymerase Inhibitor, AG14361, Sensitizes Cells to Topoisomerase I Poisons by Increasing the Persistence of DNA Strand Breaks', PhD thesis Newcastle University.
- Smith, L. M., Willmore, E., Austin, C. A. and Curtin, N. J. (2005) 'The novel poly(ADP-Ribose) polymerase inhibitor, AG14361, sensitizes cells to topoisomerase I poisons by increasing the persistence of DNA strand breaks', *Clin Cancer Res*, 11, (23), pp. 8449-57.
- Sordet, O., Larochelle, S., Nicolas, E., Stevens, E. V., Zhang, C., Shokat, K. M., Fisher, R. P. and Pommier, Y. (2008) 'Hyperphosphorylation of RNA polymerase II in response to topoisomerase I cleavage complexes and its association with transcription- and BRCA1-dependent degradation of topoisomerase I', *J Mol Biol*.
- Ström, C. E., Johansson, F., Uhlén, M., Szigartyo, C. A. K., Erixon, K. and Helleday, T. (2011) 'Poly (ADP-ribose) polymerase (PARP) is not involved in base excision repair but PARP inhibition traps a single-strand intermediate', *Nucleic Acids Res Suppl*, 39, (8), pp. 3166-3175.
- Sugimura, K., Takebayashi, S., Taguchi, H., Takeda, S. and Okumura, K. (2008) 'PARP-1 ensures regulation of replication fork progression by homologous recombination on damaged DNA', *J Cell Biol*, 183, (7), pp. 1203-12.
- Sukhanova, M., Khodyreva, S. and Lavrik, O. (2007) 'Suppression of base excision repair reactions by apoptotic 24kDa-fragment of poly(ADP-ribose) polymerase 1 in bovine testis nuclear extract', *DNA Repair (Amst)*, 6, (5), pp. 615-25.
- Suto, M. J., Turner, W. R., Arundel-Suto, C. M., Werbel, L. M. and Sebolt-Leopold, J. S. (1991) 'Dihydroisoquinolinones: the design and synthesis of a new series of potent inhibitors of poly(ADP-ribose) polymerase', *Anticancer Drug Des*, 6, (2), pp. 107-17.

- Tanizawa, A., Kohn, K. W., Kohlhagen, G., Leteurtre, F. and Pommier, Y. (1995) 'Differential stabilization of eukaryotic DNA topoisomerase I cleavable complexes by camptothecin derivatives', *Biochemistry*, 34, (21), pp. 7200-6.
- Teicher, B. A. (2008) 'Next generation topoisomerase I inhibitors: Rationale and biomarker strategies', *Biochemical Pharmacology*, 75, (6), pp. 1262-1271.
- Tell, G., Quadrifoglio, F., Tiribelli, C. and Kelley, M. R. (2009) 'The many functions of APE1/Ref-1: not only a DNA repair enzyme', *Antioxid Redox Signal*, 11, (3), pp. 601-20.
- Tentori, L. (2006) 'Inhibition of poly(ADP-ribose) polymerase prevents irinotecan-induced intestinal damage and enhances irinotecan/temozolomide efficacy against colon carcinoma', *The FASEB Journal*, 20, (10), pp. 1709-1711.
- Tentori, L., Leonetti, C., Scarsella, M., D'Amati, G., Vergati, M., Portarena, I., Xu, W., Kalish, V., Zupi, G., Zhang, J. and Graziani, G. (2003) 'Systemic administration of GPI 15427, a novel poly(ADP-ribose) polymerase-1 inhibitor, increases the antitumor activity of temozolomide against intracranial melanoma, glioma, lymphoma', *Clin Cancer Res*, 9, (14), pp. 5370-9.
- Tentori, L., Leonetti, C., Scarsella, M., Muzi, A., Mazzon, E., Vergati, M., Forini, O., Lapidus, R., Xu, W., Dorio, A. S., Zhang, J., Cuzzocrea, S. and Graziani, G. (2006) 'Inhibition of poly(ADP-ribose) polymerase prevents irinotecan-induced intestinal damage and enhances irinotecan/temozolomide efficacy against colon carcinoma', *Faseb J*, 20, (10), pp. 1709-11.
- Thomas, H. D., Calabrese, C. R., Batey, M. A., Canan, S., Hostomsky, Z., Kyle, S., Maegley, K. A., Newell, D. R., Skalitzky, D., Wang, L. Z., Webber, S. E. and Curtin, N. J. (2007) 'Preclinical selection of a novel poly(ADP-ribose) polymerase inhibitor for clinical trial', *Mol Cancer Ther*, 6, (3), pp. 945-56.
- Thompson, L. H., Brookman, K. W., Dillehay, L. E., Carrano, A. V., Mazrimas, J. A., Mooney, C. L. and Minkler, J. L. (1982) 'A CHO-cell strain having hypersensitivity to mutagens, a defect in DNA strand-break repair, and an extraordinary baseline frequency of sister-chromatid exchange', *Mutat Res*, 95, (2-3), pp. 427-40.
- Thompson, L. H., Brookman, K. W., Jones, N. J., Allen, S. A. and Carrano, A. V. (1990) 'Molecular cloning of the human XRCC1 gene, which corrects defective DNA strand break repair and sister chromatid exchange', *Mol Cell Biol*, 10, (12), pp. 6160-71.
- Tice, R. R., Agurell, E., Anderson, D., Burlinson, B., Hartmann, A., Kobayashi, H., Miyamae, Y., Rojas, E., Ryu, J. C. and Sasaki, Y. F. (2000) 'Single cell gel/comet assay: guidelines for in vitro and in vivo genetic toxicology testing', *Environ Mol Mutagen*, 35, (3), pp. 206-21.
- Trainer, D. L., Kline, T., McCabe, F. L., Faucette, L. F., Feild, J., Chaikin, M., Anzano, M., Rieman, D., Hoffstein, S., Li, D. J. and et al. (1988) 'Biological characterization and oncogene expression in human colorectal carcinoma cell lines', *Int J Cancer*, 41, (2), pp. 287-96.
- Tricoli, J. V., Sahai, B. M., McCormick, P. J., Jarlinski, S. J., Bertram, J. S. and Kowalski, D. (1985) 'DNA topoisomerase I and II activities during cell proliferation and the cell cycle in cultured mouse embryo fibroblast (C3H 10T1/2) cells', *Exp Cell Res*, 158, (1), pp. 1-14.
- Trucco, C., Oliver, F. J., de Murcia, G. and Menissier-de Murcia, J. (1998) 'DNA repair defect in poly(ADP-ribose) polymerase-deficient cell lines', *Nucleic Acids Res*, 26, (11), pp. 2644-9.
- Tsavaris, N., Lazaris, A., Kosmas, C., Gouveris, P., Kavantzias, N., Kopterides, P., Papatthomas, T., Agrogiannis, G., Zorzos, H., Kyriakou, V. and Patsouris, E. (2009) 'Topoisomerase I and IIalpha protein expression in primary colorectal

- cancer and recurrences following 5-fluorouracil-based adjuvant chemotherapy', *Cancer Chemother Pharmacol*, 64, (2), pp. 391-8.
- Tuduri, S., Crabbé, L., Conti, C., Tourrière, H., Holtgreve-Grez, H., Jauch, A., Pantesco, V., De Vos, J., Thomas, A., Theillet, C., Pommier, Y., Tazi, J., Coquelle, A. and Pasero, P. (2009) 'Topoisomerase I suppresses genomic instability by preventing interference between replication and transcription', *Nat Cell Biol*, 11, (11), pp. 1315-1324.
- Tuduri, S., Crabbe, L., Tourriere, H., Coquelle, A. and Pasero, P. (2010) 'Does interference between replication and transcription contribute to genomic instability in cancer cells?', *Cell Cycle*, 9, (10), pp. 1886-92.
- van der Zee, A. G., Hollema, H., de Jong, S., Boonstra, H., Gouw, A., Willemse, P. H., Zijlstra, J. G. and de Vries, E. G. (1991) 'P-glycoprotein expression and DNA topoisomerase I and II activity in benign tumors of the ovary and in malignant tumors of the ovary, before and after platinum/cyclophosphamide chemotherapy', *Cancer Res*, 51, (21), pp. 5915-20.
- VanAnkeren, S. C., Murray, D., Stafford, P. M. and Meyn, R. E. (1988) 'Cell survival and recovery processes in Chinese hamster AA8 cells and in two radiosensitive clones', *Radiation Research*, 115, (2), pp. 223-237.
- Venter, J. C., Adams, M. D., Myers, E. W., Li, P. W., Mural, R. J., Sutton, G. G., Smith, H. O., Yandell, M., Evans, C. A., Holt, R. A., Gocayne, J. D., Amanatides, P., Ballew, R. M., Huson, D. H., Wortman, J. R., Zhang, Q., Kodira, C. D., Zheng, X. H., Chen, L., Skupski, M., Subramanian, G., Thomas, P. D., Zhang, J., Gabor Miklos, G. L., Nelson, C., Broder, S., Clark, A. G., Nadeau, J., McKusick, V. A., Zinder, N., Levine, A. J., Roberts, R. J., Simon, M., Slayman, C., Hunkapiller, M., Bolanos, R., Delcher, A., Dew, I., Fasulo, D., Flanigan, M., Florea, L., Halpern, A., Hannenhalli, S., Kravitz, S., Levy, S., Mobarry, C., Reinert, K., Remington, K., Abu-Threideh, J., Beasley, E., Biddick, K., Bonazzi, V., Brandon, R., Cargill, M., Chandramouliswaran, I., Charlab, R., Chaturvedi, K., Deng, Z., Di Francesco, V., Dunn, P., Eilbeck, K., Evangelista, C., Gabrielian, A. E., Gan, W., Ge, W., Gong, F., Gu, Z., Guan, P., Heiman, T. J., Higgins, M. E., Ji, R. R., Ke, Z., Ketchum, K. A., Lai, Z., Lei, Y., Li, Z., Li, J., Liang, Y., Lin, X., Lu, F., Merkulov, G. V., Milshina, N., Moore, H. M., Naik, A. K., Narayan, V. A., Neelam, B., Nusskern, D., Rusch, D. B., Salzberg, S., Shao, W., Shue, B., Sun, J., Wang, Z., Wang, A., Wang, X., Wang, J., Wei, M., Wides, R., Xiao, C., Yan, C., et al. (2001) 'The sequence of the human genome', *Science*, 291, (5507), pp. 1304-51.
- Verheij, M., Vens, C. and van Triest, B. 'Novel therapeutics in combination with radiotherapy to improve cancer treatment: Rationale, mechanisms of action and clinical perspective', *Drug Resistance Updates*, 13, (1-2), pp. 29-43.
- Veuger, S. J., Curtin, N. J., Smith, G. C. and Durkacz, B. W. (2004) 'Effects of novel inhibitors of poly(ADP-ribose) polymerase-1 and the DNA-dependent protein kinase on enzyme activities and DNA repair', *Oncogene*, 23, (44), pp. 7322-9.
- Vos, S. M., Tretter, E. M., Schmidt, B. H. and Berger, J. M. (2011) 'All tangled up: how cells direct, manage and exploit topoisomerase function', *Nat Rev Mol Cell Biol*, 12, (12), pp. 827-41.
- Wall, M. E., Wani, M. C., Nicholas, A. W., Manikumar, G., Tele, C., Moore, L., Truesdale, A., Leitner, P. and Besterman, J. M. (1993) 'Plant antitumor agents. 30. Synthesis and structure activity of novel camptothecin analogs', *J Med Chem*, 36, (18), pp. 2689-700.
- Wang, H., Rosidi, B., Perrault, R., Wang, M., Zhang, L., Windhofer, F. and Iliakis, G. (2005) 'DNA ligase III as a candidate component of backup pathways of nonhomologous end joining', *Cancer Res*.

- Wang, J. C. (2002) 'Cellular roles of DNA topoisomerases: a molecular perspective', *Nat Rev Mol Cell Biol*, 3, (6), pp. 430-40.
- Wang, M., Wu, W., Wu, W., Rosidi, B., Zhang, L., Wang, H. and Iliakis, G. (2006) 'PARP-1 and Ku compete for repair of DNA double strand breaks by distinct NHEJ pathways', *Nucleic Acids Res*, 34, (21), pp. 6170-82.
- Wood, R. D. (2010) 'Mammalian nucleotide excision repair proteins and interstrand crosslink repair', *Environ Mol Mutagen*, 51, (6), pp. 520-6.
- Wu, W., Wang, M., Wu, W., Singh, S. K., Mussfeldt, T. and Iliakis, G. (2008) 'Repair of radiation induced DNA double strand breaks by backup NHEJ is enhanced in G2', *DNA Repair (Amst)*, 7, (2), pp. 329-38.
- Yu, S. W., Wang, H., Poitras, M. F., Coombs, C., Bowers, W. J., Federoff, H. J., Poirier, G. G., Dawson, T. M. and Dawson, V. L. (2002) 'Mediation of poly(ADP-ribose) polymerase-1-dependent cell death by apoptosis-inducing factor', *Science*, 297, (5579), pp. 259-63.
- Yung, T. M., Sato, S. and Satoh, M. S. (2004) 'Poly(ADP-ribosylation) as a DNA damage-induced post-translational modification regulating poly(ADP-ribose) polymerase-1-topoisomerase I interaction', *J Biol Chem*, 279, (38), pp. 39686-96.
- Zaremba, T., Thomas, H. D., Cole, M., Coulthard, S. A., Plummer, E. R. and Curtin, N. J. (2011) 'Poly(ADP-ribose) polymerase-1 (PARP-1) pharmacogenetics, activity and expression analysis in cancer patients and healthy volunteers', *Biochem J*.
- Zhang, Y. W., Regairaz, M., Seiler, J. A., Agama, K. K., Doroshov, J. H. and Pommier, Y. (2011) 'Poly(ADP-ribose) polymerase and XPF-ERCC1 participate in distinct pathways for the repair of topoisomerase I-induced DNA damage in mammalian cells', *Nucleic Acids Res*, 39, (9), pp. 3607-20.
- Zheng, W., He, J. L., Jin, L. F., Lou, J. L. and Wang, B. H. (2005) 'Assessment of human DNA repair (NER) capacity with DNA repair rate (DRR) by comet assay', *Biomed Environ Sci*, 18, (2), pp. 117-23.
- Zhou, Y., Gwadry, F. G., Reinhold, W. C., Miller, L. D., Smith, L. H., Scherf, U., Liu, E. T., Kohn, K. W., Pommier, Y. and Weinstein, J. N. (2002) 'Transcriptional regulation of mitotic genes by camptothecin-induced DNA damage: microarray analysis of dose- and time-dependent effects', *Cancer Res*, 62, (6), pp. 1688-95.